DEVELOPMENT OF CHITOSAN BASED BIOFOAMS

A Thesis Submitted to
The Graduate School of
İzmir Institute of Technology
In Partial Fulfillment of the Requirements for the Degree of

DOCTOR OF PHILOSOPHY

in Chemical Engineering

by
Aybike Nil OLCAY KURT

July 2020
İZMİR

ACKNOWLEDGMENTS

ABSTRACT

DEVELOPMENT OF CHITOSAN BASED BIOFOAMS

Chitosan is a preferred bio-foam material used in many research fields due to its unique structural features. However, chitosan foams are mechanically too weak to maintain the desired shape.

A wound infection and tissue necrosis, endanger human's lives. So, a dressing is required to protect loss of fluids from the wound and prevents any bacterial invasion replacing the function of skin temporarily. Therefore controlled drug release from a wound dressing is necessary with a biocompatibility and enough mechanical strength.

The aim of this study was the synthesis of mechanically durable - dual porosity chitosan bio-foams to provide a controlled drug release. For this purpose, oil droplets formed in a chitosan solution were used as templates to produce micropores that also contain vancomycin (a model antibiotic-hydrophylic) and curcumin (a model anti-inflammatory-hydrophobic) in the walls of chitosan matrix with large structural voids. An anionic surfactant, sodium dodecyl sulfate (SDS) alone, was used as a crosslinking agent which was a new approach. The chitosan foams have dual pore structures. 1) The intrinsic micro pores with different morphology that depends on the oil phase. 2) The structural voids, present even in the absence of an oil phase that depends on the experimental conditions. The mechanical strength of the foams were found to be much higher (up to 250 kPa) compare to the foams produced in literature and suggested to be suitable to use for wound dressing applications. The drug release mechanism of foams were found to depend on the conditions used for foam development and the released kinetics were presented with a mathematical model.

ÖZET

KİTOSAN BAZLI BİYOKÖPÜKLERİN GELİŞTİRİLMESİ

Kitosan, eşsiz yapısal özellikleri nedeniyle doku mühendisliği ve ilaç salım sistemleri gibi birçok alanda biyo-köpük üretmek için kullanılan bir malzemedir. Bununla birlikte, kitosan köpükler, dokunun yeniden oluşması ya da iyileşmesine kadar geçen sürede istenen şeklini koruması açısından mekanik olarak çok zayıftır.

Yara enfeksiyonu ve ciddi doku ölümü, insanların hayatını tehlikeye sokar. Bu nedenle, yara bölgesinden sıvı kaybını önlemek ayrıca cildin işlevini geçici olarak değiştiren bakteri istilasını engellemek için bir yara örtüsü gereklidir. Bununla birlikte, biyouyumluluğa ve yeterli mekanik mukavemete sahip yara örtülerinden kontrollü ilaç salınımı, yaraların tedavisi için önemlidir.

Bu çalışmanın amacı, kontrollü bir ilaç salımı sağlamak için mekanik olarak dayanıklı ve iki farklı tip gözenek yapısına sahip kitosan biyo-köpüklerin sentezidir. Bu amaçla, kitosan çözeltisinde oluşturulan yağ damlacıkları, büyük yapısal boşluklara sahip kitosan matrisinin duvarlarında vankomisin (model antibiyotik-hidrofilik) ve curcumin (model antiinflamatuar-hidrofobik) içeren mikro gözenekler üretmek için şablon olarak kullanılmıştır. Yeni bir fikir olarak, anyonik bir yüzey aktif madde olan sodyum dodesil sülfat (SDS) çapraz bağlama maddesi olarak kullanılmıştır. Kitosan köpükler iki farklı tip gözenek içeren yapıya sahiptir. Bunlar, 1) Kitosan matrisinin duvarlarında bulunan ve yağ fazına bağlı olarak farklı morfolojiye sahip olan gerçek mikro gözeneklerdir. 2) Kitosan matrisinin yağ fazı olmasa bile deney koşullarına bağlı olarak sahip olduğu yapısal boşluklardır. Köpüklerin mekanik mukavemetinin, literatürde üretilen köpüklere kıyasla çok daha yüksek (250 kPa 'a kadar) olduğu ve yara sargısı uygulamalarında kullanılmaya uygun olduğu görülmüştür. Köpüklerin ilaç salım mekanizmasının, köpük üretimi için kullanılan koşullara bağlı olduğu bulunmuştur ve salım kinetikleri, matematiksel bir modelle sunulmuştur.

Dedicated to my family...

TABLE OF CONTENTS

LIST OF FIGURES

xiv

LIST OF TABLES

CHAPTER 1

INTRODUCTION

Polymer foams have highly porous structures due to the gas phase that they contain. Although the porous structure supplies the material lots of properties such as having high surface area with low weight, the gas phase within the polymer do not have any effect on the chemical properties of the foams. The relation between the foam properties and porous structure depends on pore size, thickness of the pore walls, morphology, density and interconnectivity (Andrieux et al. 2019). Biofoams are materials which are bio-based, soft biomaterials, produced from renewable feedstocks (such as soybean flour/oil, cellulose, wheat gluten (WG), corn starches, chitin and chitosan (CS)) with interconnected pore structure, high swelling and absorption capacity. Biofoams can be produced by several type of methods such as solid templated, gas templated and liquid templated methods. Gas templated method is not useful for hydrophilic and glassy polymers like chitosan. In the case of gas templated method, closed pores could be obtained (Ji et al. 2011). The solid templated methods require extra porogen removal processes to have porous structures. Hence, liquid templated method looks promising among them to produce biofoams with porous structure.

Skin is the largest organ of the living structures which protect the internal organs from the environment and is about 15 wt % of the total body (Moeini et al. 2020). A wound can be described as the damage of the structure of skin and loss of its normal function due to burns, injury, chronic or genetic diseases, insect bites and surgial operations. The first thing to deal with in wounds to prevent deaths from injuries is to stop bleeding (Khan and Mujahid 2019). In addition, Gram-positive such as Staphylococcus aureus (S.aureus) and Streptococcus pyogenes (S.pyogenes) and Gram-negative bacteria such as Escherichiacoli (E.coli) and Pseudomonas aeruginosa (P.aeruginosa) which may be resulted in function loss of organ can colonized as a result of chronic wounds. Usage of suitable drugs such as vancomycin, curcumin is the most effective way to prevent wound from bacteria. In addition, controlled drug release from wound dress advantageous treatment since optimum drug release rate can be reached and change of wound dressing frequently is not needed. A succesful wound dressing

should have biocompatibility and be easily applicable with mechanical strength during usage. It should prevent infection by allowing ideal gas and liquid exchange (Michailidou et al. 2019). Traditional dressing is used in the first moments of treatment to stop wound contact with environment. They are not successful in ensuring stability and reducing the risk of infection. Hence, it is required to produce wound dressings which can prevent microorganisms. To achieve this aim, synthetic and natural polymers can be used to develop these dressing materials. Especially, natural polymers which are biocompatible, biodegradable, self treating due to features of the used raw material are preferred most of the time for biofoams as wound dressing. There are some natural polymers such as collogen, chitin, chitosan, alginate to produce biofoam wound dressings (Moeini et al. 2020).

Chitosan which is obtained by deactylation of chitin is the most commonly used polysaccharide in wound dressing applications due to being biocompatible, biodegradable, non-toxic, antimicrobial, easily applicable, easily processable and haemostatic (Khan and Mujahid 2019). Moreover, it is naturally antibacterial as a result of its amino side groups (Andrieux et al. 2019). A lot of study about chitosan based wound dressings have been carried out in literature due to its excellent properties. (Hu et al. 2018; Li et al. 2005; Khan and Mujahid 2019; Moeini et al. 2020). In literature, it was mentioned that there are some limitations due to mechanical strength of the chitosan. In addition, it was claimed that low mechanical strength is one of the major problem for the use of the polysaccharide as wound dressing (Pires and Moraes 2015; Devi et al. 2012). Hence, composites containing chitosan were prepeared or chemical modifications were applied to overcome this problem in many research. For instance, chitosan-collogen composite sponges were produced to improve the mechanical properties of the foams (Arpornmaeklong et al. 2008; Indrani et al. 2017). Devi et al. improved the mechanical properties of the foams produced as wound dressing by combining chitosan with fibrin and sodium alginate (Devi et al. 2012). Although many chitosan biofoams produced in the literature, there is little work regarding chitosan based foams (drug loaded/unloaded) which have desired mechanical properties without using composites. Moreover, foams obtained in literature have only structural voids in their structures.

In the present study, the aim was the synthesis of composite drug-bearing chitosan biofoams (as wound dressing) through liquid templated methods with optimized pore structure, mechanical strength and water affinity. Effect of molecular

weight of chitosan, chitosan concentration, type of crosslinking agent, oil type and concentration on foam sythesis were evaluated. In addition, foam-drug interactions were examined to achieve high efficiency of drug loading (modification of synthesis) and release. The release kinetics of both hydrophilic and hydrophobic drugs were studied and a release model was developed to express the process in mathematical form.

CHAPTER 2

BACKGROUND INFORMATION

This chapter starts with the description of biofoams and its synthesis methods. It continues with detailed information and literature studies about biofoams in wound dressing, chitosan, chitosan biofoams and emulsions.

2.1. Biofoams: Definition and Application Areas

Biofoams are bio-based porous materials manufactured from renewable feedstocks. Porous materials are materials with voids (pores, cavities, channels) have different properties depending on the material, composition of material, porosity, size, shape and arrangement of pores (Figure 2.1). Porosity is defined as the total volume of empty or pore parts in the material. Pore size of these materials can be changed from nanometer to milimeter and pores can have ordered or irregular pattern. Pores are classified as macropores (larger than 50 nm), mesopores (between 2 and 50 nm) and micropores (smaller than 2 nm) based on their pore size (Zhu and Ren 2014).

There are many types of raw materials for biofoams such as soybean flour/oil, cellulose, wheat gluten (WG), corn starches, chitin and chitosan. Figure 2.2. shows the different types of biobased polymers. Cellulose is the most widely used biopolymer due to being biodegradable, biocompatible and non-toxic (Ferrer et al. 2017). High surface area and tunable surface properties are some features of nanocellulose. Vegetable oils can be used to produce polyuretanes since they are renewable, easily accessible and inexpensive (Budnyak et al. 2015; MITELUȚ et al. 2015). Corn starch is an agriproduct which is degradable, renewable and has easily accessible source, usability at high temperature, short-time cooking processes without any blowing agent (Lin et al. 1995). Instead of polyurethane and polystyrene, wheat gluten is used in thermal insulation applications due to its good thermal insulation properties (Wu et al. 2017). Chitin is naturally occuring biopolymer in cell wall fungi, exoskeleton of crustacean and cuticle of insects (Zhou et al. 2014; van den Broek et al. 2015). Deacetylation of the chitin

gives chitosan which is pH sensitive, biodegradable, biocompatible, non-toxic, antimicrobial, antitumoral and antifungal biopolymer.
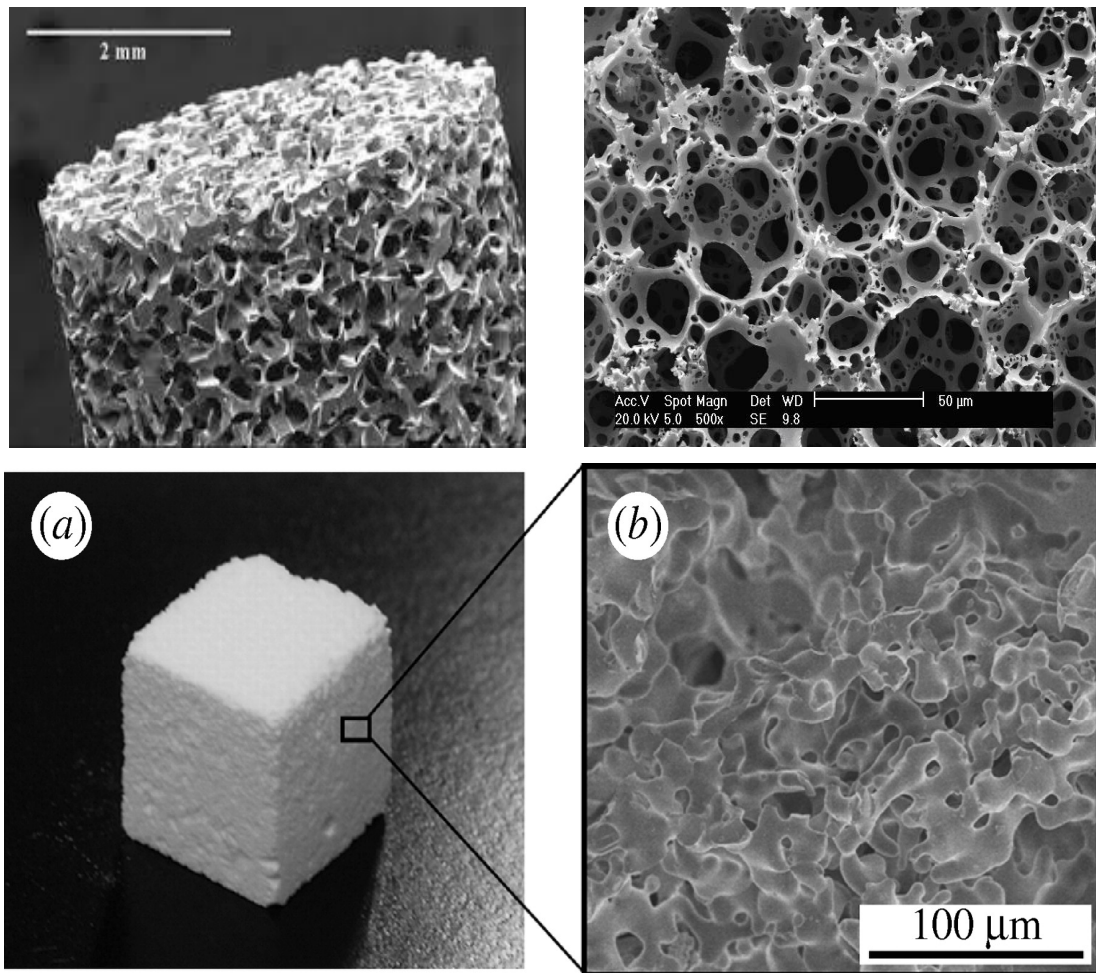
Figure 2. 1. Porous materials

(Ohtsuki et al. 2009).
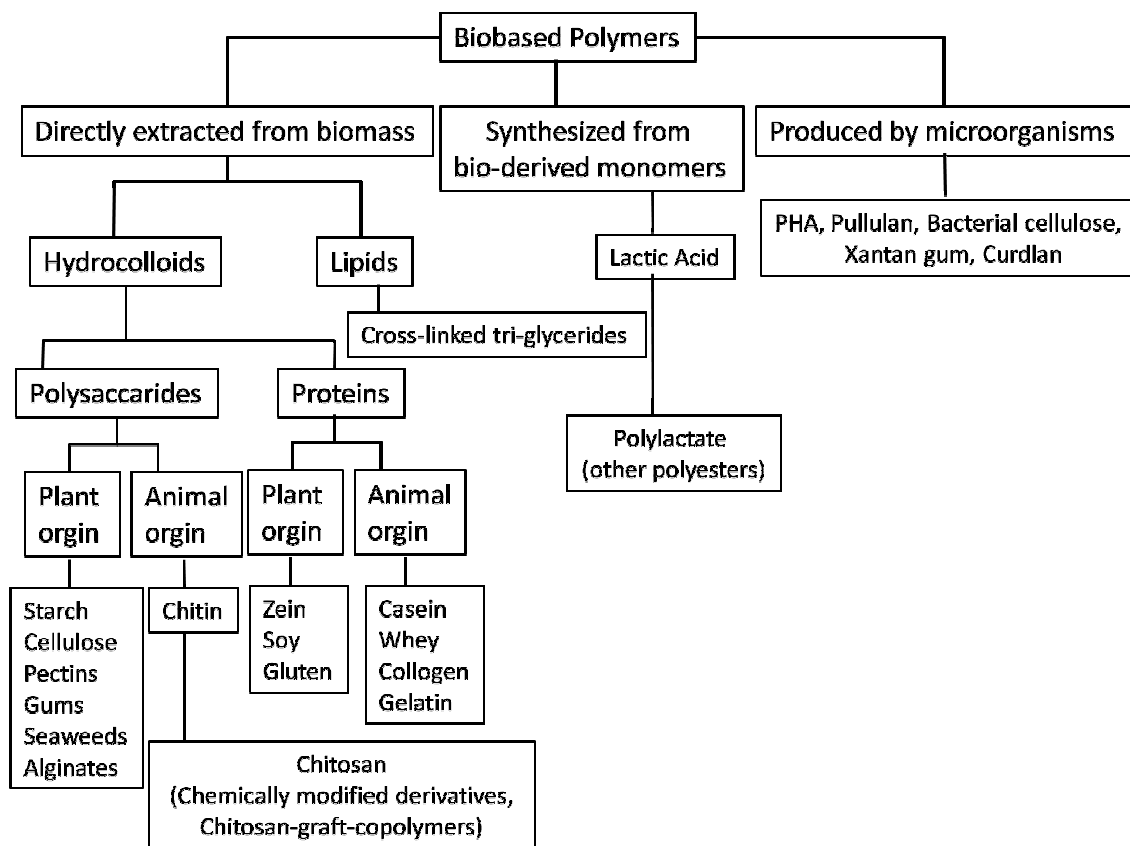
Figure 2. 2. Different types of biobased polymers
(Srinivasa and Tharanathan 2007).

Porous biomaterials have wide usage area such as wound dressing, tissue engineering, drug delivery, green packaging and etc. (Xie et al. 2012). They have high applicability due to tunable pores size, high surface area and adjustable framework (Netti 2014). In addition, usage of biofoams prevent the effects of synthetic polymers on the environment. Zhang et al. used soybean oil based polyol instead of petroleum-based polyols to produce foams as thermal insulation material. Produced foams were more stable than syhthetic polymer based foams in terms of chemical and thermal stability. Also, mechanical properties were improved by using natural polymer (Zhang and Luo 2015). As it was mentioned starch can be used as a raw material for foam production due to its biodegradability, low cost and low density. Also, starch biofoams have good thermal insulation properties when they compared with fossil-fuel based polymers (Hassan et al. 2020). Since wheat gluten has very low cost and good thermal insulation properties, wheat gluten biofoams were produced by freeze drying method and used in

thermal insulation applications. Moreover, these foams showed good liquid hold up capacity. As a result of this property, they were offered as an alternative material in applications where there is a risk of water or moisture exposure (Wu et al. 2017). The use of single-use foam packaging is increasing day by day. As a result, food packaging materials produced from plastic materials are pose a serious danger to the environment. To overcome this problem, biofoams are used instead of the synthetic foams in food packaging industry. Starch is one of the alternative biobased polymer for packaging applications (Glenn and Orts 2001). In addition to their environmental benefits, biofoams can protect the foods against microorganisms and microbes due to their natural properties. In literature, starch, antimicrobial and antioxidant, used to create bioactive packaging foams (Cruz-Tirado et al. 2020). Engel et al. developed starch-based biofoams for packaging foods with low moisture content (Engel et al. 2019). Since all biobased polymers have their own properties, sometimes it is required to use some biopolymers together to improve the properties of the biofoam. Ottenhall et al. combined low density cellulose and water stable chitosan polymers to have an alternative packaging material with desired properties (Ottenhall et al. 2018). Also, starch-cellulose composite foams were produced for use in the food industry (Soykeabkaew et al. 2004). Kaisangsri et al. prepeared cellulose enhanced starch foams as biodegradable packaging material (Kaisangsri et al. 2019). Biofoams are used in removal of industrial dyes from aqueus solutions due to their high adsorption capacities. Also, they are ecofriendly adsorption materials. Chitosan is widely used for dye removal because biofoams produced by chitosan have high surface area and porosity (Li et al. 2018). Da Rosa Schio et al. prepeared biobased chitosan-polyurethane foams for the adsorption of dye. They suggested these foams as potential dye removal materails with high adsorption capacity, high removal efficiency and good mechanical properties (da Rosa Schio et al. 2019). In another study, chitosan/hydroxyapatite foam membranes were used successfully to remove the dyes since NH_2 and OH groups of chitosan is effective for adsorption of organic contaminants and heavy metals (Shi et al. 2017). Biofoams are used widely in wound healing applications since their biocompatibility, non-toxicity, biodegradability. Nguyen et al. prepared drug loaded chitosan/gelatin composite biofoam as wound healing material (Nguyen et al. 2013). Moreover, porous biomaterials are used in ceramic industry as a slurry since they are sensible to water. In a study, chitosan based biofoams were used to process a porous ceramic material (Mathias et al. 2011).

2.1.1. Synthesis of Biofoams

Biofoams can have random or ordered pore arrangement. Random pores cause some problems during diffusion. On the other hand, ordered pore structure can overcome the diffusion limitations. Biofoams can be produced by many different methods such as gas foaming, particle leaching, phase seperation which are inexpesive and easily applicable. Although these methods have many advantages, biofoams produced by these methods have some troubles with porosity, mechanical strength, diffusion and pore structure (Mohanty et al. 2016). Techniques to have ordered structured biofoam can be classified as gas templating, solid templating and liquid (emulsion) templating.

2.1.1.1. Gas Templated

Dense gas is defined as gas which is close to its critical point. Dense gas expansion is a method to produce porous structure from polymeric materials (Ji et al. 2011). When it is compared to other methods (solid and liquid templated), toxic solvents are not used and ordered pore structure with sufficient and interconnected pores can be created. The most widely used dense gas is carbon dioxide (CO_2) since it is non-toxic, non-flammable and soluble in most of polymers. During this method, a thermoplastic material is put in a vessel which is pressured and saturated with an inert CO_2 gas. Polymer-gas solution at temperature which is lower than its glass transition temperature is obtained by supercritical CO_2 at high pressure. Then, solubility of CO_2 decreases with fast reduction in pressure to ambient pressure and bubble formation is observed due to supersaturation. Produced porous polymers are widely used as drug carrier, porous scaffold and microparticles. Figure 2.3 shows a schematic representation of the gas templating foaming method.
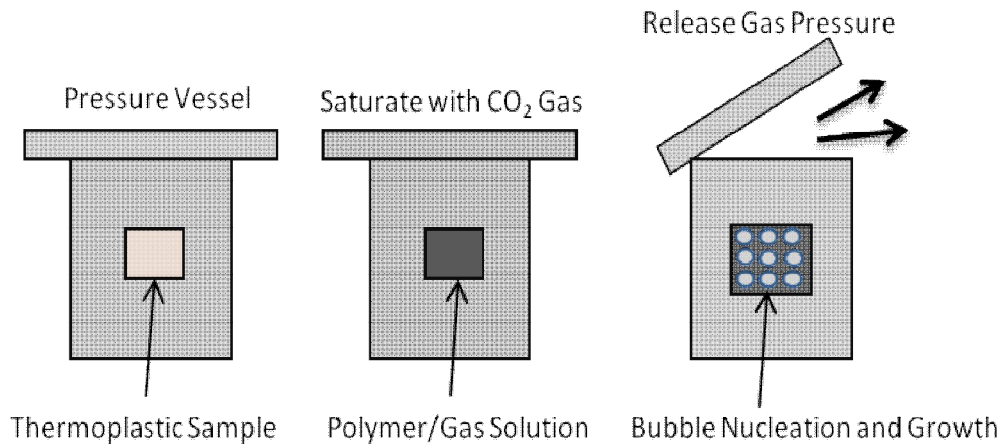
Figure 2. 3. Schematic of gas templated foam production.

Although porosity formation with supercritical CO_2 is easily applicable method, it results in a dense unfoamed surface layer since high velocity of CO_2 near the surface increases viscosity and glass transition temperature. These porous polymers can be preferred for high-strength applications. Gas templated method leads to closed pore structure which is useful for some applications such as insulation, however, closed pore structure is not desirible in tissue engineering applications (Kiran 2016). Although there is lots of study about gas (CO_2) templated method, it is highlighted that this method is not useful for hyrophilic and glassy polymers (chitosan etc.) since CO_2 is not highly soluble in these materials. Acid or ethanol as a co-solvent can be used to solve the problem about low solubility. On the other hand, while using co-solvent (such as ethanol) can result in higher solubility of the gas, open pores can not be produced and additional procedures is needed (Ji et al. 2011). Xie et al. prepared porous polycaprolactone (PCL) materials for controlled drug release studies by using CO_2 as foaming agent and procedure for porous PCL scaffolds can be seen from Figure 2.4 (Xie et al. 2012).
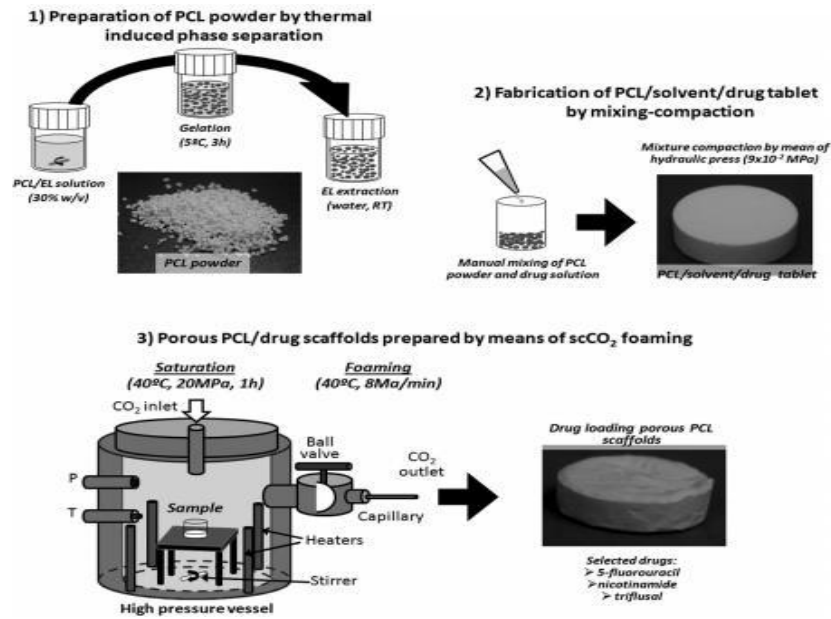
Figure 2. 4. Gas (CO$_2$) templated method for PCL scaffolds

(Xie et al. 2012).

Morphology, mean pore size and pore size distribution of drug loaded PCL porous materials produced by CO$_2$ foaming process is given in Figure 2.5.
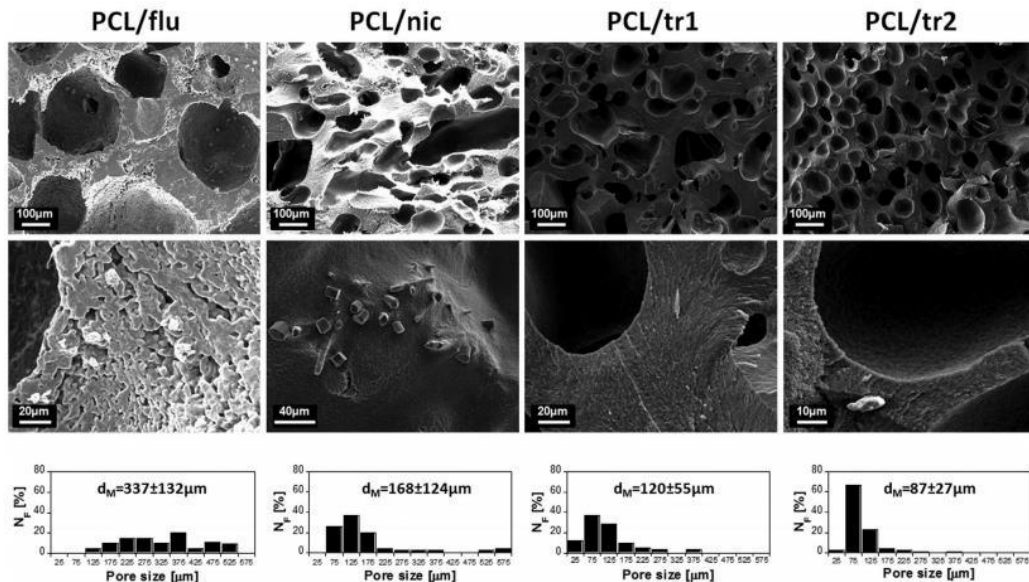
Figure 2. 5. Drug-loaded PCL-based porous scaffolds

(Xie et al. 2012).

Singh et al. produced PLGA foams by the gas templating method. Supercritical CO_2 was used as the blowing agent (Figure 2.6) (Singh et al. 2004).
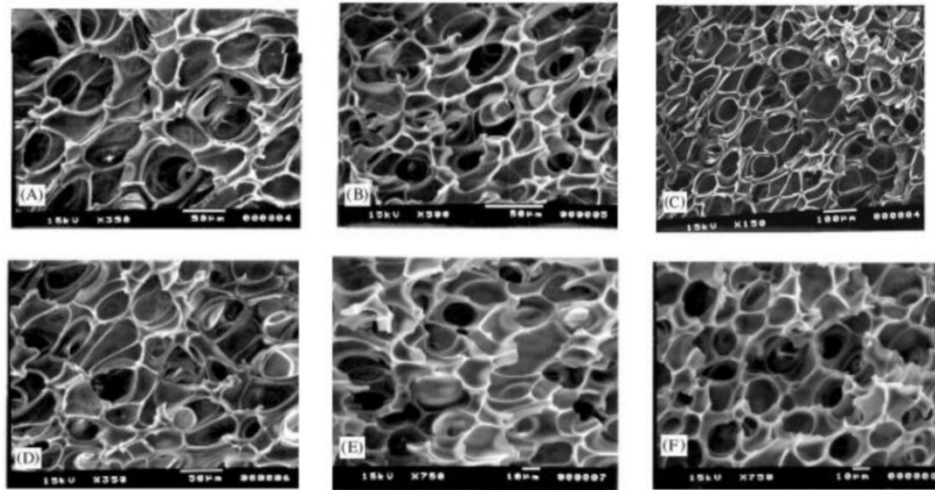
Figure 2. 6. Porous structure of poly(DL-lactide-co-glycolide) foams
(Singh et al. 2004).

An alternative gas is air for gas templating foam production method. Testouri et al. used this technique to produce porous foams from chitosan gels. In this method, chitosan solutions (with surfactant), air and crosslinking agent were given at the same time in a T-junction device (Figure 2.7). Also, surfactant was used to stabilize the foams (Testouri et al. 2010).
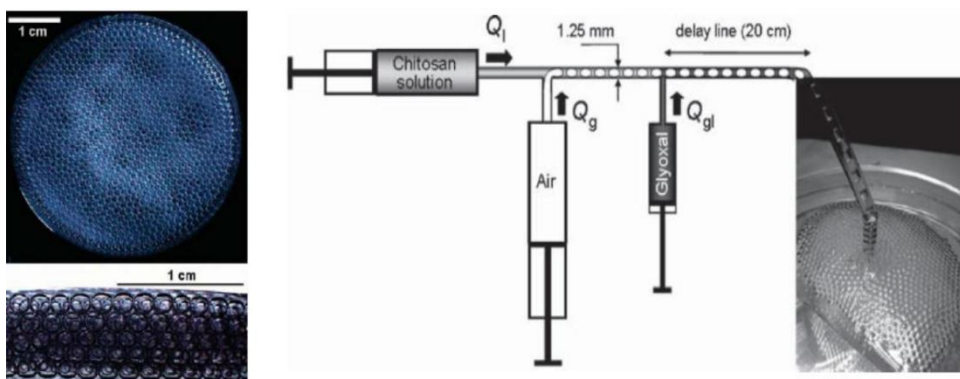
Figure 2. 7. Shematic form of the air templated foam production method
(Testouri et al. 2010).

2.1.1.2. Solid Templated

Porogen is a solid material used to produce porosity. Porous material with desired pore sizes (micropores, mesopores and macropores) and high porosity can be obtained by changing and controlling size of particles (Figure 2.8). Salt and silica can be used as porogen (Xianfang and Eli 1996). In literature, chitosan membranes were produced by using silica particles as porogen by Xianfang and Eli. While silica particles dissolve in alkaline solution, chitosan is insoluble in this solution. Hence, silica particles removed easily from the structure to create pores by using an alkaline solution (Xianfang and Eli 1996). Figure 2.9 shows the structure of the membranes produced at different chitosan silica ratios.
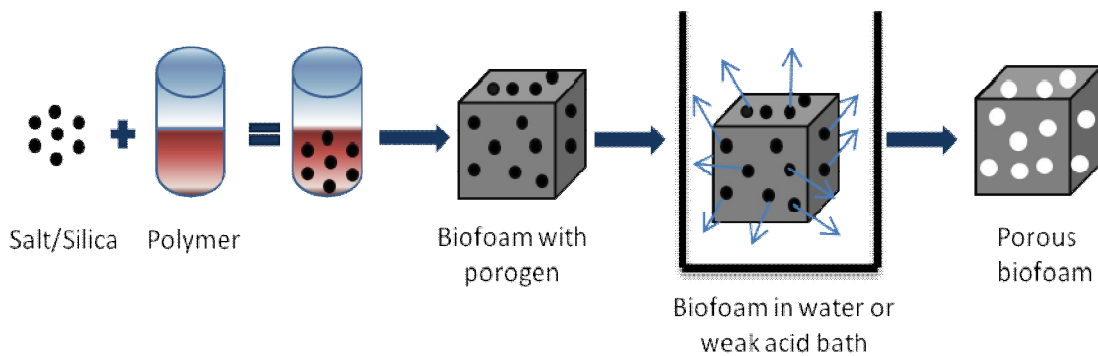
Figure 2. 8. Schematic of solid templated foam production.
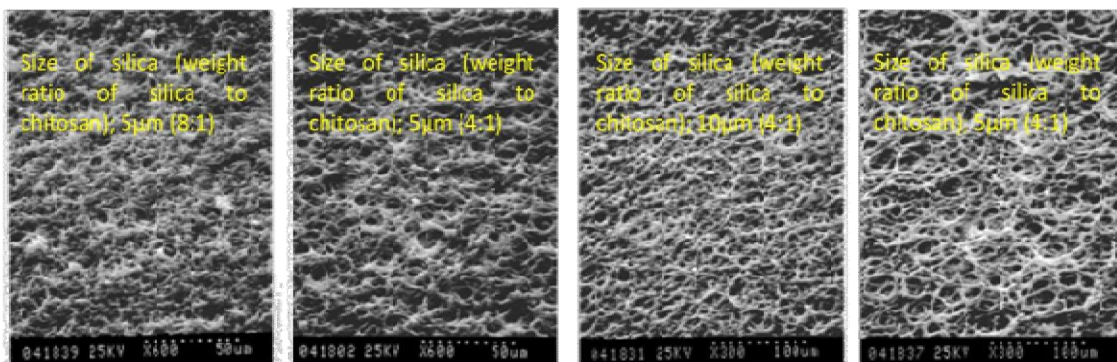
Figure 2. 9. Structures of chitosan membranes

(Xianfang and Eli 1996).

Chao et al. used sodium cloride (NaCl) as a porogen and genipin as a crosslinking agent for solid templated chitosan membrane production (Figure 2.10). NaCl particles was removed by using deionized water. Effect of porogen on mean pore diameter and porosity was studied by using NaCl and silica. The pore diameter and porosity of the materials which was produced by NaCl were lower than the materials using silica particles as porogen due to dissolving and size reduction of NaCl particles in acidic chitosan solution (Chao et al. 2006).
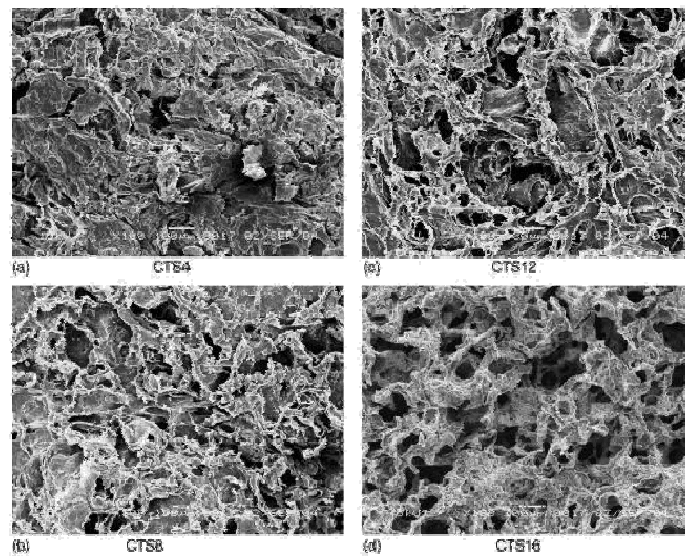
Figure 2. 10. Surface morphologies of chitosan membranes prepared with different NaCl:chitosan concentrations (Chao et al. 2006).

Lim et al. prepeared chitosan scaffold by solid templated method using sodium acetate as a porogen and examined the structure by SEM (Figure 2.11). Since chitosan is soluble in acidic conditions, the tendency of the salt to ionize in low acidic conditions should be taken into account and a salt eith low ioniation trend should be used as a porogen to produce porous material (Lim et al. 2011).
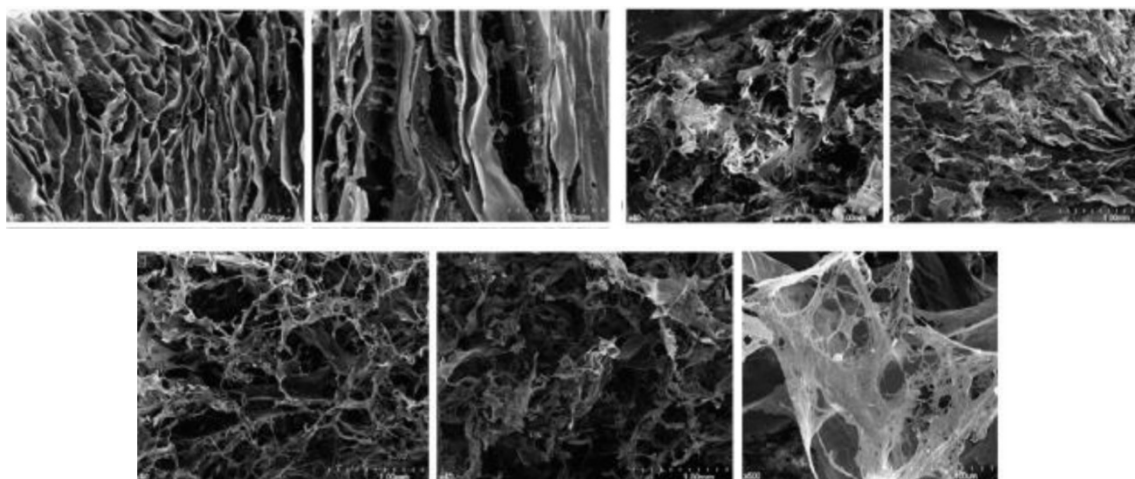
Figure 2. 11. Scanning electron microscope (SEM) images of sodium acetate templated chitosan scaffold (Lim et al. 2011).

Although solid templated method is used to produce porous structures, there is some disadvantages of the method. For instance, residual impurities are formed after the foam production and extra porogen removal methods are needed. Also, high solid concentrations are needed to create open pores and foam shows low mechanical strength due to high solid concentration.

2.1.1.3. Liquid Templated

In liquid templated method, porous structure is formed by liquid phase such as emulsion or microemulsion. Pore size can vary from nanaometer to micrometer, depending on liquid system used (Silverstein 2014). In this method, biphasic system is present and while continuous phase is polymerized, volatile liquid phase is removed after polymerization to produce porous structure (Figure 2.12).
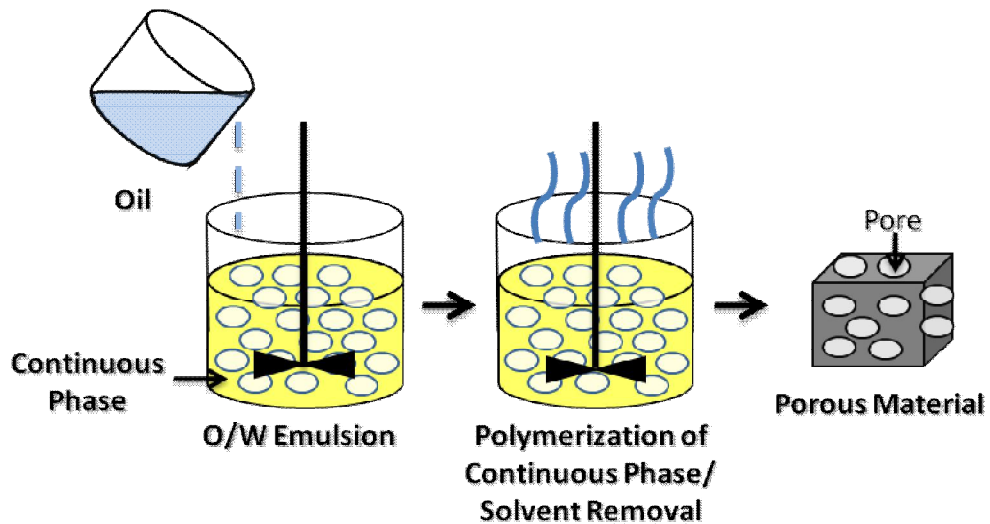
Figure 2. 12. Schematic of liquid templated foam production.

Miras et al. generated chitosan biofoams by using liquid templated method. Oil-in-water emulsions was used to create porous structure and chitosan was crosslinked by genipin. Volatile components were removed by freeze drying. SEM images of synthesized chitosan macroporous foams can be seen from Figure 2.13 (Miras et al. 2013).
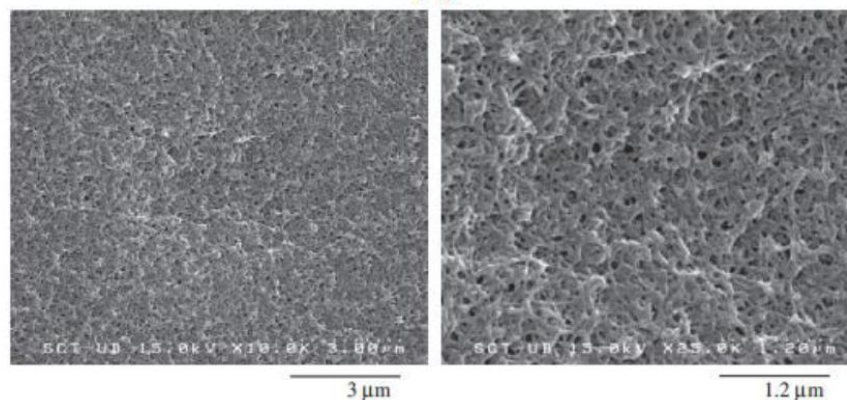
Figure 2. 13. SEM images of chitosan porous foam
(Miras et al. 2013).

Franks et al. desired to develop a new method to produce chitosan scaffolds by controlling porous structure in terms of volume fraction and pore size. 2,5-dimethoxy-2,5-dihydrofuran (DHF) was used as crosslinking agent to polymerize the chitosan

solution which is continuous phase. Oil is used to produce dispersed emulsion phase. The crosslinked scaffold was dried at room temperature. While a problem such as shrinking of scaffold was encountered during the drying phase, no cracking was observed in the scaffolds. It was observed that pores was created with lower sizes by increasing the cationic surfactant, CTAB concentration which was used to reduce the interaction with the cationic chitosan. Pore size of the structure was always higher than calculated and expected. There could be two reasons for this; 1) Size of the pores is not monodisperse and as a result while pores with small size have higher surface area, pores with larger pores can have less surface area, 2) There can be some surfactants which could not be removed in solution. It can be deduced that amount of surfactant affect the pore size of the structure (Franks et al. 2006). Figure 2.14, Figure 2.15, Figure 2.16 and Figure 2.17 show the SEM images of scaffold produced with different oil amount and droplet size.
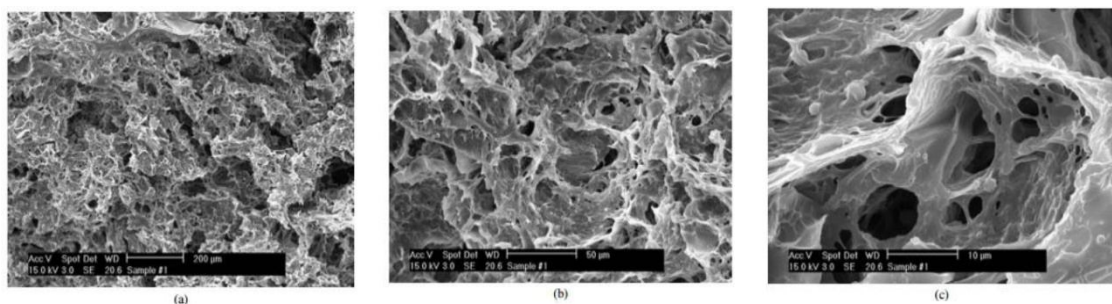
Figure 2. 14. Structure of the scaffold (30 % oil and 3 µm droplets)
(Franks et al. 2006).
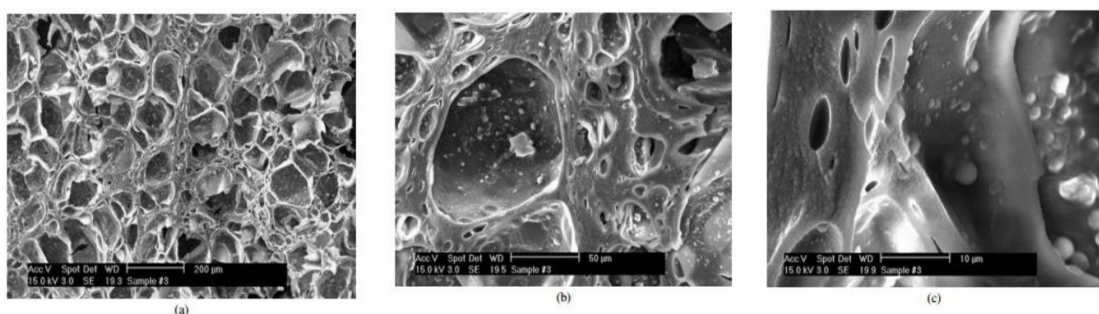
Figure 2. 15. Structure of the scaffold (30 % oil and 30 µm droplets)
(Franks et al. 2006).
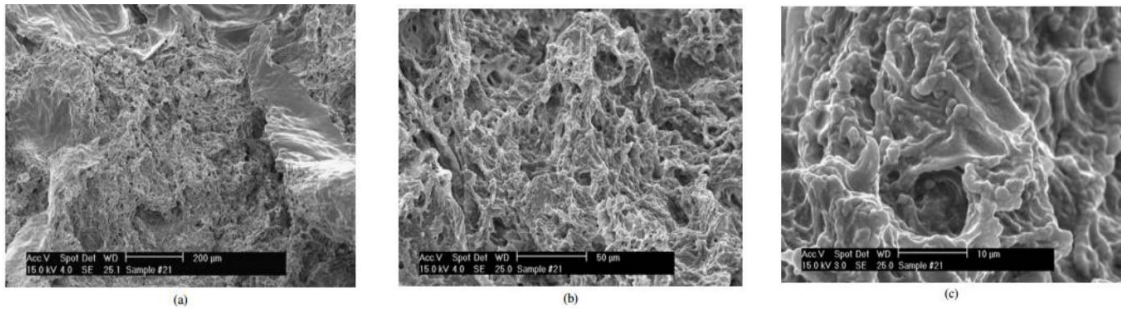
Figure 2. 16. Structure of the scaffold (50 % oil and 3 µm droplets)
(Franks et al. 2006).
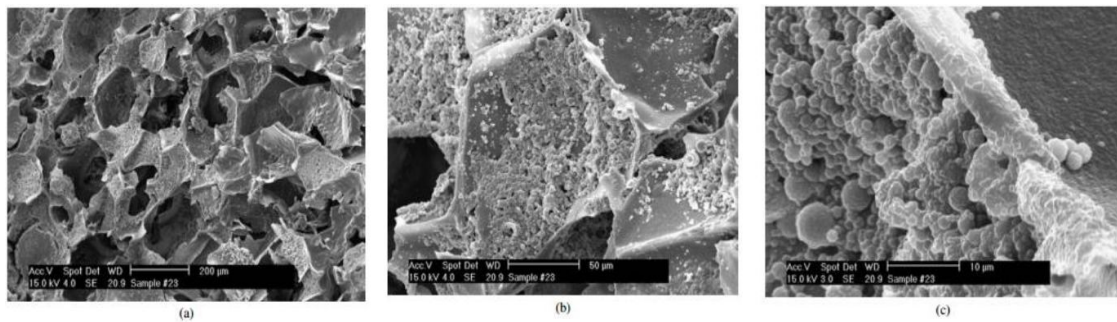
Figure 2. 17. Structure of the scaffold (50 % oil and 30 µm droplets)
(Franks et al. 2006).

Zhong et al. produced chitosan-poly(e-caprolactone) (PCL) composite hydrogels having different volume ratios by liquid (emulsion) templated method. Emulsion was obtained by Span-80 as an emulsifier and homogenity of the emulsion was provided by sonication. The polymerized mixture was frozen and lyophilized to create porous structure by ice sublimation under vacuum (Zhong et al. 2011). Figure 2.18 gives the results of SEM analysis of chitosan with different PCL amount.
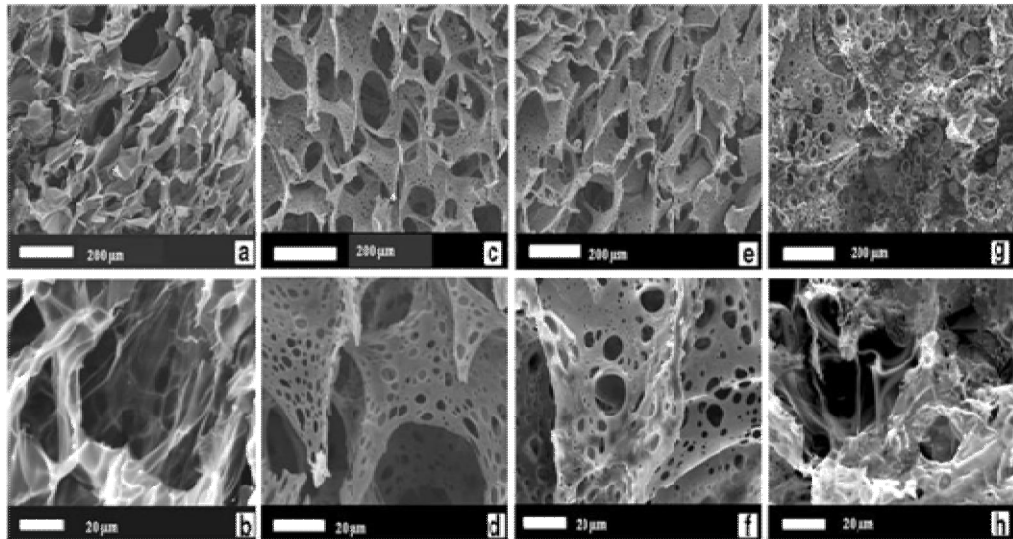
Figure 2. 18. SEM images of pure chitosan (a, b), composite hydrogels, 25 wt % PCL (c,d), 50 wt % PCL (e,f) and 75 wt % PCL (g,h) (Zhong et al. 2011).

In addition, the change in pore size by freezing temperature prior to lyophilisation was examined in the study. Liquid nitrogen was used at -196 ^{o}C to freeze the polymer solution and resulting pores had very small sizes which are not found favorable for tissue engineering applications. Otherwise, hydrogels frozen at -20 ^{o}C got larger pores as can be seen from Figure 2.19 (Zhong et al. 2011).
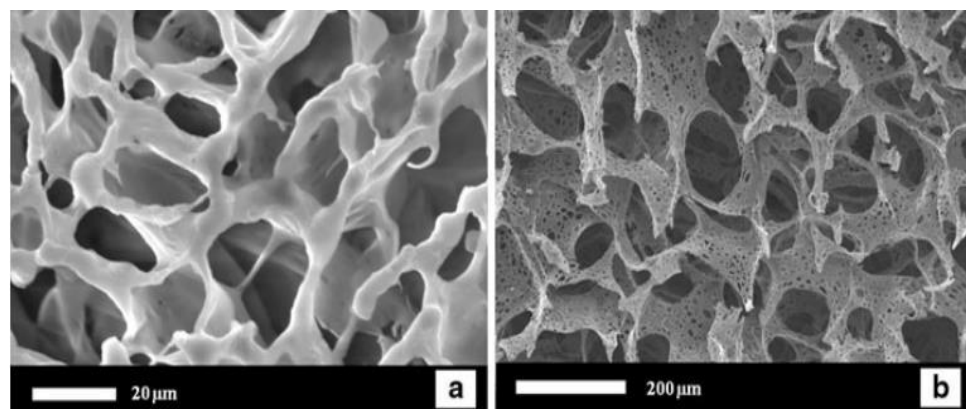
Figure 2. 19. SEM images of composite hydrogel frozen at (a) liquid nitrogen (-196°C) and (b) -20°C (Zhong et al. 2011).

2.1.1.4. Freeze Drying

Freeze drying is a technique used to produce porous material by sublimation of ice under vacuum after polymer solution is frozen at a low temperature (Chen et al. 2015). This technique is easy to apply and highly efficient. Since this process is a physical process between polymers and ice crystals, biofoams produced by the freeze drying process do not contain impurities and do not require extra purification steps. Water is environment-friendly solvent hence sustainable and green ice crystals are widely used to obtain porous structure (Zhou et al. 2014). Schematic representation of the freeze-drying method can be seen from the Figure 2.20.
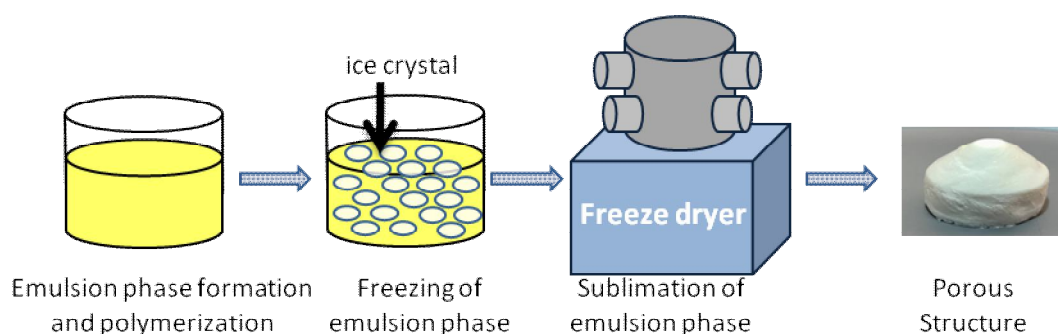
Figure 2. 20. Schematic of Freeze-Drying.

2.1.2. Biofoams in Wound Dressing

Skin covers the all of human body and is the largest organ of the body. It has many duties such as preventing infections by microorganisms, balancing body temperature, fat, water and vitamin. In addition, skin preserve the body against light, heat and injury. Many people suffer from skin diseases or skin losing due to physical, chemical and health reasons. Infections caused by skin injuries can endanger human life. A wound can be elucidated as the injury of usual structure and function of a living tissue. For example, as a result of the chemical explosions in industries or injuries in wars, many people suffer from skin burns. If all skin layer is destroyed in third degree burn, healthy part of the patient's own skin can be transfered to the burned area. Burned area should be protected from infections and fluid accumulation and also wound healing is speeded up during this

treatment. Open wounds have high risk in terms of infection. For example, orhopaedic wounds can suffer from infection. To prevent patient from morbidity and mortality, infection of the wounds should be prevented to improve antimicrobial protection (Noel et al. 2010). Dressing is a solution for preserving the skin from bacteria spreadwhich distrups the structure of the skin. Also, it is required to stop protein, body fluid and function loss from the wound by appropriate dressing (Hu et al. 2018). Tissue engineering works to create solution for the repair damaged tissues or develop new solutions such as hydrogels, hydrocolloids and biofoams for replace the tissues (Michailidou et al. 2019). There is some requirements for designing and producing a material in tissue engineering such as being biocompatible and biodegradable, required/adequate mechanical strength and interconnected, appropriate pore structure (Xu et al. 2017). Biofoams are bio-based, flexible and soft materials manufactured from renewable feedstocks with interconnected pore structure. As a result of the their structural properties, biofoams have high absorption capacity and cell connection. However, they especially do not have high mechanical strength to maintain their shape for the desired time. Hence, biofoams can be conveniently used as wound dressing or healing material. A wound dressing material must have some features such as being non-toxic, non-allergic, obstacle to microorganisms, having high absorption capacity of wound exudate, enable gaseous transfer and ensuring that the wound surface is kept at the required humidity. Biofoams can satisfy the requirements of biofoams with high liquid absorption capacity, healing ability due to natural properties of raw material (Jayakumar et al. 2011). Many types of raw material are used to produce biofoams as a wound dressing. For instance, collagen biofoams can be loaded by antibiotics. Toxicity is one of the disadvantage of the collagen. Chitosan is also used as a raw material of biofoams due to being biodegradable, biocompatible and effective drug carrier. In addition, chitosan is used widely as a wound treatments in US military to control injury bleeding (Noel et al. 2010).

Chronic wounds contain a wide variety of types and high amounts of bacteria such as Staphylococcus aureus and Pseudomonas aeruginosa. These pathogens are caused by gram-positive and gram-negative microorganisms in wound area (Albaugh et al. 2013). Antibiotics are used to prevent wound from organisms. Vancomycin is a hydrophilic antibiotic. Vancomycin is effective against Gram-positive bacteria which is not destroyed by other antibiotics (Zaric et al. 2018). This antibiotic can be used as initial treatment for complicated infections caused by Staphylococcus aureus such as

bone, joint, bloodstream and skin (Talebian and Mansourian 2017). Xu et al. prepeared vancomycin loaded chitosan nanoparticles and they had excellent antibacterial activity against the Gram-positive bacterium Staphylococcus aureus (Xu et al. 2015). Drugs obtained from natural sources have an importance for healthcare. Curcumin is natural, hydrophobic polyphenolic compund which is an active agent of the herb Curcuma longa (commonly known as turmeric). It has incredible properties such as anticancer, antioxidant, anti-inflammatory, hyperlipidemic, antibacterial, wound healing. Bioactivity of curcumin is provided by double bonds, diketone and phenolic hydroxyl groups in the structure. Drug release is a process where the loaded drug is released in the body by dissolution or diffusion. Not only active component of the drug but also solubility and diffusibility is important for effective drug release. Since curcumin has poor solubility in aqueous solutions, efficiency of the drug release is limited. To overcome release limitations, advanced drug delivery systems with emulsions, micelles, nanoparticles have been enhanced (Gunathilake et al. 2018). Hence, solubility and stability of curcumin can be increased to improve effectiveness of therapeutic ability (Cuomo et al. 2018).

Drug release process includes drug loading, absorption, distribution, acting periods. It is important to be aware about new drug dosage in terms of drug release and dissolution. Drug dissolution and release is intensively researched by pharmaceutical industries. Mathematical derivations which are function of drug amount are used for the quantitative drug analysis. Mathematical models can be obtained during release process. By using mathematical models, emprical results/equations can be justified and new drug delivery systems can be designed. With the mathematical model, the number of experiments is reduced, saving money and time. As a result, mathematical modeling enable researcher to development new formulations. Kinetic models define the amount of the released drug from the structure as a function of time. The objectives of mathematical models can be listed as follows:

- Deduction of appropriate drug release system via general release behaviour.
- Avoiding further experiments by obtaining drug release/diffusion rate and behavior.
- Determination of optimum conditions for release kinetic.
- Determination of drug release mechanism.
- Obtaining how the drug release rate is affected by design parameters such as size, amount, shape, composition.

2.2. Chitosan

Chitin is the second widely used polysaccharide after cellulose. About 10^{11} tones of chitin is obtained per year from insects, mollusks or crustacean shells (Kumar 2000). Chitin consist of -(1–4)-N-acetyl-d-glucosamine units. After the raw material is pretreated, chitin is obtained by applying demineralization, deproteination, deodorization, drying processes, respectively (Srinivasa and Tharanathan 2007). Deacetylation of the chitin gives chitosan which have a a copolymer of glucosamine (at least 60 % of D-glucosamine residues) and N-acetylglucosamine units. Chitosan is the preferred biopolymer due to its properties such as pH sensitivity, biodegradability, biocompability, non-toxicity, antimicrobial, antitumoral and antifungal (Xie et al. 2012; Kanimozhi et al. 2016). Chemical structure of chitin and chitosan can be seen from Figure 2.21.
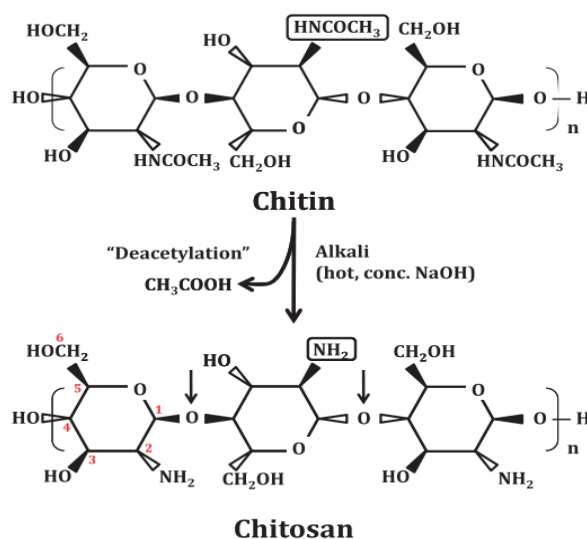
Figure 2. 21. Chemical structure of chitin and chitosan.

Chitosan has different polar functional groups such as hydroxyl (OH), primary amine (NH_2), ether (C-O-C), and residual carbonyl (C=O) groups. Due to the these functional groups, chitosan have water absorption capacity (Madeleine-Perdrillat et al. 2016). Chitosan is the cationic biopolymer since its positive charge on the amino group under acidic conditions. Chitosan is weakly basic due to the amino and hydroxyl groups

in its structure (Wan et al. 2008). Some properties of chitin and chitosan can be seen from Table 2.1. Crosslinking process is performed to improve mechanical strength and biostability of chitosan by interconnection of polymeric chains to form 3D network. Ionic and covalent crosslinking agents can be to polymerize the chitosan. While polyanions such as triphosphate, hyaluronic acid and alginate are some examples for the ionic crosslinking agent, glutaraldehyde and genipin can be given as examples for covalent crosslinking (Jayakumar et al. 2011). Crosslinking agents can be classified into two groups as toxic and non-toxic. Non-toxicity of the material makes it possible to use them as biomaterials (Miras et al. 2013; Sionkowska et al. 2014). Genipin and tripolyphosphate (TPP) crosslinked materials are less toxic than those crosslinked by glutaraldehyde, formaldehyde and epoxy compounds, hence they are generally preferred for use in biomaterials. Tripolyphosphate (TPP) can have interaction with chitosan due to its negative charge and electrostatic forces creates ionic crosslinked materials. Also, TPP has high gelling ability. Polymerization of chitosan by TPP and genipin can be seen from Figure 2.22 and Figure 2.23, respectively.
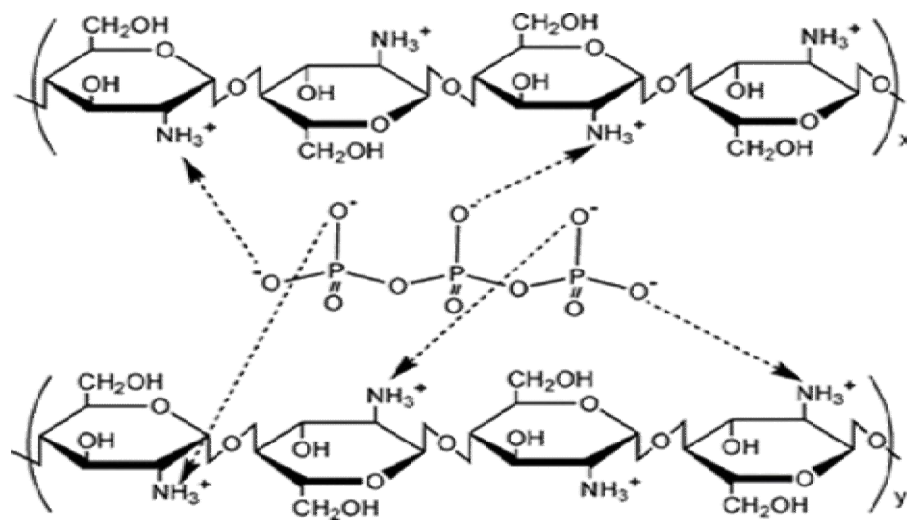
Figure 2. 22. Polymerization of chitosan with TPP.
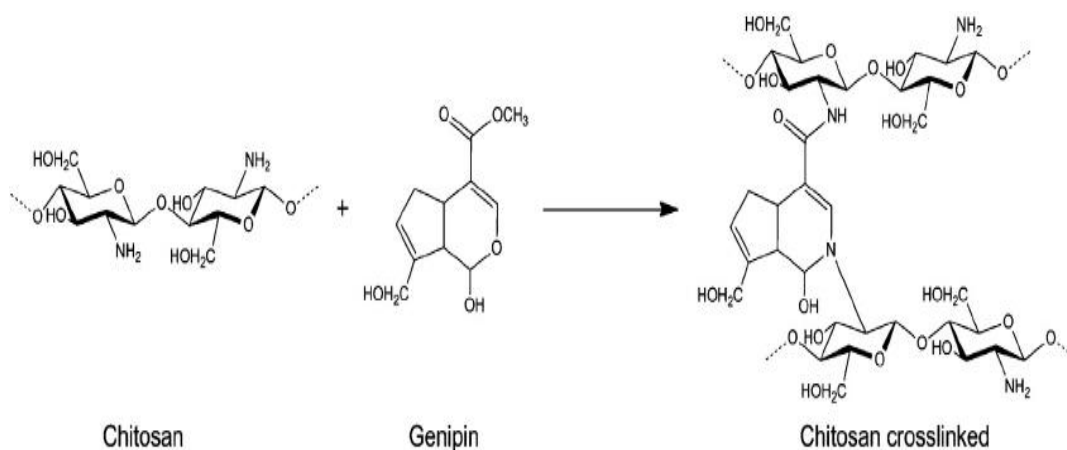
Figure 2. 23. Polymerization of chitosan with genipin.

Chemical and physical properties of chitosan can be listed as follows (Srinivasa and Tharanathan 2007; Xie et al. 2012; Croisier and Jérôme 2013);

- Natural polysaccharide with positive charge.
- Low solubility except in acidic conditions.
- Solubility of chitosan varies with pH and this property makes it available in many applications.
- All deacetylation degree, molecular weight and acetyl group distribution of chitosan have effect on solution properties.
- Chitosan can have covalent bond due to the alcohol and amino groups of the polysaccharide.
- Specific properties of the chitosan depend on the protonable amino group along D-glucosamine residues.
- Etherification and esterification reactions can occur since chitosan have alcohol functions.
- Chitosan can have interation with mucin due to its positive charge in acidic medium. Increasing deacetylation degree of chitosan gives the higher mucoadhesion since positive charges increases with deacetylation degree.
- Deaceylation degree and molecular mass of chitosan affect its degradation rate.

Table 2. 1. Some properties of chitin and chitosan

(Croisier and Jérôme 2013)

Property	Chitin	Chitosan
Molecular Weight	$(1\text{-}1.03) \times 10^6$ to 2.5×10^6	10^5 to 5×10^3
Degree of Deacetylation	$\sim 10~\%$	60-90
Viscosity of 1 % solution in 1 %, cps	-	200-2000
Moisture content		6-7
Solubility	DMAc-LiCl/TCA-MC	Dilute Acids TCA-MC

As a result of these properties, chitosan has a great application areas such as food packaging, waste treatment, cosmetics, paper industry, biotechnology, tissue engineering, drugs and pharmaceuticals (Table 2.2) (Madeleine-Perdrillat et al. 2015; El-Hefian et al. 2014). Chitosan can be treated as scaffolds, beads, membranes/sponges, films, nanofibers, microgel/nanogel, hydrogel, nanofibers and micro/nano particles (Anitha et al. 2014).

Although chitosan has many benefits due to the properties of the polymer, there is lack of tensile strength and elasticity which are the properties required for wound dressing and tissue applications. Usage of composites of chitosan and synthetic/natural polymers or development of new preperation methods can overcome the deficiencies.

Table 2. 2. Application areas of chitosan

(Source: El-Hefian, Nasef et al. 2014)

Application	Examples
Water Treatment	Filtration, removal ions, sponges, membranes, dental plaque inhibition, cholesterol reducing agent, tumor inhibition, contact lens
Medical	Controlled release of drugs, bone release of drugs, wound healing material, drug carriers, burned area treatment, drug delivery system, artificial kidneys
Cosmetics	Make-up powder, nail polish, moisturizer, bath lotion and hair treatment, face, hand and body creams, toothpaste
Paper industry	Surface treatment, photographic paper, carbonless copy paper
Biotechnology	Enzyme immobilization, protein separation, glucose electrode, chromattography
Agriculture	Seed coating, hydroponic/fertilizer
Food	Removal of dyes, solids, acids animal feed additives, color stabilization
Chemical industry	Solvent separation, permeability control

2.3. Chitosan Biofoams

An ideal wound dressing material should have some properties such as acceleration of tissue regeneration, easy application, low infection risk, high absorption capacity of wound exudate. These requirements can be provided by cationic wound dressing. Chitosan is a cationic biopolymer which is a polysaccharide obtained from chitin. Chitosan is one of the raw material used to produce biofoams since it is biodegradable, biocompatible, non-toxic, antimicrobial, antitumoral and antifungal (Jayakumar et al. 2011). Antimicrobial properties of the polymer is important to prevent the wound from infections. In addition, effectivieness of macrophages and inflammatory cells can be accelerated by chitosan. N-acetyl glucosamine which increases the re-epithelialization is produced during chitosan biodegradation. Not only

chitosan absorb wound exudates but also it increases tissue regeneration. Also, stability of drug is improved in the presence of chitosan. Interconnected porous structures with high fluid hold up capacity can be obtained by chitosan (Hu et al. 2018). In literature, chitosan biofoams are widely used as wound dressing due to its properties (Jayakumar et al. 2011; Dragostin et al. 2016). Nguyen et al. produced hydrophobic drug (curcumin) loaded chitosan/gelatin composite sponge for wound treatment applications. They used phosphate buffer solution, pH 7.4 for in vitro drug release. They were obtained improved wound healing propeties by combining gelatin and chitosan in the presence of curcumin (Nguyen et al. 2013). Karri et al. used curcumin incorpared chitosan nanoparticles in collogen scaffolds to have improved stability and solubility (Karri et al. 2016). Huang et al. compared chitosan biofoams and gelatin sponges as hemostatic wound dressing. They obtained smaller pore size, high swelling capacity by chitosan sponges. Also, blood loss is lower for chitosan biofoams than gelatin biofoams. Chitosan foams provided a faster recovery of the wound (Huang et al. 2015). Shao et al. produced chitosan/silver sulfadiazine (CS/AgSD) foams in order to enhance the biomaterial for wound dressing. They concluded that this composite can be used as antimicrobial wound healing material against E.coli, C. albicans, S. aureus and B. subtilis (Shao et al. 2017). Sankar et al. prepared chitosan biofoams using freeze drying and glutaraldehyde (as crosslinking agent). The results of the study demonstrated that chitosan foams have high absorption capacity and sterility was appropriate. Non-toxicity of chitosan foam was obtained in vivo experimets. It was concluded that produced biofoam is suitable for blood haemostasis application with good biocompability (Sankar et al. 2017).

Producing the foams with sufficient and desired mechanical properties are very important. There is some important mechanical properties of biofoams such as porosity, pore size, swelling capacity and mechanical strength for the usage of the foams in wound dressing applications (Xie et al. 2018). Characteristic features of the chitosan biofoams in terms of the mechanical and biological properties depend on deacetylation degree and molecular wieght, and on sponge production method. Nwe et al. tried to fabricate chitosan foam using both high moleular weight and low molecular weight chitosan. Freeze drying was used to fabricate porous structure. As a result, it was obtained that low molecular weight chitosan is more appropriate than high molceular weight chitosan. In addition, higher mechanical strength was achieved by low molecular weight chitosan (Nwe et al. 2009). Ikeda et al. examined effect of chitosan

concentration on mechanical strength by producing chitosan foams using freeze drying. There was similarity in pore size and structure due to changing chitosan concentration except 4 wt % chitosan. It was observed that since chitosan concentrations increase as 1 wt %, 2 wt % and 4 wt %, pore diameter decreases as 158.5 μm, 142.5 μm, 74.5 μm, respectively. The study showed that increasing chitosan concentrations formed thicker pore walls, increased homogenity and dense surface structure. Mechanical properties of the foam was increased as a result of decreasing pore size and increasing wall thickness. It was proved that mechanical properties can be improved by higher chitosan concentrations. However, when chitosan concentration was raised up to 10 wt %, the solution started to create aggregates which results in decreased porosity due to high viscosity. In addition, it was obtained that mechanical properties of the foams were affected by porosity change and, Young's modulus and tensile strength decreased with increasing porosity. In other words, when the solution concentration was increased, tensile strength was increased. Moreover, it was given that foams having larger pore size have better mechanical properties than foams with smaller pores. Desired pore sizes and pore structures can be obtained by changing and optimizing the process conditions (Ikeda et al. 2014). In literature, chitosan solution was frozen in cylindrical vessel and lyophilized to produce biofoams which have open pore structure with interconnectivity. Due to the cylindrical geometry of the vessel, pores had radial structure (Madihally and Matthew 1999). Hsieh et al. produced chitosan foams by freeze drying and examined the process parameters on the mechanical properties. It was found that the tensile stress and strain were 35 kPa and 41 %, respectively (Hsieh et al. 2007). Since mechanical strength of the biofoams are important due to be in contact with skin, compressive strength was tested and found as 54 kPa for 40 % strain (Hu et al. 2018). Li et al. applied compression test to foams which was dried by freeze dryer. For the pure chitosan, compressive strength and Young's modulus were found as 0.125 MPa and 2.6 MPa, respectively (Li et al. 2005). As a result of the studies, it can be said that chitosan foams has great option to used as a wound dressing.

Porosity is the ratio of pore volume to total volume. Porosity value can change between 0 and 1. The porosity is one of the most important property for the wound dressing since it allows required fluid and drug transfer. In literature, it was stated that material with more than 80 % porosity is suitable for wound dressing. Ikeda et al. produced chitosan foam and obtained 83 %, 80 % and 79 % porosity for the 1 wt %, 2 wt % and 4 wt % chitosan concentration, respectively. It can be clearly said that

porosity was decreased with increasing chitosan concentration and produced chitosan foams have enough porosity to achieve effective migration of the fluids (Ikeda et al. 2014). Furthermore, Shirosaki et al. produced chitosan sponges by freeze drying and the porosity of the foams found as 83 % (Shirosaki et al. 2008).

2.4. Surfactants and Emulsions

An emulsion is a mixture/colloid of two or more liquids which are immiscible in normal conditions and one liquid contains a dispersion of the other liquids. Also, emulsion can be defined as special mixture produced by two or more non-miscible liquids (López-Montilla et al. 2002). Emulsions do not have static inner structure due to being in liquid form. The dispersion medium is the medium in which the droplets are distributed throughout a liquid matrix. Different types of the emulsions can be produced such as oil in water emulsion (O/W) or water in oil emulsion (W/O). While the oil droplets are dispersed in water for an oil in water emulsion, water is dispersed in oil for a water in oil emulsion, with. Further, they can form multiple emulsions, such as water in oil in water (W/O/W) and oil in water in oil (O/W/O) (Figure 2.24).
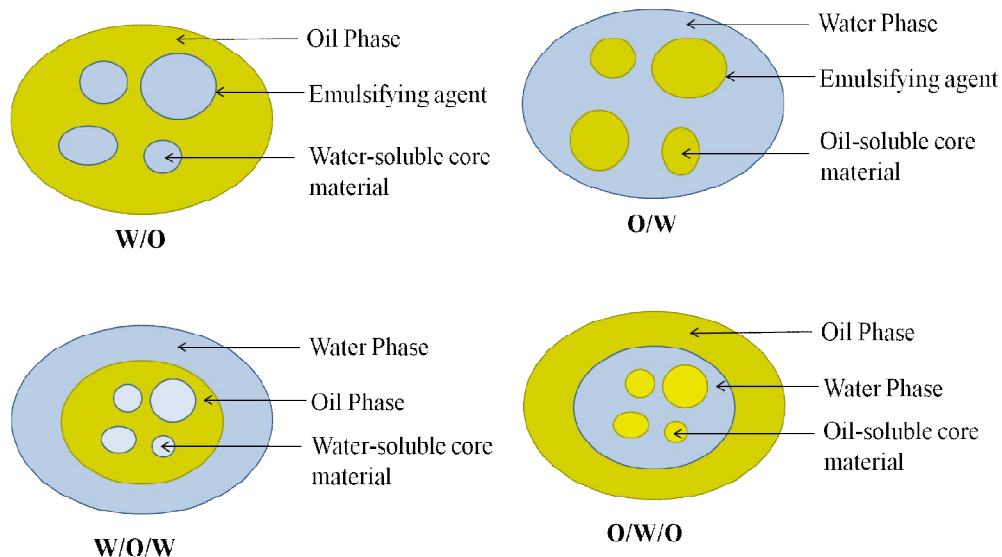
Figure 2. 24. Types of emulsion.

To have stable emulsion, mechanical force is needed to have suspended small droplets of dispersed phase in the continuous phase. In addition, the smaller the drops are desired, the more mechanical energy should be applied since work is defined as W=γΔA (ΔA: the change in the total interfacial area, γ: interfacial tension). Different devices can be used to apply the mechanical energy such as blender, homogenizer and whisk. When more mechanical energy is applied, smaller droplets and the resulting more stable emulsion are obtained. Nevertheless, although the droplets are small, phases can easily separate without using an emulsifier/emulgent which is the substance that makes emulsion stable. Emulsifiers allow molecules to have different polarity and increase the kinetic stability of a mixture. Surfactants are used as emulsifiers (Shahidzadeh et al. 1999). Emulsifier decreases the surface tension between two immiscible liquid by creating a film over one liquid and emulsification come true. It can be seen from Figure 2.27 that how the emulsifier molecules position themselves to make an oil droplet more stable.

Spontaneous Emulsions

Spontaneous emulsification can be defined as self-emulsification. Spontaneous emulsion is formed when two immiscible liquids which are not in equilibrium produce droplets in the absence of mechanical energy due to chemical potential gradients between immiscible phases. On the other hand, it can be explained as follows; required energy to increase the interface is positive and large when the immiscible liquids are in equilibrium thermodynamically. If the energy required to increase the interface is defined as γΔA (γ: the interfacial tension, ΔA: the increase in interfacial area) and energy due to the entropy change is given as TΔS (T: the absolute temperature, ΔS: the increase in entropy), total free formation energy which is ΔG=γΔA−TΔS is obtained as positive. As a result, external energy have to be applied to system for emulsification. Nevertheless, emulsion can be produced spontaneously when the immiscible liquids are not in equilibrium and emulsification free energy is negative due to chemical potential gradient between phases (Solans et al. 2016).

Surfactants are short for surface active agents which are chemicals that adsorb at surfaces or interfaces due to their structures: both hydrophilic and hydrophobic part in one molecule. In the presence of surfactants, contact area between liquid and other substance increases since surface active agents decreases the surface tension of liquid by creating film. The main idea of the work of surfactants is adsorption. Surfactants have two parts which are hydrophilic (water-liking) and hydrophobic (water-disliking)

(Figure 2.25). The hydrophobic part (nonpolar carbon chain) is formed by long carbon chain and hydrophilic head (polar head group) has ionic or polar structure. In a reverse micelle, while hydrophilic part creates the core of a micelle, hydrophobic part forms the outer shell.
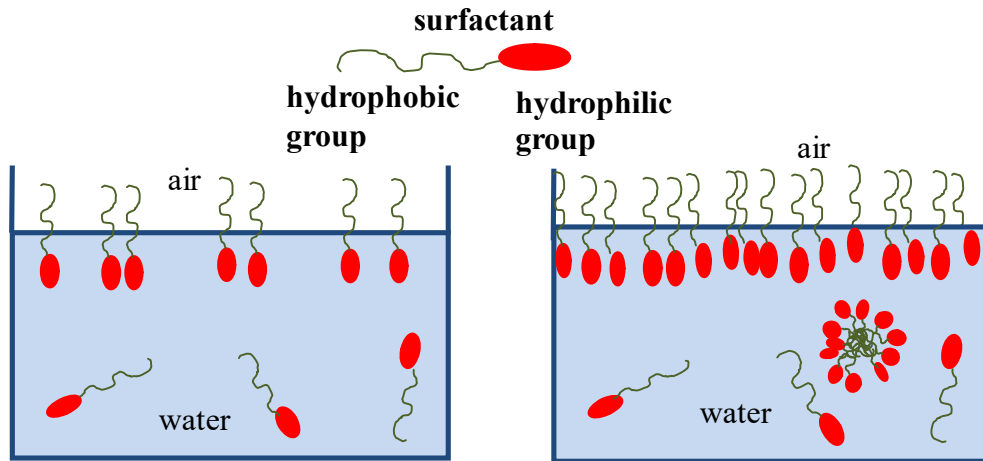
Figure 2. 25. Surfactants in bulk and surface.

Several types and combination of hydrophobic and hydrophilic parts give many different surfacant type. According to their hydrophilic head group, they can be classified into four main types: anionic, cationic, nonionic and zwitterionic (Möbius et al. 2001). The anionic surfactants have hydrophilic parts with negative charged while the cationic surfactants have positive charged group. On the other hand, the surface-active portion in the nonionic surfactants have no ionic charge while zwitterionic surfactants possess both positive and negative charged head groups. Schematic form of surfactant structure can be seen from Figure 2.26.
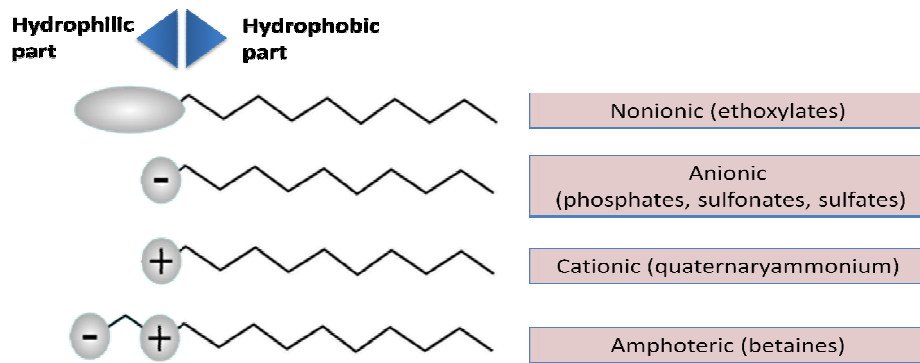
Figure 2. 26. Schematic form of surfactant structure.

The critical micelle concentration (CMC) is the concentration where surfactants start to aggregate to form micelles. Core-shell micelle structure is formed due to the association of hydrophobic parts of block copolymers to reduce the contact area with water. At low surfactant concentration, surface tension has the highest value. When surfactants are added to solution, surface tension starts to fall down and decreases down to the critical micelle concentration. At this point surface is full of surfactant. If surfactants are added after this point, surfactants start to aggregate to form micelles and the surface tension remain constant because there is no change at the surface. Due to these properties surfactants are widely used as emulsifier. The structure of surfactants as an emulsifier and micelles can be seen from Figure 2.27.
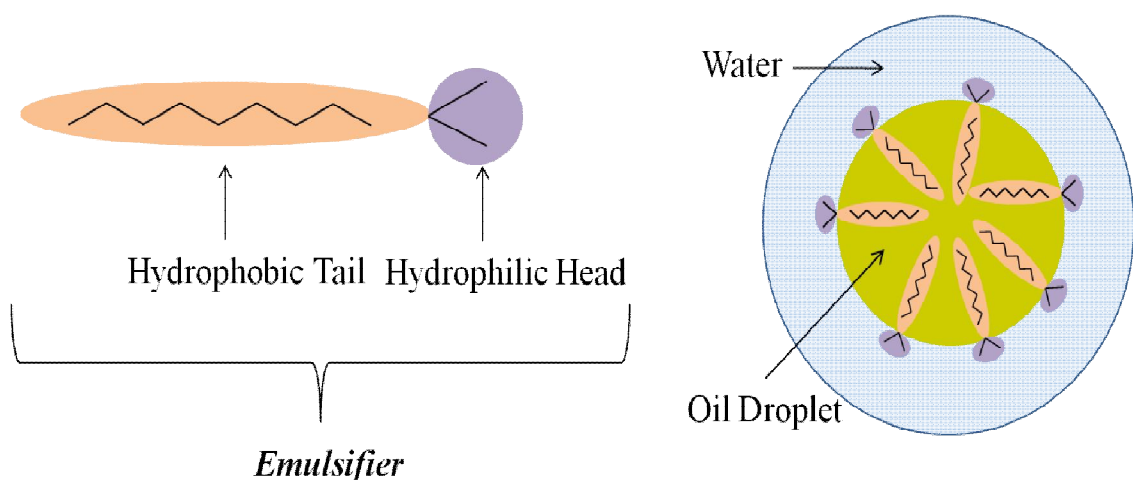
Figure 2. 27. Surfactant as a emulsifier in oil/water emulsions.

When amphiphilic block copolymers come together spontaneously above their critical micelle concentration in aqueous solution, polymeric micelles which have hydrophobic and hydrophilic blocks with core-shell nanostructure are formed. Most of the micelles have spherical structure with hydrophobic core and hydrophilic corona. Hydrodynamic diameter of the spherical micelles changes between 20 nm and 80 nm (Petrov et al. 2008). Hydrophobic drugs which are poorly water-soluble have some problems such as aggregation, low bioavailability and low absorption during pharmaceutical applications. Polymeric micelles are widely used to overcome the dissolution problem in drug studies. While the outer shell of the hydrophilic part conserves the drug from water, hydrophobic drug stays in the inner hydrophobic core and as a result effciency of the drug increases (Figure 2.28) (Kedar et al. 2010). Hydrophobic parts of the polymers have hydrophobic interaction in the inner core of the micelles. Due to this property polymeric micelles are most preferred subtance to make hydrophobic drugs soluble in water. There are two types of the block copolymers as diblock and triblock copolymers. Diblock copolymer can be shown as X-Y (X: hydrophilic block and Y: hydrophobic block). Triblock copolymers have two different types which are produced from two type polymers, XYX and three type polymer, XYZ. Both X-Y and X-Y-X type block copolymers are widely used as drug carrier since the properties of micelles and polymers are similar to this types copolymers. There are some properties which should be supplied by block copolymers used in drug delivery systems. For instance, they should be formed spontaneously in water, high drug solubility and loading effciency, and be nontoxic and biocompatible. Pluronics; Most of the time, polypropylene oxide (PPO), polyesters; polylactic acid (PLA), hydrophobic polyamino acids, lactic acid copolymers, glycolic acid and polycaprolactone (PCL) are used as micelles in drug delivery applications (Xu et al. 2013). Pluronic block copolymer, PEO-PPO-PEO, is one of the triblock copolymer formed by poly (ethylene oxide) (PEO) and poly (propylene oxide) (PPO) which are hydrophilic and hydrophobic, respectively. Pluronic P123 (PEO20- PPO70-PEO20) compose of average 40 PEO and 70 PPO repeat units. This copolymer ensures high drug loading efficieny, since it has high hydrophobic block. Hydrophobic PPO parts encapsulate the hydrophobic drug by forming micelles in aqueous solution and hydrophilic PEO block make the micelles stable in the medium (Su et al. 2016).
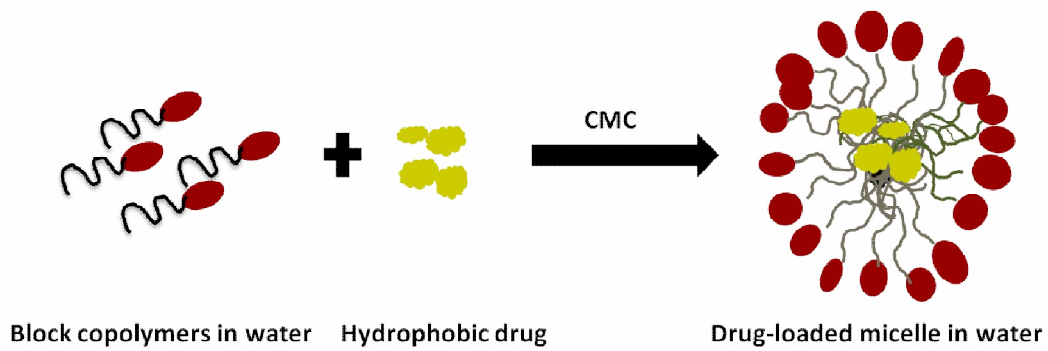
Figure 2. 28. Hydrophobic drug inside block copolymer.

Su et al. prepeared polymeric micelles by Pluronic P-123 and curcumin to enhance the solubility and bioavailability of curcumin. Thin-film evoparation technique was used to form the P-123-curcumin micelles. Drug release of curcumin from P-123-curcumin micelles was observed as 6 %, 30 % and 75 % within 3 h, 12 h and 48 h, respectively. This release mechanism can be explained by the the rapid desorption of a small amount of curcumin absorbed in the micelle surface or in the hydrophilic layer coated by the force of van der Waals. Swelling or erosion of biopolymer can be a reason for slow drug release (Su et al. 2016).

CHAPTER 3

MATERIALS AND METHODS

This chapter gives the properties of materials used in this study and summarizes the experimental methods for chitosan biofoam production and characterization. The methodology of the synthesis methods is given in the following paragraphs.

3.1. Materials

Low molecular weight chitosan was used as a raw material to produce biofoam due to the favored properties such as biodegradable, good biocompatible, high adhesion ability, pH stability in wide range. In some studies, high molecular weight chitosan was also used to form biofoams to observe the effect of molecular weight on the synthesis. Sodium tripolyphosphate (TPP) and anionic surfactants such as sodium dodecyl sulfate (SDS), octadecyl sulfate sodium salt and mono-N-dodecyl phosphate were used as crosslinking agents. Pentane, hexane and heptane were used as oil phases for emulsions. Pentane is the most volatile component among them. Normal boiling and melting points of pentane are 36 ^{o}C and -139 ^{o}C, respectively. Hexane is a highly volatile substance whose normal boiling and melting points are 67-69 ^{o}C and -94 ^{o}C, respectively. n-Hexane is well known for its high hydrophobicity and low bioavailability (Cheng et al. 2016). Properties of pentane and hexane are very similar. Normal boiling point and melting points of heptane are 98 ^{o}C and -90.59 ^{o}C, respectively. Heptane does not have the environmental and health concerns that are associated with hexane hence because of the similarity of the oils, heptane can be an alternative oil. Vancomycin was selected as model hydrophilic antibiotic which is used to treat infections. Curcumin and Amphotericin-B as model hydrophobic drugs were used. Amphotericin-B treats fungal infections. Curcumin is antioxidant, anticancer, anti-inflammatory and antibacterial drug. A polymeric surfactant, P-123 (Polyethylene glycol-block-polypropylene glycol-block-polyethylene glycol) was used to form micelles and enclose the hydrophobic drugs. In addition, nonionic surfactants, TX-100, Tween 20 and Tween 80 were used to

form smaller sized O/W emulsions and to make curcumin (hydrophobic surfactant) soluble. Properties of selected materials can be seen from Table 3.1.

Table 3. 1. Used chemicals and their properties

Name	MW (g/mol)	Explanation	Chemical structure
Chitosan-Low Molecular Weight CS	50000-190000 Da	Raw material for foam *77% DA chitosan was used.*	
Chitosan-High Molecular Weight, CS	310000-375000 Da	Raw material for foam	
Sodium Dodecyl Sulfate SDS $NaC_{12}H_{25}SO_4$	288	Anionic surfactant	$CH_3(CH_2)_{10}CH_2O-\overset{O}{\underset{O}{\overset{\|}{\underset{\|}{S}}}}-ONa$
Octadecyl Sulfate Sodium Salt $CH_3(CH_2)_{17}OSO_3Na$	372	Anionic Surfactant	$CH_3(CH_2)_{16}CH_2-O-\overset{O}{\underset{O}{\overset{\|}{\underset{\|}{S}}}}-ONa$
Mono-N-Dodecyl Phosphate $C_{12}H_{27}O_4P$	266	Anionic Surfactant	
Sodium tripolyphosphate TPP $Na_5P_3O_{10}$	368	Crosslinking agent	
Vancomycin $C_{66}H_{75}Cl_2N_9O_{24}.HCl$	1485.73	Hydrophilic Drug *An antibiotic used to treat infections*	
Curcumin $C_{21}H_{20}O_6$	378.38	Hydrophobic Drug *Antioxidant, anticancer, antibacterial drug*	
Amphotericin-B $C_{47}H_{73}NO_{17}$	924.08	Hydrophobic Drug *Treat possibly fungal infections*	
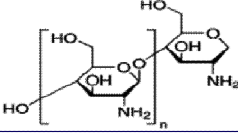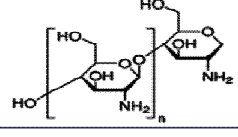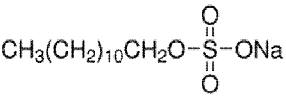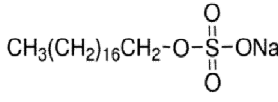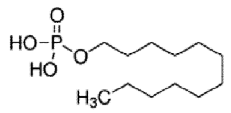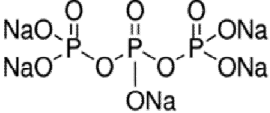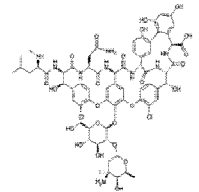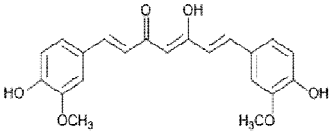
(cont. on next page)

36
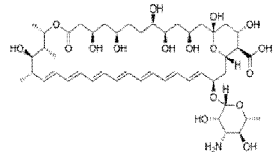
Table 3.1. (cont.)

Name	MW (g/mol)	Explanation	Chemical structure
Poly(ethylene glycol)-block-poly(propylene glycol)-block-poly(ethylene glycol) P-123 $(C_3H_6O.C_2H_4O)x$	5800	Polymeric surfactant	
Hexadecyl Trimethyl-Ammonium Bromide CTAB $C_{19}H_{42}BrN$	364	Simple, cationic surfactant	
Octylphenol Ethoxylate, Triton X-100 TX-100 $C_{14}H_{22}O(C_2H_4O)_n(_{n=9-10})$	625	Nonionic surfactant	
Polysorbate 20 Tween-20 $C_{58}H_{114}O_{26}$	1227.54	Nonionic surfactant	
Polysorbate 80 Tween-80 $C_{64}H_{124}O_{26}$	1310	Nonionic surfactant	
Pentane C_5H_{12}	72.15	Oil *Highly volatile, hydrophobic, low bioavailability* *B.P: 36 ^{0}C , M.P: -139 ^{0}C*	
Hexane C_6H_{14}	86.18	Oil *Highly volatile, hydrophobic, low bioavailability* *B.P: 67 ^{0}C , M.P: -94 ^{0}C*	
Heptane C_7H_{16}	100.21	*Oil* *B.P: 98 ^{0}C , M.P: -90 ^{0}C* *Does not have the environmental and health concerns*	

3.2. Experimental Methods

As mentioned above, although there are some studies in literature using liquid templated method, it looks like there is not much success to obtain chitosan foams with desired structures and properties. Also, there is no detailed study on drug release through kinetic models and optimization of the foam structure for best drug loading/release. First of all, methods were developed and parameters were studied in detail for the foam production. Interaction of molecules in the foam production system was examined to clarify drug release behaviours. The flow sheets of the liquid templated methods applied in this study are given in the following paragraphs.

3.2.1. Foam Production

First, the O/W emulsion templated method in the absence of surfactant was used to produce foams using ultrasonic probe (Bandelin Sonopuls, HD 3200). Four different chitosan concentrations (1-4 %) and five different oil phases concentrations (5, 10, 15, 17, 20 volume %) were studied for synthesis. Hexane and heptane were the oil phases and sodium tripolyphosphate (TPP) was the crosslinking agent. Freeze drying (LABCONCO Freeze Dryer) was applied to all samples to remove volatile components which creates pores. Operation condition for freeze dryer was 0.016 mBar and -52 $^{\text{o}}$C. Then the characterization of foams were conducted by SEM analysis and mechanical tests (Figure 3.1).

Then, the same O/W emulsion templated method was used in presence of surfactants to produce foams using ultrasonic probe (Figure 3.1). The surfactants used were: 1) a nonionic polymeric surfactant, P-123, 2) a cationic surfactant, CTAB, 3) an anionic surfactant, SDS and 4) a nonionic simple surfactant, TX-100. Two different chitosan concentrations (2 % and 4 %) were used. In addition, 15 volume % hexane as an oil phase was selected. Biofoams produced were analyzed by SEM and mechanical tests.
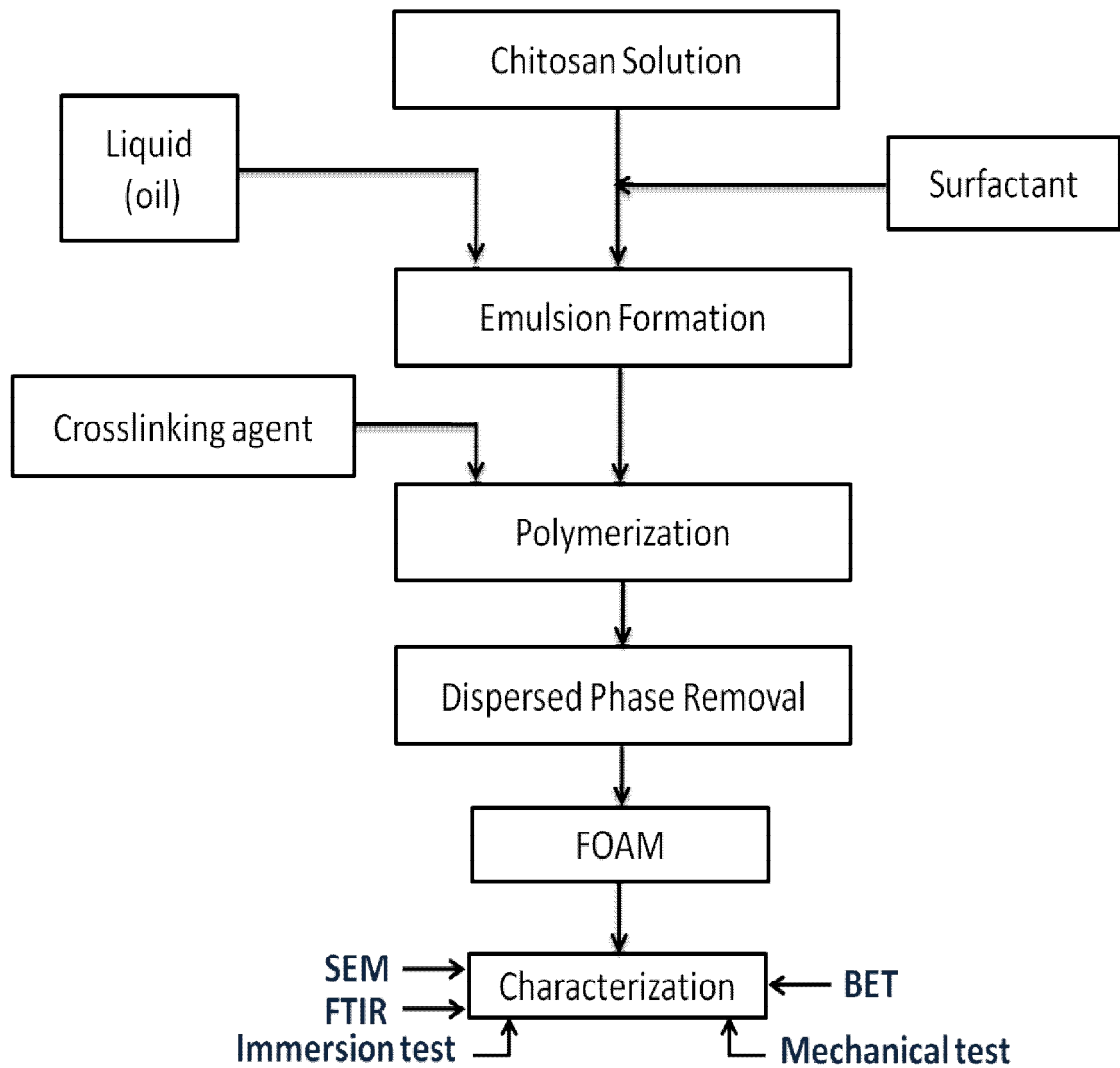
Figure 3. 1. O/W emulsion templated method.

Figure 3.2 gives the flowsheet of liquid templated method when emulsion is produced spontaneously. In this case two types of surfactants were used to freeze the oil droplets. One in oil phase (Span 80), the other is water phase (Tween 20). The concentrations of these surfactants were 10^{-2} M. In this case, it was possible to measure size of emulsion droplets by DLS.
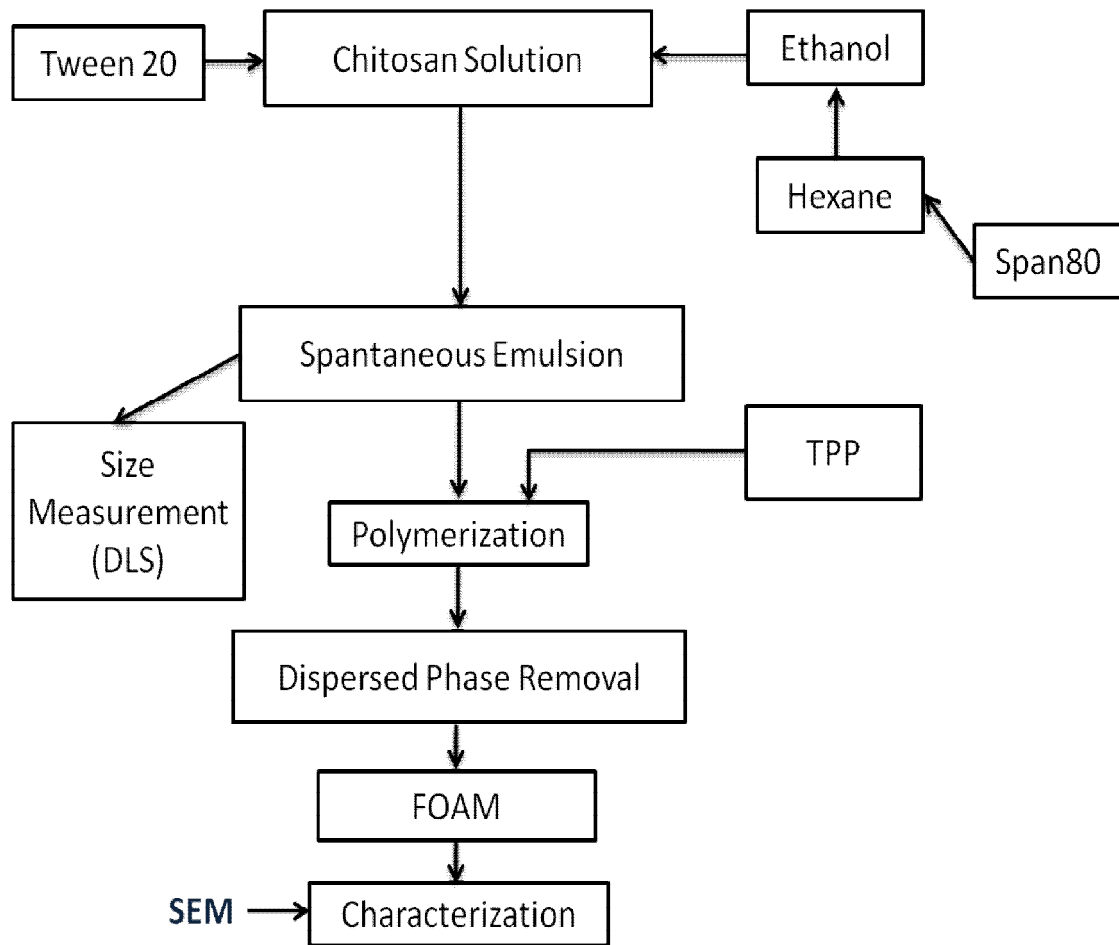
Figure 3. 2. O/W spontaneous emulsion templated method.

Moreover, high molecular weight chitosan (HMW chitosan) was also used to produce foams (Figure 3.1) in the absence of surfactants to see effect of molecular weight. However, in this case, high concentrations could not be studied due to the higher viscosities chitosan solution for the similar conditions of low molecular weight (such as acetic acid ratio etc.). Hence, 1 % HMW chitosan was used to be able to produce biofoams at different hexane concentrations (10, 15, 17 volume %).

In addition, SDS was used as a crosslinking agent because of its negative charge like TPP (Figure 3.1). The effect of SDS was tested at different concentrations (10^{-2} and 10^{-3} M) with different oil phases (pentane, hexane and heptane). Freeze drying was applied to all samples to remove volatile components which creates pores. In addition, the following testes were conducted: 1) the type and concentration of oil phase, 2) similar type anionic surfactant. Foams were characterized by SEM, mechanical test, FTIR and BET. In addition to sodium dodecyl sulfate, octadecyl sulfatesodium salt and

mono-N-dodecyl phosphate were used as an anionic crosslinking agent. In this period of the study, concentrations of chitosan and hexane were set as 4 % and 15 %, respectively. As before, freeze drying was applied to all samples to remove volatile components. Produced foams were characterized by SEM.

3.2.2. Porosity and Water Release Behavior of the Chitosan Foams

To determine hold-up capacity of the foams produced, water immerse tests were applied to calculate the amount of water that hold-up in biofoam and releasing behavior of water with time can be determined. Foams were produced by o/w emulsion templated method which is given in Figure 3.1 (in the absence of surfactants). Hexane was used as an oil phase. Foams were crosslinked by SDS. The effect of chitosan (2-4 %) and oil phase (15 and 25 %) concentrations on the release behaviour were studied. First, all the samples were dried at 50 $^{\circ}$C in oven and weighed. Then, they kept in ultrapure water at 25 $^{\circ}$C and weighed as a function of time again after removed from water.

The porosity of the foams were calculated using results of immerse test and the effect of chitosan/oil phase concentrations on the porosity were determined. First, the dimensions of the foams were measured and weighted after dried. The details of the calculations are as follows. Air volume was calculated by using Equaiton 3.1. Porosity (Φ) of the foams were calculated by using foam volume and air volume (Equation 3.2). Chitosan density was used as 0.8 g/cm^3 as mentioned in literature (Lin et al. 2005).

$$V_{air} = \frac{V_{total}*\rho_{chitosan} - M_{total}}{\rho_{chitosan} - \rho_{air}} \tag{3.1}$$

$$\Phi = \frac{V_{air}}{V_{total}} \tag{3.2}$$

where V_{air} is the volume of the air, M_{total} is the total mass of the foam, V_{total} is the total volume of the foam, $\rho_{chitosan}$ is density of chitosan and ρ_{air} is the density of air.

3.2.3. Production of Drug-Loaded Chitosan Biofoams

In this part of the study, the production of chitosan foams were done in the presence of a model hydrophilic drug, Vancomycin Hydrochloride, and a model hydrophobic drug Curcumin to see the effect of drug type on foam structure. In these studies, an ultrasonic probe was used to produce oil/water type of emulsions to use as templates. Both TPP and SDS (due to its negative charge) were used as crosslinking agents. The chitosan concentration was fixed as 2 % to decrease the risk of dissolution problems. As before, freeze drying was applied to all samples to remove volatile components which creates pores. Foams produced were characterized by SEM.

3.2.3.1. Hydrophilic Drug-Loaded Chitosan Biofoams

In this part of the study, the production of chitosan foams were done in the presence of a model hydrophilic drug, Vancomycin Hydrochloride. In the first method, vancomycin hydrochloride, was dissolved in chitosan solution and O/W emulsion was produced using hexane. The amount of Vancomycin used was 3 mg/mL. Two different chitosan concentrations (2 % and 4 %) were studied. Oil (hexane) concentration was selected as 15 %. Both SDS (10^{-2} M) and TPP (2 % and 4 %) were selected as crosslinking agent. The flow sheet of the method applied is presented in Figure 3.3. SEM and FTIR analyses were done on the foams.
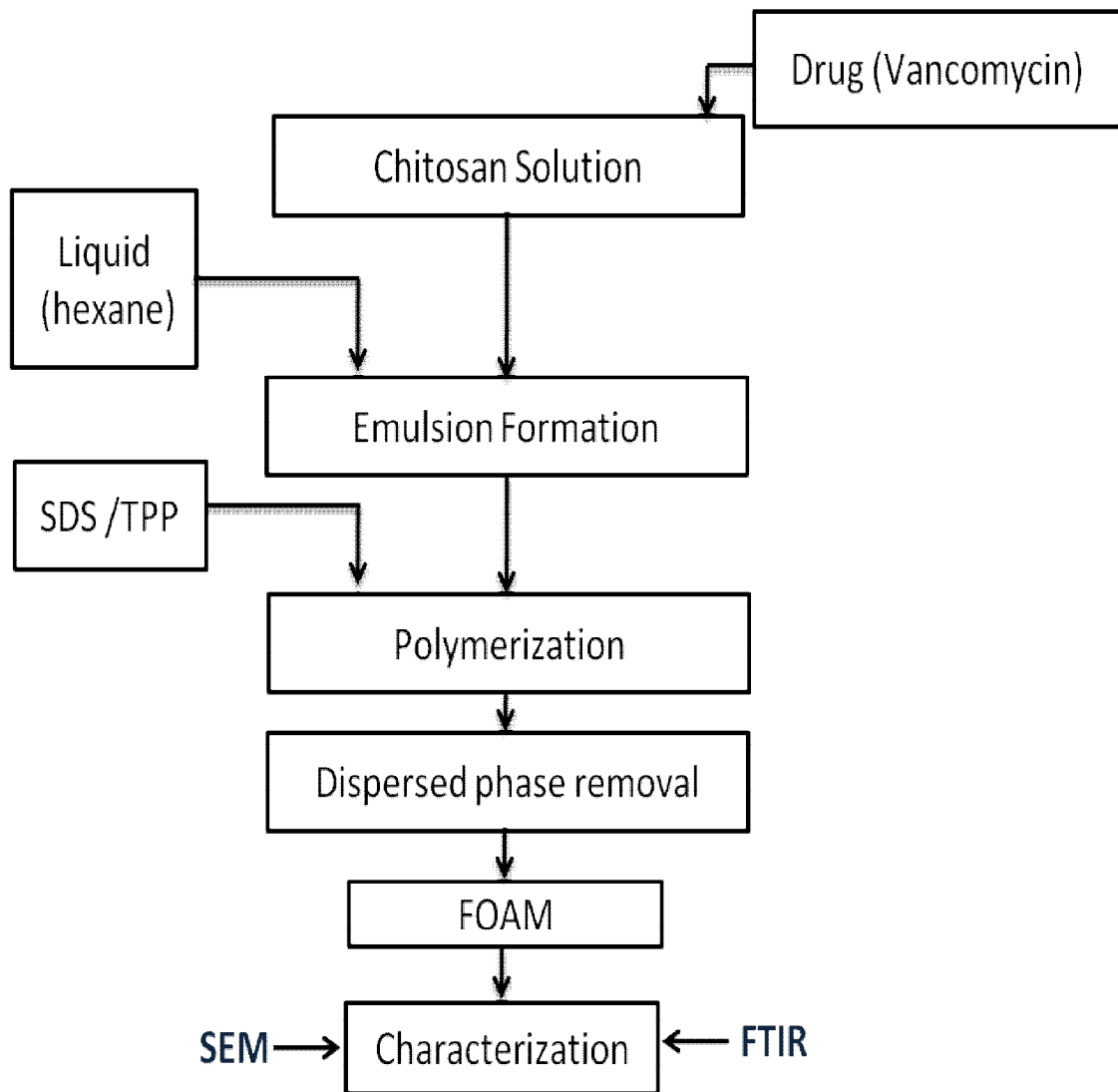
Figure 3. 3. Production of vancomycin-loaded chitosan biofoam production by O/W emulsion templated method.

In another emulsion templated method to produce vancomycin loaded chitosan foams, the foams were immersed in drug solution to load foams. Chitosan concentration was selected as 2 % while hexane concentration was used as 15 %. SDS (10^{-2} M) was used as a crosslinking agent. The flow sheet of the method designed is presented in Figure 3.4.
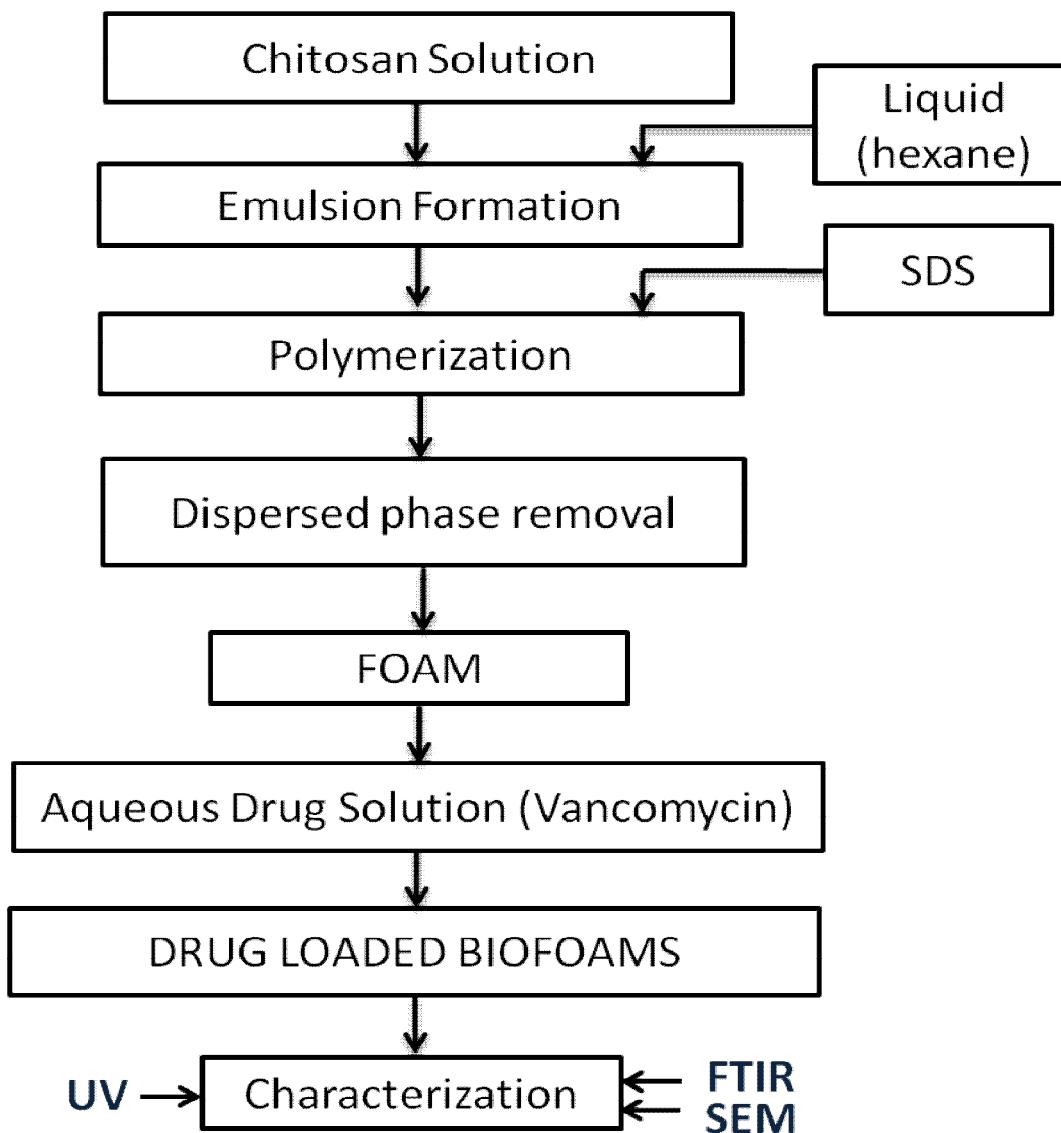
Figure 3. 4. Production of chitosan biofoam by O/W emulsion templated method and drug loading of the foam by immersion in drug.

3.2.3.2. Hydrophobic Drug-Loaded Chitosan Biofoams

Amphotericin-B and Curcumin were chosen as model hydrophobic drugs for this part of the study. The chitosan concentration was fixed as 2 % to reduce the risk of dissolution problems. Different drug loading methods were applied to produce chitosan foams to achive the most effective drug release. The first method was the thin film evaporation method coupled with O/W emulsion template method in which the hydrophobic drug was enveloped in P-123 micelles (10^{-3} M). Chitosan was crosslinked

by SDS to produce Amphotericin-B loaded foams. SDS and TPP were both used as crosslinking agent to produce curcumin loaded foams. SEM analysis was done on the foams. The flowsheet of the methods designed is presented in Figure 3.5 for Amphotericin-B and Curcumin.
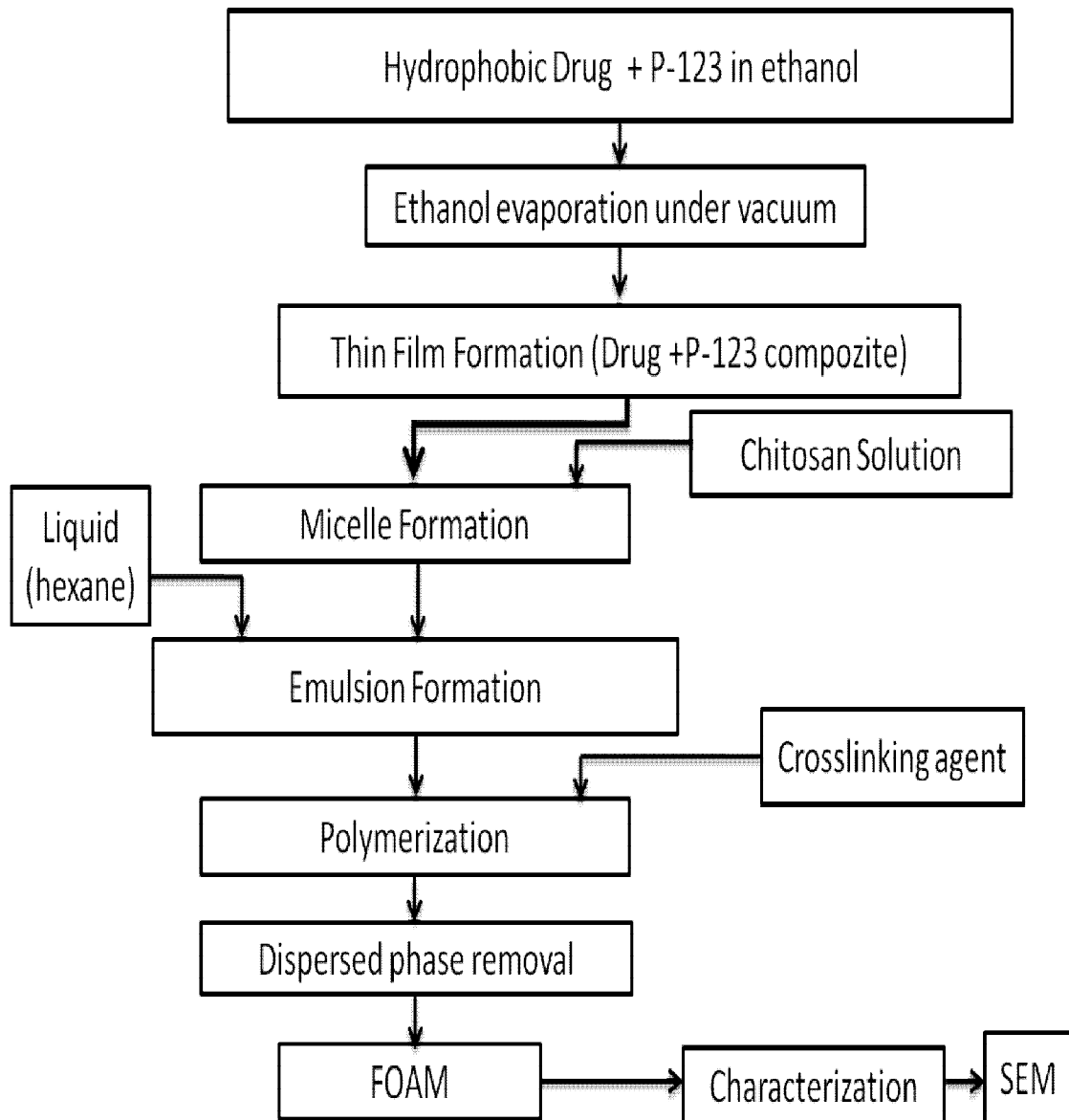
Figure 3. 5. Hydrophobic drug-loaded chitosan biofoam production by thin film formation coupled with O/W emulsion templated method.

In the second method used, curcumin was dissolved in water by using different nonionic surfactants (TX-100, Tween 20 and Tween 80). Then curcumin solution was mixed with chitosan solution. TPP was used as crosslinking agent (Figure 3.6).

```
┌──────────────────┐   ┌────────────────────────────────────────┐
│ Chitosan Solution │   │ Drug (Curcumin)+ TX-100/ Tween 20/ Tween 80 │
└──────────────────┘   └────────────────────────────────────────┘
         │                              │
         ▼                              ▼
      ┌─────────────────────────────────────┐
      │    Chitosan Solution within Curcumin │
      └─────────────────────────────────────┘
  ┌──────────┐            │
  │ Liquid   │─────┐      │
  │ (hexane) │     │      │
  └──────────┘     ▼      ▼
              ┌─────────────────────┐
              │  Emulsion Formation │
              └─────────────────────┘
  ┌──────────┐        │
  │   TPP    │────┐   │
  └──────────┘    ▼   ▼
              ┌─────────────────────┐
              │    Polymerization   │
              └─────────────────────┘
                       │
                       ▼
              ┌─────────────────────┐
              │ Dispersed phase removal │
              └─────────────────────┘
                       │
                       ▼
              ┌─────────────────────┐
              │        FOAM         │
              └─────────────────────┘
                       │
                       ▼
              ┌─────────────────────┐
              │   Characterization  │──▶ SEM
              └─────────────────────┘
```
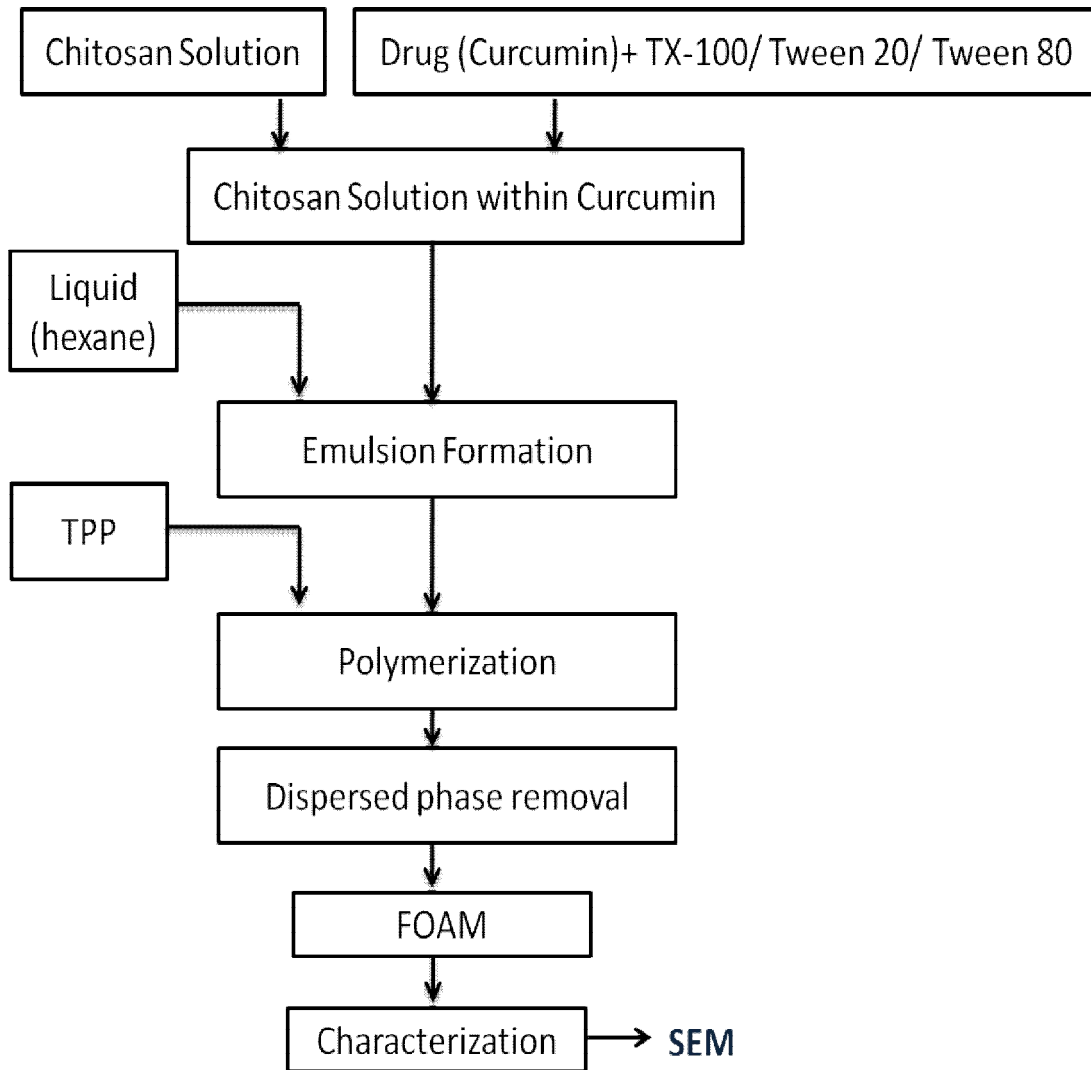
Figure 3. 6. Drug loaded chitosan biofoam production by O/W emulsion templated method (nonionic surfactants to make hydrophobic drug soluble).

3.2.4. Examination of Interaction of Molecules in the Foam Production System

While different production methods were applied, the interactions between molecules were studied in detailed to clarify the release behavior. Size measurement were applied to P-123 micelles in water, P-123 micelles in water in the presence of chitosan molecules, P-123 micelles in chitosan solutions, P-123 micelles with drug curcumin and curcumin molecules in ethanol. Charge measurements were applied to P-123 micelles to characterize the surfactant molecules. Also, FTIR analyses were applied to these molecules.

3.2.5. Drug Release from Chitosan Biofoams

In drug release part of the study, all chitosan foams were produced (clarified in previous section) in the presence of a model hydrophilic drug and in the presence of a model hydrophobic drug with various chitosan and drug concentrations used for release studies. First of all, calibration curves for vancomycin and curcumine (both in ethanol and in P-123 micelles) were obtained to determine the amount of the drug released (Figure 3.7 and Figure 3.8). The release of drug from drug-loaded chitosan biofoams were evaluated using phosphate buffer at pH 5.6 and pH 8.2. Phosphate buffer was prepared by using dipotasyumfosfat (K_2HPO_4) and mono potasyumfosfat (KH_2PO_4). Molarities of K_2HPO_4 and KH_2PO_4 are 0.0058 M and 0.0942 M, respectively, for pH 5.6. Moreover, Molarities of K_2HPO_4 and KH_2PO_4 are 0.0935 M and 0.0065 M, respectively, for pH 8.2. The release study was carried out at 37 ºC applying a shaking and at the time intervals of 0.2, 1, 3, 6, 24 and 48 hours, the sampling was performed. All samples (supernatants) were examined by UV-spectrophotometer and calibration curve to determine the quantity of releasing drug. Characteristic peaks of vancomycin and curcumin are 281 nm and 425 nm, resprectively. The flowsheets of the methods designed for release studies are presented in Figure 3.9 and Figure 3.10 for Vancomycin and Curcumin, respectively.

The amount of drug release is calculated by the given relationship:

Release % = Released Drug/Total Drug x 100
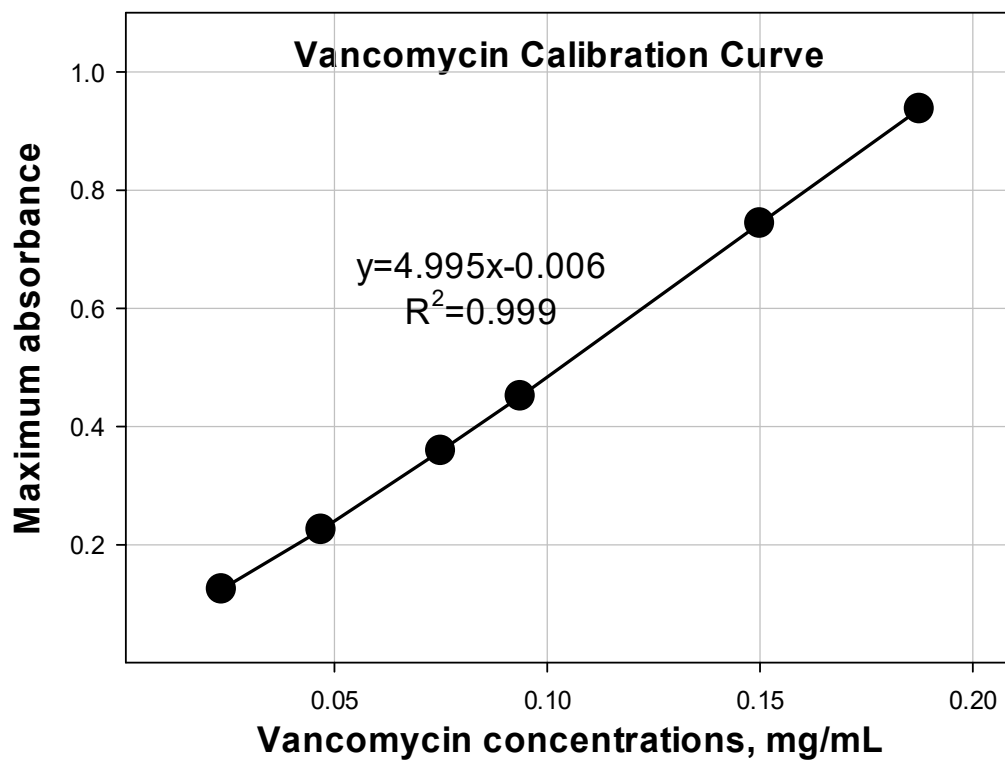
Figure 3. 7. Calibration curve for vancomycin.
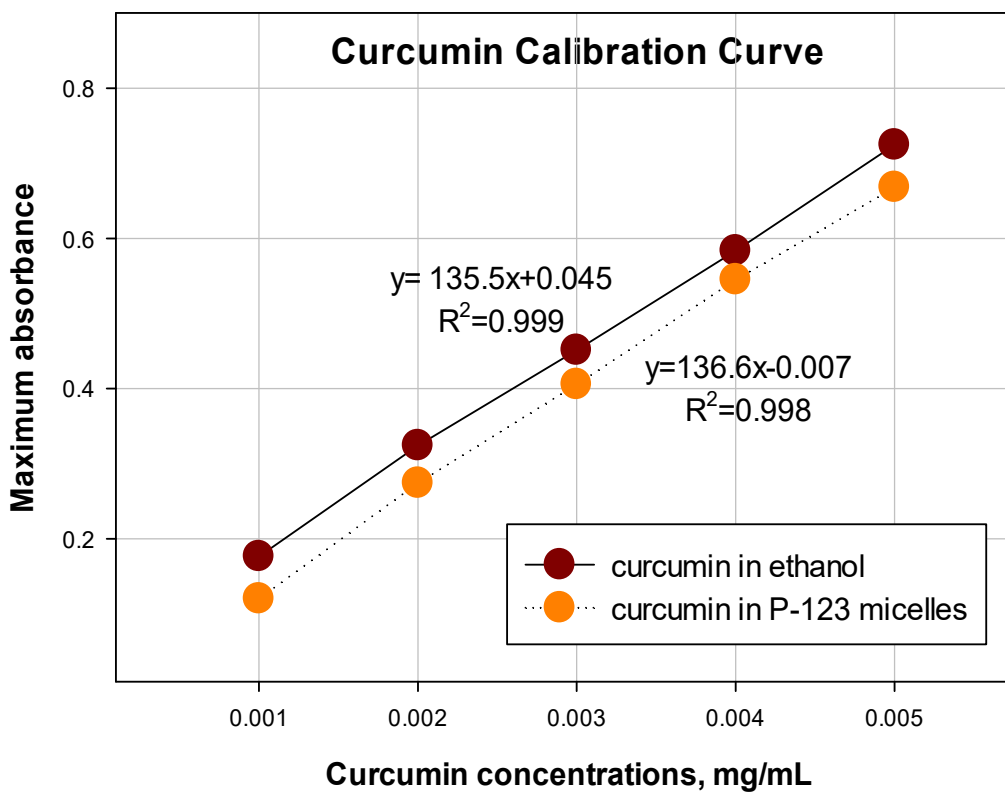
Figure 3. 8. Calibration curve for curcumin.
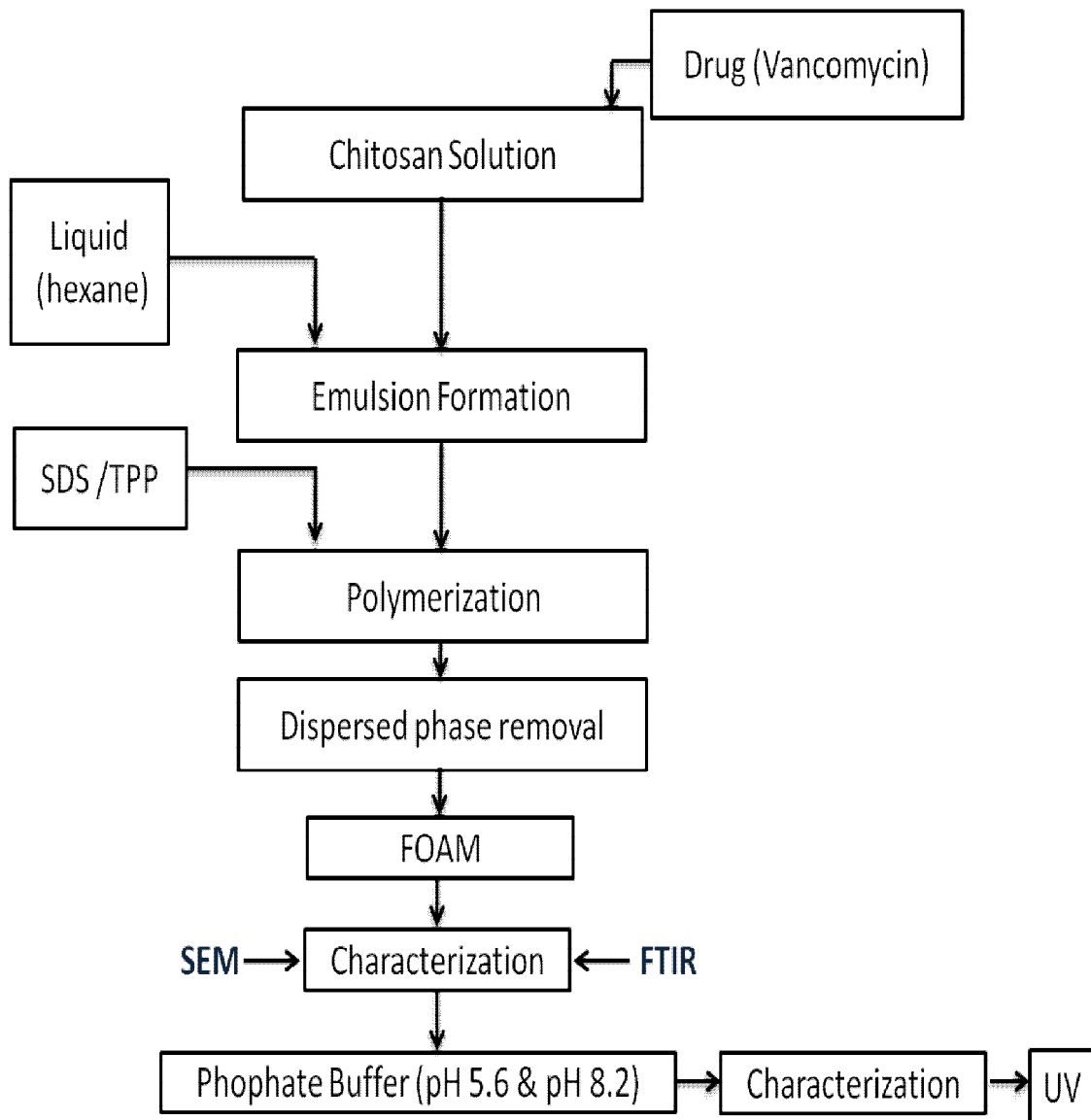
Figure 3. 9. Hydrophilic drug release from chitosan foams.
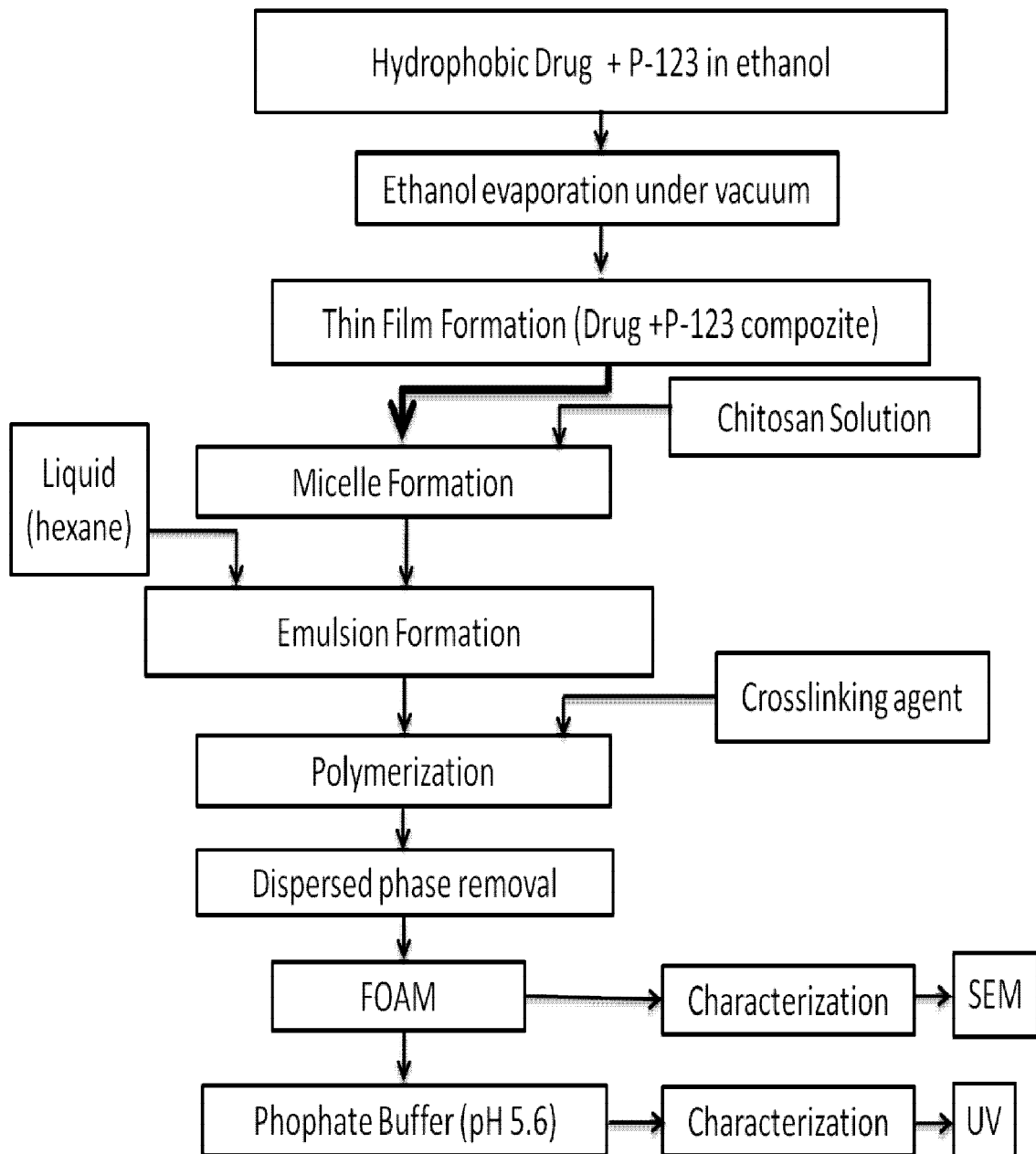
Figure 3. 10. Hydrophobic drug release from chitosan foams.

3.2.6. Application of Kinetic Models

In this part, mathematical models were used to describe the drug release mechanisms for drug-loaded biofoams. First order, Second order, Higuchi and Korsmeyer–Peppas models were applied.

First Order Kinetic Model:

First Order Kinetic Model clears up the absorption of the drugs release. The drug release can be given by the equation given below when described by first order kinetic model:

$$\ln(m_0 - m_t) = \ln(m_0) - k_1 t$$

where t is the time, m_0 is the amount of the drug in the structure, m_t is the released drug amount with time t, and k_1 is the first-order release rate constant (Wójcik-Pastuszka et al. 2019). The plot can be obtained by using remaining drug with time. This model is suitable to examine the water soluble drug in porous structures (Shaikh et al. 2015).

Second Order Kinetic Model:

In the second-order kinetics, the rate depends as a second power of drug concentration. The second-order kinetics model is given as:

$$1/(m_0 - m_t) = 1/m_0 + k_2 t$$

where m_t shows the released drug amount with time t, m_0 is the amount of the drug in the formulation before dissolution and k_2 is the second-order rate constant (Wójcik-Pastuszka et al. 2019).

Higuchi Model:

Higuchi Model is most widely used mathematical description for drug release of water soluble or low soluble drugs in solids. This model is often applicable to the different structures and porous system. The Higuchi model is as follows;

$$m_t = k_H t^{0.5}$$

where k_H is the Higuchi rate constant, m_t is the released drug amount with time t (Wójcik-Pastuszka et al. 2019). This model was studied for several drug dosages and for water soluble drugs (Shaikh et al. 2015).

Assumptions for this model are given as (Siepmann and Peppas 2011);
a. Diffusion of the drug is one dimensional.
b. Diffusivity of the drug is constant.
c. Dissolution of matrix is negligible.
d. Sufficient amount of drug which is higher than solubility is presentd.

Korsemeyer-Peppas Model:

Korsemeyer-Peppas Model describes the release of drug from a polymeric system. The Korsmeyer-Peppas model is as follows;

$$\log(\frac{m_t}{m_\infty})=\log(k_{K-P})+n\log(t)$$

where m_∞ is the mass of the released drug after an infinitive time (in this research after 24 h), k_{K-P} is the Korsmeyer-Peppas rate constant, and n is the drug release parameter (Table 3.2) (Wójcik-Pastuszka et al. 2019). It should be underlined that the data we have been fitting to the model refer to the diffusion through low retention/high retention barriers.

The following assumptions were made for this model;

a. Drug release is one dimensional.
b. The ratio of the lenth to thickness should be equal or higher than 10.

Table 3. 2. Drug release parameter the Peppas equation and drug release mechanism (Siepmann and Siepmann 2008)

Exponent, n			Drug Release Mechanism
Thin film	Cylinder	Sphere	
0.5	0.45	0.43	Fickian diffusion
$0.5 < n < 1.0$	$0.45 < n < 0.89$	$0.43 < n < 0.85$	Anomalous transport on non Fickian transport
1.0	0.89	0.85	Polymer swelling

3.3. Characterization

Scanning electron microscope (SEM), Transmission electron microscope (TEM), Scanning transmission electron microscopy (STEM) and Atomic force microscope (AFM) analyses were used for morphological characterization of foams produced. Fourier transform infrared (FTIR) spectroscopy was used for chemical characterization and to examine the interactions between molecules present in the foams. Size measurements of P-123 micelles in water, P-123 micelles in water in the presence of chitosan molecules, P-123 micelles in chitosan solutions, P-123 micelles

with drug curcumin and curcumin molecules in ethanol were determined. Charge of P-123 micelles were also measured. Ultraviolet–Visible Spectroscopy (UV-Vis) was used to determine the calibration curves and to determine the quantities of drug during the release studies. Water immerse tests and mechanical tests were also used to characterize the porous structure of foams produced.

3.3.1. Scanning Electron Microscope (SEM)

The scanning electron microscope (SEM) images were used for morphological characterization (size and shape) of the biofoams produced. Surface is characterized by high-energy electrons which are generated by SEM. Human eye can differenciate the points in 0.2 mm away from each other. Microscope is used to enable to see the points which have lower distance than 0.2 mm. The magnifications can be between 20X and 30000X.

3.3.2. Scanning Transmission Electron Microscopy (STEM)

Scanning transmission electron microscopy (STEM) analyses were used to characterize (size, shape and structure) the P-123 micelles using a Quanta 250FEG type instrument. Image is obtained by counting of backscattered electrons of the reflected electron beams in STEM analysis. Both properties and working principles of SEM and TEM are combined in STEM. Samples should be very thin for STEM. Like TEM, STEM uses secondary electrons, characteristic X-rays and scattered beam electrons. STEM scans the samples by electron beams like SEM.

3.3.3. Transmission Electron Microscope (TEM)

The transmission electron microscope was used to characterize (size, shape and structure) the P-123 micelles. TEM is a very useful analysis method for material science. The working principle of the TEM is similar to light microscope. The TEM

uses electrons instead of light since electrons have smaller wavelength than the light of light microscope. Hence, resolution of TEM images is better and details in the structure of samples can be examined. A high energy electron beam is sent to the sample and images are obtained as a result of interactions between electrons and atoms of the sample. The magnifying power of TEM is up to 2 million times. If TEM is compared with SEM, it can be said that SEM is based on scattered electrons while TEM is based on transmitted electrons. In adddition, TEM has much higher resolution than SEM. TEM provides a 2-dimensional picture while SEM provides a 3-dimensional image.

3.3.4. Atomic Force Microscope (AFM)

P-123 micelles were characterized (size, shape and structure) by Atomic Force Microscope using a Bruker – MultiMode Nanoscope8. The principle of operation is based on measuring the force between the tip and the sample. The force is caused by different types of interactions such as electrostatic, magnetic, van der Waals, ionic and capillary forces, elastic/plastic deformations. Hooke's Law (F=-k.x ; F: the Force, k: the spring constant, and x: the cantilever deflection) can be used to describe the force between the sample and the probe which is put at the end of cantilever. This force depends on the spring constant of the cantilever and the distance between probe and sample.

3.3.5. Fourier Transform Infrared (FTIR) Spectroscopy

FTIR analyses were performed for chemical characterization of chitosan foams (Whether to see if the foams contained heptane or hexane). FTIR is the most widely used type of infrared spectroscopy. When infrared radiation is absorbed, signals are observed. All chemical structures have own signal spectral fingerprints in FTIR. For instance, the pure chitosan shows characteristic bands at 3441 cm^{-1} for O-H (hydroxyl) stretching, at 2856 cm^{-1} for C-H stretching, at 1630 cm^{-1} for C=O stretching (Amide-I) and at 1317 cm^{-1} for C-N (aliphatic amine) stretching (Figure 3.11).
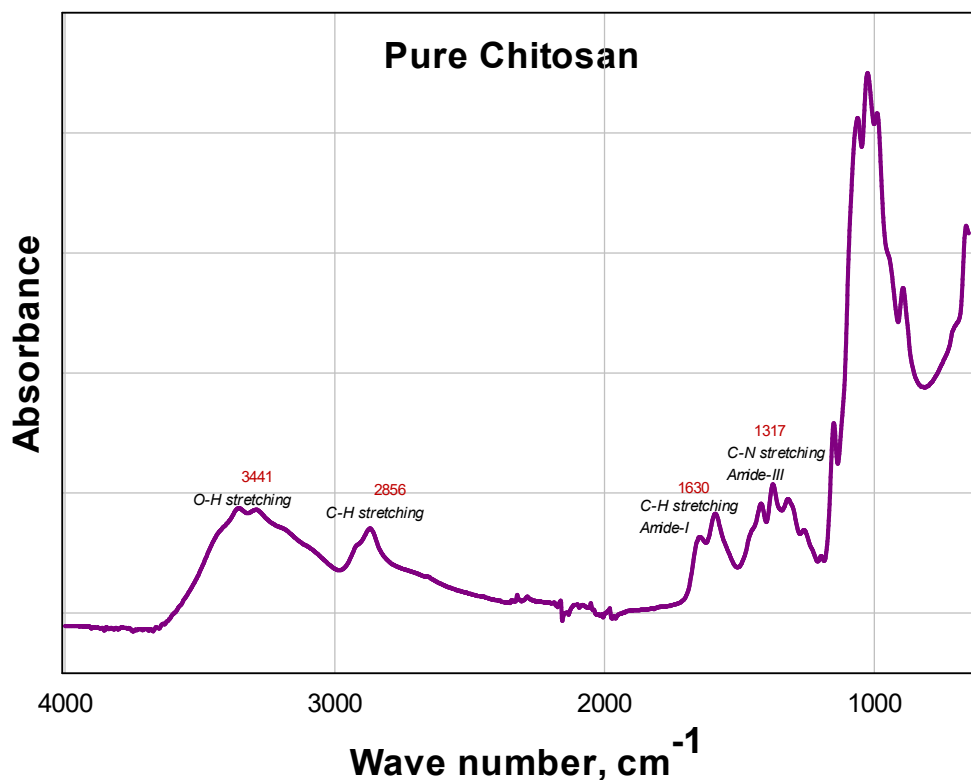
Figure 3. 11. FTIR spectrum of chitosan.

Before the characterization of the foams produced, SDS which was used as crosslinking agent was examined by appliying FTIR analysis to see the effect of it on the produced foams. Figure 3.12 shows the FTIR spectrum for SDS. SDS gave peak near 3450 cm^{-1} for the bending vibration of adsorbed molecular water. In addition, SDS have peak at 2950 cm^{-1} for asymmetric stretching vibration of CH_3. Peaks at 2920 and 2850 cm^{-1} representing the asymmetric and symmetric stretching of CH_2, respectively. The bands at 1470 and 1380 cm^{-1} shows the asymmetric and symmetric deformation vibrations of CH_3, respectively. SDS have characteristic peaks at 1220 and 1108 cm^{-1} for asymmetric and symmetric stretching of the S=O. The peak at 995 cm^{-1} shows the asymmetrical stretching vibration of C–O–S.
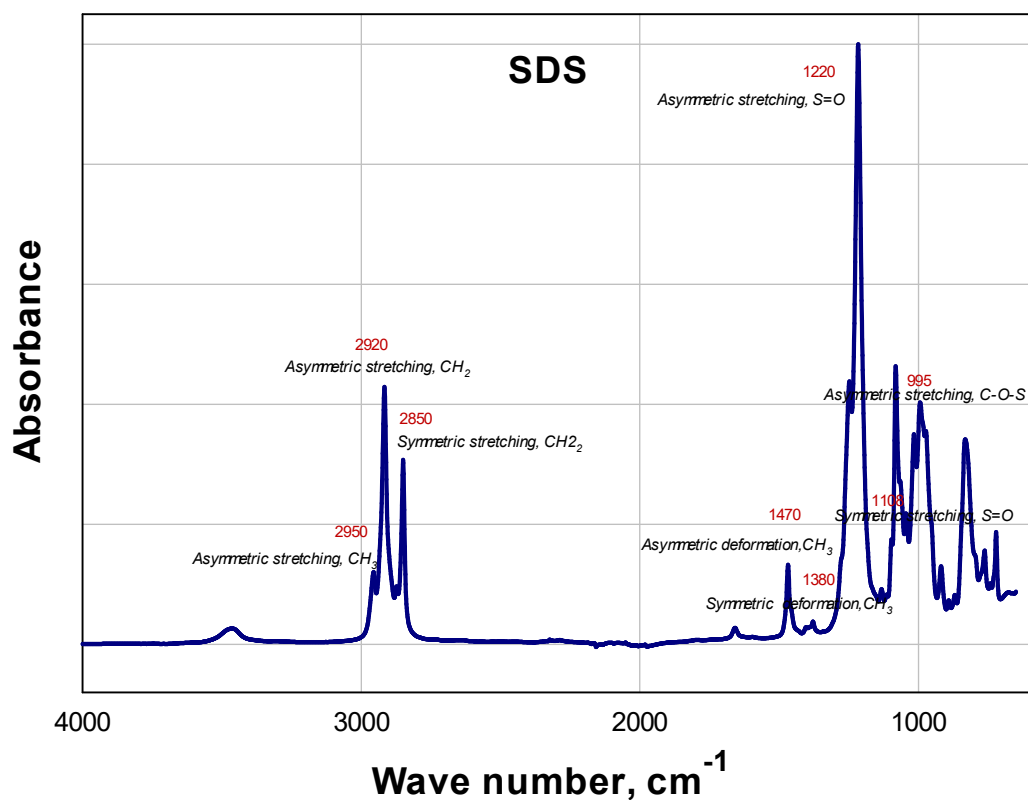
Figure 3. 12. FTIR analysis of SDS.

Vancomycin was used as model hydrophylic drug to produce drug loaded biofoams. Figure 3.13 gives characteristic peaks of the drug. The characteristic absorption bands of vancomycin are found at 3450 cm^{-1} for O-H (hydroxyl) stretching, at 1655 cm^{-1} for C=O stretching (Amide-I), at 1504 cm^{-1} for C=C stretching (aromatics), at 1231 cm^{-1} for C-O-C stretching (phenols) and at 1062 cm^{-1} for C-N (aliphatic amine) stretching.

Figure 3.14 gives the FTIR analysis for P-123. As it is seen, the peaks corresponding to appear in the range of 2850-3000 cm^{-1} -CH stretching. The peak between 1000 and 1100 cm^{-1} is assigned to the C–O–C stretch of the ether bond, which is a feature of the Pluronic copolymer.
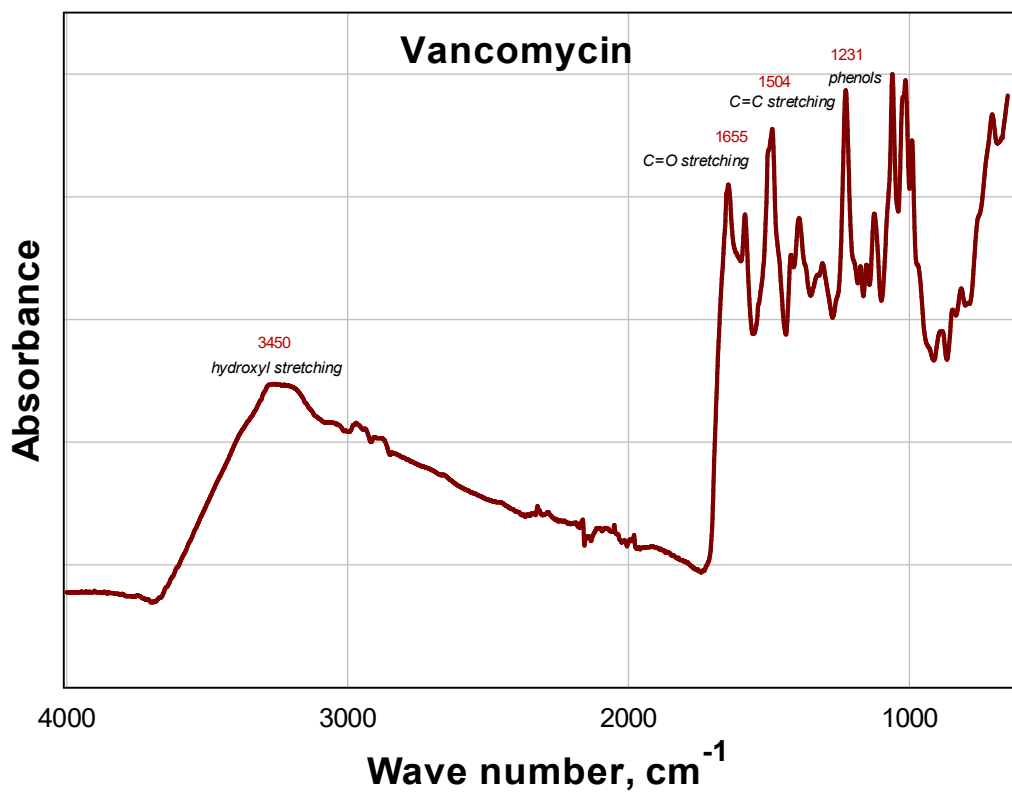
Figure 3. 13. FTIR analysis of vancomycin.
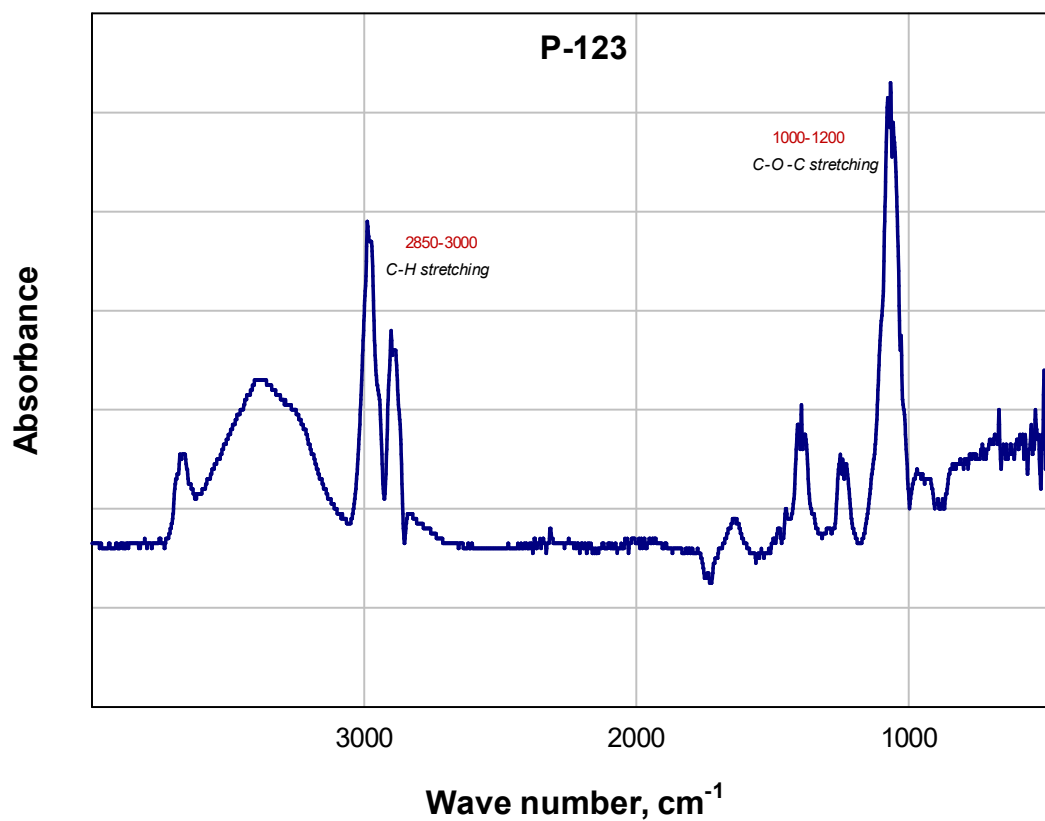
Figure 3. 14. FTIR graph for P-123.

3.3.6. Water Hold-Up Capacity and Release Studies

It is important to know hold-up capacity of the produced foams. Water immerse test was applied to the chitosan foams to see amount of water that hold-up in biofoam and releasing behavior of water with time. First of all, the samples were dried and weighed. Then, they stayed in water and weighed with time again after removed from water.

3.3.7. Mechanical Test

To observe the mechanical properties of the foams and the effect of the parameters, compression test was applied to samples by using TA.XTplus Texture Analyser. Strain of 40 % was applied with the load of 5 kg. The mechanical properties of biofoams produced for wound dressing applications are very important during the applications. The mechanical and biological properties of chitosan foams depend on the properties of chitosan and preparation method used.

3.3.8. Brunauer-Emmett-Teller (BET) Surface Area Analysis

BET analyses were used to characterize the structure and pore sizes of the foams produced. This method is based on the gas adsorption on solid surfaces. Adsorption is the adhesion of gas molecules or atoms to a surface. Temperature and pressure of gas, surface area and interaction between the molecules are parameters for the adsorbed gas amount. Nitrogen is used as a gas in BET surface analysis since it has high purity and availability. Nitrogen gas with known amount is given to the device. Then, samples are removed after adsorption layers are produced. Heat is applied to release adsorbed nitrogen. BET isoterm is obtained as a function of adsorbed gas amount and releative pressure.

3.3.9. Ultraviolet–Visible Spectroscopy (UV-Vis)

UV-Vis spectroscopy was used to determine the amount of drug releaseased and also to examine the interactions between P-123 molecules, chitosan and drug molecules.

The working principle of the UV is the measurement of beam of light after reflection. While visible region ranges from 400 to 800 nm, ultraviolet region is between 190 and 400 nm. The analyisis can be both quantitative and qualitative. UV-Vis spectroscopy involves the region between 200-800 nm. The absorbance (A) of the sample can be obtained by the equation given below:

$$A = log_{10} \left(\frac{I_0}{I} \right)$$

where I_o is intensity of light passing through the reference cell and I is intensity of light passing through the sample cell. Light is absorbed when intensity of light passing through the sample cell is lower than intensity of light passing through the reference cell. Light is converted to the current and high current shows higher intensity. Concentration of the substance is proportional to the absorbance according to the Beer-Lambert Law. Calibration curve is obtained by measuring absorbances at the known concentrations. Then unknown sample amounts are determined by using calibration curve.

3.3.10. Size and Charge Measurements

Size and charge measurements of P-123 micelles in water, P-123 micelles in water in the presence of chitosan molecules, P-123 micelles in chitosan solutions, P-123 micelles with curcumin and curcumin molecules in ethanol were carried out using Malvern Zeta Sizer Nano ZS. This device combines the laser Doppler velocimetry and Phase Analysis Light Scattering. Malvern Zeta Sizer Nano ZS has working principle based on dynamic light scattering distribution of particles as a function of particle size. While small particles scatter light at small angles, large particles scatter light at small angles relative to the laser beam. Molecules have random collosion due to Brownian motion. Stokes-Einstein equation describes the relationship between particle size and

speed of particles due to Brownian motion. Zeta Sizer uses this relation to determine the size of particles (Figure 3.15).
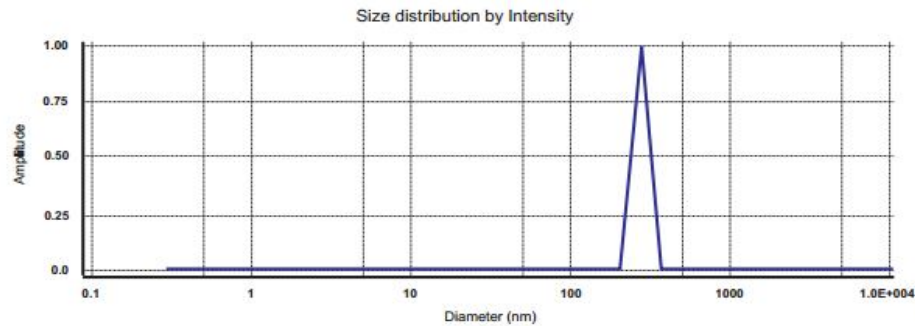
Figure 3. 15. General size distribution graph.

Zeta Potential can be defined as potential of the particle surface or surface charge of particles. Henry equation given below is used to get zeta potential by Malvern Zeta Sizer Nano ZS (Figure 3.16)

$$UE = \frac{(2 \, \mathcal{E} \, z \, f \, (Ka))}{3\eta}$$

where UE: Electrophoretic mobility, $\mathcal{E}$: Dielectric constant, z: Zeta potential, η: Viscosity, f(Ka): Henrys function, f(Ka) value generally used as 1.5 or 1.0. The magnitude of the zeta porential shows how the colloidal system is stable. Particles which have low zeta potential come together while particles which have large zeta potential repel each other.
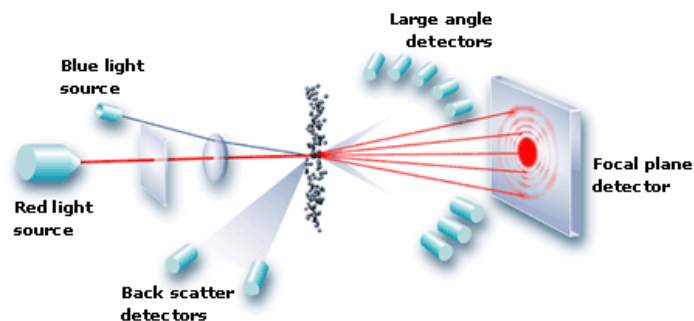
Figure 3. 16. Malvern Mastersizer 2000 Laser Diffraction.

CHAPTER 4

PRODUCTION AND CHARACTERIZATION OF CHITOSAN BASED BIOFOAMS

Production of chitosan biofoams was done by O/W emulsion templated synthesis in the absence and presence of surfactants for different chitosan and oil phase concentrations and types. For these experiments, TPP and SDS (as an alternative) were used as the crosslinking agents. O/W emulsions were prepared using ultrasonic probe as mentioned above in experimental section. For this purpose three types of oil phases such as pentane, hexane and heptane were employed at various concentrations. First of all, the structure of chitosan foams produced without an oil phase were characterized as a base line. The results of all these studies were discussed in the following paragraphs.

4.1. Foam Production Using O/W Emulsion Templated Method: In the Absence of Surfactants

In this part of the study, O/W emulsions were produced using an ultrasonic probe in the absence of surfactants at four different chitosan concentrations. Chitosan was crosslinked by TPP and hexane and heptane were used as oil phases in these studies. The pictures of the foams produced are presented in Figure 4.1 a and b. It is easily seen with a naked eye that there is a big difference between the foams produced with low and large amounts of chitosan. That is, it seems that the chitosan amount has a large effect on both the pore structure and the mechanical strength of foams. The SEM images of these foams were also presented in Figures 4.2 and 4.3 (at different magnifications) for the cases of 2 % and 4 % chitosan, respectively. It is clearly seen that the high chitosan concentration resulted in larger pore size. Although the pores are large, the structure seems robust. Detailed studies for the oil phase and concentrations are given below.
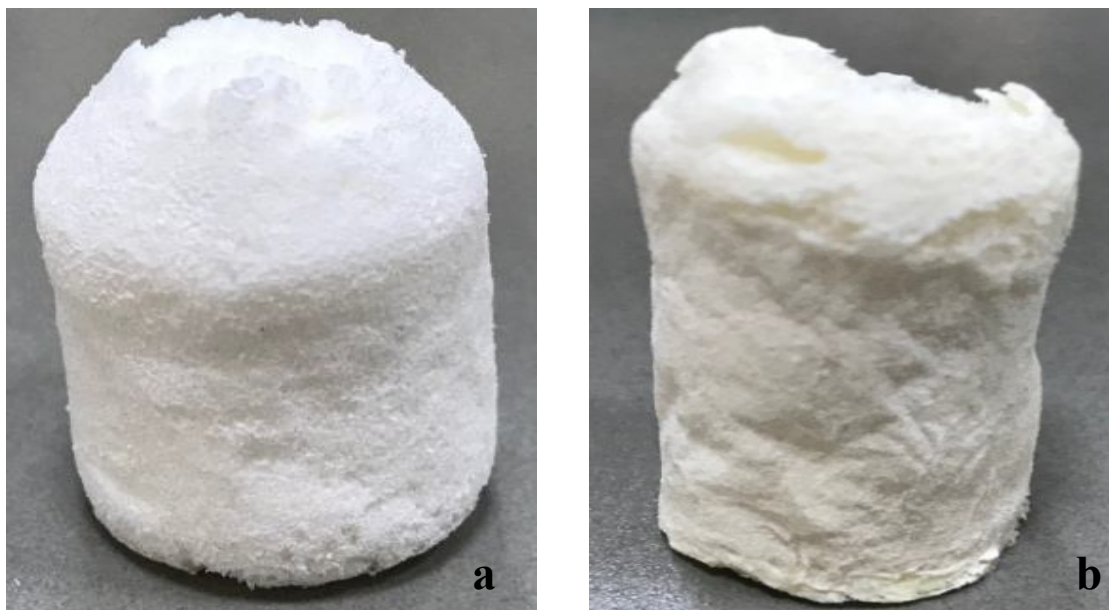
Figure 4. 1. Chitosan foams produced by O/W emulsion templated method in the absence of surfactant (a) 2 % chitosan (b) 4 % chitosan.

HV	spot	det	mag ☐	HFW	WD	pressure	12/8/2017	⊢——— 10 µm ———⊣
5.00 kV	2.0	ETD	10 000 x	41.4 µm	9.7 mm	1.85e-3 Pa	10:20:27 AM	IYTEMAM

HV	spot	det	mag ☐	HFW	WD	pressure	12/8/2017	⊢——— 4 µm ———⊣
5.00 kV	2.0	ETD	25 000 x	16.6 µm	9.8 mm	2.97e-3 Pa	10:17:38 AM	IYTEMAM
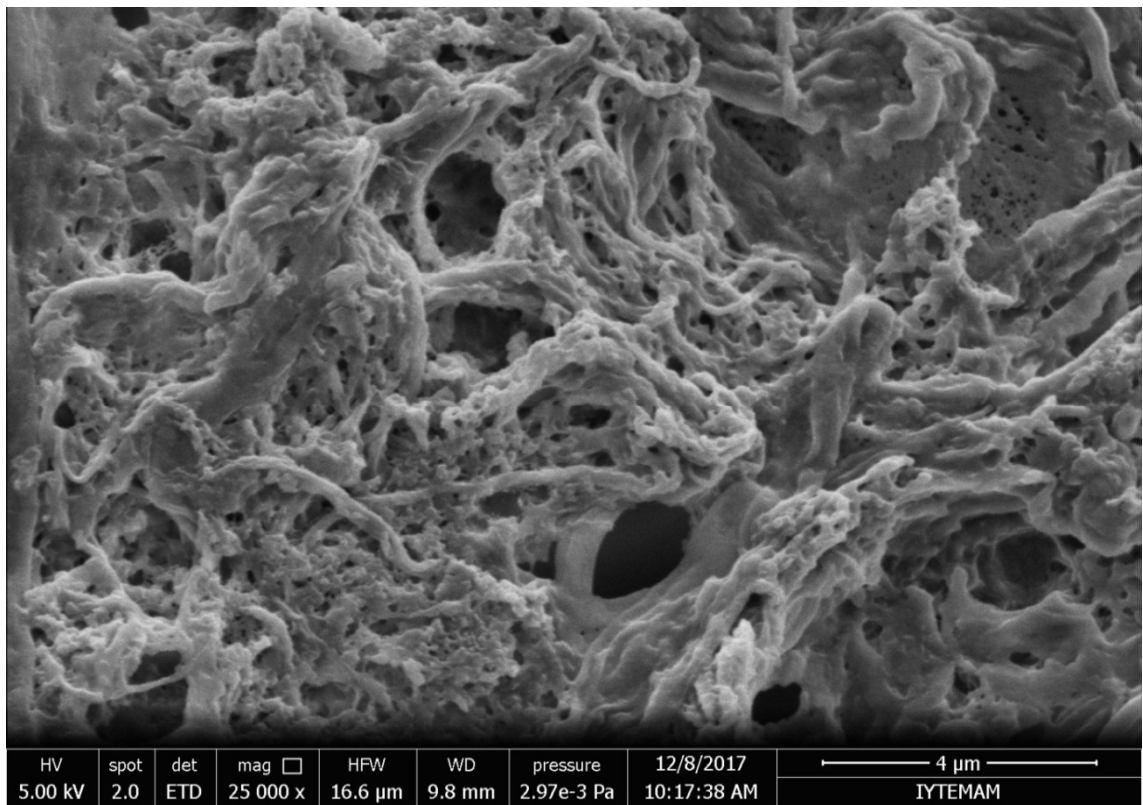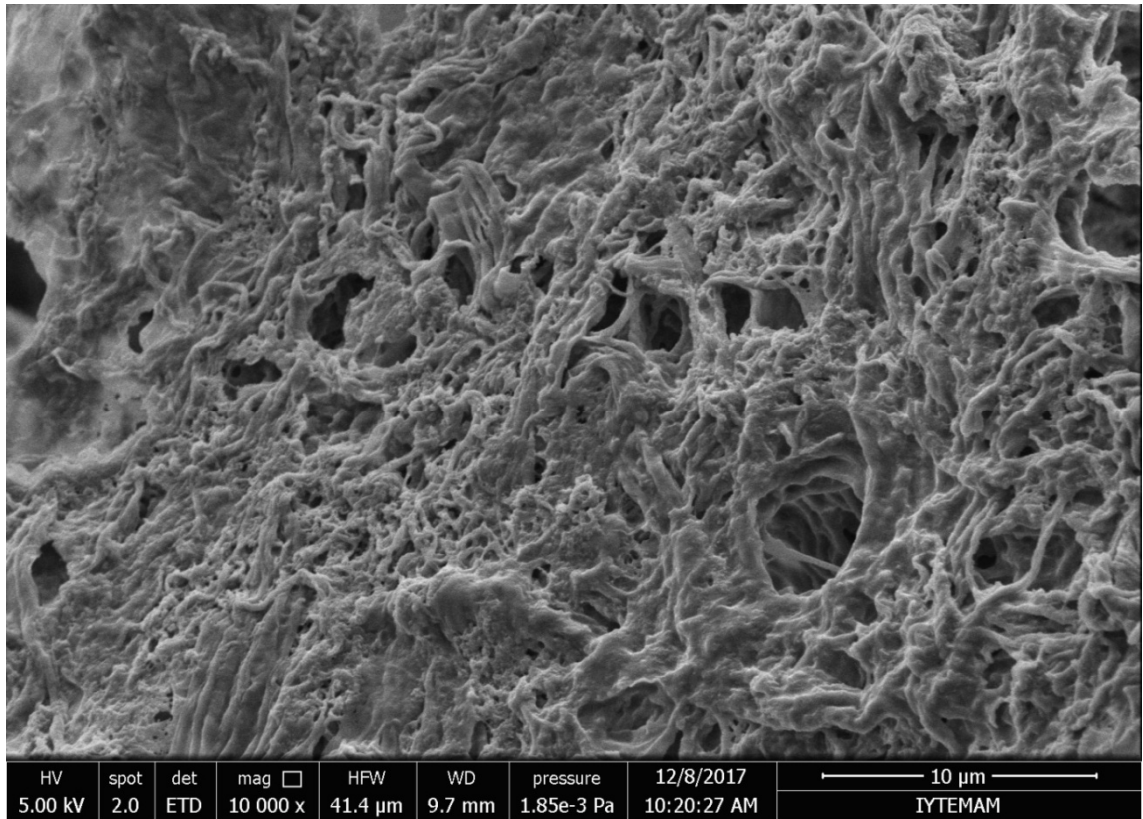
Figure 4. 2. Chitosan foam in the absence of surfactant (2 % chitosan).

| HV | spot | det | mag □ | HFW | WD | pressure | 12/8/2017 | 400 µm |
| 5.00 kV | 2.0 | ETD | 250 x | 1.66 mm | 10.1 mm | 1.32e-3 Pa | 10:23:13 AM | IYTEMAM |

| HV | spot | det | mag □ | HFW | WD | pressure | 12/8/2017 | 100 µm |
| 5.00 kV | 2.0 | ETD | 1 000 x | 414 µm | 10.1 mm | 1.15e-3 Pa | 10:24:22 AM | IYTEMAM |
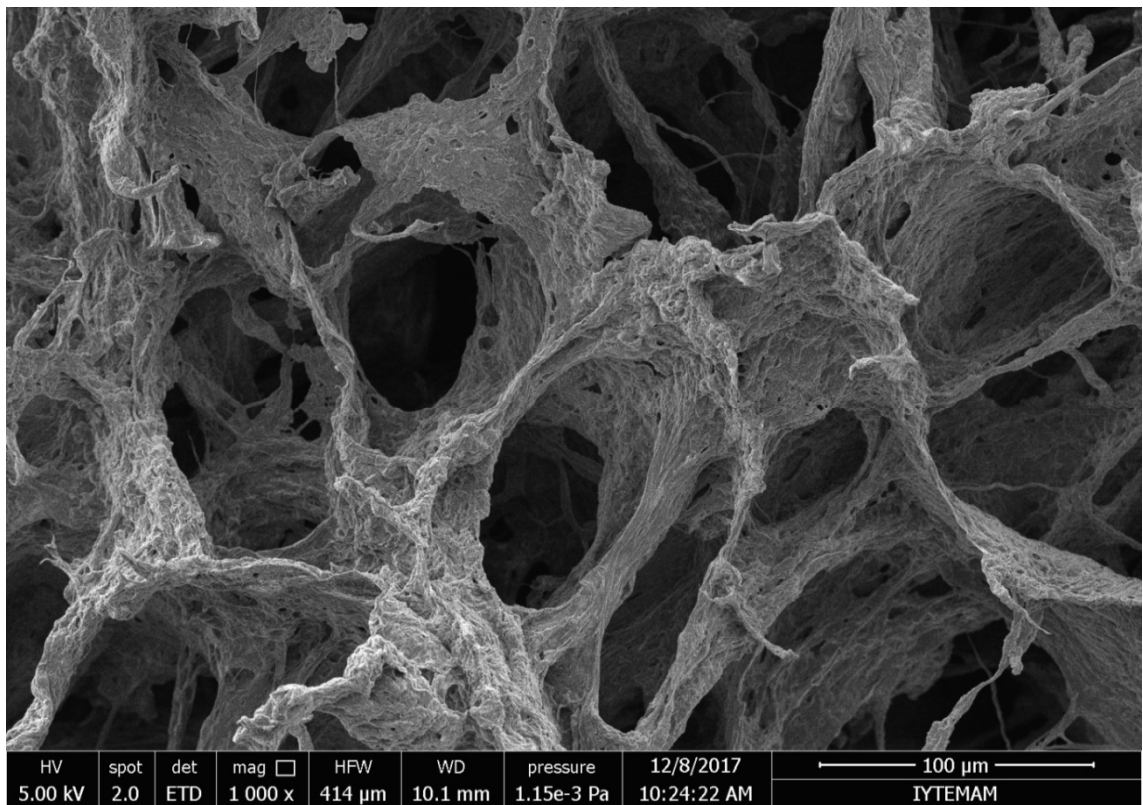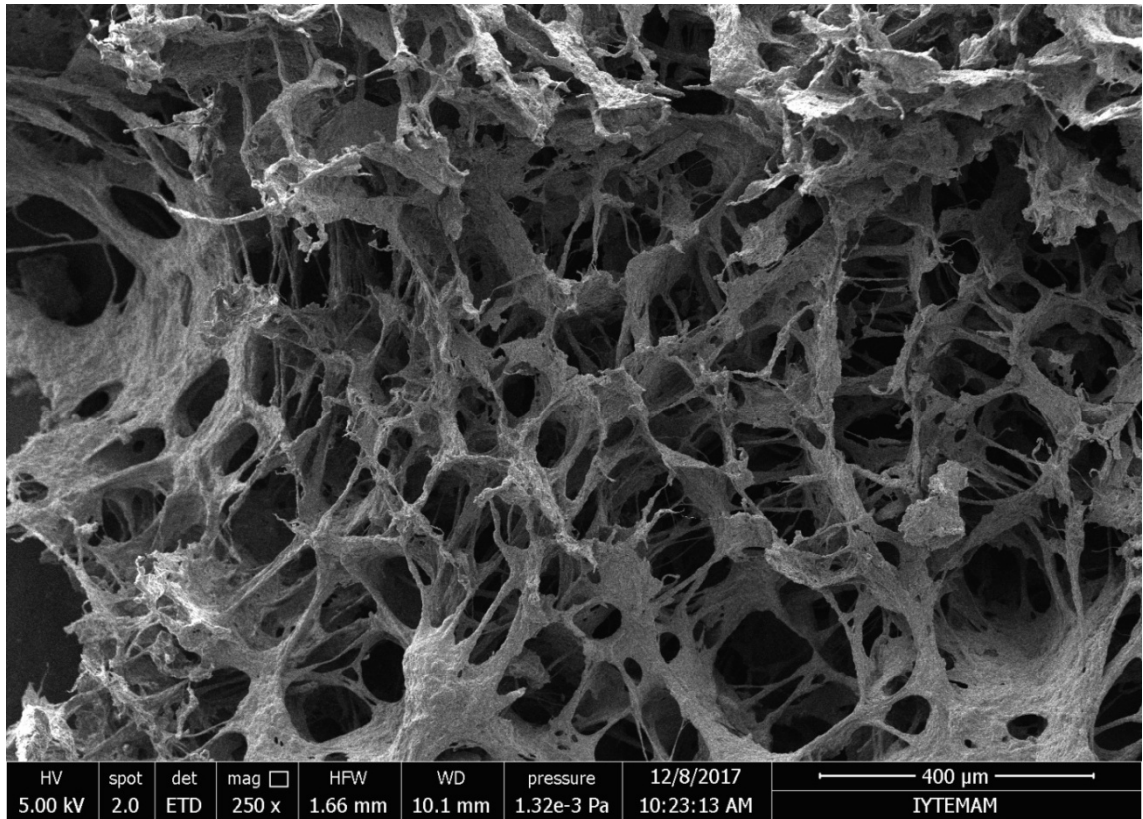
Figure 4. 3. Chitosan foam in the absence of surfactant (4 % chitosan).

4.1.1. Hexane as an Oil Phase

As discussed in methods section above, different chitosan concentrations were used in the range of one to four percent. Hexane concentrations were chosen as 5, 10, 15, 17, 20 volume %. Pore size and structure of these foams were characterized by SEM and the SEM images were presented in Figure 4.4 for all the conditions. It can be seen from images that all structures have almost porous structure. The chitosan amount seems to have a large effect on both the pore structure and the mechanical strength of foam. Increasing chitosan concentration results in smaller pore size. Moreover, it is also seen that the concentration of oil phase is important and about 15 volume % of oil produce better structures. Based on these results one can conclude that the foam is better in terms of both the strength (Table 4.1) and the pore structure when 2-4 % chitosan was used with 15-17 volume % hexane.

Chitosan Concentration, %
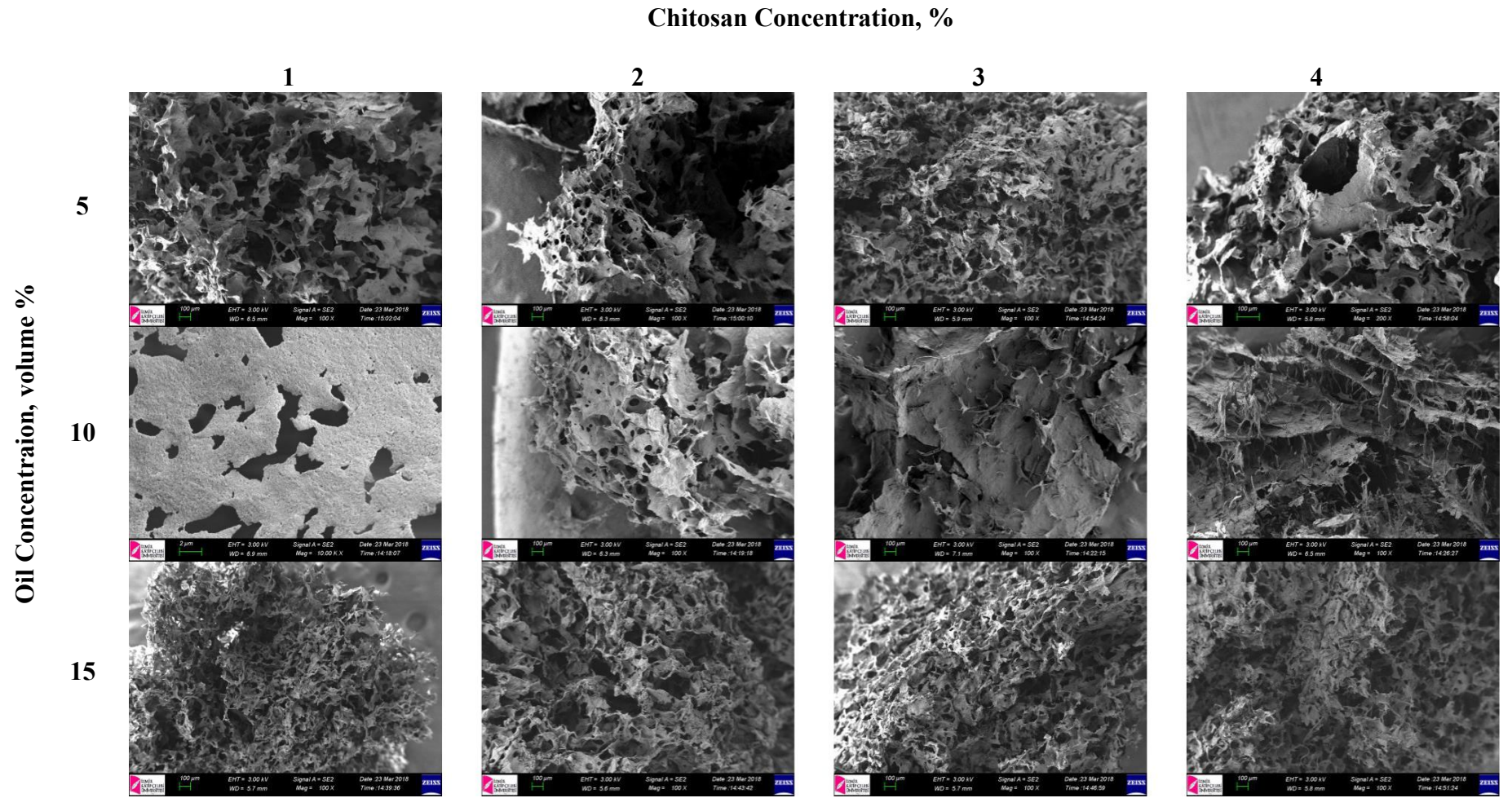
Figure 4. 4. SEM images of chitosan foam which produced with different chitosan and hexane concentrations.

Chitosan Concentration, %

1   2   3   4

17

20

Figure 4. 4. (cont.)

Oil Concentraion, volume %
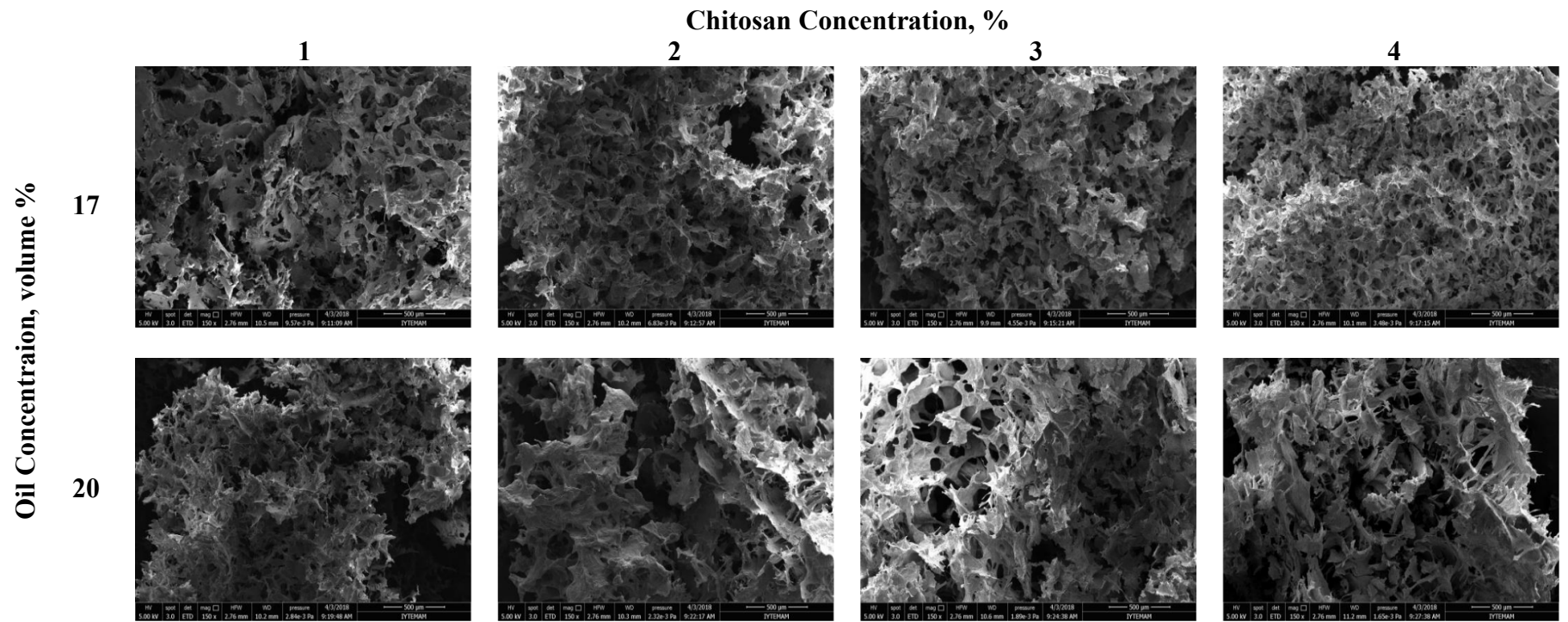
The mechanical properties of these foams with different concentrations were evaluated by compressive strength measurements. The compressive strength gives the stress that is needed to destroy the sample by crushing. These results were listed in Table 4.1. It is seen that the strain values for 4 % chitosan are different due to the irregular shape of samples. When the stress and strength values are compared for similar strain values, it can be said that higher chitosan and hexane amounts give better mechanical properties. The mechanical properties of a scaffold used for tissue engineering are very important due to the need for the structural stability to oppose the various stresses incurred during culture in vitro or implantation in vivo. In one example study from literature found that the compressive stress values at 40 % strain in compressive testing was about 50 kPa for chitosan foams (Hu et al. 2018).

Table 4. 1. Mechanical test results for foam produced by hexane/water emulsion templated method

Sample Content	Compressive Strength (kPa)
2 % CS, 5 % hexane	19
2 % CS, 10 % hexane	20
3 % CS, 10 % hexane	23
4 % CS, 13 % hexane	66
4 % CS, 17% hexane	87

4.1.2. Heptane as an Oil Phase

Heptane does not have the environmental and health concerns that are associated with hexane hence because of the similarity of the oils, heptane was also used as an oil phase to produce chitosan foams. Similar to the foam productions conducted with hexane, chitosan at different concentrations (1 - 4 %) and heptane at concentrations (5, 10, 15, 17, 20 volume %) were used in these experiments. Pore size and structure of these foams were characterized by SEM and presented in Figure 4.5. It can be seen from the figures that all the conditions of 4 % chitosan concentration with different oil concentrations resulted porous structures as expected. For the other chitosan concentrations (2 % and 3 %), high heptane concentrations give porous structure.

Chitosan Concentration, %

Figure 4. 5. SEM images of chitosan foams which produced with different chitosan and heptane concentrations.

Table 4.2 gives the mechanical test results for chitosan biofoams produced by heptane/water emulsion templated method. Similar to the results of hexane, it can be clearly seen that increasing chitosan concentration increases mechanical strengths of the foams with higher compressive stress values.

Table 4. 2. Mechanical test results for for foam produced by heptane/water emulsion templated method

Sample Content	Compessive Strength (kPa)
2 % CS, 5 % heptane	9
2 % CS, 10 % heptane	13
2 % CS, 17 % heptane	12
4 % CS, 10 % heptane	52
4 % CS, 13 % heptane	74
4 % CS, 17 % heptane	78
4 % CS, 20 % heptane	62

4.2. Foam Production Using O/W Emulsion Templated Method: In the Presence of Surfactants

As discussed in the experimental methods section above, some selected surfactants (P-123, SDS, CTAB and TX-100) were used to increase both the stability and the number of oil droplets to form emulsions as templates. The size and shape of oil droplets were observed using a microscope (Figure 4.6 a, b, c and d). As it is seen from the figures that the sizes of oil droplets are between 220-270 µm in the case of P-123, around 170 µm in the case of SDS, around 170 µm in the case of CTAB and between 80 and 250 µm in the case of the mixture, TX-100.
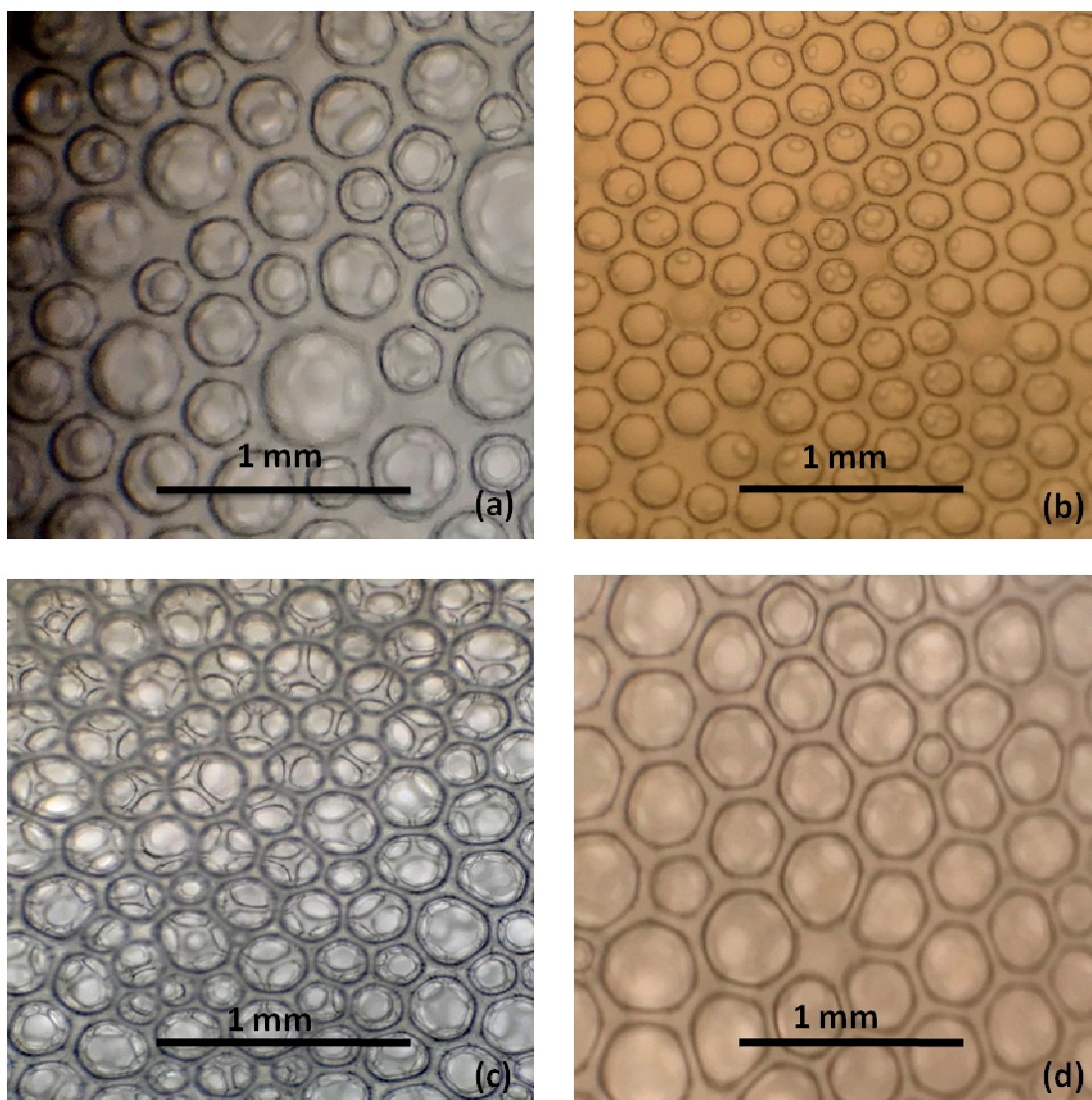
Figure 4. 6. Microscope images of emulsions with different surfactants (a) P-123 (b) SDS (c) CTAB (d) TX-100.

Figure 4.7 shows the chitosan foams produced using these emulsions in the presence of surfactants. It can be seen from the figures that all structures are so brittle compare to the ones produced in the absence of surfactants. The porous structures of these foams are also look better from the foams produced in the presence of surfactants. This is suprizing and can become very important conclusion about surfactants. They are expected to be miracle molecules and used in any application.
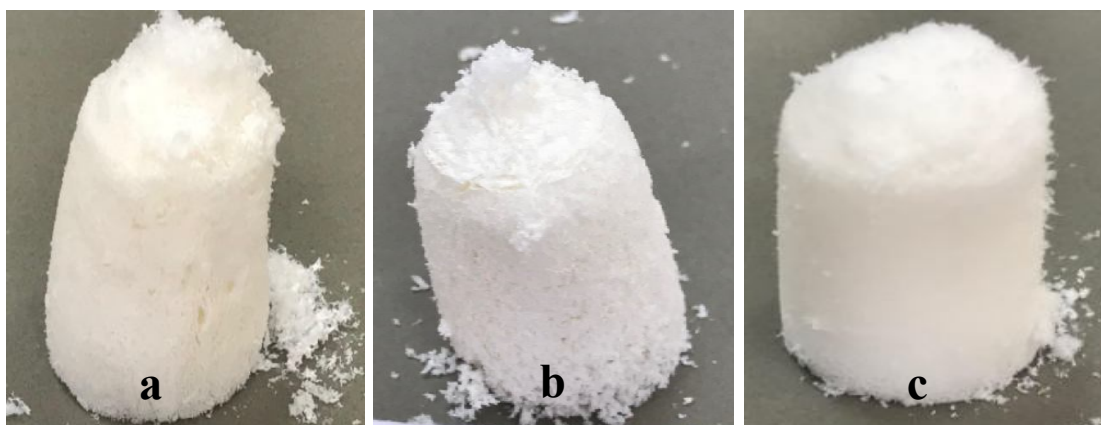
Figure 4. 7. Produced foams by using O/W emulsion templated method in the presence of surfactant (a) SDS (b) CTAB (c) P-123.

The foams produced in the presence of hexane and different types of surfactants at two chitosan concentrations as 2 % and 4 % were also characterized by SEM analysis and given in Figures 4.8 - 4.15. As can be seen from figures, except SDS, biofoams with other surfactants give porous structure. Although they have very good porous structure, they are all so brittle. Especially the one which was prepared in the presence of SDS was not durable and scattered during sample preparation for SEM analysis.

Compare to the SDS, the network structure of chitosan foam produced in the presence of CTAB was better (Figure 4.10 and Figure 4.11) but not enough in terms of the size and shape of the pores. Even though there are both small and large pores in the structure, they are not uniform and ordered.

Similar type of foams were obtained in the presence of P-123. As it is seen that the foams are better in terms of both the strength and the pore structure (Figure 4.12 and Figure 4.13). If one compares this structure with the one in the case of CTAB, it is more ordered and uniform. There are no very large pores.

SEM images of the foams produced in the presence of TX-100 are similar to the foams produced in the presence of P-123. These two surfactants are both nonionic. However, there is big difference in their moleculer weights (Figure 4.14 and Figure 4.15).
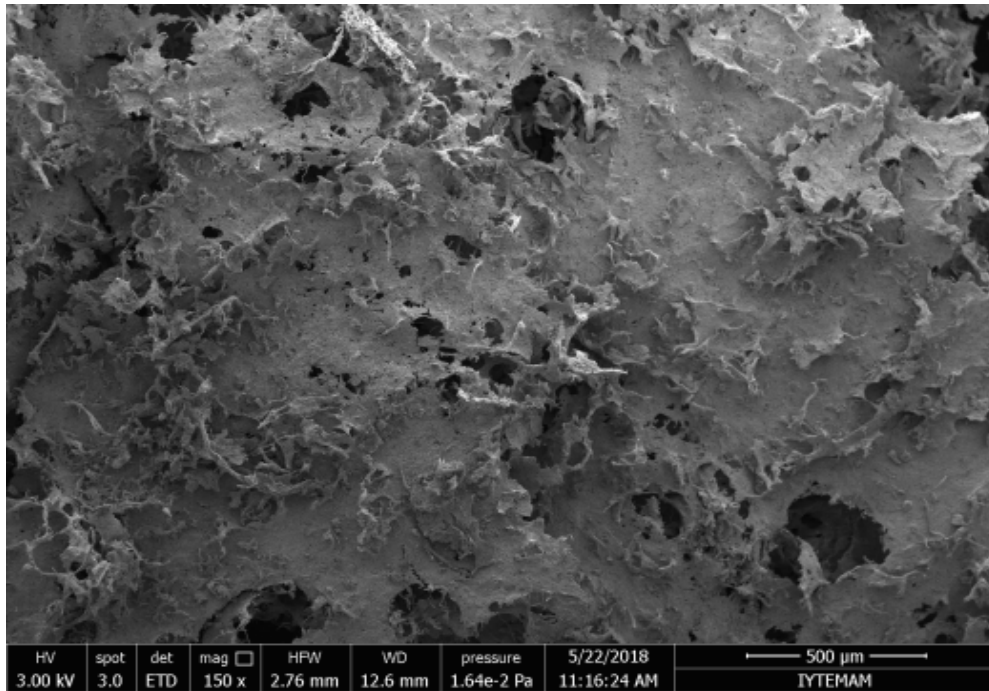
Figure 4. 8. O/W Emulsion templated foam in the presence of SDS (2 % CS, 15 % hexane).
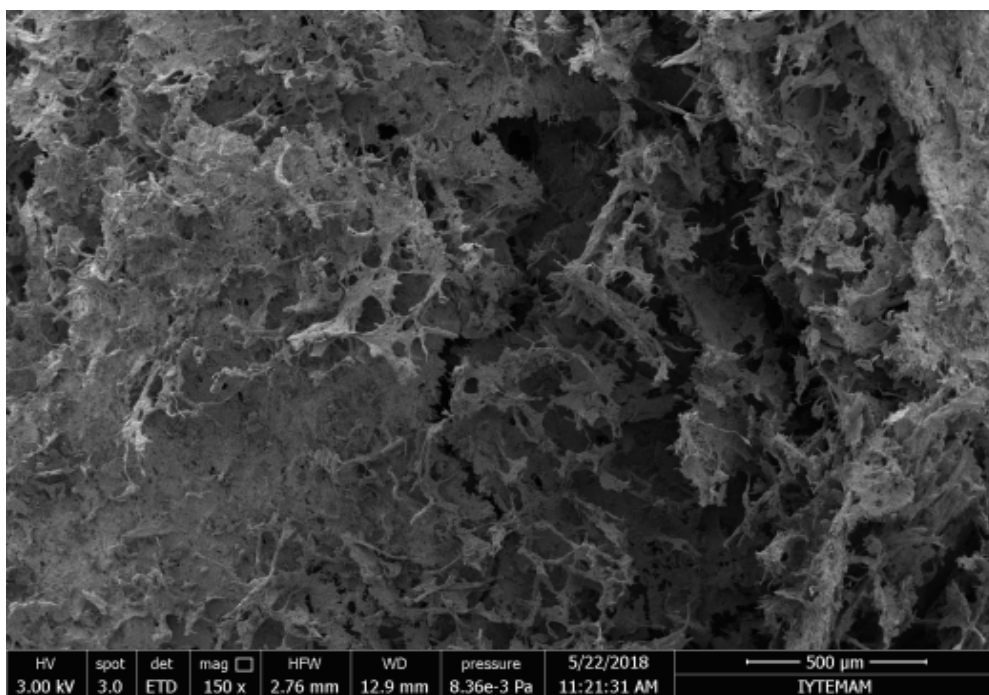
Figure 4. 9. O/W Emulsion templated foam in the presence of SDS (4 % CS, 15 % hexane).
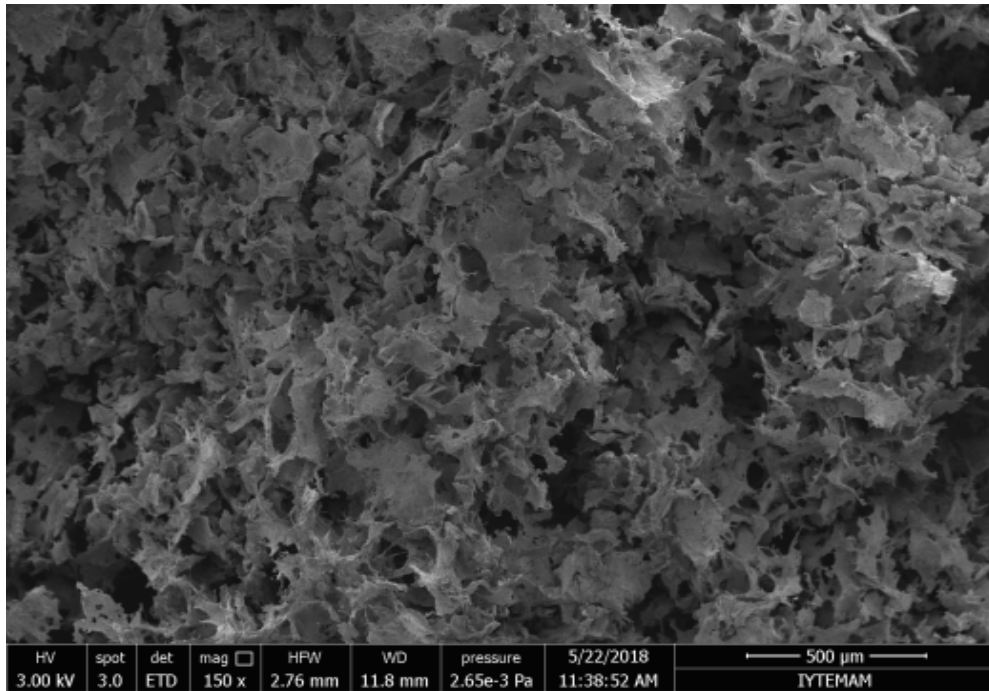
Figure 4. 10. O/W Emulsion templated foam in the presence of CTAB (2 % CS, 15 % hexane).
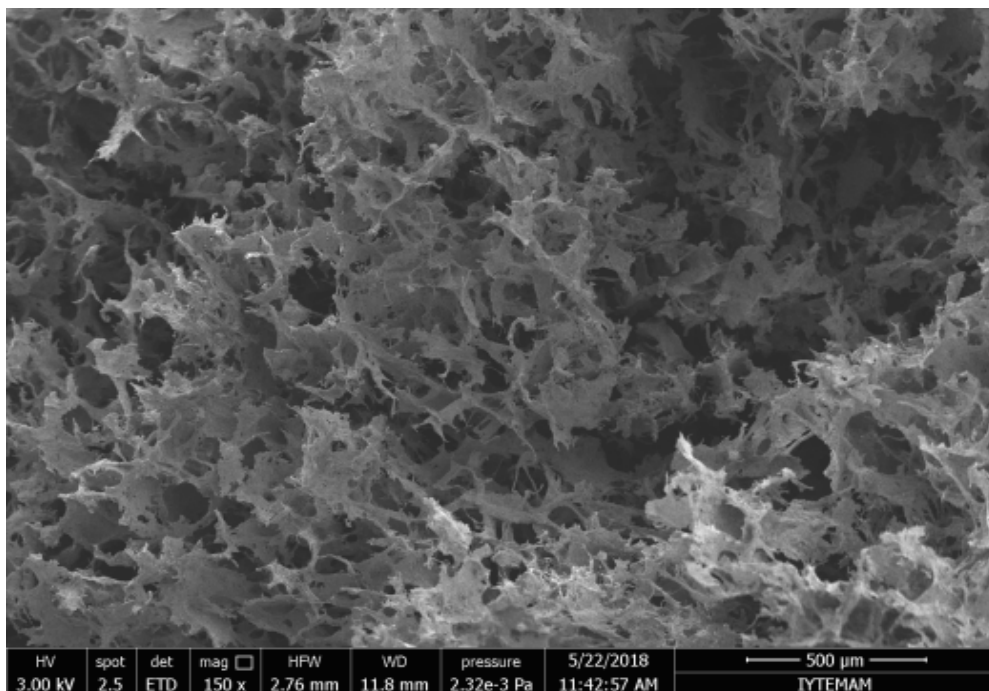
Figure 4. 11. O/W Emulsion templated foam in the presence of CTAB (4 % CS, 15 % hexane).
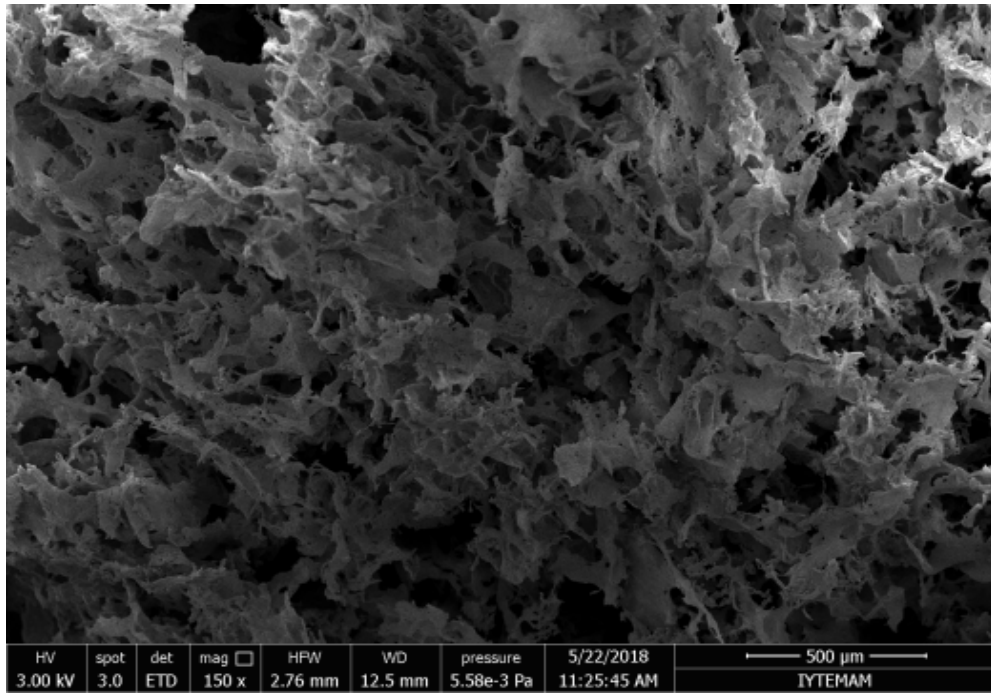
Figure 4. 12. O/W Emulsion templated foam in the presence of P-123 (2 % CS, 15 % hexane).
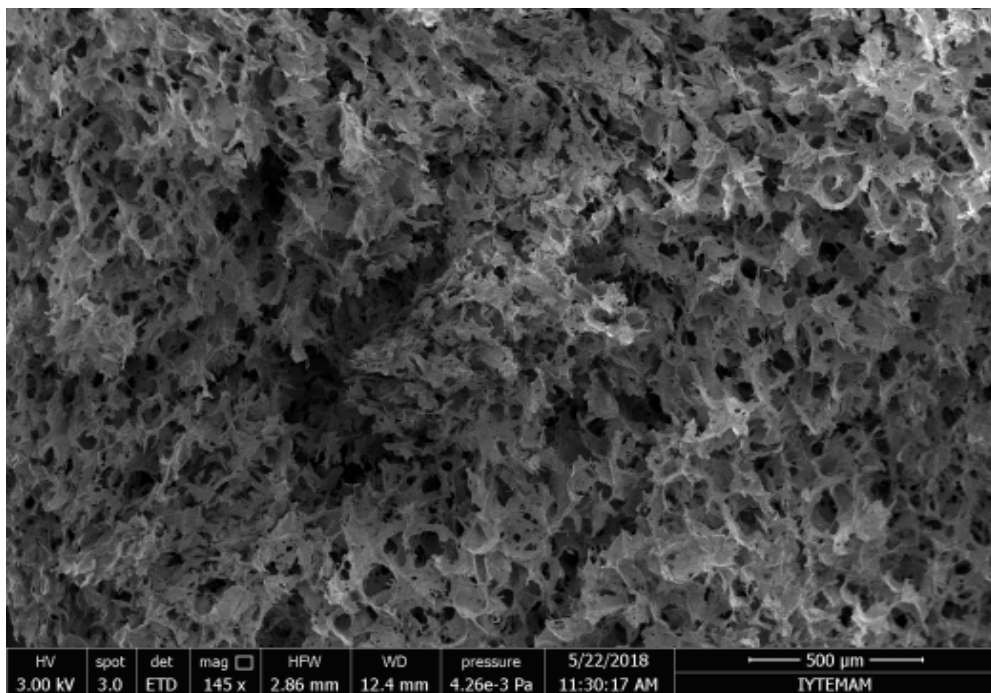
Figure 4. 13. O/W Emulsion templated foam in the presence of P-123 (4 % CS, 15 % hexane).
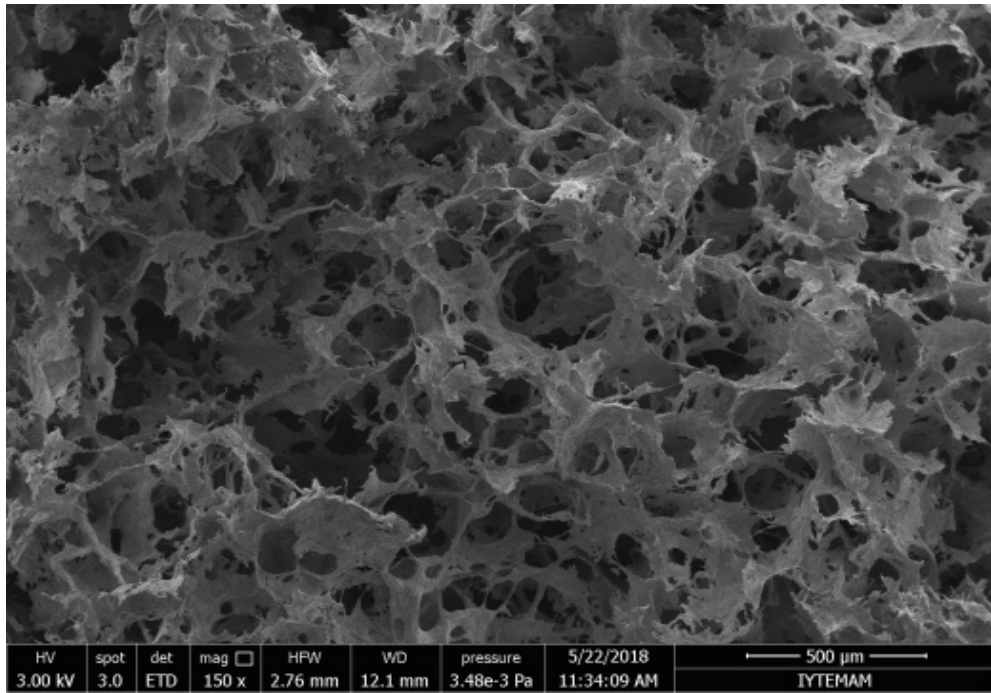
Figure 4. 14. O/W Emulsion templated foam in the presence of TX-100 (2 % CS, 15 % hexane).
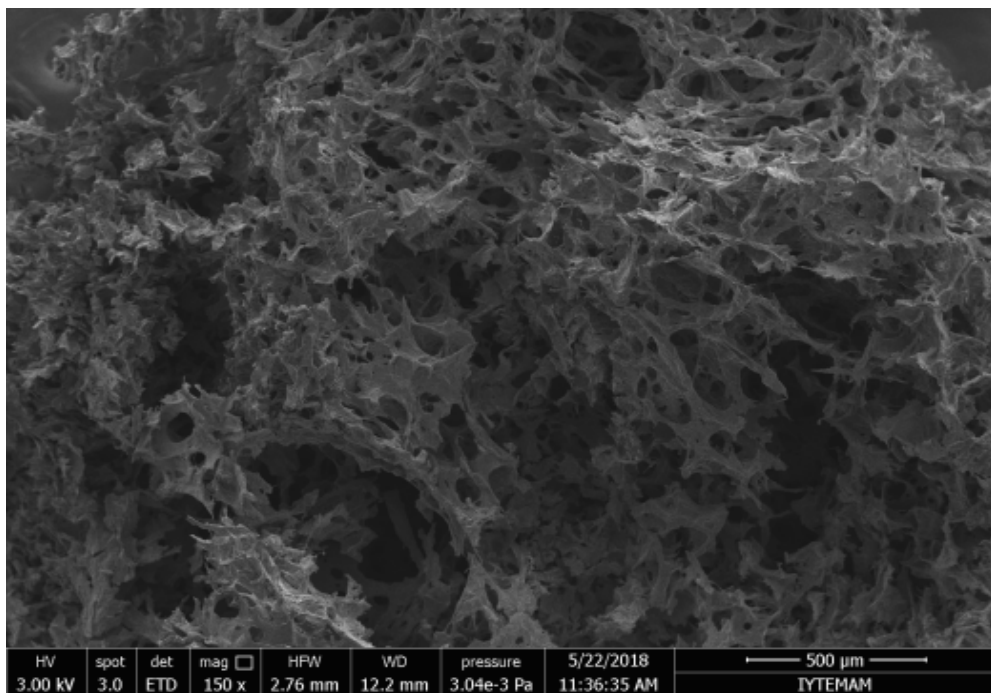
Figure 4. 15. O/W Emulsion templated foam in the presence of TX-100 (4 % CS, 15 % hexane).

Compressive strength measurements of these foams were conducted and given in Table 4.3. As it is expected, the britle sample produced in the presence of SDS have the lowest value. The foams with P-123, however, shows the higher mechanical strength in direct proportion to SEM results. In addition, the comressive strength of the foams which were produced in the presence of surfactant are lower than the foams produced in the absence of surfactants.

Table 4. 3. Mechanical test results for foam produced by hexane/water emulsion templated method in the presence of surfactants

Sample Content	Compressive Strength (kPa)
4 % CS, 17 % hxn, 10^{-2} M SDS	19
4 % CS, 17 % hxn, 10^{-3} M P-123	48
4 % CS, 13 % hxn, 10^{-2} M CTAB	21
4 % CS, 17 % hxn, 10^{-2} M TX-100	38

4.3. Foam Production Using O/W Emulsion Formed Spontaneously

O/W emulsions formed spontaneously were prepeared in the presence of Span 80 in hexane together with ethanol and Tween 20 in chitosan solutions (discussed above in experimental methods section). The size distributions of emulsions were obtained by Dynamic Light Scattering (DLS). DLS performs measurements three times. It is seen that the average size of oil droplets are about 1600 nm and have narrow size distributions (Figure 4.16). The picture of foam produced by forming spontaneous emulsion is given in Figure 4.17. As it is seen from the picture that the structure is very brittle and distributes easily. The pore structure, on the other hand, looks uniform and small sized (Figure 4.18).
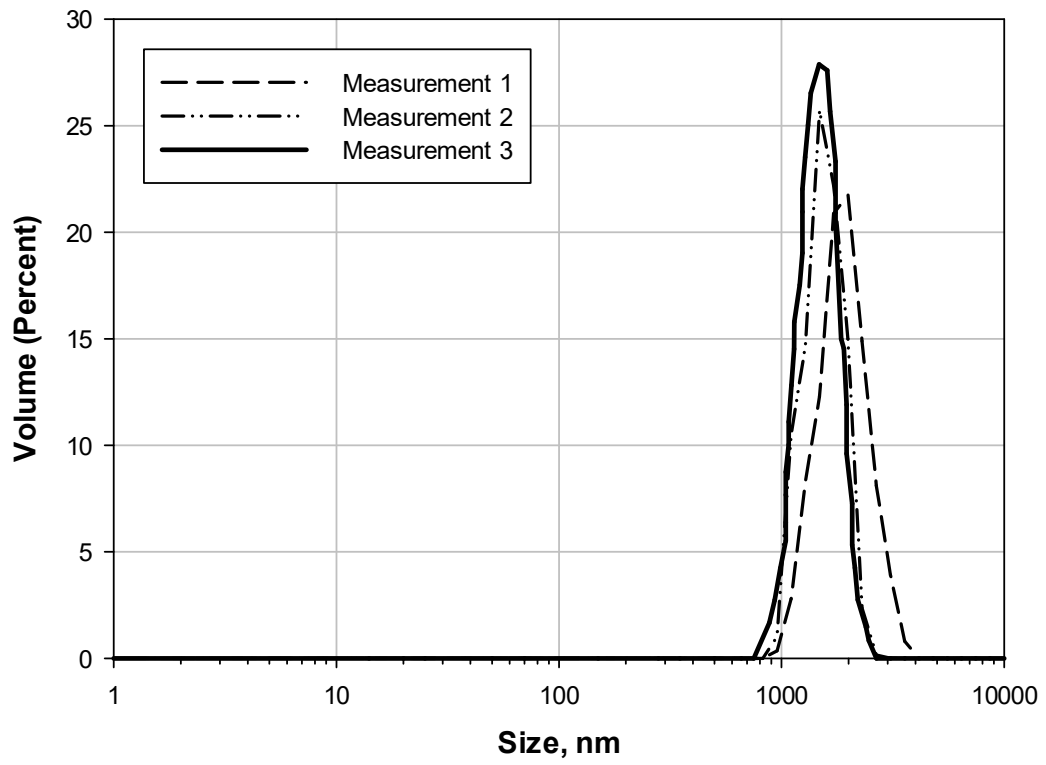
Figure 4. 16. Size distribution of O/W spontaneous emulsion.

Figure 4. 17. Produced foam by using O/W spontaneous emulsion templated method.
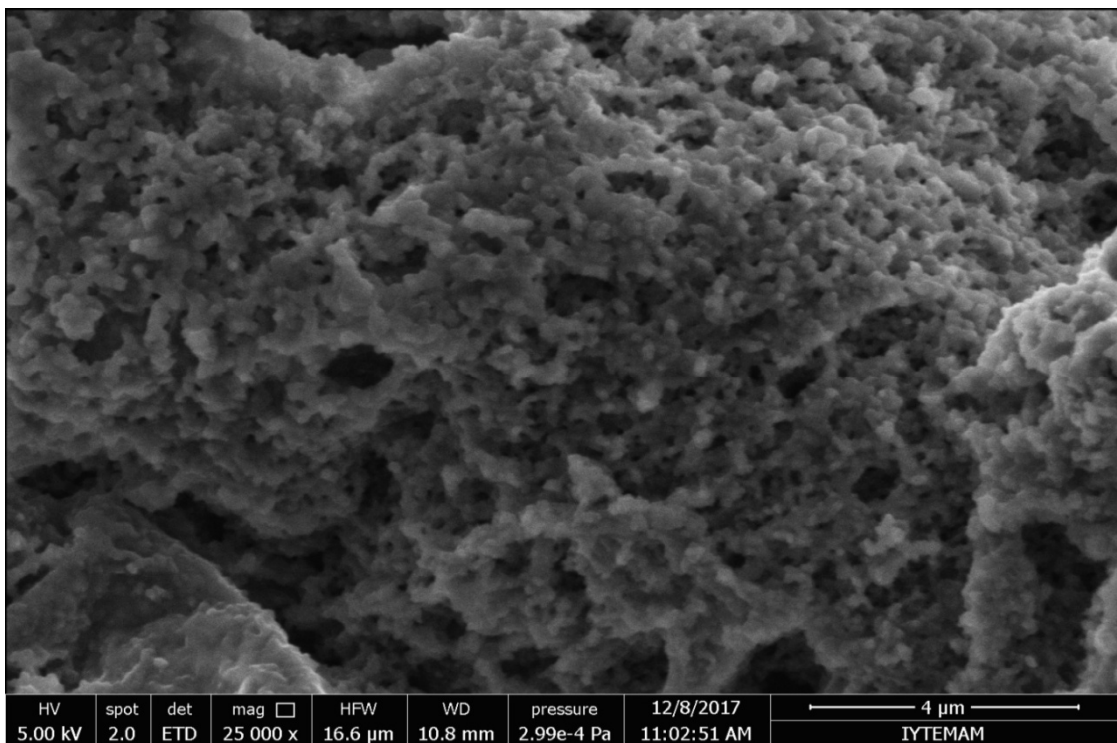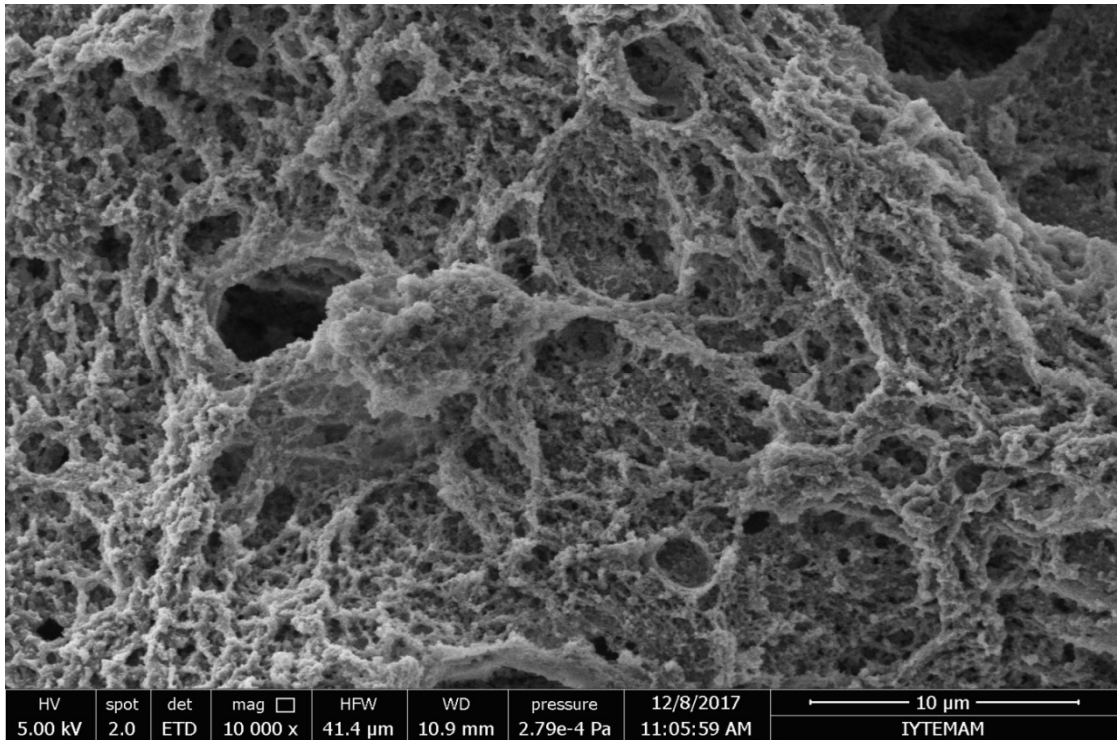
Figure 4. 18. O/W spontaneous emulsion templated foam.

4.4. Foam Production using O/W Emulsion Templated Method: High Molecular Weight Chitosan

High molecular weight (HMW) chitosan was used to test the effect of molecular weight on biofoam production. High concentrations of chitosan were not used because of the high viscosity of the resulting chitosan solution and inadequate mixing. One percent chitosan was used by changing hexane concentrations (10, 13 and 17 volume %). Samples did not maintain their shape after freeze drying process as can be seen from Figure 4.19. SEM images for HMW chitosan foams are given in Figure 4.20. It can be seen that pore structure is more disordered when compared with low molecular weight chitosan. As a result, it can be concluded that the low molecular weight chitosan is more favorable for production of biofoams.

Figure 4. 19. Biofoams produced by using high molecular weight chitosan (a) 1 % HMW CS, 10 volume % hexane, (b) 1 % HMW CS, 13 volume % hexane (c) 1 % HMW CS, 17 volume % hexane.
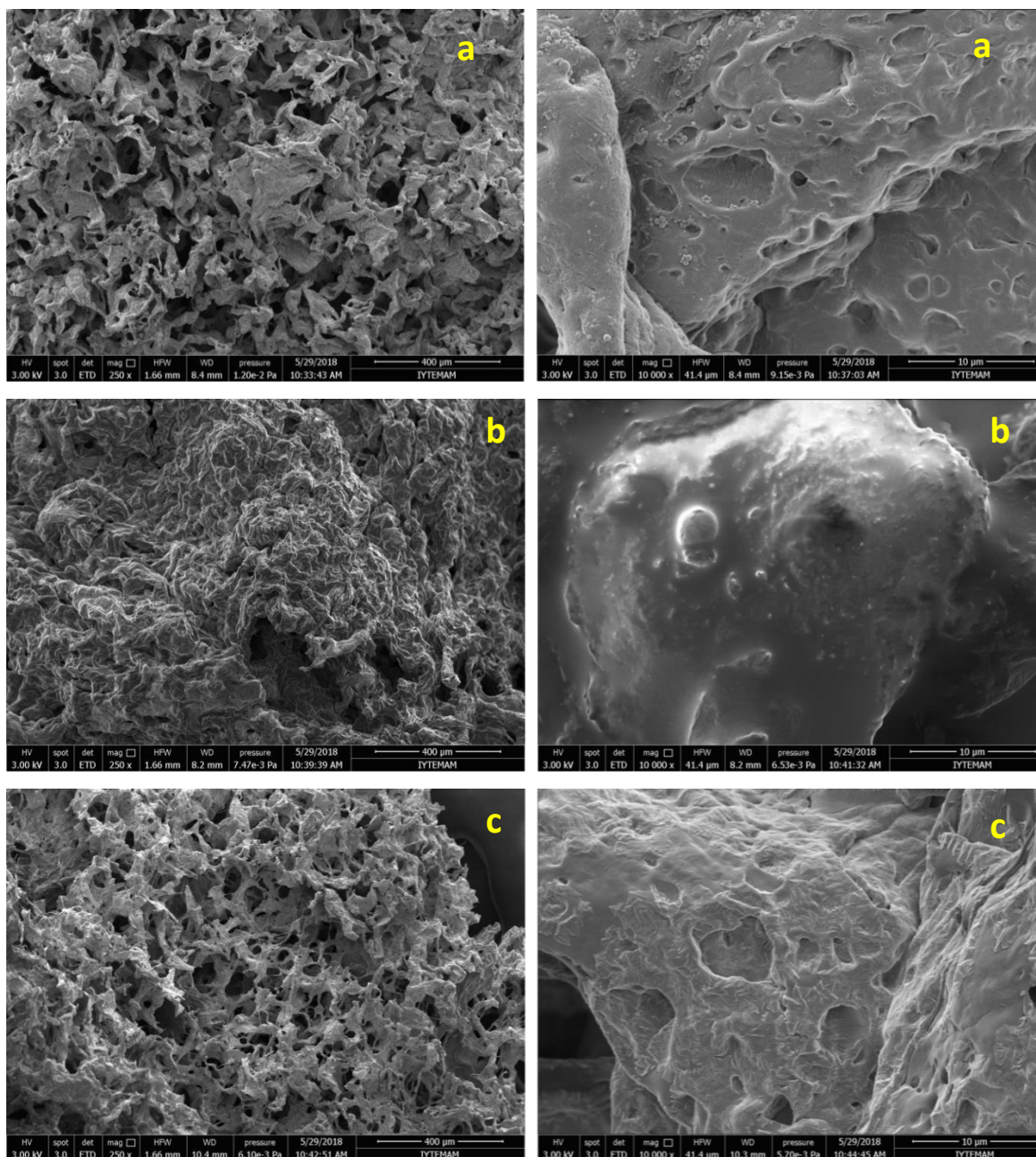
Figure 4. 20. SEM images for biofoams produced by using high molecular weight chitosan (a) 1 % HMW CS, 10 volume % hexane, (b) 1 % HMW CS,13 volume % hexane (c) 1 % HMW CS, 17 volume % hexane.

4.5. Foam Production Using O/W Emulsion Templated Method: SDS as a Crosslinking Agent

In this part of the study, SDS alone without TPP was used as an alternative crosslinking agent due to its negative charge. As it was discussed above the foams produced in the presence of SDS as a surfactant besides TPP were so brittle compared to the other surfactants. When it is used alone, on the other hand, produces much different foams. In these studies, hexane concentration was chosen to be 15 % with chitosan concentrations 2 % and 4 %. Two different SDS concentrations (10^{-2} and 10^{-3} M) were tested and the SEM images were presented in Figure 4.21. It can be seen from the images (Figure 4.21) that all SDS concentrations produced smaller sized porous structures compared to the ones crosslinked by TPP. Also, walls of the chitosan matrix have porous structure. After freeze drying, no deformation in the structure was observed in the case of SDS crosslinking.

The mechanical strengths of these foams were conducted and compression strength values were presented Table 4.4. It is seen that the biofoams which were crosslinked by SDS have higher compressive strength values compared with the other foams produced in this study (using TPP) and the literature. In this respect, chitosan biofoam crosslinked by SDS might be quite beneficial in wound dressing applications in terms of providing mechanical flexibility. As a result, it was thought that SDS can act as a crosslinking agent due to its negative charge similar to TPP.

Table 4. 4. Mechanical properties of the foams crosslinked by SDS

Sample Content	Compressive Strength (kPa)
4 % CS, 15 % hexane, 10^{-3} M SDS	201
4 % CS, 15 % hexane, 10^{-2} M SDS	255
2 % CS, 15 % hexane, 10^{-2} M SDS	186
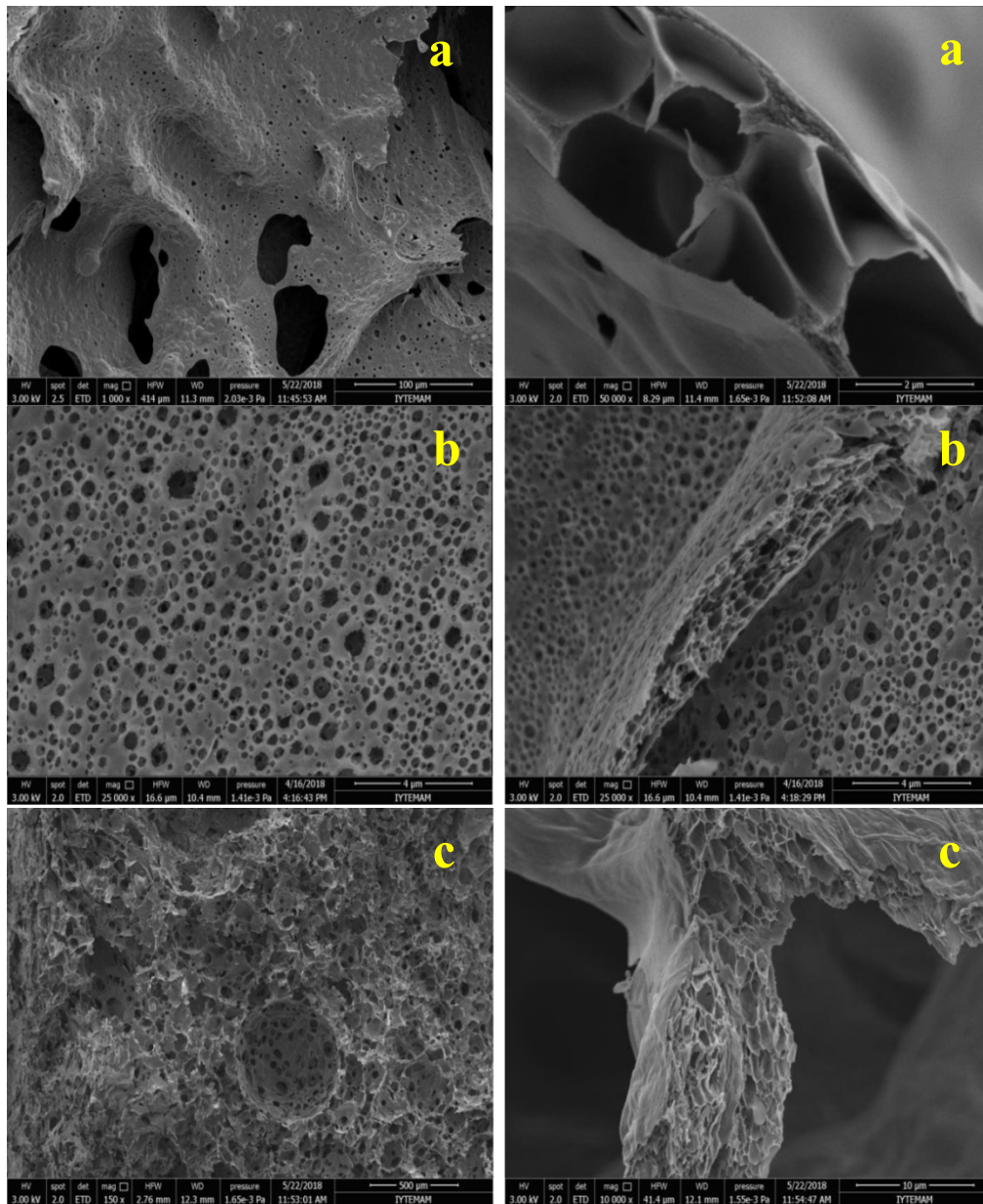
Figure 4. 21. SDS crosslinked chitosan foams (a) 4 % CS, 15 volume % hexane, 10^{-3} M SDS (b) 4 % CS, 15 volume % hexane, 10^{-2} M SDS (c) 2 % CS, 15 volume % hexane, 10^{-2} M SDS.

4.6. Foam Production Using O/W Emulsion Templated Method: Different Anionic Surfactants as Crosslinking Agents

The studies showed that the foams produced with SDS as a crosslinking agent have better pore structures and mechanical properties. This was attributed to the negative charge of SDS. Therefore, different type of anionic surfactants were also tested as crosslinking agents to clarify the effect of surfactant structure on forming foams. Octadecyl sulfate sodium salt has straight chain similar to the SDS and mono-N-dodecyl phosphate has helical chain. Hexane (15 %) was used as an oil phase to produce emulsions in these studies. SEM images of these foams are presented in Figure 22. As can be seen from the images that the both surfactants were also formed porous structures. However, the walls of the foams do not have porous structure. As a result, SDS can be choosen as an appropriate crosslinking agent for this system.
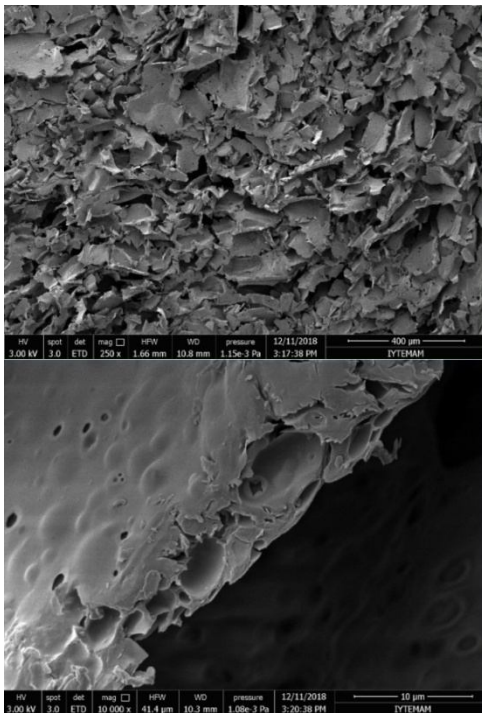
Octadecyl Sulfate Sodium Salt   **Mono-N-Dodecyl Phosphate**
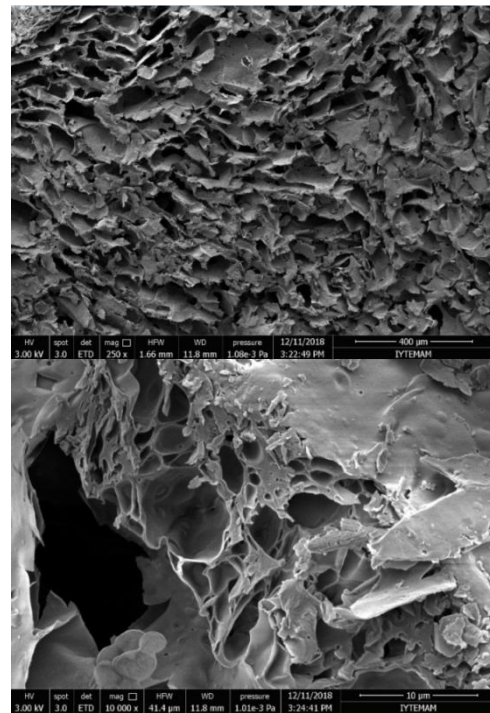
Figure 4. 22. SEM images of chitosan foam which was produced by O/W emulsion templated method in the presence of different anionic crosslinking agents.

4.7. The Role of an Oil Phase on Foam Production (SDS as a Crosslinking Agent)

After choosing the suitable cross linking agent as SDS, the role of oil phase in foam production was investigated. For this reason, first chitosan foams were produced in the absence of an oil phase. Then, the effect of an oil phase and oil concentration on the structure and mechanical strengths of foams were studied.

4.7.1. Chitosan Biofoam Production without an Oil Phase

In this part of the study, biofoams were produced in the absence of an oil phase to clarify the role of an oil phase in foam production. These experiments were carried out in two different concentrations of SDS as a crosslinking agent and the structure of the foams produced were characterized by SEM and the images were given in Figure 4.23. As can be seen from the SEM images that the foams show a porous structure even in the absence of an oil phase. However, the walls of the chitosan matrix seems to have no pores. This observation suggests the presence of two types of pores in the structure. One is the structural voids (macropores) produced even in the absence of an oil phase (at least oil phase is not directly responsible) and the other one is the intrinsic micro pores (micropores) produced in the walls of the chitosan matrix. The air phase that is involved (uncontrolled way) during the synthesis, may be mainly responsible from the structural large voids. But the shape and the size of pores might be still affected by the presence of an oil phase. The effect of oil phase, on the other hand, seems to be on the matrix structure of the foams (the porous in the walls). The structural voids were characterized using small SEM magnifications (x250) and the intrinsic micro pores were characterized using large SEM magnifications (x10,000).
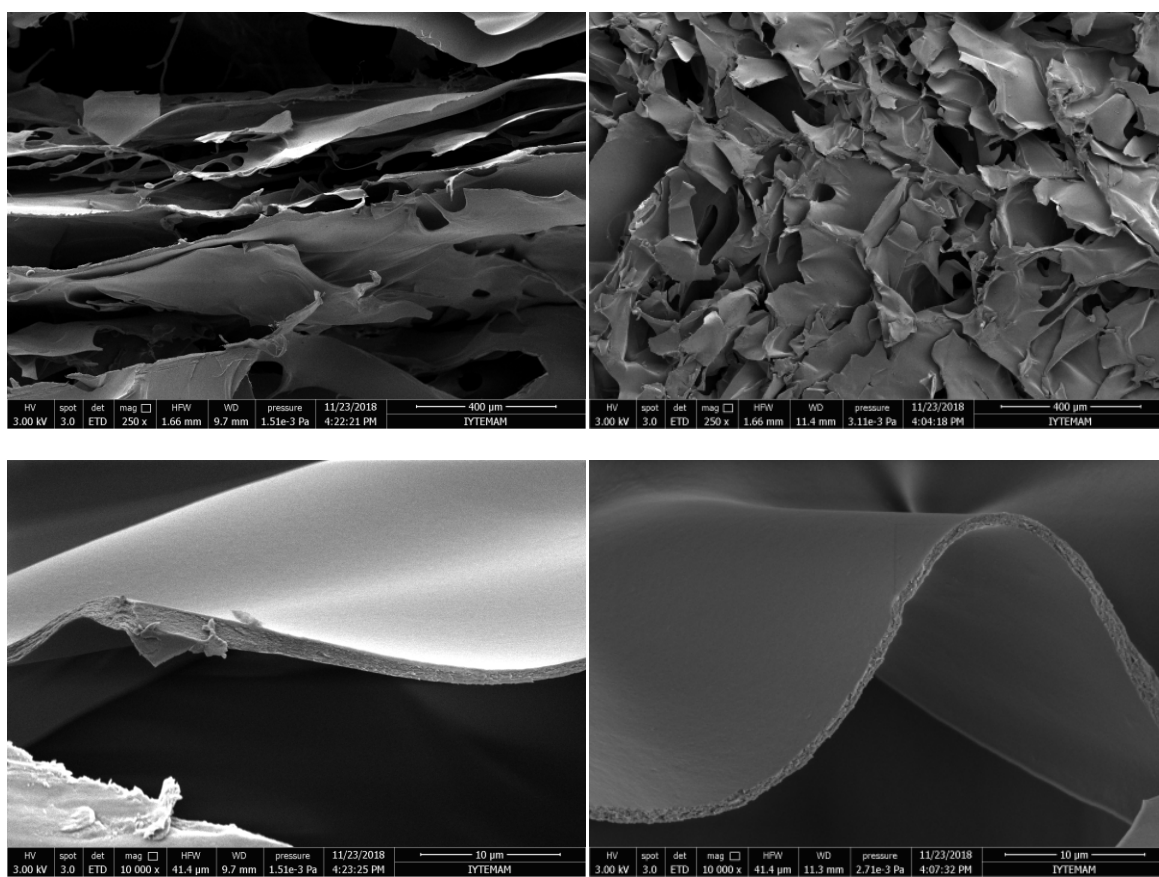
Figure 4. 23. SEM images of chitosan foam produced in the absence of oil phase (Cross linking agent: SDS).

BET analyses were conducted to estimate the surface area and micropore areas of porous materials. BET surface area and t-plot micropore area was found as 3.6083 m^2/g and 0.2608 m^2/g, respectively.

4.7.2. Effect of Oil Phase Type and Oil Concentration (SDS as a Crosslinking Agent)

In this part of the study, three types of oil (pentane, hexane and heptane) were used to see the effect of carbon chain length. The results of these studies were discussed in the following paragraphs.

4.7.2.1. Pentane as an Oil Phase

Pentane has a smaller carbon chain length compare to the those of haxane and heptane. The pentane concentrations were chosen as 15 and 25 volume %. Pore size and structure of these foams were characterized by SEM and the SEM images were presented in Figure 4.24. It can be seen from the images that the structures have both structural voids and intrinsic micro pores.

SDS Concentration, M

10⁻²   10⁻³

Pentane Concentration, volume %

15

25
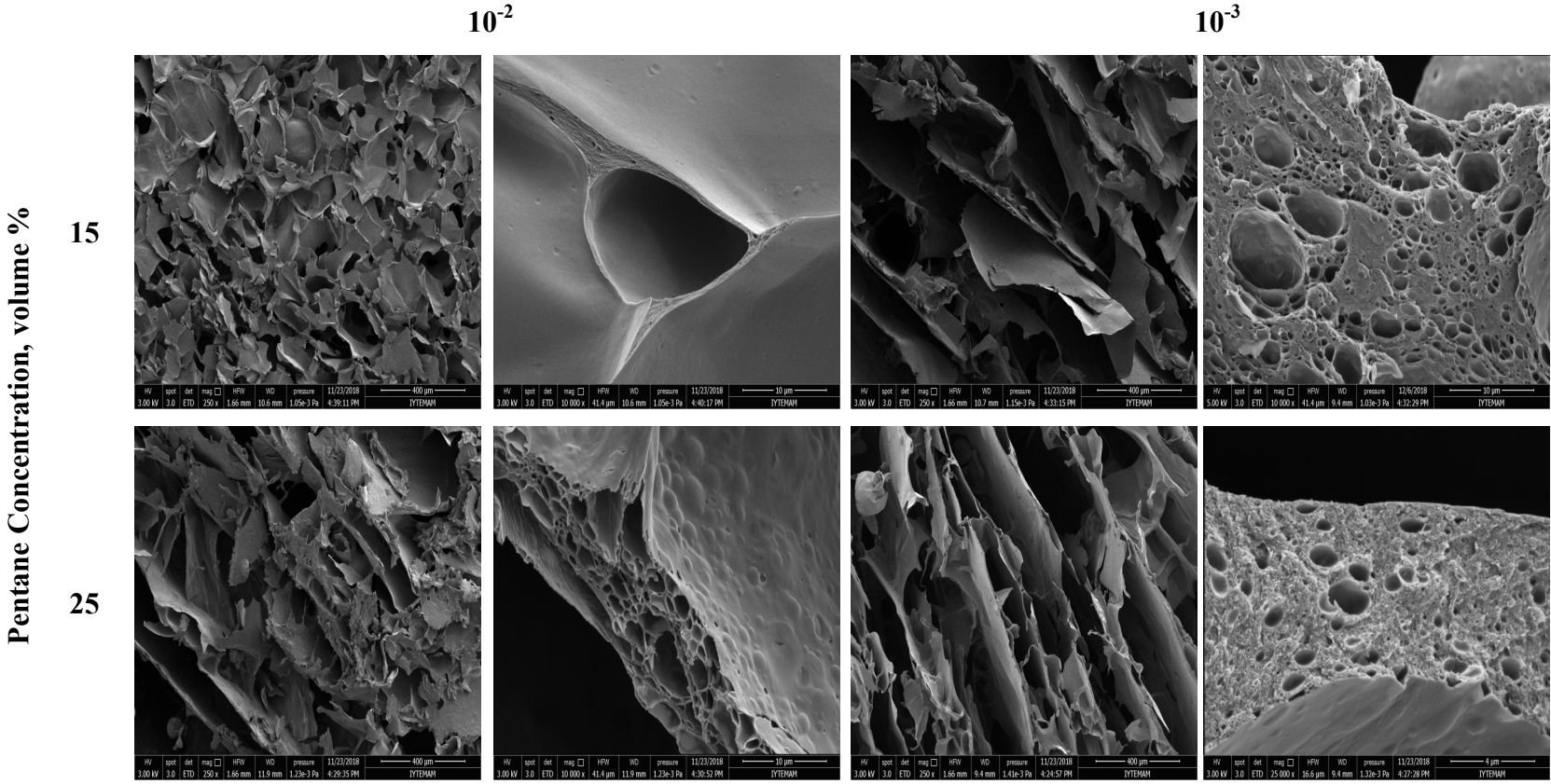
Figure 4. 24. SEM images of chitosan foam which produced with different SDS and pentane concentrations (Crosslinking agent: SDS).

It is important to remove all volatile oil phase during freeze process. Therefore, FTIR (with different spectral finger prints chemical structures/molecules) is used to check whether the samples contain any pentane. Figure 4.25 gives the results of FTIR analysis for all the samples and pentane itself alone. It can be seen from the figure that the characteristic bands of pentane in the 3000-2850 cm^{-1} region due to C-H stretch, almost disappears in the case of foams produced. However, there is also SDS as a cross linking agent in the system. The very small peaks in this region may belong to SDS which also have a peak at this region for C-H stretching. Hence, it can be said that all pentane was removed by applying freeze drying process and the foams produced do not contain any pentane.
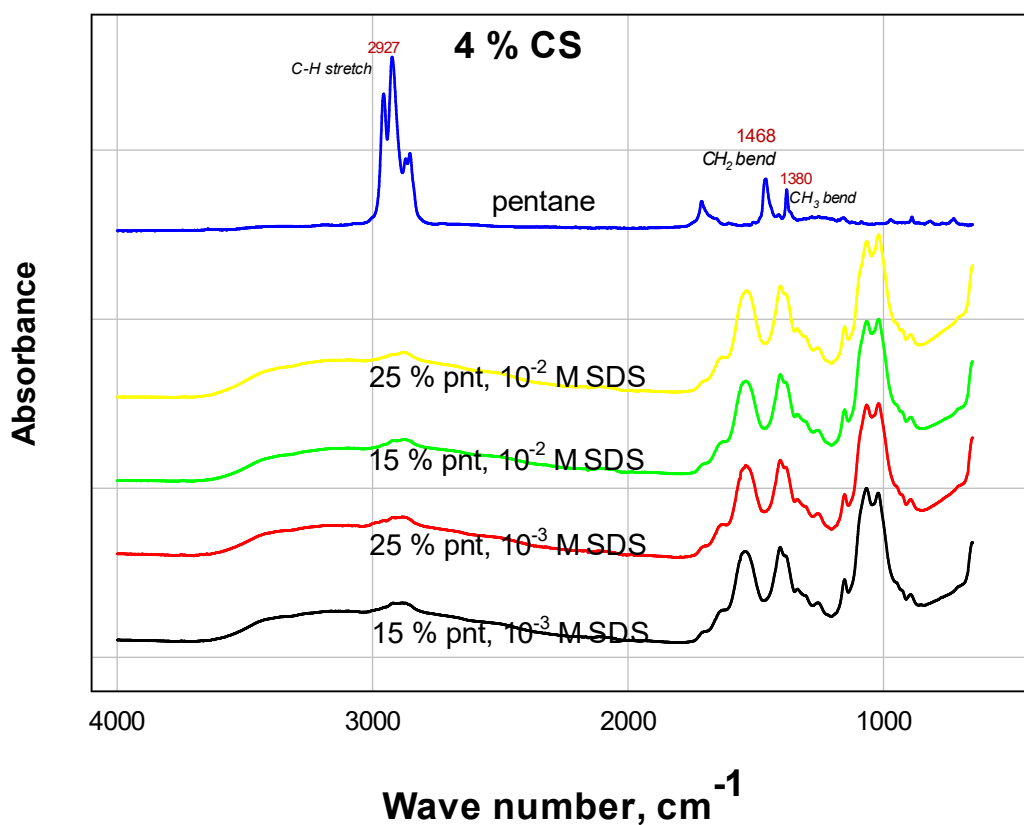
Figure 4. 25. FTIR results of foams produced by pentane/water emulsion templated method.

The BET analyses were done for the samples produced by 25 % pentane and 10^{-2} M SDS. BET surface area and t-plot micropore area were found as 9.4118 m^2/g and 10.6123 m^2/g, respectively.

The mechanical properties of these samples were evaluated by compressive strength measurements. The compression test results of the foams are given in Table 4.5. It can be seen that the foams produced have good mechanical strength when it is compared with literature. In addition, they have better compressive strength than the foams produced in the absence of oil phase.

Table 4. 5. Mechanical test results for foam produced by pentane/water emulsion templated method (4 % CS)

Sample Content	Compressive Strength (kPa)
15 % pentane, 10^{-3} M SDS	166
15 % pentane, 10^{-2} M SDS	180
w/o oil, 10^{-3} M SDS	76
w/o oil, 10^{-2} M SDS	12

4.7.2.2. Hexane as an Oil Phase

Hexane has higher carbon chain than pentane and smaller carbon chain than heptane. The hexane concentrations were chosen as 15 and 25 volume %. Pore size and structure of these foams were characterized by SEM and the images were presented in Figure 4.26. It can be seen from the images that the structures have both structural voids and intrinsic micro pores.

Crosslinking Agent (SDS) Concentrtion, M

10⁻²   10⁻³

Hexane Concentration, volume %

15
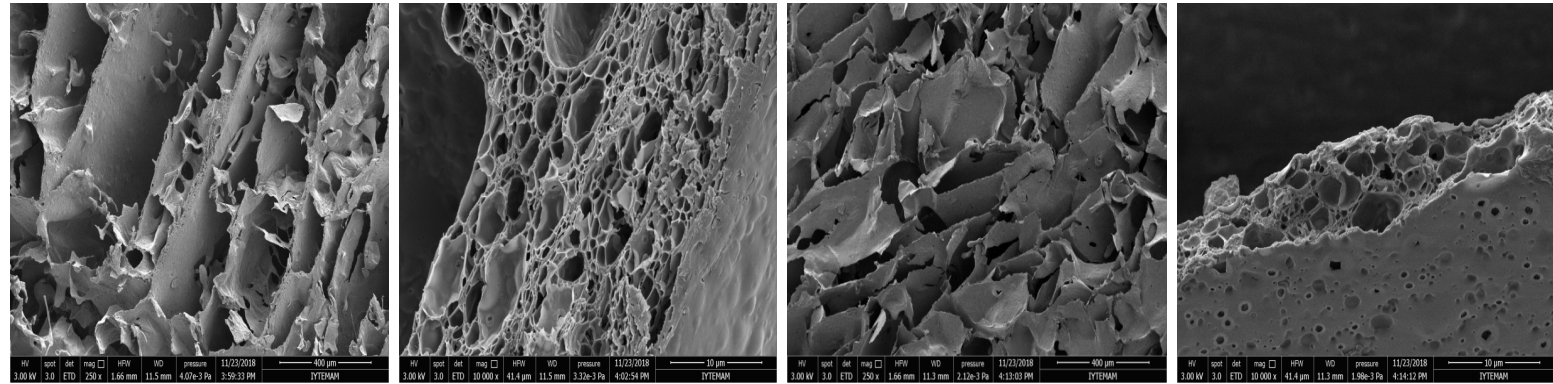
25
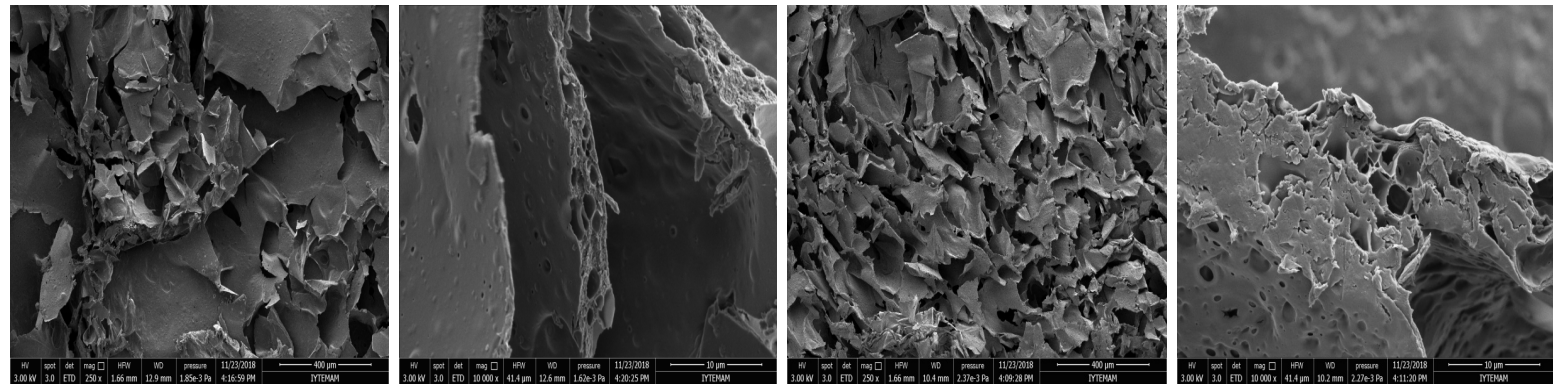
Figure 4. 26. SEM images of chitosan foam which produced with different SDS and hexane concentrations.

As mentioned before, it is important to remove all volatile oil phase during freeze process. Therefore, FTIR (with different spectral finger prints chemical structures/molecules) is used to check whether the samples contain any hexane. Figure 4.27 gives the results of FTIR analysis for all the samples and hexane itself alone. It can be seen from the figure that the characteristic bands of hexane in the 3000-2850 cm^{-1} region due to C-H stretch, almost disappears in the case of foams produced. However, there is also SDS as a cross linking agent in the system. The very small peaks in this region may belong to SDS which also have a peak at this region for C-H stretching. Hence, it can be said that all hexane was removed by applying freeze drying process and the foams produced do not contain any hexane.
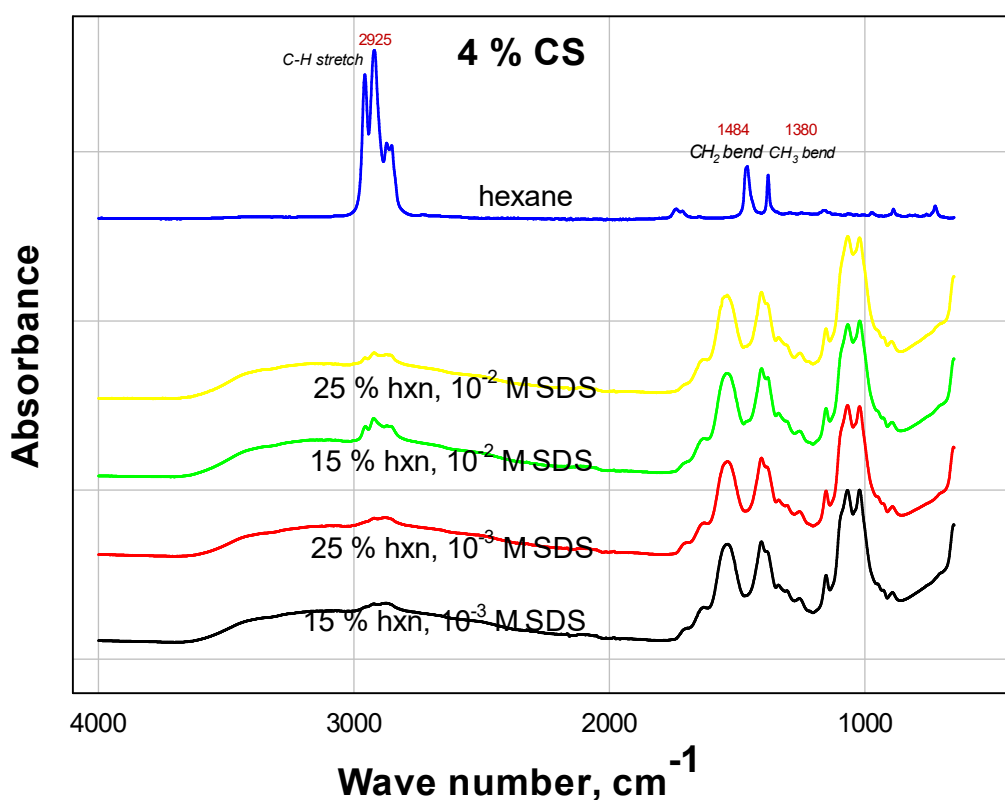
Figure 4. 27. FTIR results for foam produced by hexane/water emulsion templated method.

The BET analyses were done for the samples produced by 25 % hexane and 10^{-2} M SDS. BET surface area and t-plot micropore area were found as 1.8112 m^2/g and 3.7425 m^2/g, respectively.

The mechanical properties of these samples were evaluated by compressive strength measurements. The compressive strength of chitosan foams at 40 % strain was found to be 50 kPa in literature. The compression test results of our foams are given Table 4.6. It can be seen that the foams produced have good mechanical strength when it is compared with literature. In addition, they have better compressive strength than the foams produced in the absence of oil phase and in the presence of pentane.

Table 4. 6. Mechanical test results for foam produced by hexane/water emulsion templated method (4 % CS)

Sample Content	Compressive Strength (kPa)
15 % hexane, 10^{-3} M SDS	201
15 % hexane, 10^{-2} M SDS	255
w/o oil, 10^{-3} M SDS	76
w/o oil, 10^{-2} M SDS	12

4.7.2.3. Heptane as an Oil Phase

Heptane does not have the environmental and health concerns that are associated with pentane and hexane hence because of the similarity of the oils, heptane was used as oil phase to produce chitosan foam. Heptane has longer carbon chain length than both pentane and hexane. Heptane concentrations were chosen as 15, 25 volume %. Pore size and structure of these foams were characterized by SEM and the images were presented in Figure 4.28. It can be seen from the images that the structures have both structural voids and intrinsic micro pores. In addition, as can be seen from the images that there is bubbles on the surface. This may be explained by high carbon chain and low volatility of heptane.

Crosslinking Agent (SDS) Concentration, M

10^{-2} 10^{-3}
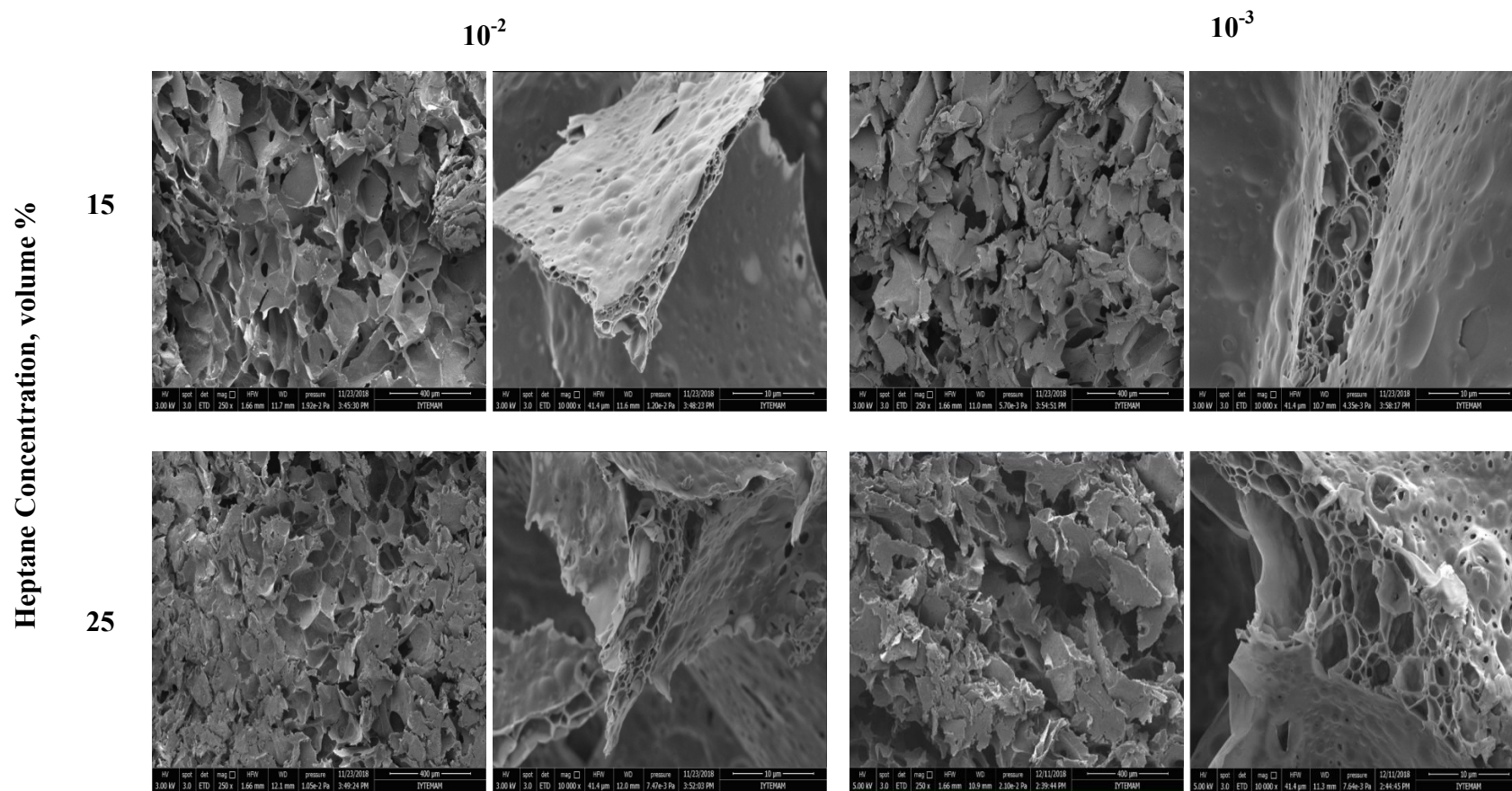
Figure 4. 28. SEM images of chitosan foam which produced with different SDS and heptane concentrations.

FTIR (with different spectral finger prints chemical structures/molecules) are used to check whether the samples contain any heptane. Figure 4.29 gives the results of FTIR analysis for all the samples and heptane itself alone. It can be seen from the figure that the characteristic bands of heptane in the 3000-2850 cm^{-1} region due to C-H stretch. Although almost all bands of heptane disappear in the case of foams produced, foams which produced by higher amount of heptanes have more significant peaks than others. The small peaks might be due to unremoved heptane. However, there is also SDS as a cross linking agent in the system. The very small peaks in this region may belong to SDS which also have a peak at this region for C-H stretching.
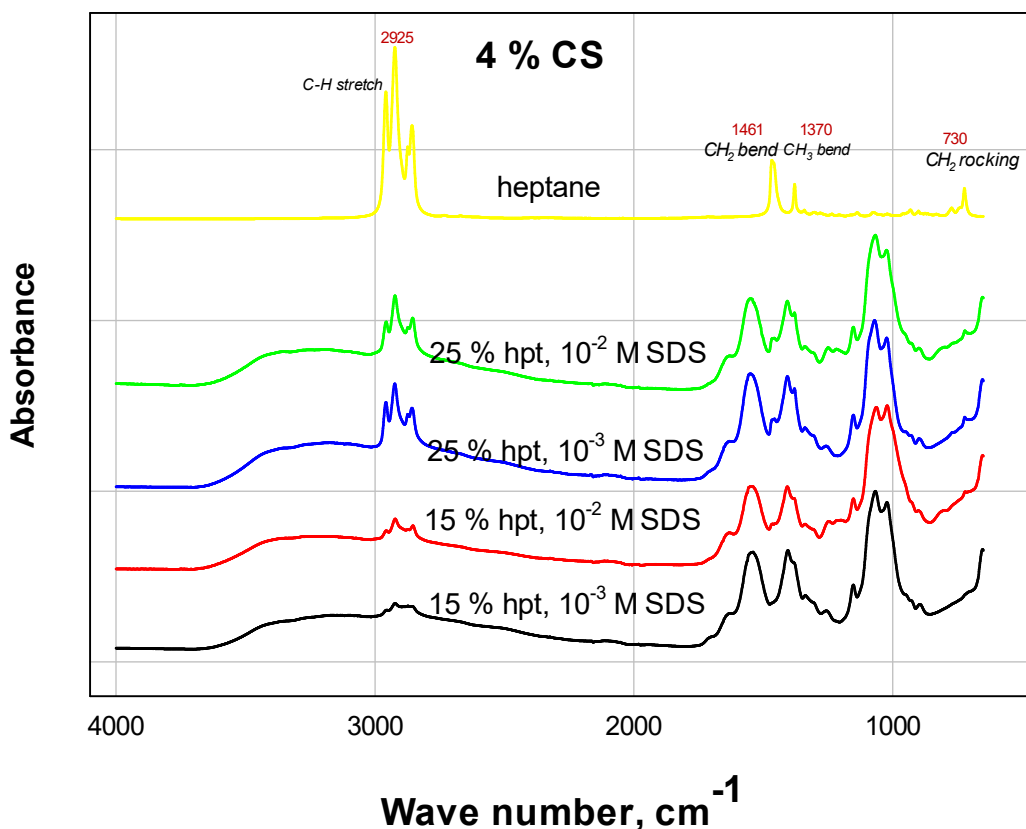
Figure 4. 29. FTIR results for foam produced by heptane/water emulsion templated method.

The BET analyses were done for the samples produced by 25 % heptane and 10^{-2} M SDS. BET surface area and t-plot micropore area were found as 8.3991 m^2/g and 2.1562 m^2/g, respectively. If the results are compared with pentane (10.6123 m^2/g) and hexane (3.7425 m^2/g), t-plot micropore areas for samples produced by pentane is

smaller. These results show that oil phase with smaller carbon chain produces higher micropore areas due to high volatility and low molecular weight. Also foam produced in the absence of oil phase has the smallest micropore area (0.2608 m^2/g). This may be due to not presence of intrinsic micro pores.

The mechanical properties of these samples were evaluated by compressive strength measurements. The compressive strength of chitosan foams at 40 % strain was found to be 50 kPa in literature (Hu et al. 2018). The compression test results of our foams are given in Table 4.7. It can be seen that the foams produced have good mechanical strength when it is compared with literature. In addition, they have better compressive strength than the foams produced in the absence of oil phase.

Table 4. 7. Mechanical test results for foam produced by heptane/water emulsion templated method

| Sample Content	Compressive Strength (kPa)
15 % heptane, 10^{-3} M SDS	148
15 % heptane, 10^{-2} M SDS	103
10^{-3} M SDS	76
10^{-2} M SDS	12

4.7.2.4. Porosity and Water Hold-up/Release Behavior of the Chitosan Foams

To determine the porosity and water hold-up/release behavior of the chitosan foams, foams were produced at three different chitosan concentrations and two different concentrations of oil phase. SDS was the crosslinking agent (Figure 4.30). As can be seen from the SEM images that the chitosan foams show two types of porous structure as intrinsic micro pores and structural voids. As it was discussed in the previous part of the study, the intrinsic micro pores (micropores) were produced in the walls of the chitosan matrix in addition to the structural voids (macropores). The effect of oil phase seemed to be on the matrix structure of the foams (the pores in the walls). The structural voids were characterized using small SEM magnifications (x500) and the intrinsic

micro pores were characterized using large SEM magnifications (x10,000). Both structural voids and micropores are smaller for low chitosan concentrations.
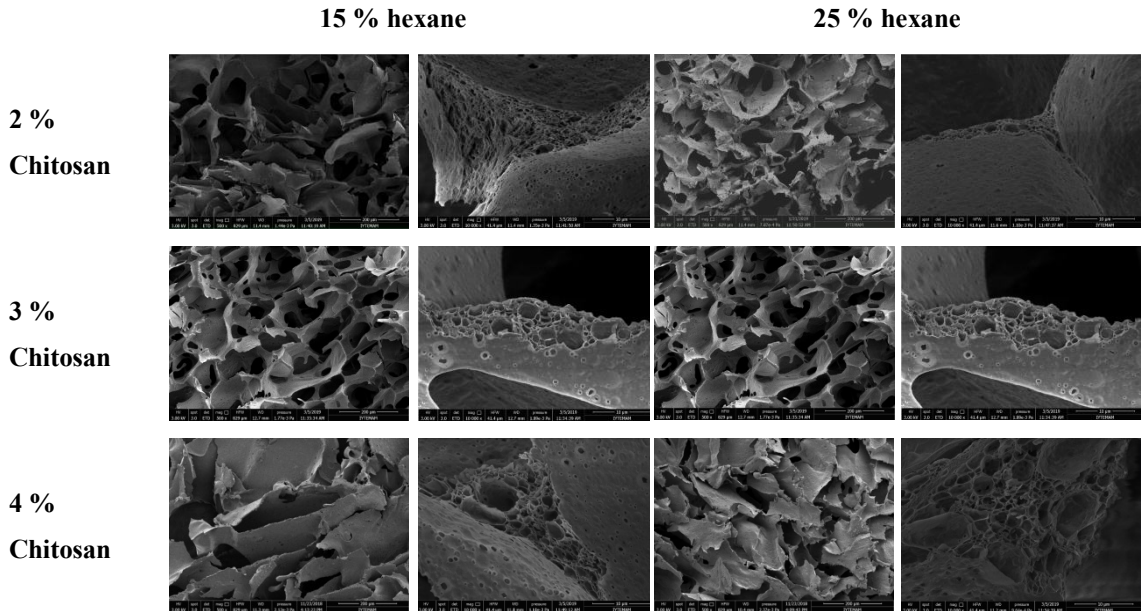
Figure 4. 30. Structure of produced chitosan biofoams for different chitosan and hexane amount.

Then, water immerse tests were conducted using chitosan foams to observe the amount of water that hold-up in structure and its release behavior with time. Effect of chitosan concentration and oil phase (hexane) percentages on release behavior was studied. For this purpose, first, the samples were dried at 50 ^{o}C in oven and weighed. Then, they are left in water for some time to weight again to determine the amount of water hold-up. The results of these studies were presented in Figure 4.31. It can be said that almost all foams can hold water nearly twenty times of their weight.
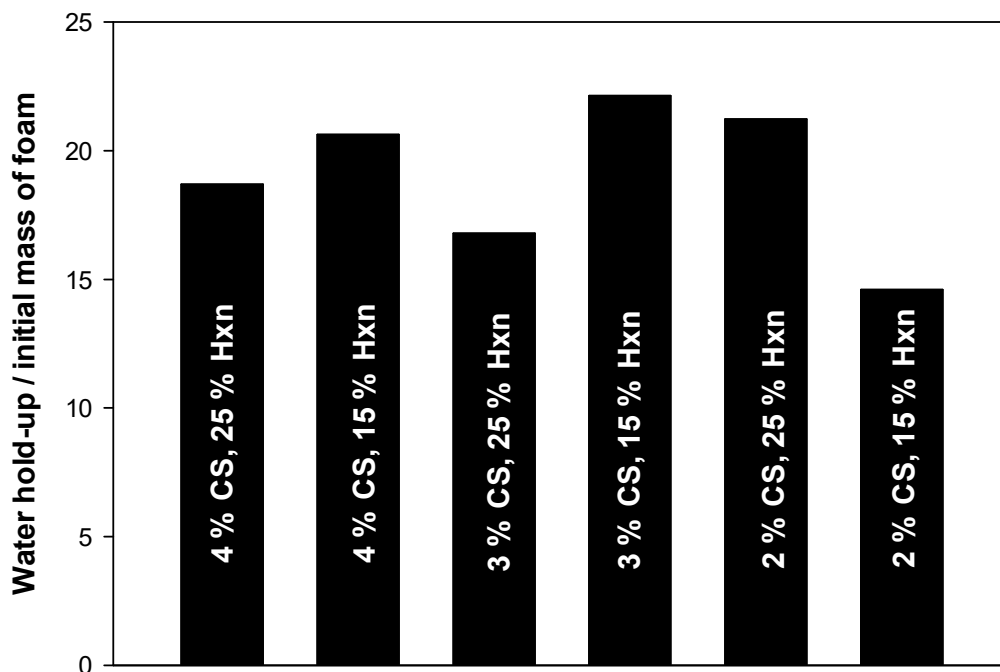
Figure 4. 31. Water hold-up ratios to initial mass of foams.

For the water release tests, the foams were dried and then immersed in water for a day. Then, they were weighted in time intervals to see the release amount of water. As can be seen from Figure 4.32 that water release is slower for the higher chitosan concentration. This can be due to high pore size and low porosity of the foams produced by high chitosan concentration. There is no significant effect of the hexane amount on water release behavior.
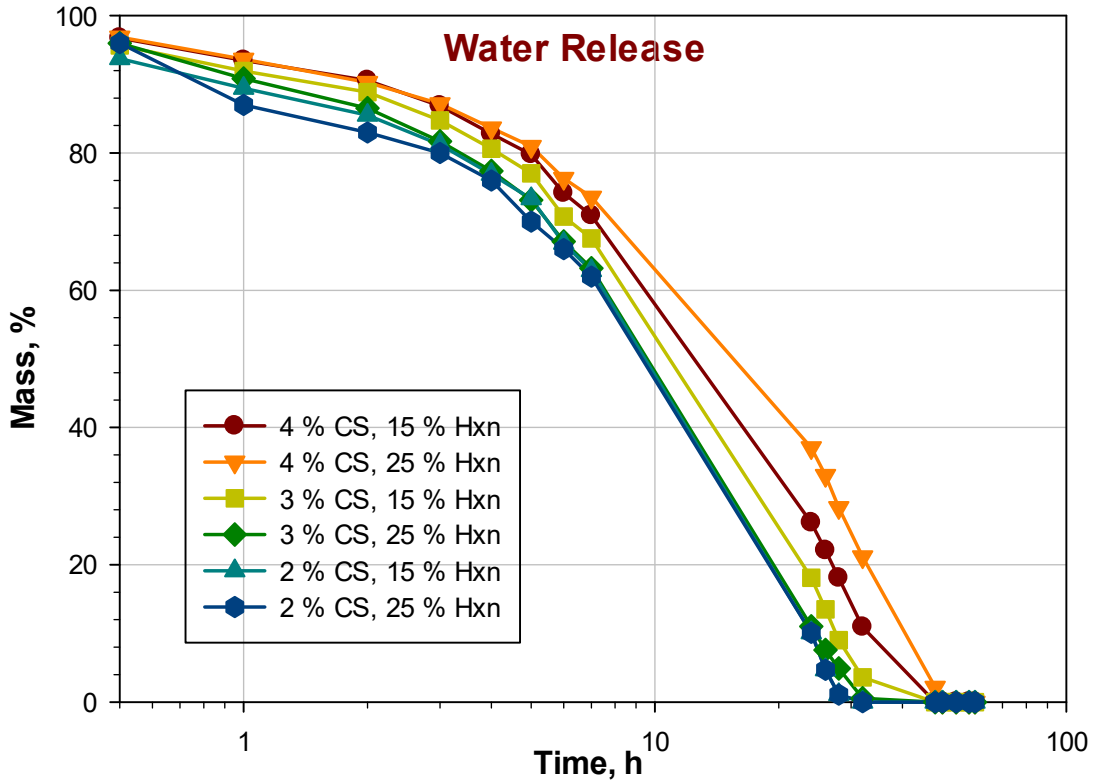
Figure 4. 32. Water release behaviour of the chitosan foams.

Based on these results the porosities of foams were calculated and the results are presented in Table 4.8. Dimensions of the chitosan foams produced were measured and they were dried to weigh. Air volume and porosity was calculated using equations given above (Equation 3.1 and Equation 3.2) for chitosan foams with varying chitosan and oil phase concentrations. As can be seen from the table that, the porosity of the foams depends on the percentage of chitosan and oil phase. The porosity increases with decreasing chitosan concentration and decreasing oil concentration. Moreover, the porosity of all the foams are higher than the ideal value, 80 % mentioned in literature (Ikeda et al. 2014). Hence, one can conclude that the foams produced in this study will be all suitable for wound dressing applications.

Table 4. 8. Porosities of the foams for different chitosan and oil phase concentrations

Sample	Porosity, %	
4 % CS, 15 % hxn	91.25	
4 % CS, 25 % hxn	90.47	
3 % CS, 15 % hxn	93.96	
3 % CS, 25 % hxn	93.75	
2 % CS, 15 % hxn	95.04	
2 % CS, 25 % hxn	94.83	
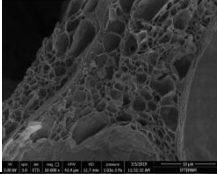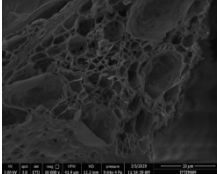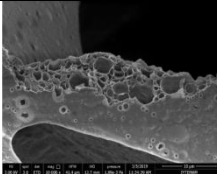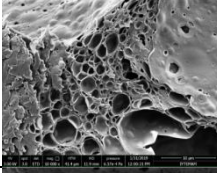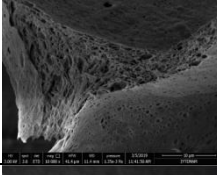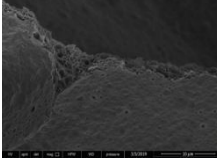
CHAPTER 5

PRODUCTION OF DRUG LOADED CHITOSAN FOAMS

This part of the study is on the production of drug loaded chitosan foams. For this purpose two types of drugs as hydrophilic and hydrophobic were selected. The hydrophobic drugs used were curcumin and amphotericin-B (a model anti-inflammatory and antibiotic drugs) and the hydrophylic drug was a model antibiotic vancomycin hydrochloride which is used to treat infections. The morphological and chemical characterization of chitosan foam structures (drug loaded in these experiments) were done by SEM and FTIR as usual.

5.1. Hydrophilic Drug Loaded Foam Production using O/W Emulsion Templated Method

To produce drug loaded chitosan foams, hexane was used as an oil phase to produce emulsions as templates and drug was dissolved in chitosan solution. The system was polymerized by both SDS and TPP, separately. The SEM images of the foams are presented in Figure 5.1. As can be seen from the figure that the foam have both structural voids and intrinsic micro pores. In addition these foams which were crosslinked by SDS were found to have a durable structure. However, the foams crosslinked by TPP has broken into small peices. SEM images of these foams look very much the same with the foams without drug. This is most probably due to the dispersion of hydrophilic drug within the chitosan matrix. Therefore the presence of drug was demonstrated using FTIR analysis.

SDS	TPP
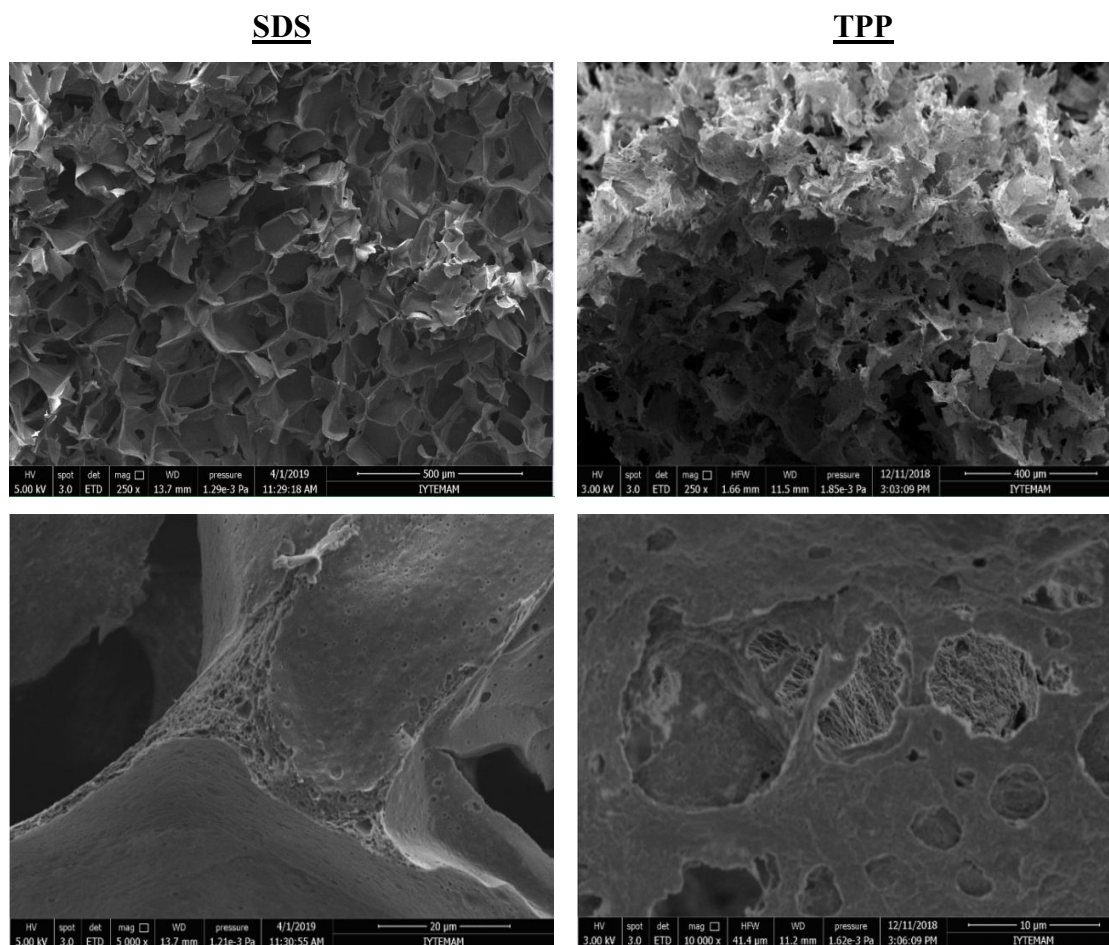
Figure 5. 1. SEM images of vancomycin loaded chitosan biofoam production by O/W emulsion templated method.

FTIR analyses were carried out to confirm the presence of drug vancomycin in the chitosan biofoam structure. The FTIR spectra of chitosan, vancomycin, and foams produced which were crosslinked by SDS and TPP are shown in Figure 5.2 and 5.3, respectively. The characteristic absorption bands of vancomycin were found at 3450 cm^{-1} for O-H (hydroxyl) stretching, 1655 cm^{-1} for C=O stretching (Amide-I), 1504 cm^{-1} for C=C stretching (aromatics), 1231 cm^{-1} for C-O-C stretching (phenols) and 1062 cm^{-1} for C-N (aliphatic amine) stretching. The pure chitosan shows characteristic bands at 3441 cm^{-1} for O-H (hydroxyl) stretching, 2856 cm^{-1} for C-H stretching, 1630 cm^{-1} for C=O stretching (Amide-I) and 1317 cm^{-1} for C-N (aliphatic amine) stretching. The produced biofoams involved these characteristic peaks of the chitosan and vancomycin. As can be seen from the figures, the hydroxyl stretching existed in the chitosan and vancomycin was less obvious in the biofoams. This can be explained by hydrogen

bonding between the vancomycin and chitosan through amine and hydroxyl groups. In additon, SDS have peaks 2850-2950 cm^{-1} band for C-H stretching and biofoam crosslinked by SDS have these peaks as can be seen in Figure 5.2.
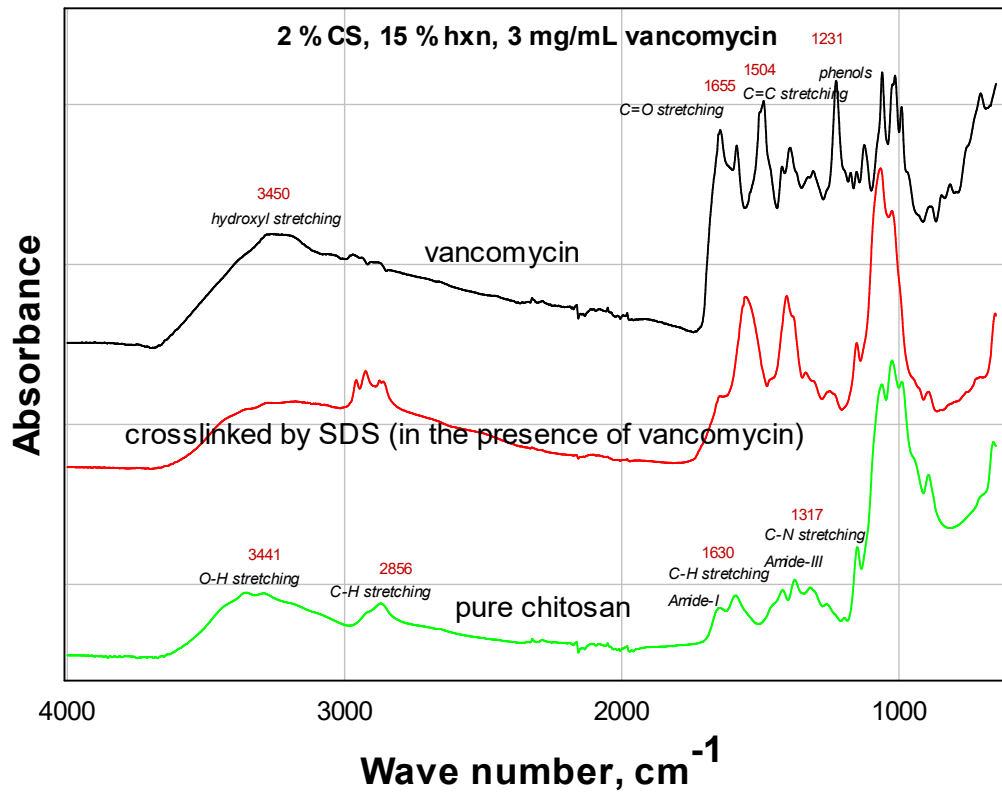
Figure 5. 2. FTIR analysis of drug loaded chitosan biofoam production by O/W emulsion templated method (SDS as a crosslinking agent).
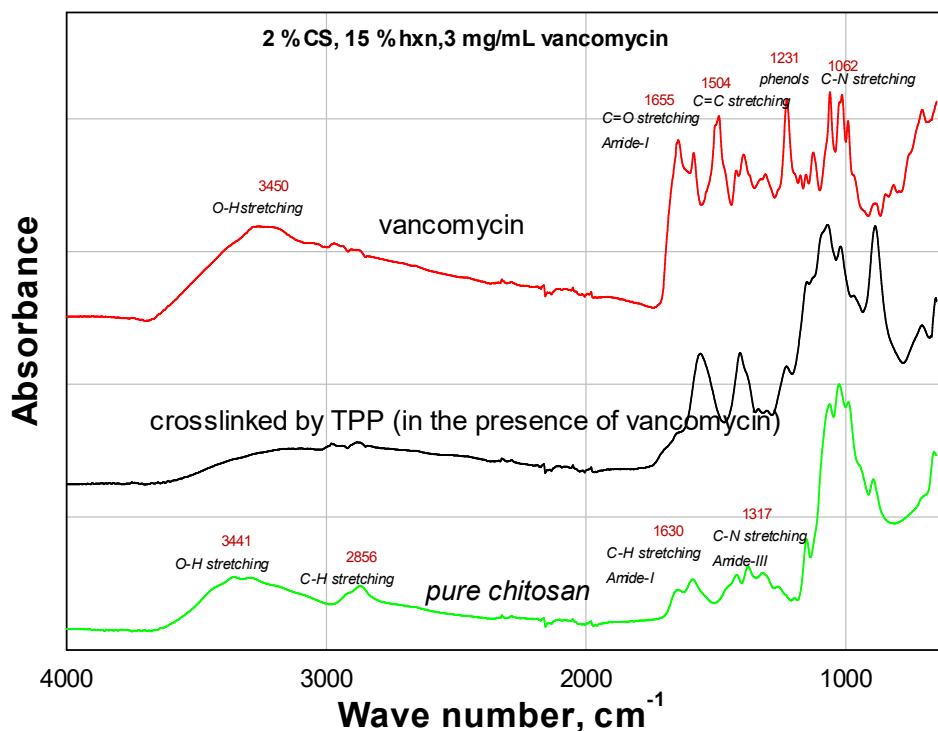
Figure 5. 3. FTIR analysis of drug loaded chitosan biofoam production by O/W emulsion templated method (TPP as a crosslinking agent).

5.2. Hydrophobic Drug Loaded Foam Production Using a Thin Film Evaporation Method Coupled with the O/W Emulsion Templated Method

Hydrophobic drug loaded chitosan foams were produced with a thin film evaporation method coupled with the O/W emulsion template method. In thin film evaporation part of the method, the micelles of P-123 molecules that envelope hydrophobic drugs were produced. Therefore, this part of the method will be discussed in detail in the following paragraphs.

5.2.1. Preparation and Characterization of P-123 Micelles with and without Curcumin

Before producing drug loaded chitosan foams, P-123 micelles were characterized with and without curcumin. Also, effect of micelle formation methods was examined.

5.2.1.1. P-123 Micelles in Water

First of all, drug loaded P-123 micelles were produced using the procedure given in experimental part. In this method, both P-123 and curcumin were dissolved in ethanol and ethanol was evaporated and a thin film of P-123 and curcumin was obtained. When this film was dissolved in water, drug loaded micelles were produced. The details of this method were given above. These micelles were characterizated using several different methods such as DLS, STEM, TEM. The size and charge distributions of P-123 micelles formed at concentration of 10^{-3} M were presented in Figures 5.4 and 5.5, respectively. Figure 5.4 gives the size distribution of P-123 micelles obtained by DLS. It can be clearly seen that average size of micelles are around 20 nm as also mentioned in literature (Dutra et al. 2015). In addition, size of micelles were also observed by STEM and TEM (Figure 5.6). These results also show that the size of P-123 micelles are around 20 nm. In addition, P-123 micelles were found to be slightly negatively charged (Figure 5.5) as expected.
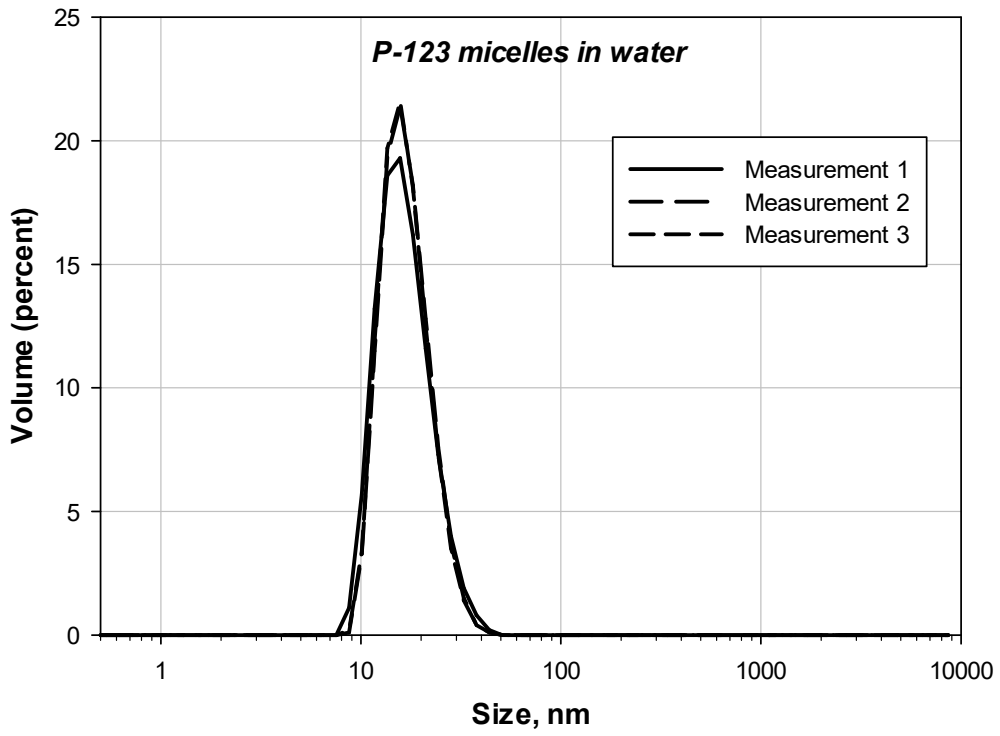
Figure 5. 4. Size distribution of P-123 micelles in water by DLS.
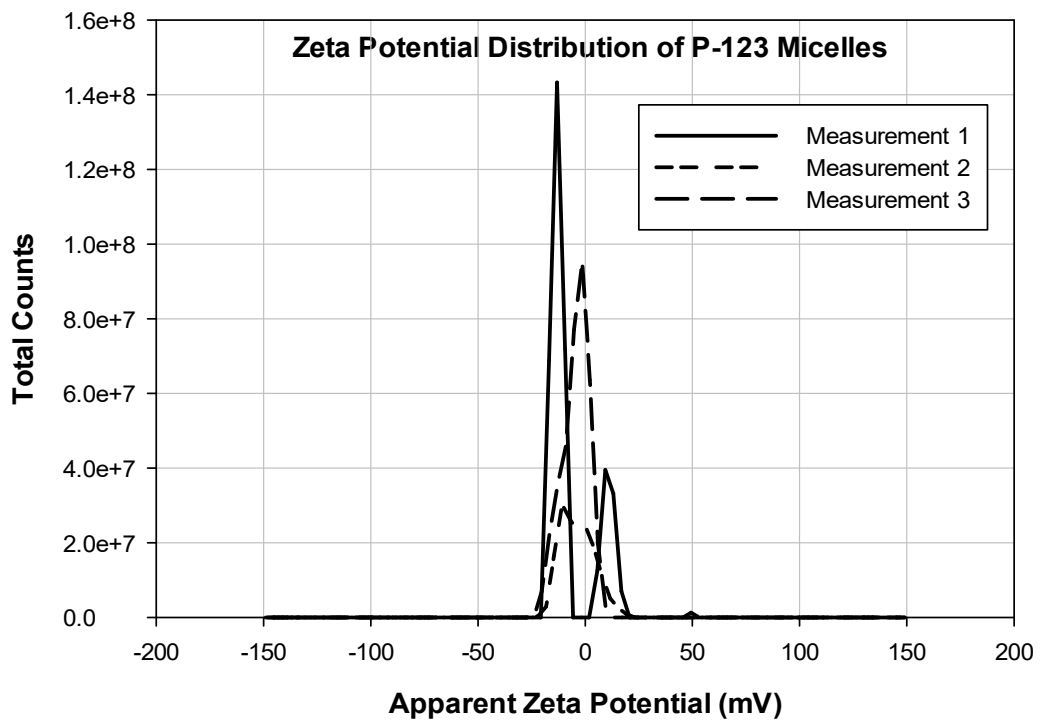
Figure 5. 5. Charge of P-123 micelles in water.

STEM

AFM

TEM
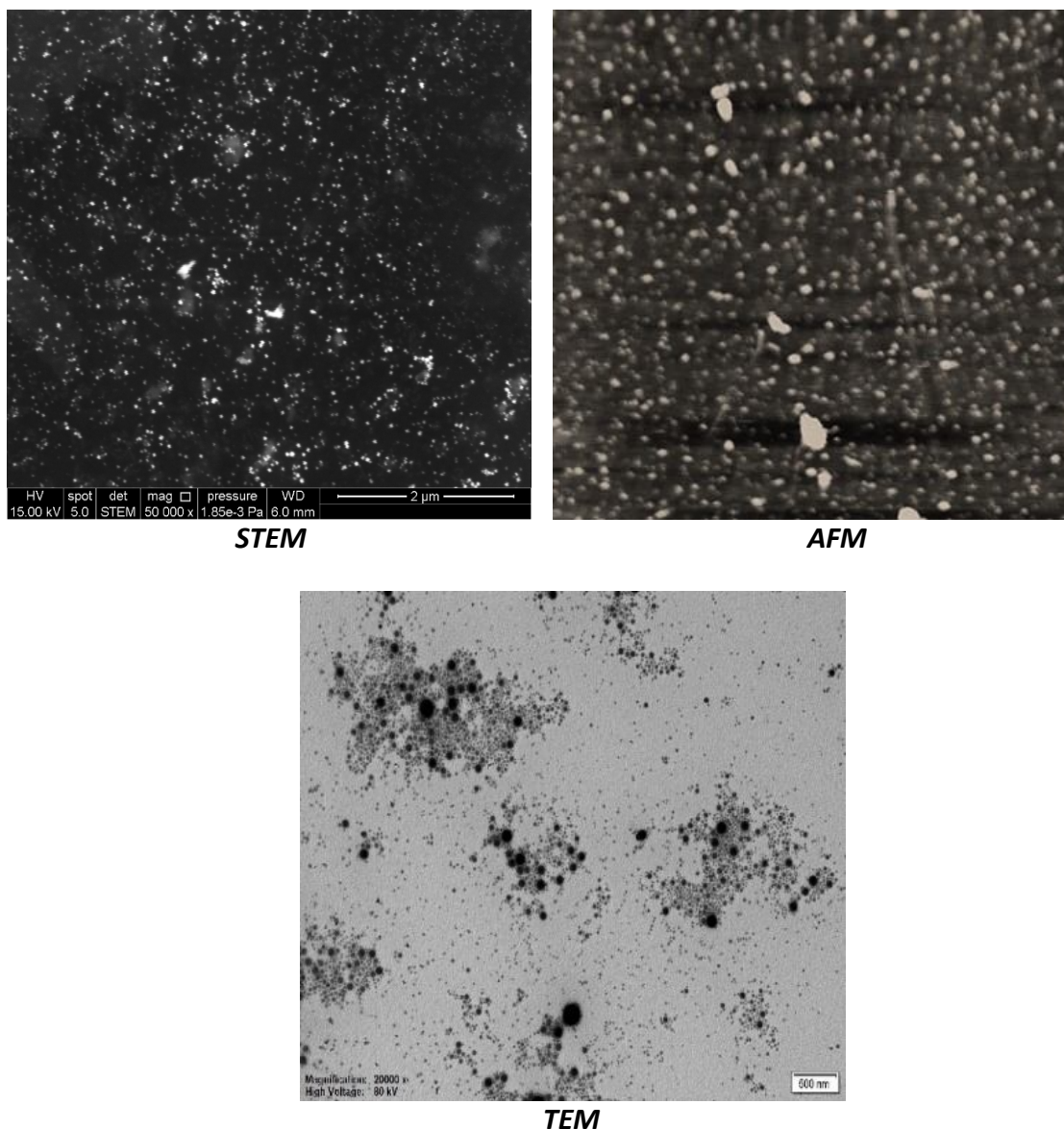
Figure 5. 6. Characterization of P-123 micelles by STEM, AFM and TEM.

5.2.1.2. P-123 Micelles in Water in the Presence of Chitosan Molecules

The stability of P-123 micelles in the presence of chitosan molecules were studied by mixing with chitosan solutions at different concentrations. That is, first P-123 micelles were formed in water and then chitosan molecules were added at different amounts. Figure 5.7 gives the size distribution for P-123 micelles in water in the presence of chitosan molecules. It can be seen that an increase in chitosan concentration increases the size of P-123 micelles. Since, there is only one mode size distribution, one can conclude that chitosan molecules contribute to the structure of micelles. As can be

seen from Figure 5.8 that the size of P-123 micelles increases with increasing chitosan concentration up to 160 nm in the presence of 2 % chitosan.
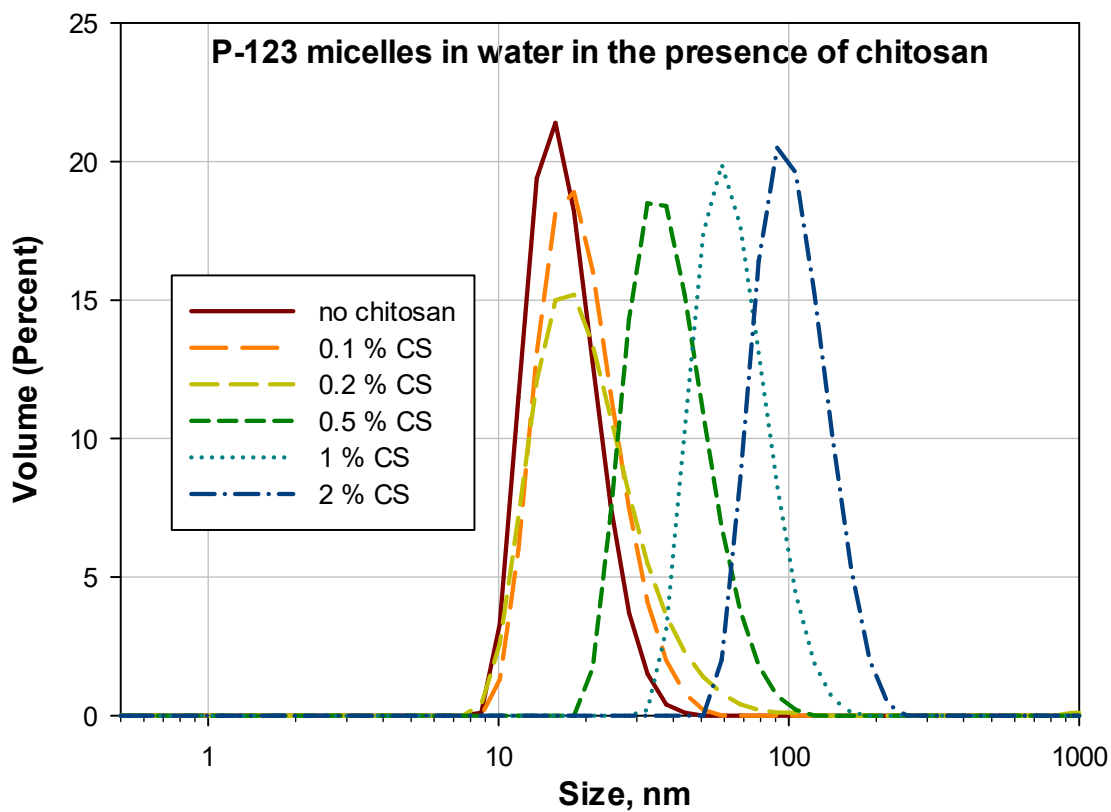
Figure 5. 7. Size distribution of P-123 micelles in water in the presence of chitosan.
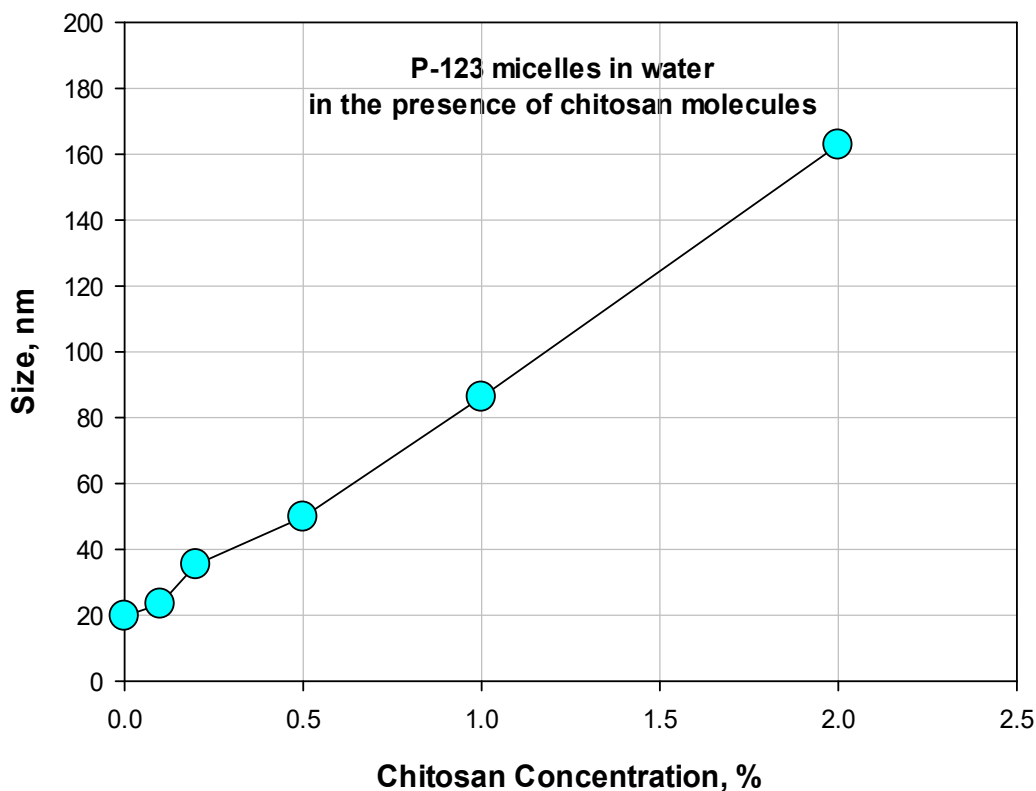
Figure 5. 8. Effect of chitosan concentration on P-123 micelle size in water in the
presence of chitosan.

5.2.1.3. P-123 Micelles Formed in Chitosan Solution

In this part of the study, P-123 micelles were directly formed in chitosan
solutions. First, chitosan molecules in water without P-123 micelles at different
concentrations were analyzed and presented in Figure 5.9. It is seen that the size of
chitosan molecules are larger than 1 micron on average (Figure 5.10). The size of a
chitosan molecule, on the other hand, is over 1 micron on average which is in the range
given literature (Sreekumar et al. 2018).
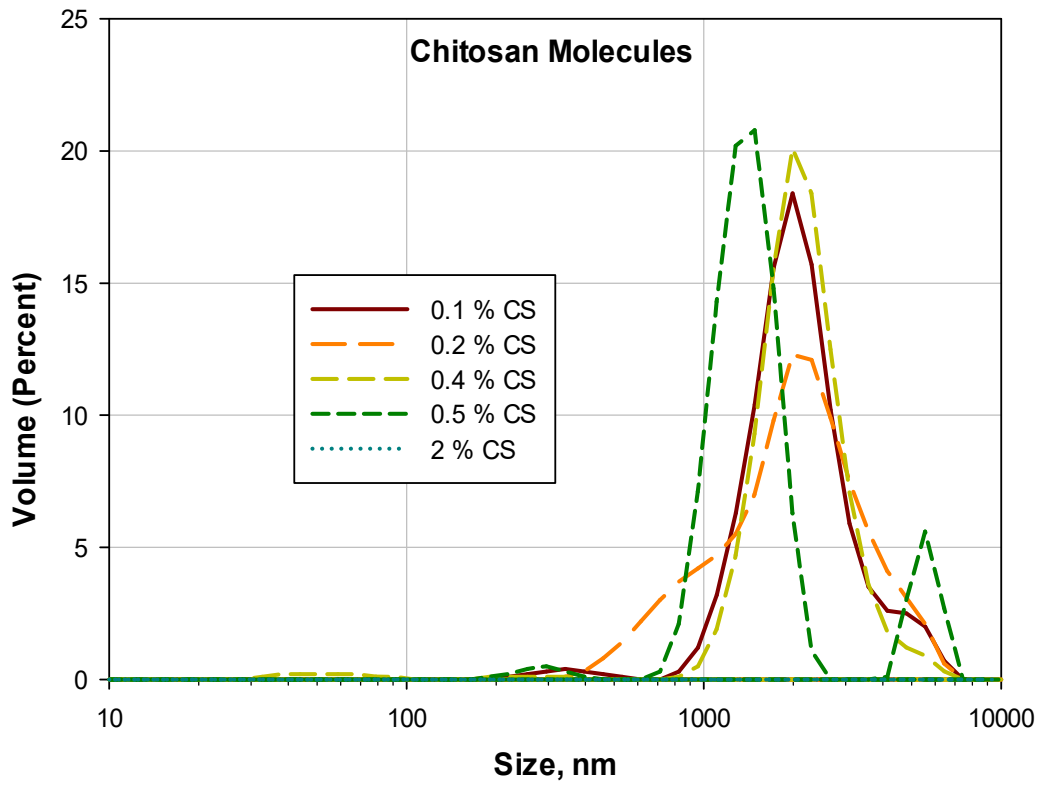
Figure 5. 9. Size distribution of chitosan solutions at different concentrations.
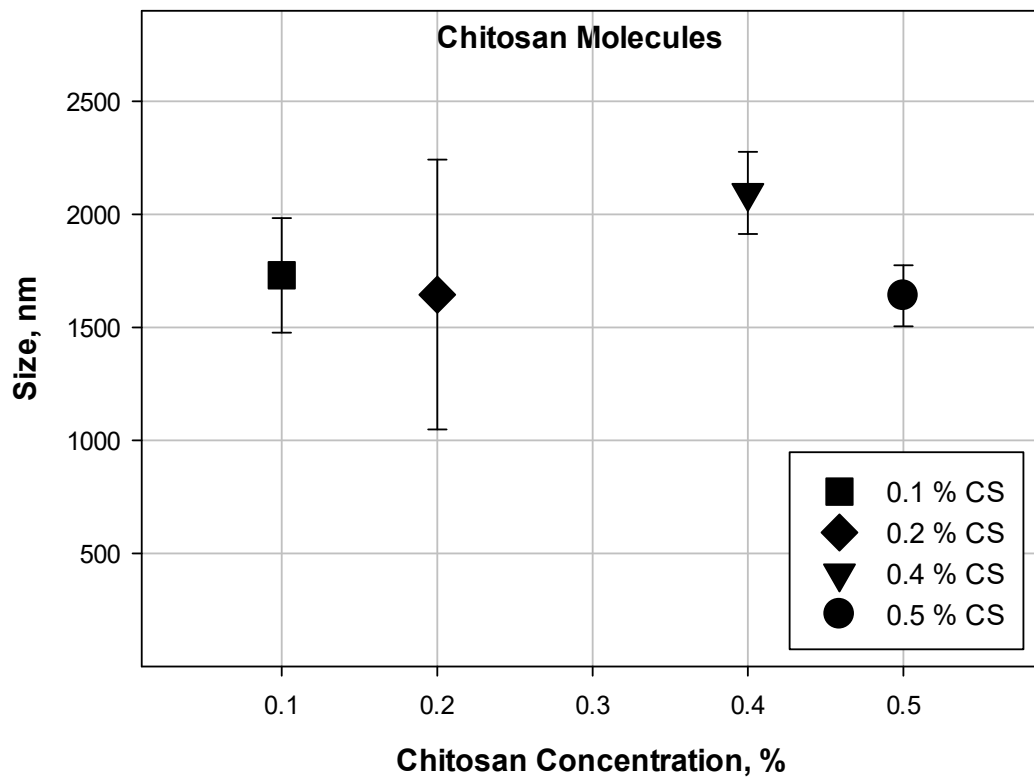
Figure 5. 10. Average sizes of chitosan molecules for different concentrations.

P-123 micelles in chitosan solutions give size distributions very similar to the ones that chitosan added to the P-123 micelle solution later (Figure 5.11). It is seen that the size of micelles increases with increasing chitosan concentrations. When it was compared with the chitosan molecules, it can be seen that sizes of chitosan molecules seem to decrease in the presence of P-123 micelles.
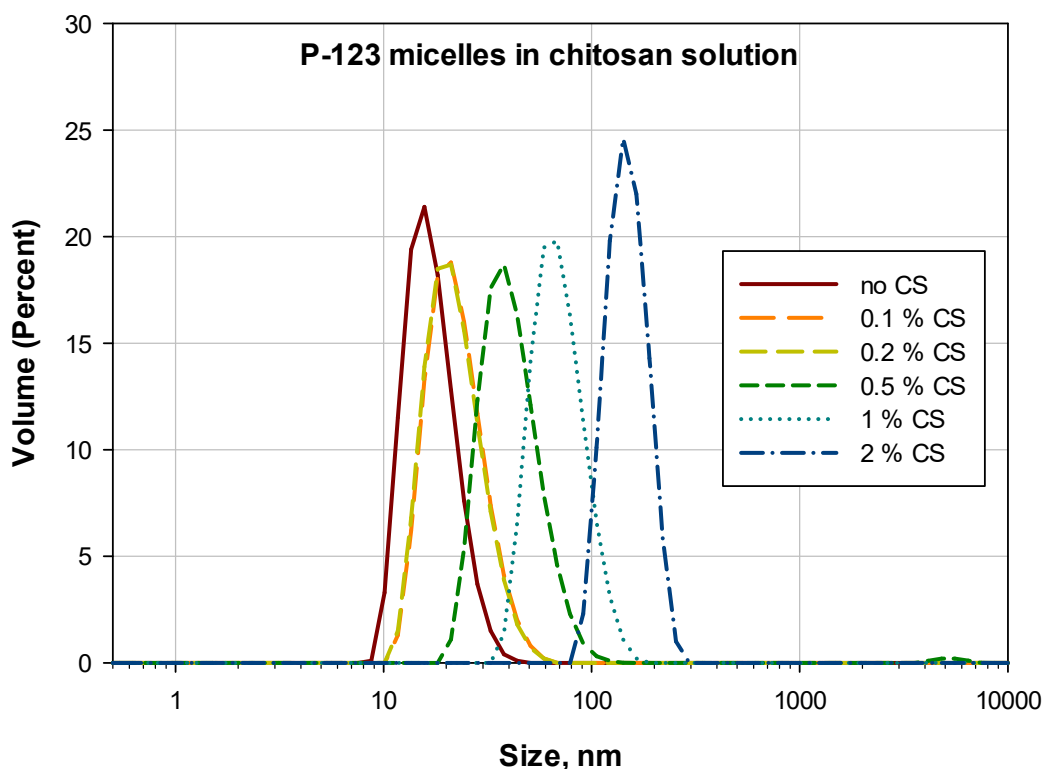
Figure 5. 11. Size distribution of P-123 micelles in chitosan solutions.

As can be seen from Figure 5.12 that the size of P-123 micelles were able to increase up to 160 nm (2 % chitosan) when P-123 micelles formed in chitosan solutions.

Figure 5.13 gives the effect of chitosan concentration on P-123 micelles for both micelle formation conditions (P-123 micelles in water in the presence of chitosan and in chitosan solution). It can be said that there is no effect of P-123 micelle formation method clearly. So, chitosan molecules get into the structure of P-123 micelles however that they were prepared.
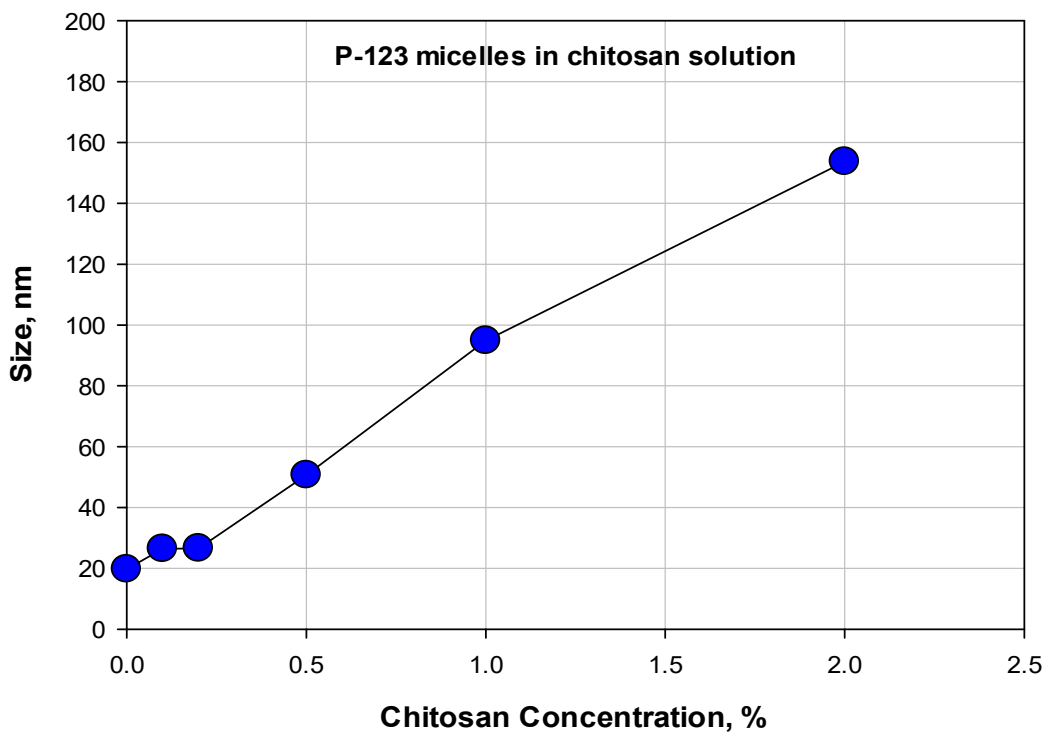
Figure 5. 12. Effect of chitosan concentrati on on P-123 micelle size in chitosan solution.
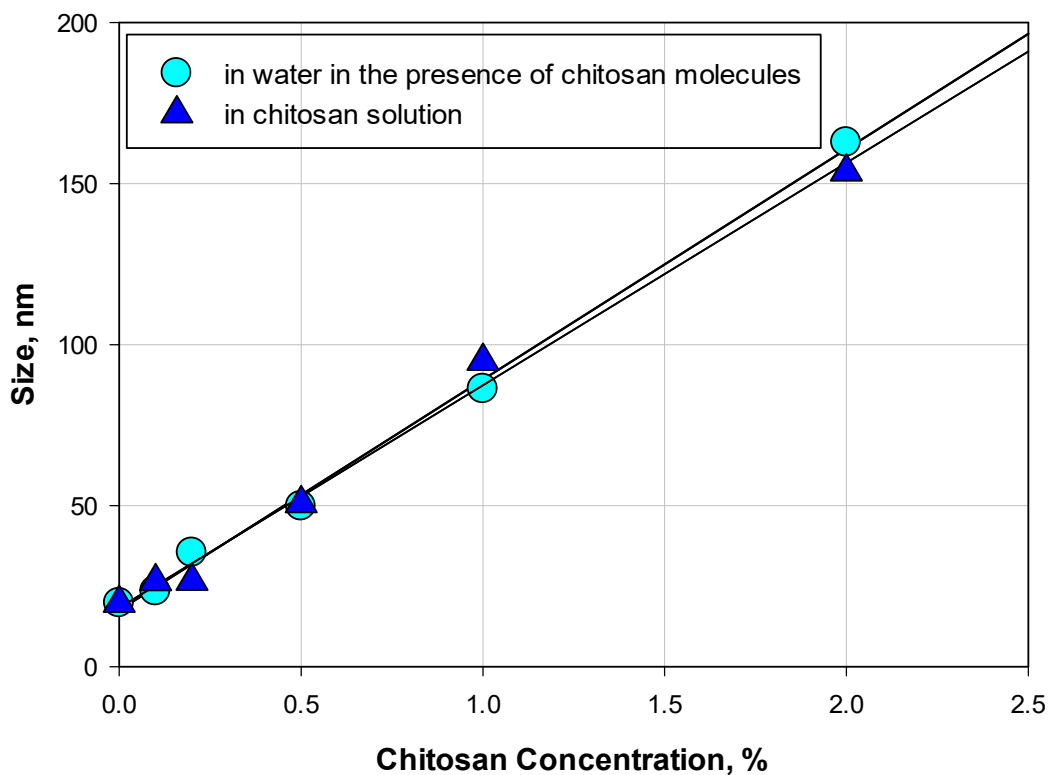
Figure 5. 13. Effect of chitosan concentration on P-123 micelle size in water in the presence of chitosan molecules and in chitosan solution.

In addition to the size measurements by DLS, UV-spectrophotometer was also used to see the difference in their absorbance values, if any, in the case of micelles with different methods (Figure 5.14). Similar to the other analysis, the same results were also obtained with UV-spectrophotometer for the two formation conditions. As a result, it can be said that both P-123 micelles in water in the presence of chitosan or P-123 micelles in chitosan solution can be used to envelope drug.
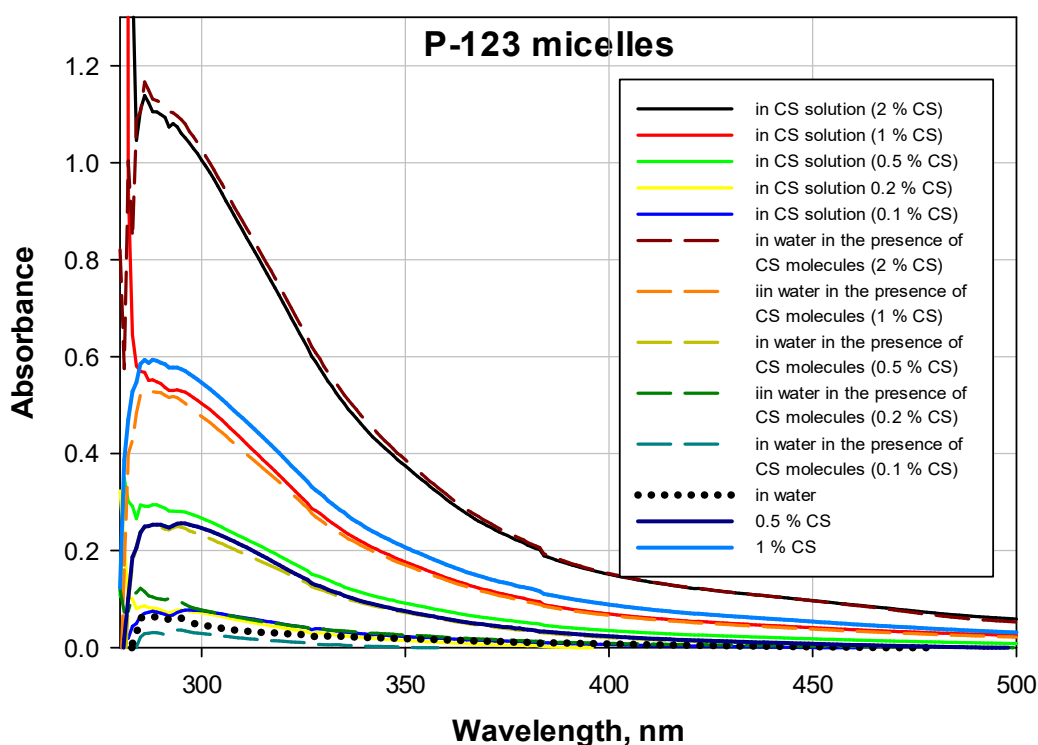
Figure 5. 14. UV-spectrophotometer analysis for P-123 micelles in water in the presence of chitosan molecules and in chitosan solution.

5.2.1.4. Curcumin Loaded P-123 Micelles in Water

As it was mentioned above in the experimental section, thin film evaporation method was coupled with O/W emulsion templated method to envelope hydrophobic drug, curcumin, in P-123 micelles. For this purpose, several chitosan foams contain different drug amounts were used. Figure 5.15 gives the size distributions of P-123 micelles in the absence and presence of curcumin molecules at different drug concentrations. As can be seen form the DLS results that the presence of drug in

micelles seem to not effect the size distribution of micelles very much. This might be due to the low amounts of drugs used in this study. The STEM images, on the other hand, clearly show the change in the size distribution of drug loaded P-123 micelles as presented in Figure 5.16. However, the distribution of drug molecules among micelles seems to be non-uniform and therefore the size distribution of P-123 micelles gets broader.
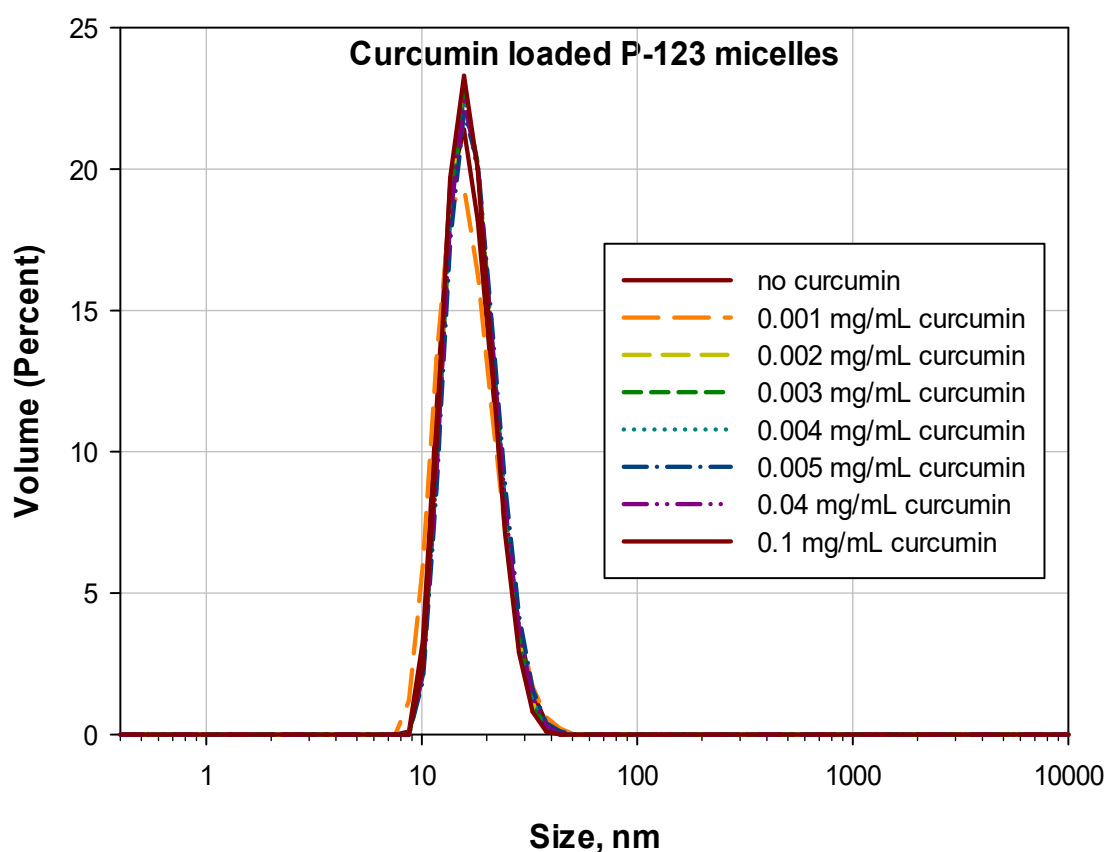
Figure 5. 15. Size distribution of curcumin loaded P-123 micelles.
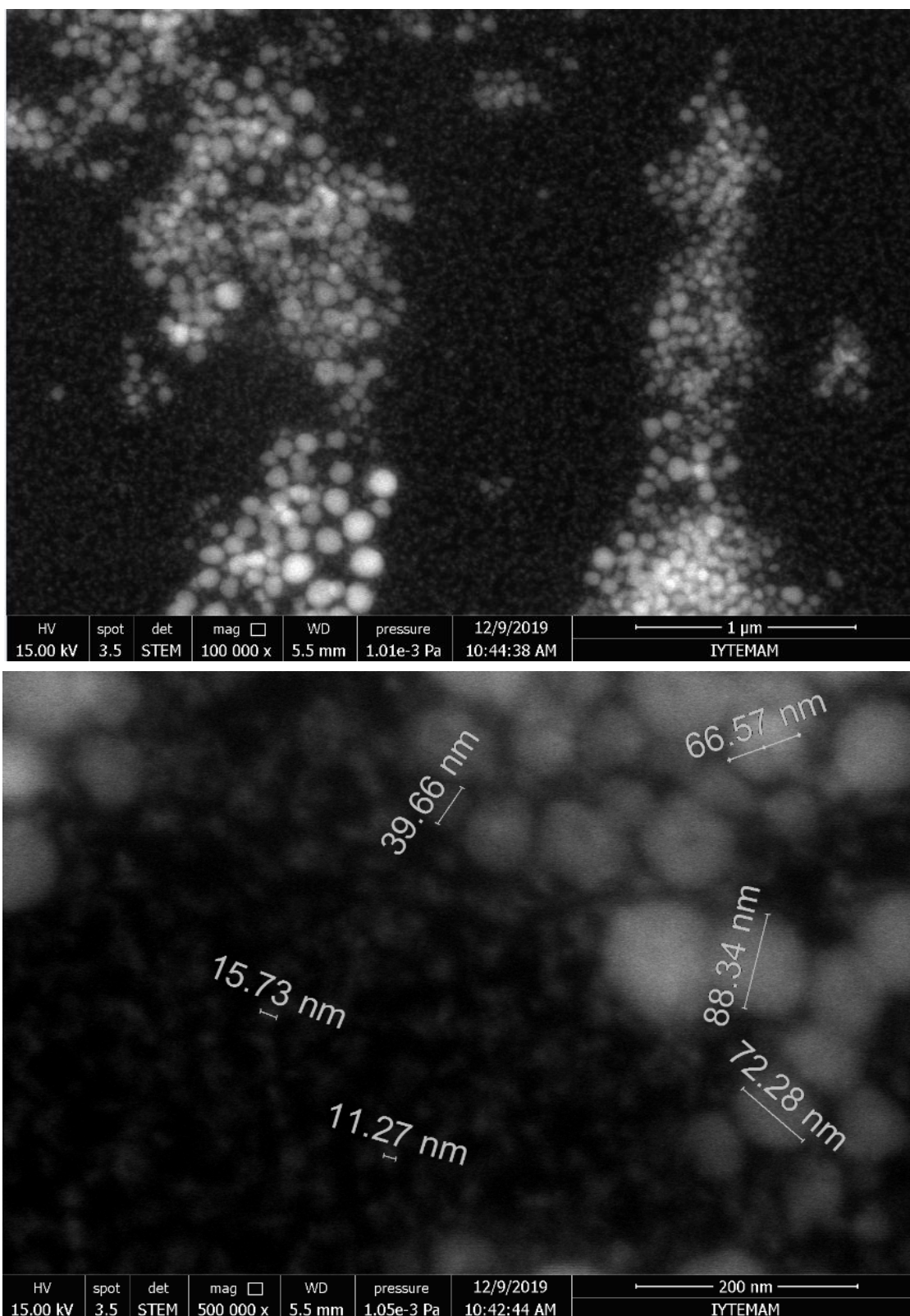
Figure 5. 16. Characterization of curcumin loaded P-123 micelles by STEM.

5.3. Production of Drug Loaded Chitosan Foams

Amphotericin-B and curcumin were hydrophobic drugs. Hexane was the oil phase to produce O/W emulsions. The polymerization of chitosan was performed by SDS for amphotericin-B and chitosan was polymerized by SDS and TPP at different curcumin concentrations. The morphological characterization of the hydrophobic drug-loaded foams was characterized by SEM and presented in Figures 5.17-5.25. As it is seen the drugs dispersed drug in chitosan matrix can not be identified in the SEM images. However, the foams produced by different cross linking agents were unlike in terms of their pore structures. Foams crosslinked by SDS have both structural voids and intrinsic micro pores. However, the foams crosslinked by TPP have only structural voids (macropores).
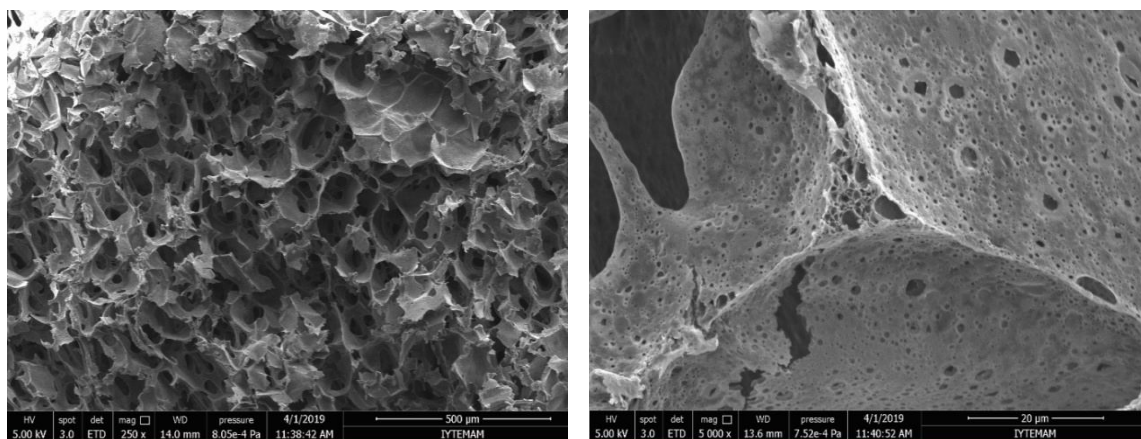
Figure 5. 17. SEM images of amphotericin-B loaded chitosan biofoams.
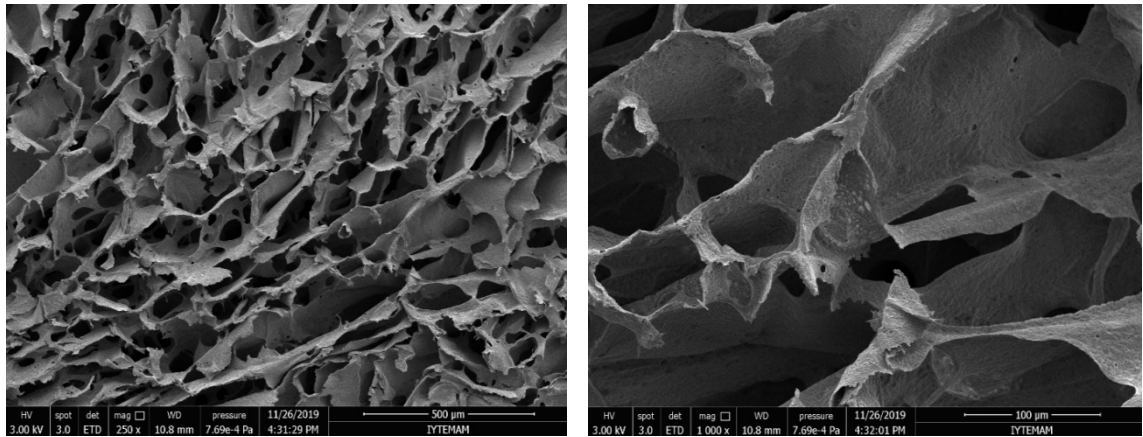
Figure 5. 18. SEM images of curcumin (0.04 mg/mL) loaded chitosan biofoams (SDS).
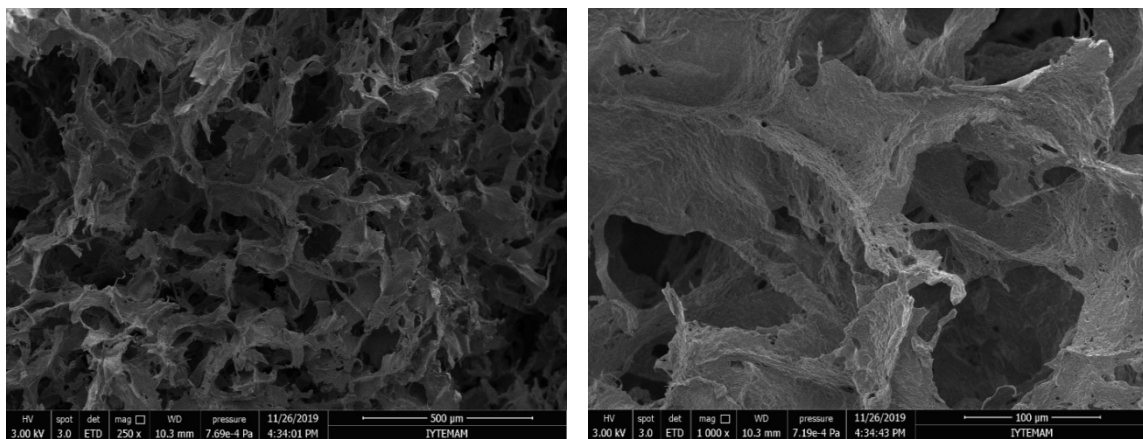
Figure 5. 19. SEM images of curcumin (0.04 mg/mL) loaded chitosan biofoams (TPP).
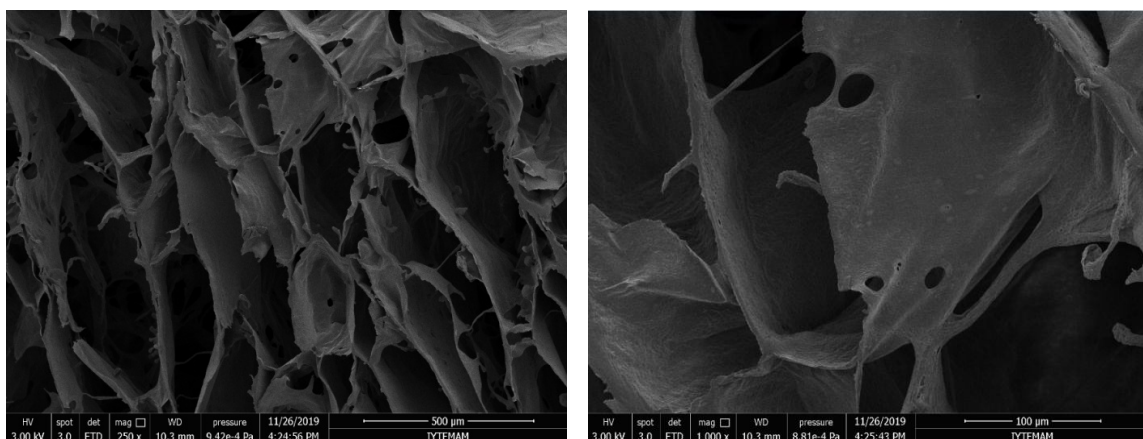
Figure 5. 20. SEM images of curcumin (0.08 mg/mL) loaded chitosan biofoams (SDS).
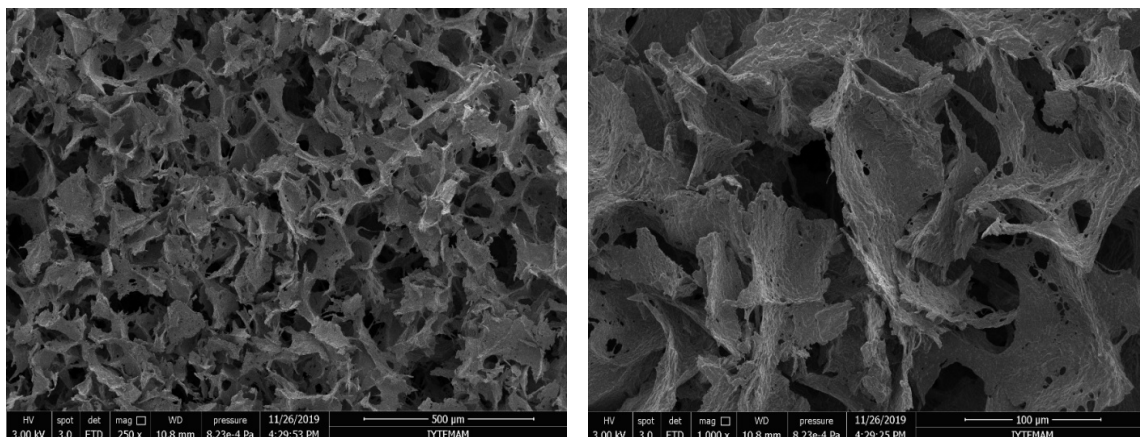
Figure 5. 21. SEM images of curcumin (0.08 mg/mL) loaded chitosan biofoams (TPP).
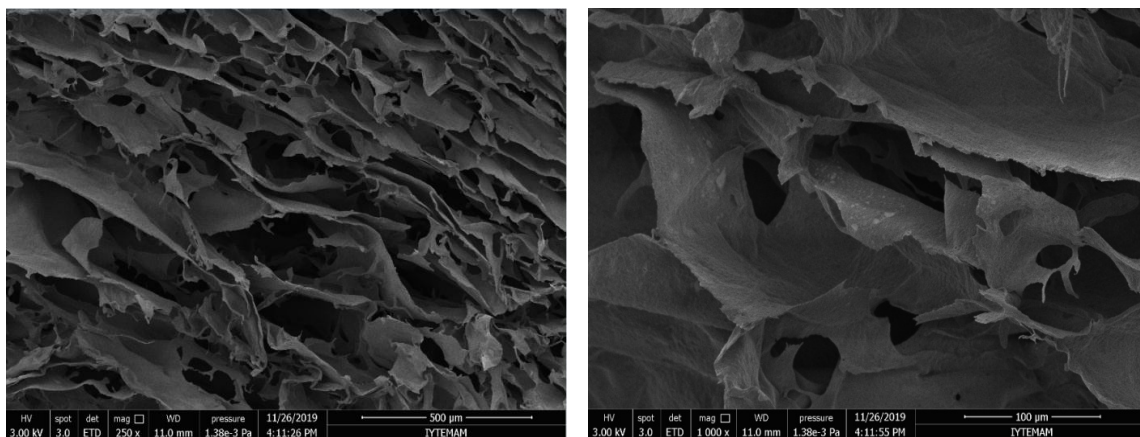
Figure 5. 22. SEM images of curcumin (0.1 mg/mL) loaded chitosan biofoams (SDS).
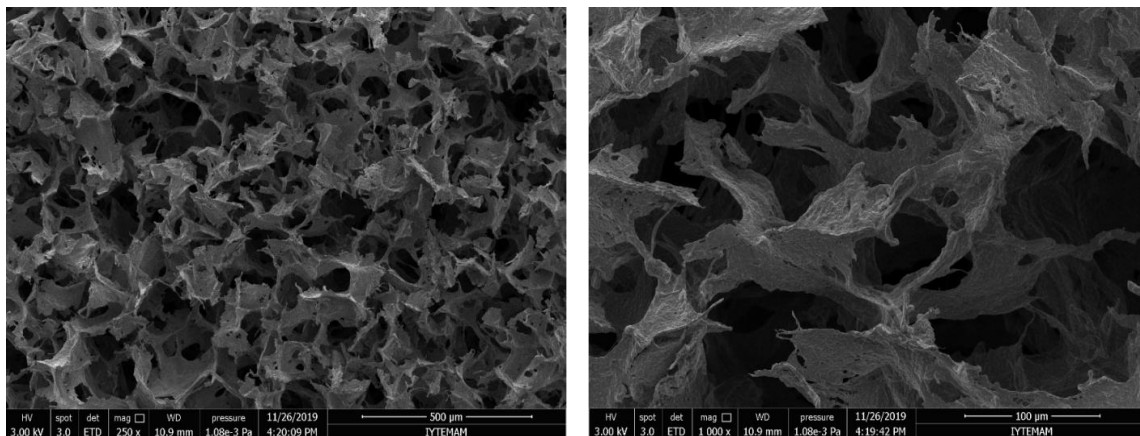
Figure 5. 23. SEM images of curcumin (0.1 mg/mL) loaded chitosan biofoams (TPP).
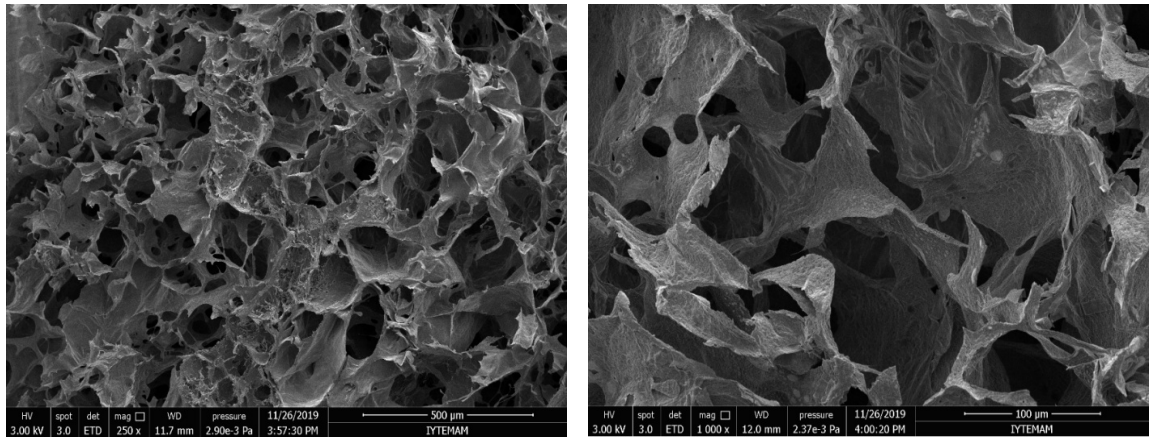
Figure 5. 24. SEM images of curcumin (0.2 mg/mL) loaded chitosan biofoams (SDS).
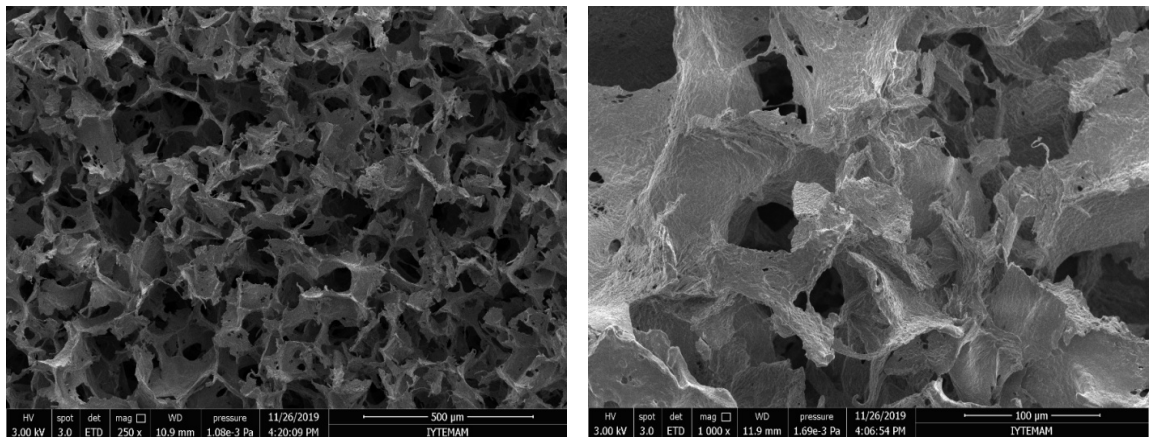
Figure 5. 25. SEM images of curcumin (0.2 mg/mL) loaded chitosan biofoams (TPP).

CHAPTER 6

DRUG RELEASE STUDIES

This chapter includes, tests to observe the drug release behaviour of foams for both hydrophobic and hydrophylic drugs. For release studies, a selected drug, curcumin, was used as a model hydrophobic, anti-inflammatory drug. Vancomycin was selected as a model hydrophilic antibiotic which is used to treat infections. These studies were conducted for different chitosan concentrations at pH 5.6 and pH 8.2 in phosphate buffer. The quantitative analyses of released drugs were done using UV-Vis analysis as discussed above in methods section.

6.1. Hydrophobic Drug: Curcumin

Before release studies, it was important to understand the system in detail to clarify the interactions between molecules as P-123 micelles with and without curcumin and chitosan molecules. For this purpose, the UV-Vis absorption data (UV-spectrophotometer), FTIR analysis, STEM images were used. In addition size and charge measurements were conducted using DLS. All these results were evaluated together to understand the possible effects on the release of a hydrophobic drug before studying the kinetics for all types of foams in detail.

6.1.1. Determination of Curcumin by UV-Vis Analysis

Curcumin has poor solubility in water at ambient conditions of pressure and temperature. Further, it is soluble in polar organic solvents, such as methanol, ethanol, dimethyl sulfoxide, among others. Hence, the real amount of curcumin was first determined in ethanol to see the difference when drug was in micelles. Three measurements were done for all curcumin concentrations. The size distributions of these

samples were also determined and given in Figure 6.1. Average sizes of curcumin molecules for different concentrations are shown in Figure 6.2. As can be seen from the figure that curcumin molecules are very small molecules when compared with P-123 micelles.
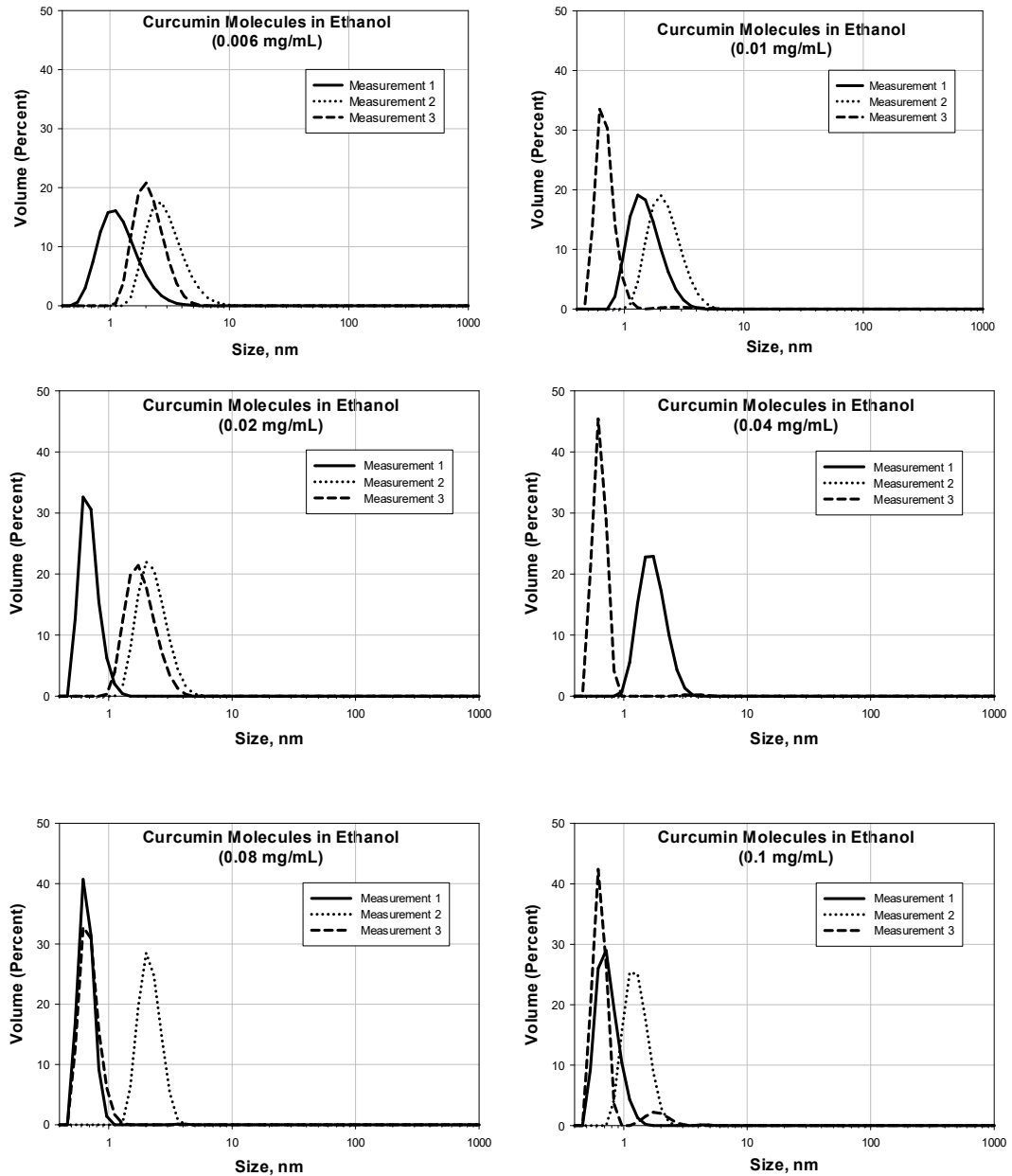
Figure 6. 1. Size distribution of curcumin for different concentrations.
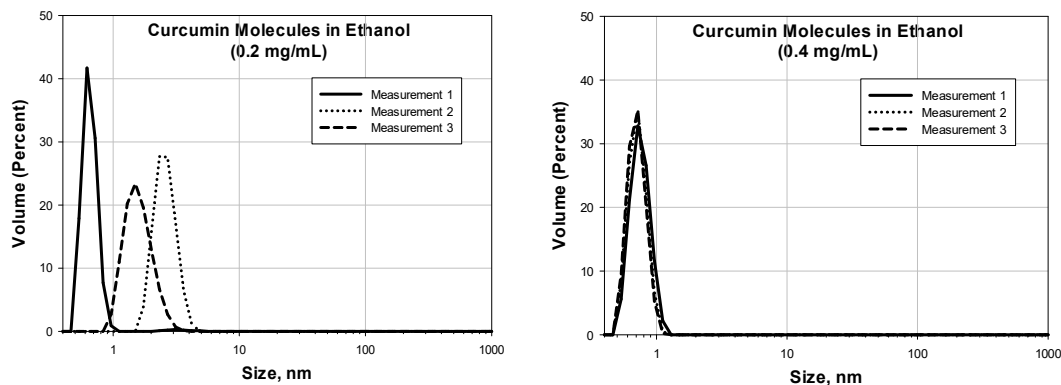
Figure 6.1. (cont.)
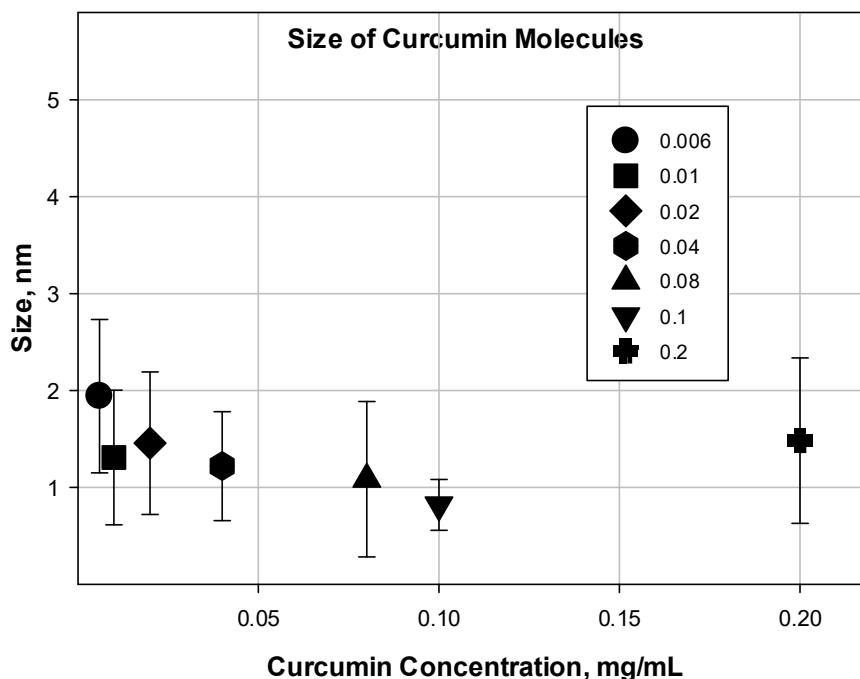
Figure 6. 2. Average sizes of curcumin molecules for different concentrations.

The UV-absorbances for curcumin molecules in ethanol and in P-123 micelles were presented together in Figure 6.3. These analysis were done by different curcumin concentrations as 0.05 mg/mL, 0.04 mg/mL, 0.03 mg/mL, 0.02 mg/mL, 0.01 mg/mL. As can be seen from the figures that the higher curcumin amounts give higher absorbance values as expected. In addition, when compared with curcumin in ethanol, curcumin in P-123 micelles gives lower absorbance values for the same amounts. That is, the presence of P-123 micelles around curcumin reduce the absorbanse of UV-Vis.
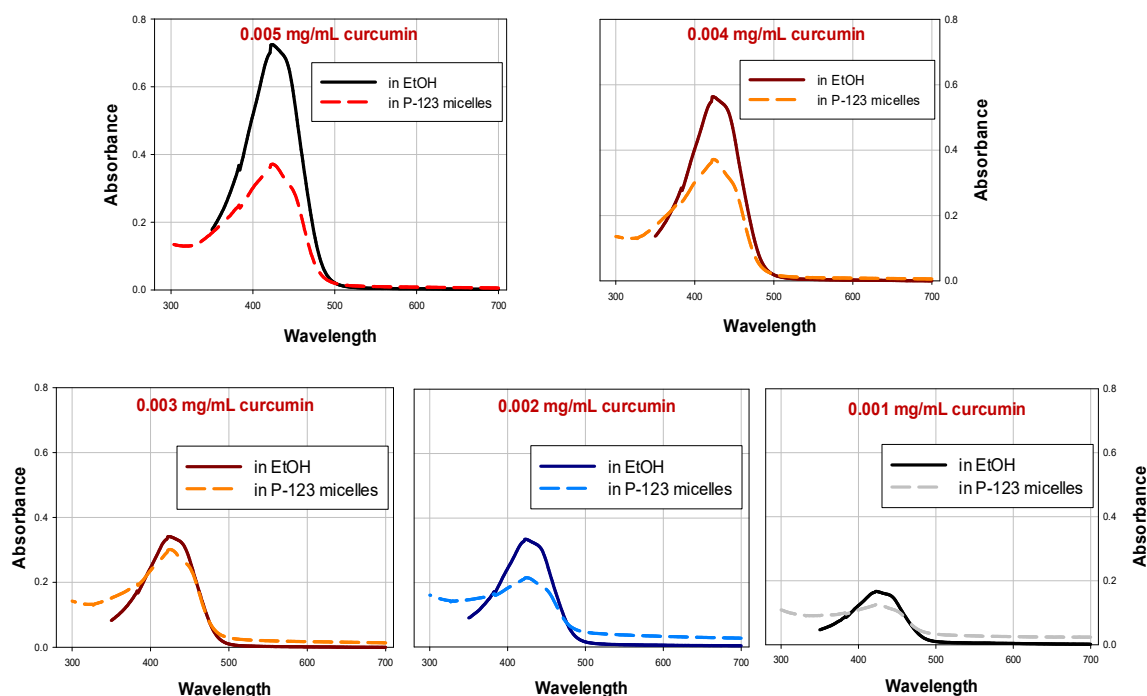
Figure 6. 3. UV analysis of curcumin in ethanol and in P-123 micelles.

6.1.2. Release Studies with Curcumin

In this part of the study, the release of hyrophobic drug enveloped in chitosan foams was studied. For this purpose, curcumin was selected as a model drug (hydrophobic) and several chitosan foams were prepared with different amounts of drug and chitosan. The details of the method used was discussed above which was the thin film evaporation method coupled with O/W emulsion template method to envelope drug in P-123 micelles. The amounts of chitosan were 2 % while the amounts of curcumin were 0.2 mg/mL, 0.1 mg/mL, 0.08 mg/mL, 0.04 mg/mL. Hexane (15 %) was used as an oil phase to produce W/O emulsions. SDS and TPP were the crosslinking agents. The release studies were conducted in phosphate buffer at pH 5.6. These studies were carried out at 37 ºC by shaking the solutions in bottles that contains a chitosan foam. The sampling was performed at the preset time intervals to for kinetic release studies. All the samples (supernatants) were analyzed by UV-spectrophotometer and calibration curve (obtained earlier, given above) to determine the quantity of the curcumin released. The drug release percentage was calculated for the conditions of 2 % CS. It is seen that the release percentage of curcumin increases with an increase in the amount of

curcumin for the cases where chitosan was crosslinked by TPP (Figure 6.4). In the case of chitosan foams crosslinked by SDS, on the other hand, the release percentage of curcumin is really low (Figure 6.5). This might be due to the possible interactions between drug, chitosan and SDS.

Figure 6.6 gives the release data both for SDS and TPP crosslinked chitosan foams. It can be clearly seen that the the release percentage of curcumin is higher in the case of foams crosslinked by TPP. Hence, one could conclude that the amount of drug release could be increased if chitosan foams crosslinked with TPP.
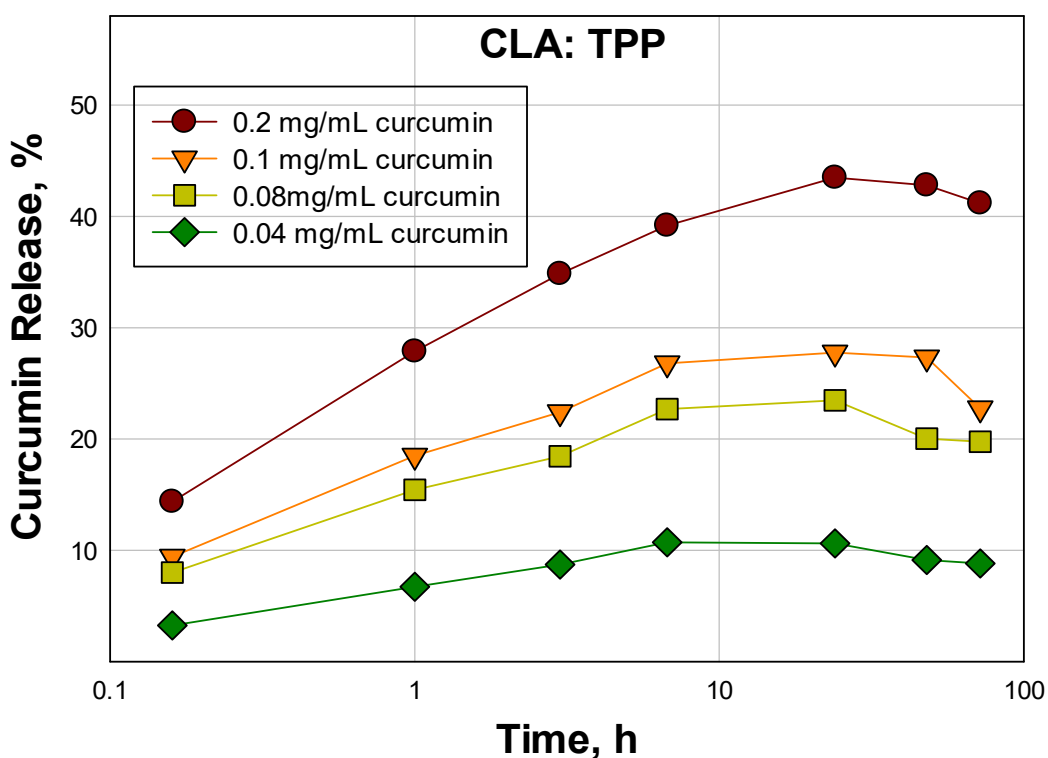
Figure 6. 4. Hydrophobic drug (curcumin) release from chitosan foams crosslinked by TPP.
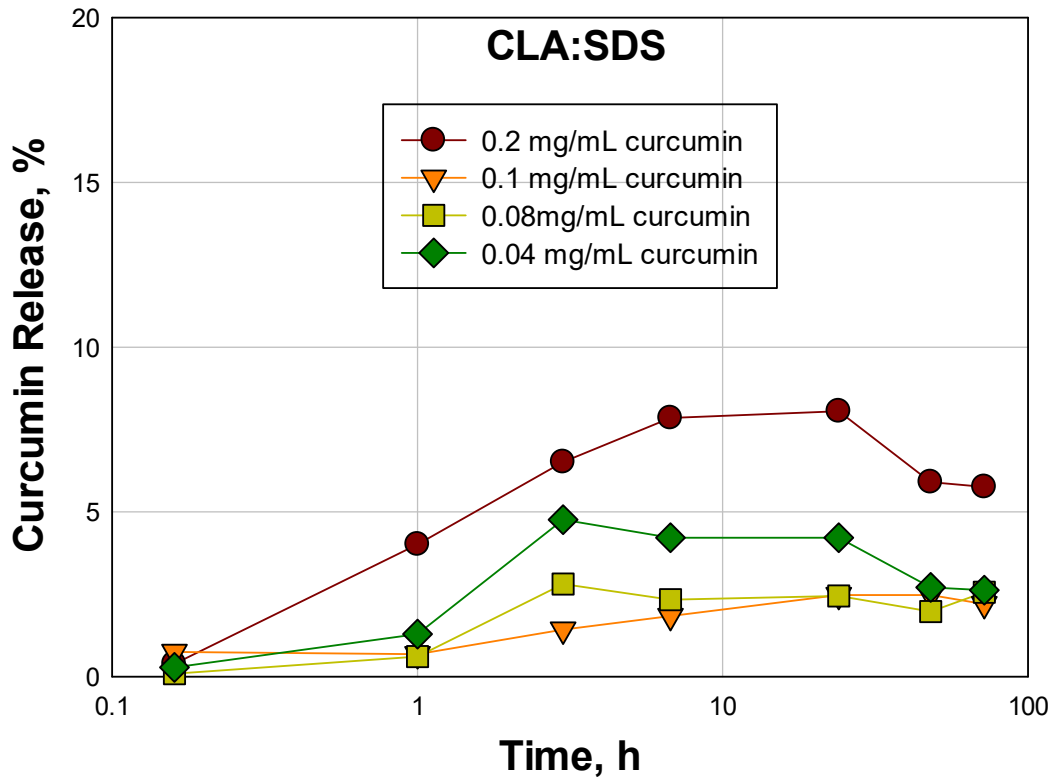
Figure 6. 5. Hydrophobic drug (curcumin) release from chitosan foams crosslinked SDS.
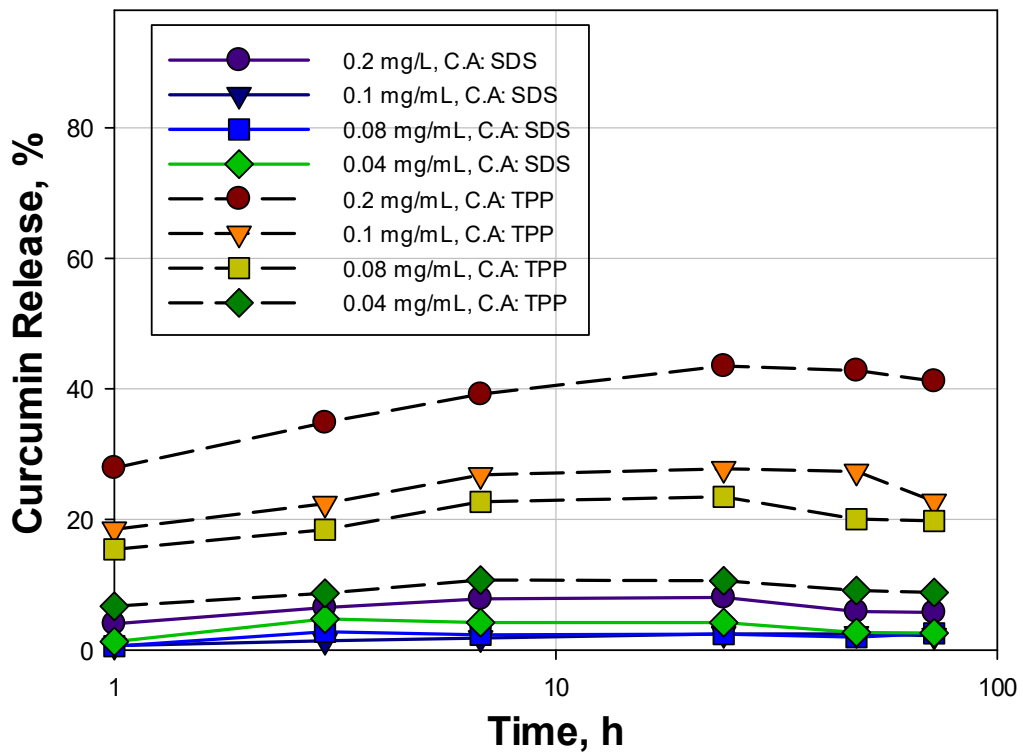
Figure 6. 6. Hydrophobic drug (curcumin) release from chitosan foams.

125

The release data obtained for hydrophobic drug, curcumin (crosslinked by TPP and SDS) were analyzed by first and second order kinetics and commonly used Higuchi and Korsemeyer-Peppas Models (Figure 6.7 and 6.8). The details of the models were discussed above in materials and method section. The figures show that the drug release fits the second order kinetics much better among others in the case of TPP. The data with SDS, on the other hand, seem to not fit any of the models applied.
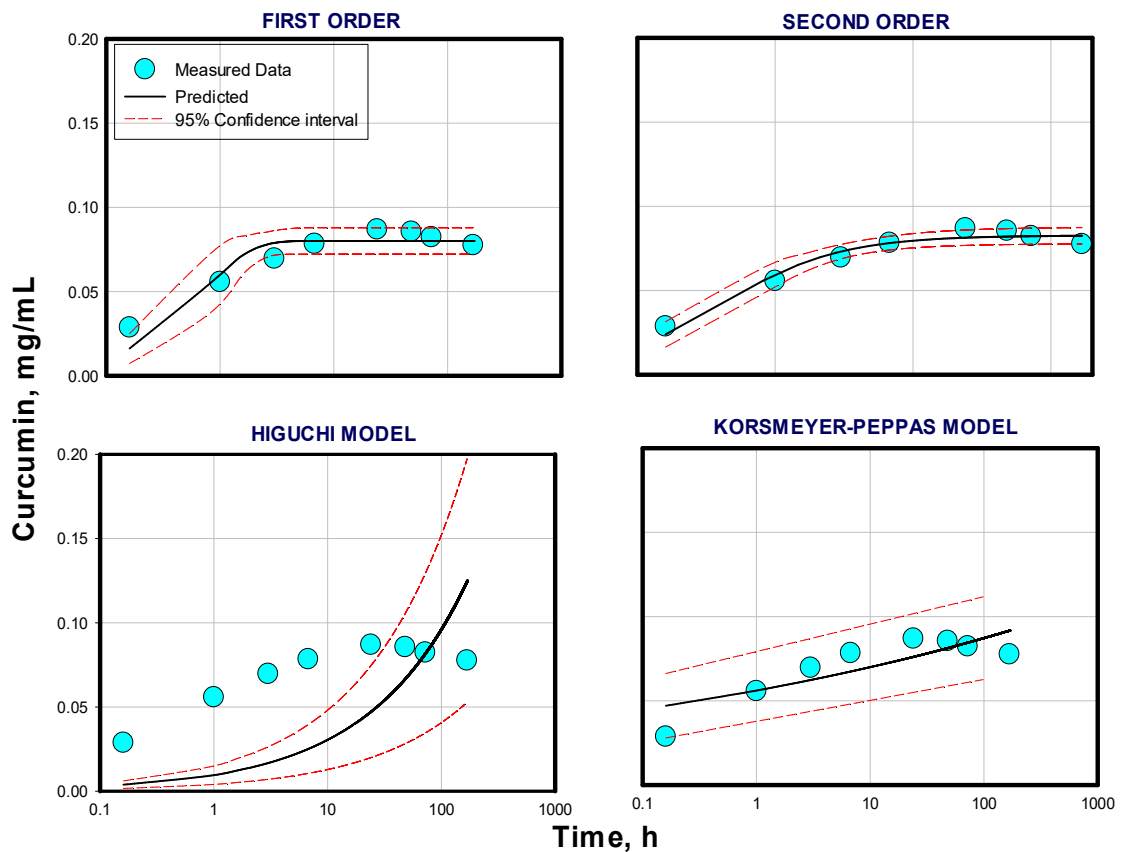
Figure 6. 7. Drug release data fitted to various kinetic models (0.2 mg/mL curcumin, CLA:TPP).
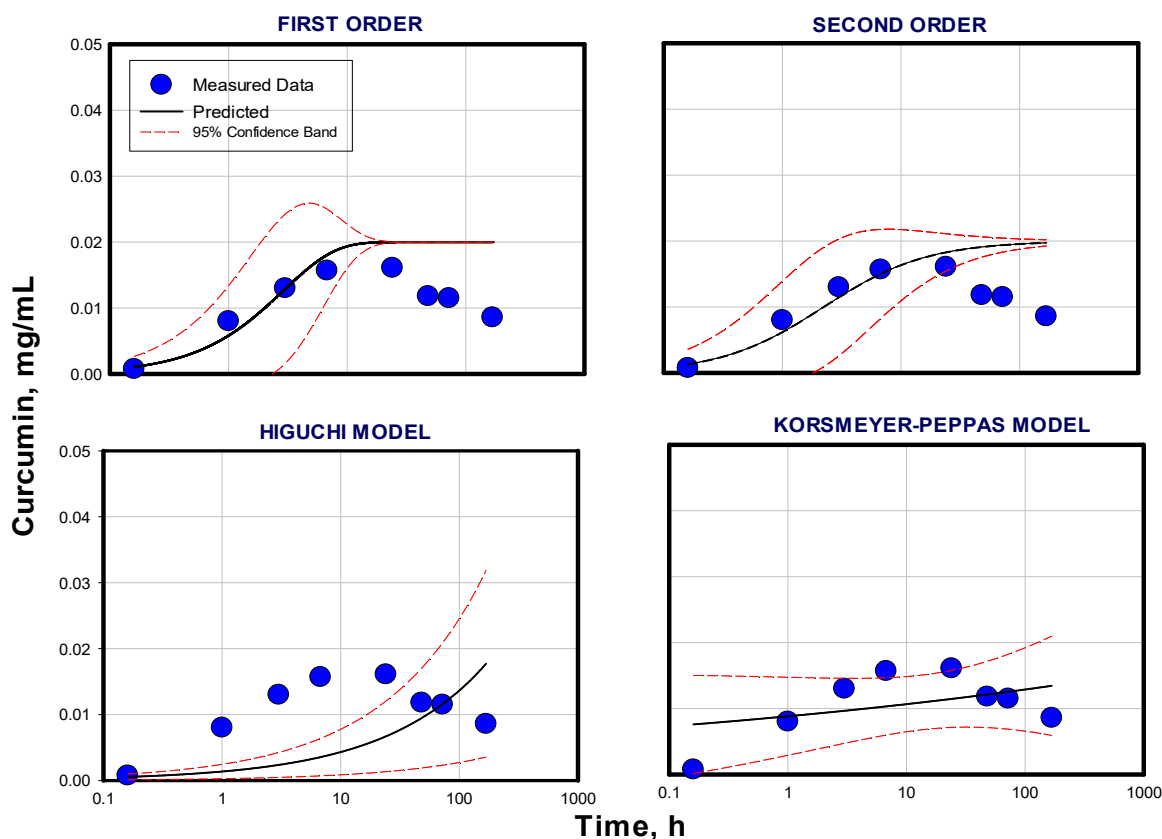
Figure 6. 8. Drug release data fitted to various kinetic models (0.2 mg/mL curcumin, CLA:SDS).

6.2. Hydrophilic Drug: Vancomycin Hydrochloride

In this part of the study, the release of hydrophilic drug from chitosan biofoams was determined. Vancomycin Hydrochloride was the model hydrophilic drug. Hexane was used as an oil phase to produce emulsions. Chitosan concentrations were chosen as 2 % and 4 %. The system was polymerized by SDS. The release of vancomycin from vancomycin-loaded chitosan biofoams were evaluated using phosphate buffer at pH 5.6 and pH 8.2 (Figure 6.9). These studies were carried out at 37 ºC by shaking the solutions in bottles that contain a chitosan foam and the sampling was performed at the preset time intervals to perform kinetic release studies. All the samples (supernatants) were examined by UV-spectrophotometer and a calibration curve (obtained earlier and given in Method section) to determine the quantity of vancomycin released (Figure 3.7).

It can be seen from the figure that the release of vancomycin from loaded foams was found to be higher at pH 5.6 than pH 8.2 (in case of 2 % chitosan) due to the higher solubility of chitosan under acidic conditions. The release of vancomycin was also lower in the case of 4 % chitosan compared to the 2 % chitosan as expected due to its structure with lower porosity as discussed above.
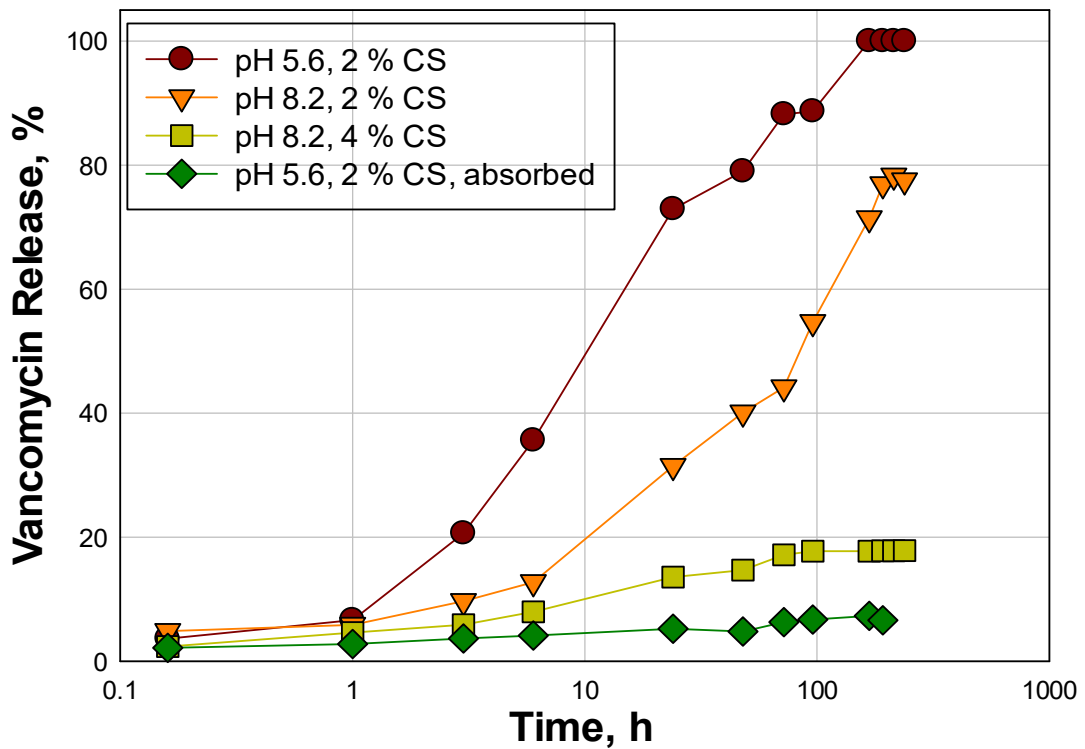
Figure 6. 9. Hydrophilic drug (vancomycin) release from chitosan foams.

The release data obtained was analyzed by first and second order kinetics and commonly used Higuchi and Korsemeyer-Peppas Models (Figure 6.10). The details of the models were discussed above in materials and method section. The figure shows that the drug release fits the second order kinetics much better among others.
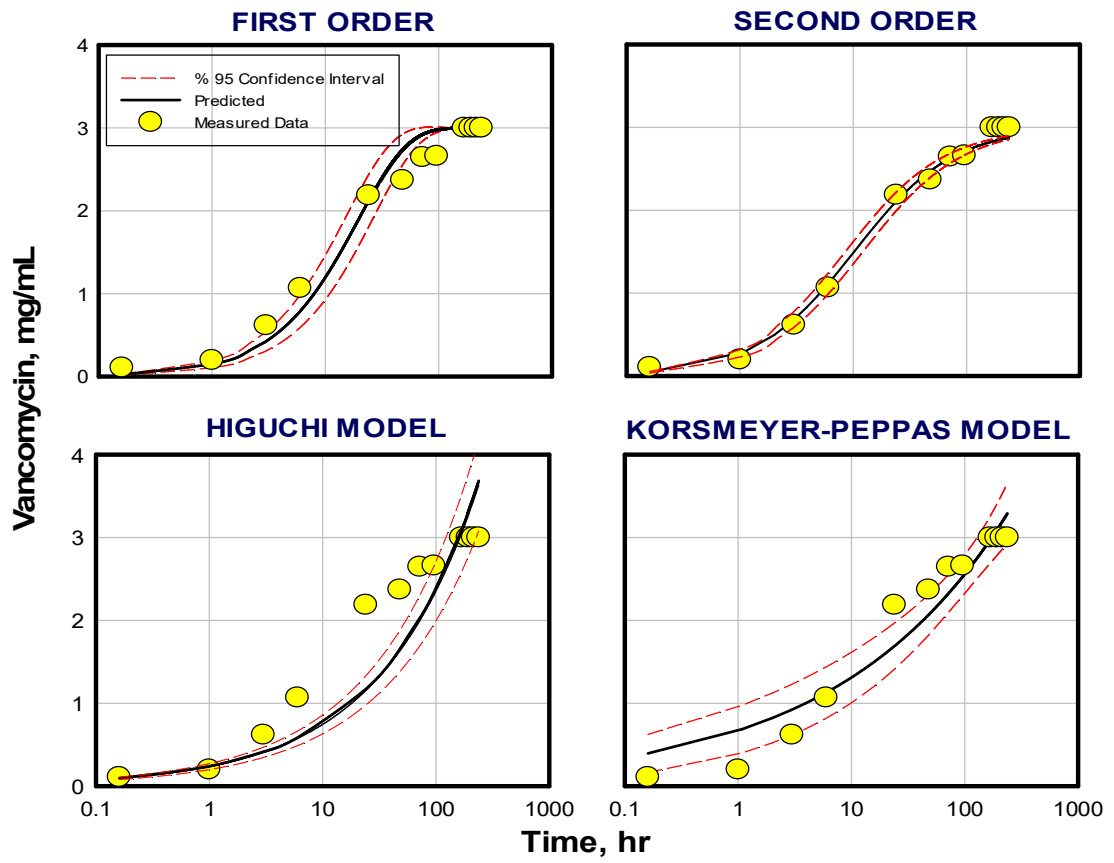
Figure 6. 10. Drug release data fitted to various kinetic models (2 % CS, pH 5.6).

CHAPTER 7

DEVELOPMENT OF A RELEASE MODEL FOR THE DRUG MOLECULES FROM CHITOSAN FOAMS MATRIX

Since the drug release mechanism has great importance, this chapter includes the development of a model for drug release from chitosan foams. First of all, details about produced foams in terms of pore structure are given. Then, physical model is described. Derived equations are given in detail in the following parts.

7.1. Chitosan Foams

In this study, chitosan biofoams were produced by o/w emulsion templated method as given in detail in the previous part. To summarize, an ultrasonic probe was used to produce oil/water type of emulsions to use as templates. Freeze drying was applied to all samples to remove volatile components which creates pores. In addition, biofoams were produced in the absence of an oil phase to clarify the role of an oil phase in foam production. Structures of the foams produced were characterized by SEM.

It could be seen from the SEM images in Section 4. Production and Characterization of Chitosan Based Biofoams that the foams show a structure composed of two different levels of porosity. The first type is rather large structural voids (or nearly spherical chambers) in sizes larger than 100 micrometer (μm). These chambers are separated by thin walls whose thicknesses are in the order of 10 micrometer. The walls contain the second level intrinsic pores which are nearly spherical with diameters in the order of 1 micrometer.

It was mentioned in Section 4 that the structural voids (or the chambers) form irrespective of whether the oil is present during the synthesis. This suggests that the structural voids are created by some other means, most probably due to the presence of air bubbles created by the strong ultrasonic energy applied during the synthesis.

However, the walls of the chamber in the absence of the oil contain no intrinsic pores. When the oil is present, both the structural voids and the instrinsic pores on their walls are present. This clearly indicates that the instrinsic micro pores are generated by the evaporating oil phase.

The foams were also synthesized in the presence of both hydrophilic (vancomycin hydrochloride), and hydrophobic (curcumin) drugs in the presence of oil. The dispersion method of the drugs into the chitosan matrix was completely different as explained in Section 3. Materials and Methods. SEM images of the foams in the presence of the drugs are very similar to those generated in the absence. No residual separate drug phase was observed in the foam structures even though the mass ratio of the drug to the polymer is close to 10 % (30 mg drug in around 0.4 gr polymer). This is an initial indication that complete dispersion of the drugs in the chitosan matrix was achieved as aimed.

Figure 7.1 displays a cross view of a sectioned representative chitosan foam where the chamber structure (structural voids) can be seen very clearly. Figure 7.2 shows a magnified portion of the same photograph which shows the instrinsic pores on the chamber walls. A comparison of the figures shows that the size of the chambers are several order of magnitude larger than the the instrinsic pores.

Measurements have been carried out on the SEM photographs show that the measured and calculated geometrical properties of the system (as averages) can be summarized as follows:

Measured from geometry

The diameter of the chambers:	~100(μm)
The thickeness of the walls (2L):	~10 μm
The radius of the instrinsic pores (R):	~0.5μm
Number of pores in 1cm^2 chamber surface:	8.6x10^7 #/1 cm^2

Calculated from geometry

The volume of a single chamber:	3.38x10^{-6}cm^3
The total surface area of chamber:	4.61x10^{-4}cm^2
Number of chambers:	3.42x10^7 #/cm^3
Total number of pores:	1.85x10^{12}
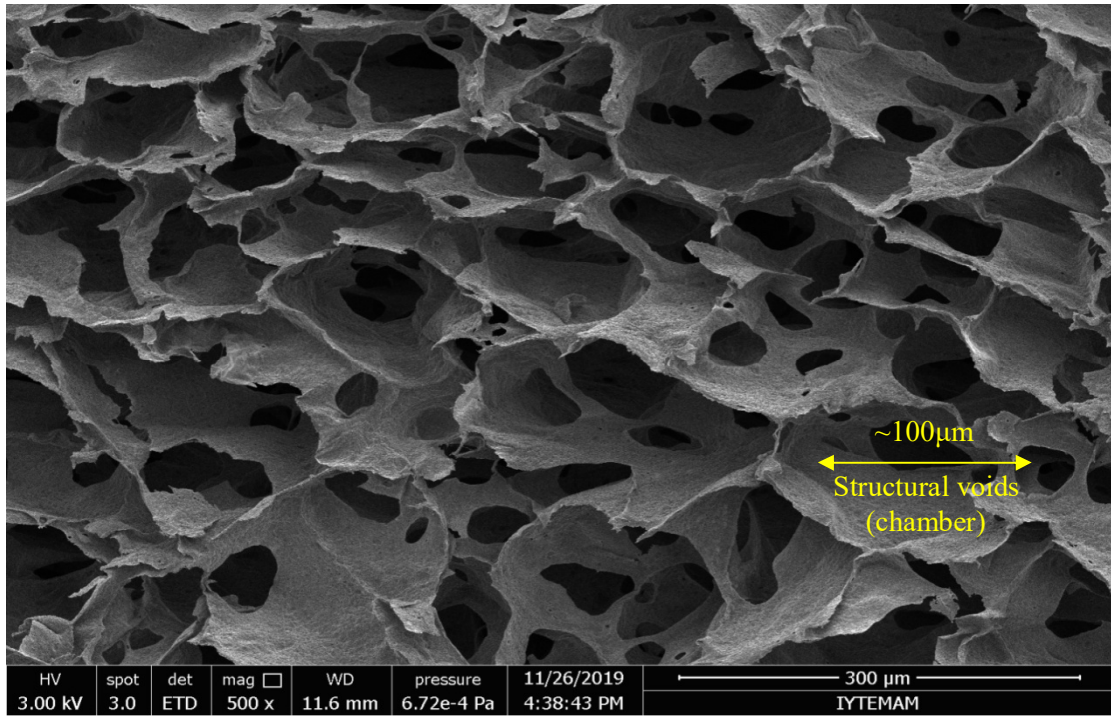
Figure 7. 1. Structural voids (chambers) of the foams.
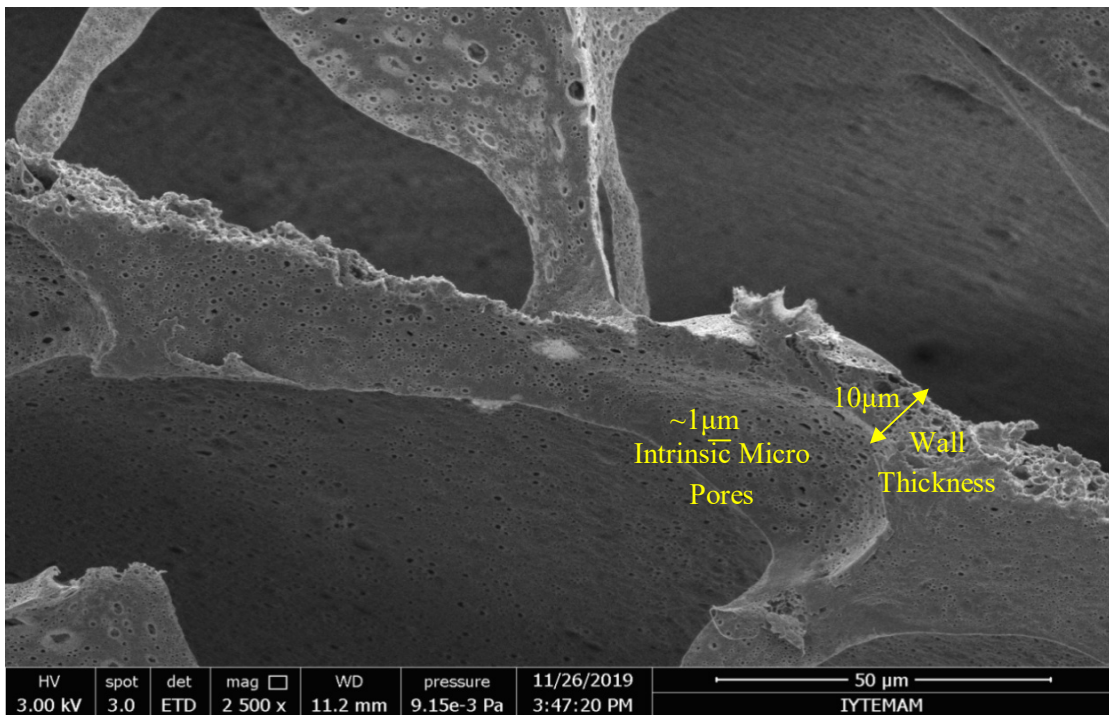
Figure 7. 2. Wall thickness of the foams and size of intrinsic micro pores.

7.2. Development of the Model

7.2.1. Model Geometry

The physical model is based on the main assumption that the drug is homogeneously dispersed in the chitosan matrix and the dissolution kinetics of chitosan from the pore walls directly gives the dissolution rate of the drug. Therefore, the model aims to determine the chitosan dissolution rate from the pores in a chitosan matrix which is in contact with a buffer solution in a diffusion controlled manner.

Since the size of the chambers in the foam is very large, any drug released into the chambers can be considered to be in total solution volume. In other words, the change of the drug concentration in the chambers with time can approximate to the drug concentration in solution $C_{sol}(t)$. Also, it was assumed that the intrinsic pores on the walls maintain a cylindirical geometry through the wall with a pore radius R. Considering possible tortuosity, the minimum pore length will be equal the wall thickness 2L (Figure 7.3).

A pore is situated in the z-axis between z=-L and z=+L and is symmetrical around z=0. In terms of the radial distances, the position of the pore is between r=-R and r=+R and there is also a complete symmetry around r=0. One end of the pore opens into a chamber at z=L with a solution concentration of $C_{sol}(t)$ at time t. The concentration at the pore mouth (z=L) is constant at $C_{sol}(t)$ for all r at any given time. The chitosan solution concentration on the pore surface (r=R), on the other hand, is constant at a value C_s for all z where C_s is the solubility limit of the chitosan polymer in given solution conditions. It can be seen that these boundary conditions will require a series solution of a periodic function.

The solute flux in the pore (0<r<R and 0<z<L) depends on the local concentration gradient C(r,z) according to the Fick's 1st Law. The flux from the pore wall will be governed by the the local concentration gradient which becomes equal to chitosan solubility C_s at r=R. The flux at the pore entrance will be governed by the local concentration gradient which becomes equal to solution concentration $C_{sol}(t)$. The flux in the z-direction is zero at the middle of a pore along the z-axis (z=0) due to the

symmetry requirement. Also, the flux in the r-direction is zero at the center of a pore along the r-axis (r=0).

The solution of the system requires the following:

1. Setting up the 2-D mass balance which leads to the Laplace's equation,
2. Solution of the Laplace's Equation in terms of the periodic Bessel's functions which leads to the concentration profile C(r,z) within the pore,
3. Calculating the in-flux from the walls to the pore and the out-flux from the pore to chamber using the C(r,z) profile,
4. Integrating the out-flux from the pore to chamber with respect to time to determine the time-dependent solution concentration,
5. Calculating the foam sequence,
6. Fitting the experimental data to a developed model.
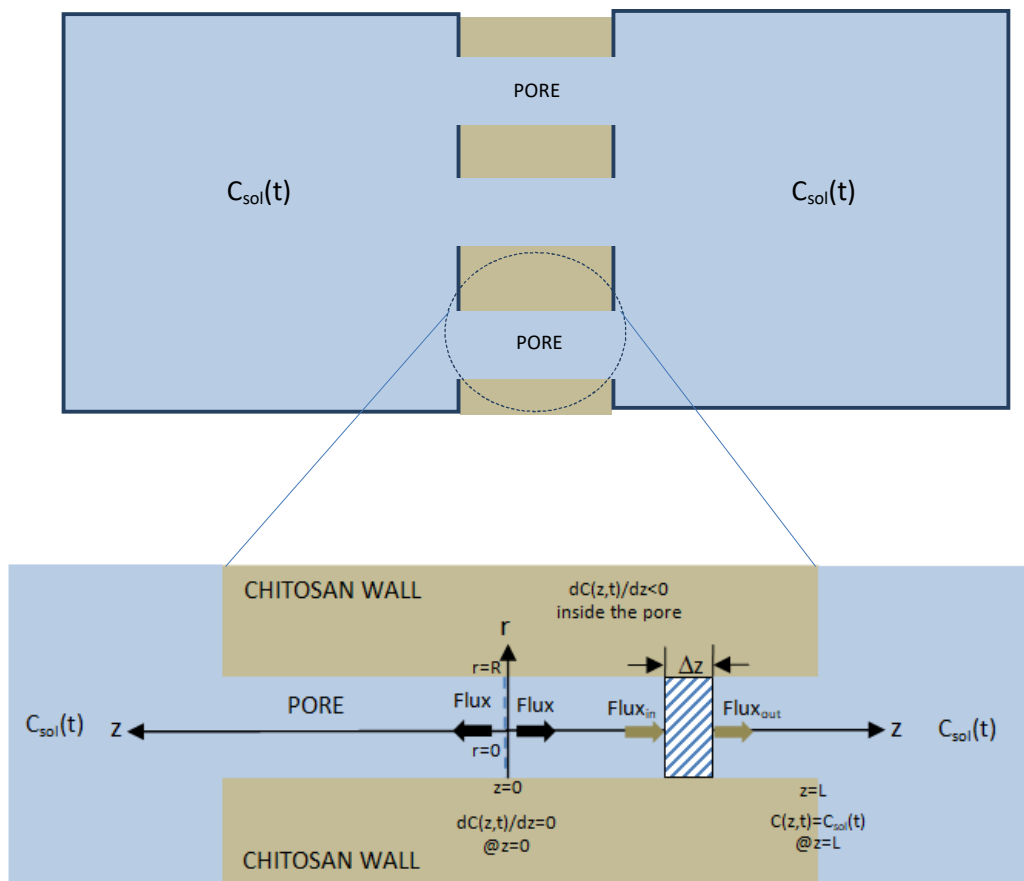
Figure 7. 3. Schematic presentation of the pores.

7.2.2. Development of the Mass Balance Equation

The net flux through the infinite small volume, δV, can be shown as (Figure 7.4);

$$J_{net}=J_{out}-J_{in} \tag{7.1}$$
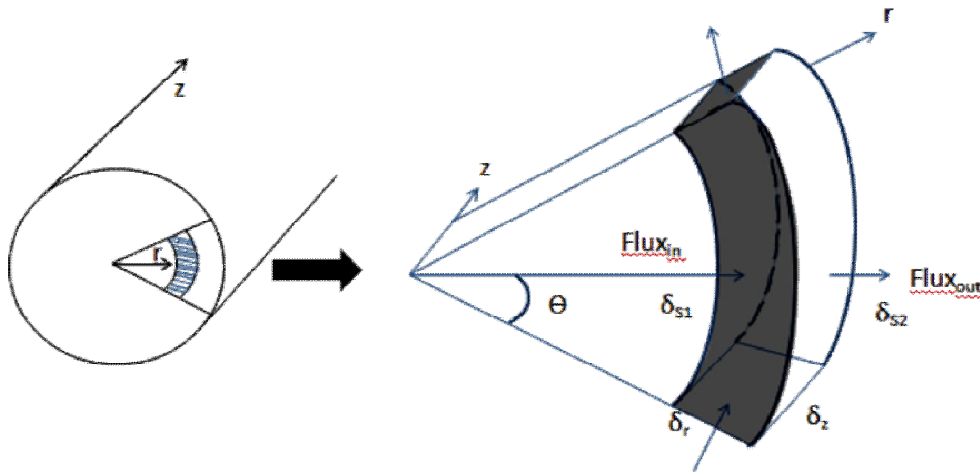
Figure 7. 4. The net flux through the infinite small volume, δV.

The mass balance in an infinite small volume element of a cylindiral pore δV can be obtained by recognizing that change in the mass content of in this volume will be equal to;

$$\frac{dm}{dt} = \dot{m}_{in} - \dot{m}_{out} + Generation \tag{7.2}$$

If it is asssumed that; 1) no generation in δV, 2) steady state, Equation 7.2 can be written as;

$$\dot{m}_{in} = \dot{m}_{out} \tag{7.3}$$

Mass of the flux crossing the area per unit time in a given direction, is proportional to the gradient of solute concentration in that direction and described by Fick's First Law;

$$J = -D\left(\frac{\partial C}{\partial l}\right)A \tag{7.4}$$

where D: molecular diffusion coefficient, C: concentration, l: distance, A: area, J: mass flow rate.

m goes in & out in r, Θ and z directions. If flux equations are examined in cylindrical coordinates;

r-Direction:

$$\frac{\partial C}{\partial r} > 0 \; in \; r - direction \; and \; flux \; is \; (-) \; in \; r$$

$$J_r = -D\left(\frac{\partial C(r,\theta,z)}{\partial r} - \frac{\partial}{\partial r}(\frac{\partial C(r,\theta,z)}{\partial r}\frac{\delta r}{2})\right)r\delta\theta\delta z$$
$$- \left[-D\left(\frac{\partial C(r,\theta,z)}{\partial r} + \frac{\partial}{\partial r}(\frac{\partial C(r,\theta,z)}{\partial r}\frac{\delta r}{2})\right)(r + \delta r)\delta\theta\delta z\right] \tag{7.5}$$

Θ-Direction:

The system is radially symmetrical due to Θ direction, hence there is no change in concentration with Θ.

z-Direction:

$$\frac{\partial C}{\partial z} < 0 \; in \; z - direction \; and \; flux \; is \; (+) \; in \; z$$

$$J_z = -D\left(\frac{\partial C(r,\theta,z)}{\partial z} - \frac{\partial}{\partial r}(\frac{\partial C(r,\theta,z)}{\partial z}\frac{\delta z}{2})\right)r\delta\theta\delta r$$
$$- \left[-D\left(\frac{\partial C(r,\theta,z)}{\partial z} + \frac{\partial}{\partial r}(\frac{\partial C(r,\theta,z)}{\partial z}\frac{\delta z}{2})\right)\right]r\delta\theta\delta r \tag{7.6}$$

Net flux through δV:

$$\frac{\partial^2 C}{\partial r^2} r(\delta r \delta \theta \delta z) + \left[\frac{\partial C}{\partial r} + \frac{\partial^2 C}{\partial r^2}\frac{\partial r}{2}\right]\delta r \delta \theta \delta z + \frac{\partial^2 C}{\partial z^2} r(\delta r \delta \theta \delta z) = 0 \qquad (7.7)$$

If the equation is divided by $\delta r \delta \theta \delta z$;

$$r\frac{\partial^2 C}{\partial r^2} + \frac{\partial C}{\partial r} + \frac{\partial r}{2}\frac{\partial^2 C}{\partial r} + r\frac{\partial^2 C}{\partial z^2} = 0 \qquad (7.8)$$

Divide by r and collect;

$$\frac{\partial^2 C}{\partial r^2}\left[1 + \frac{\partial r}{2r}\right] + \frac{1}{r}\frac{\partial C}{\partial r} + \frac{\partial^2 C}{\partial z^2} = 0 \qquad (7.9)$$

Since $\partial r \rightarrow 0$, $1 + \frac{\partial r}{2r}\rightarrow 1$

Hence two dimensional steady state diffusion equation in a cylindrical pore is obtained as given below and this is the Laplace Equation;

$$\frac{\partial^2 C(r,z)}{\partial z^2} + \frac{1}{r}\frac{\partial}{\partial r}\left[r\frac{\partial C(r,z)}{\partial r}\right] = 0 \qquad (7.10)$$

7.2.3. Solution of the Laplace Equation in Two-Dimension

Since the Laplace Equation for steady state flux in cylindrical coordinated in 2-dimension is obtained as;

$$\frac{\partial^2 C(r,z)}{\partial z^2} + \frac{1}{r}\frac{\partial}{\partial r}\left[r\frac{\partial C(r,z)}{\partial r}\right] = 0 \qquad (7.11)$$

Boundary Conditions for C(r,z);

$c(R, z) = C_s$ The concentration on the pore surface (r=R) is constant at C_s for all z. C_s is the maximum concentration which chitosan may reach in solution (solubility limit).

$c(r, L) = C_{sol}$ The concentration at the pore mouth (z=L) is constant at C_{sol} for all z. At the pore end (chamber) the concentration is equal to solution concentration).

$\frac{dC(r,z)}{dz}\big|_{z=0} = 0$ The flux at the pore end (z=0) is zero (Pore is symmetric on both sides of z=0). This means no flux at z=0.

$\frac{dC(0,z)}{dr}\big|_{r=0} = 0$ The flux at the pore center (r=0) is zero (Pore is symmetrical around r).

Since C(r,z) at r=R is constant and equal to C_s, it can be said that;

$$C(r,z) = \chi(r,z) + C_s \qquad (7.12)$$

Note that, χ(r,z) must be equal to 0 at r=R (since we want to solve for the roots of the Bessel Function).

$$\chi(R,z) = 0 \qquad (7.13)$$

This can be generalized for all r;

$$C(r,z) = \chi(r,z) + C_s \qquad (7.14)$$

It follows that;

$$\frac{\partial C(r,z)}{\partial z} = \frac{\partial \chi(r,z)}{\partial z} \qquad (7.15)$$

Note that the boundary conditions for C(r,z) are satisfied for χ(r,z);

$$\left[\frac{\partial \chi(r,z)}{\partial r}\right]_{r=0} = 0 \qquad\qquad \left[\frac{\partial \chi(r,z)}{\partial z}\right]_{z=0} = 0$$

Since the general solution of the Laplace Equation for diffusion in cylindrical coordinates is given in 7.11, it follows that;

$$\frac{\partial^2 \chi(r,z)}{\partial z^2} + \frac{1}{r}\frac{\partial}{\partial r}\left[r\frac{\partial \chi(r,z)}{\partial r}\right] = 0 \qquad\qquad (7.16)$$

If the Equation 7.16 is separated into variables and χ(r,z) defined as;

$$\chi(\text{r,z}) = R(r)Z(z) \qquad\qquad (7.17)$$

Integration of Equation 7.17 two times gives;

$$\frac{\partial^2 \chi(r,z)}{\partial z^2} = R(r)\frac{\partial^2 Z}{\partial z^2} \qquad\qquad (7.18)$$

If Equation 7.18 is used for the first term of the Equation 7.11;

$$\frac{\partial d^2 C(r,z)}{\partial z^2} = \frac{\partial^2 \chi(r,z)}{\partial z^2} = R(r)\frac{\partial^2 Z(z)}{\partial z^2} \qquad\qquad (7.19)$$

Now, Equation 17 is used for the second term of the Equation 7.11 becomes;

$$\frac{1}{r}\frac{\partial}{\partial r}\left[r\frac{\partial \chi(r,z)}{\partial r}\right] = \frac{1}{r}\frac{\partial}{\partial r}\left[r\frac{\partial R(r)Z(z)}{\partial r}\right] = \frac{1}{r}\frac{\partial}{\partial r}\left[rZ\frac{\partial R}{\partial r}\right] \qquad (7.20)$$

When the derivative of the product is taken, second term of the Equation 7.11 can be written as;

$$\frac{1}{r}\frac{\partial}{\partial r}\left[r\left(z\frac{\partial R}{\partial r}\right)\right] = \frac{1}{r}\left[z\frac{\partial R}{\partial r} + z\frac{\partial^2 R}{\partial r^2}r\right] = Z(z)\left[\frac{1}{r}\frac{\partial R}{\partial r} + \frac{\partial^2 R}{\partial r^2}\right] \qquad (7.21)$$

If the Equation 7.19 and Equation 7.21 is put into Equation 7.11;

$$R(r)\frac{\partial^2 Z(z)}{\partial z^2} + Z(z)\left[\frac{1}{r}\frac{\partial R}{\partial r} + \frac{\partial^2 R}{\partial r^2}\right] = 0 \tag{7.22}$$

When Equation 7.22 is divided by R(r)Z(z);

$$\frac{1}{Z(z)}\frac{\partial^2 Z(z)}{\partial z^2} + \frac{1}{R(r)}\left[\frac{1}{r}\frac{\partial R(r)}{\partial r} + \frac{\partial^2 R(r)}{\partial r^2}\right] = 0 \tag{7.23}$$

While Equation 7.11 have two functions which depends 2-variables (r and z), Equation 7.23 is obtained with two functions which depends only 1-variable (r or z) by separating into variables. Then, they can be integrated separately. Terms of the Equation 7.23 should only be equal to each other when they are equal to a constant. If the constant is defined as $-\lambda^2$;

$$-\frac{1}{Z(z)}\frac{\partial^2 Z(z)}{\partial z^2} = +\frac{1}{R(r)}\left[\frac{1}{r}\frac{\partial R(r)}{\partial r} + \frac{\partial^2 R(r)}{\partial r^2}\right] = -\lambda^2 \tag{7.24}$$

If the Equation 7.24 is solved for Z(z) and R(r) separately Equation 7.25 and 7.26 is obtained;

$$Z(z) = A_3 e^{\lambda z} + A_4 e^{-\lambda z} \tag{7.25}$$

$$R(r) = A_1 J0(\lambda r) + A_2 Y0(\lambda r) \tag{7.26}$$

If the Equation 7.25 and 7.26 are used in Equation 7.17, general solution for concentration in a cylindrical pore with an opening is obtained (Equation 7.27);

$$\chi(r,z) = [A_1 J0(\lambda r) + A_2 Y0(\lambda r)]\left[A_3 e^{\lambda z} + A_4 e^{-\lambda z}\right] \tag{7.27}$$

Evaluating the Equation 7.27 at r=0 gives;

$$\chi(0,z) = [A_1 J0(\lambda.0) + A_2 Y0(\lambda.0)]\left[A_3 e^{\lambda z} + A_4 e^{-\lambda z}\right] \tag{7.28}$$

Since J0(0)=1, YO[0] = $-\infty$, to make the concentration finite A_2 should be 0. Then, the equation 7.28 can be given as;

$$\chi(r,z) = [A_1 JO(\lambda r)]\left[A_3 e^{\lambda z} + A_4 e^{-\lambda z}\right] \qquad (7.29)$$

Applying the boundary conditions that there is no flux at z=0 and derivation of the Equation 7.29 is zero due to symmetry;

$$\frac{dC(r,z)}{dz}\Big|_{z=0} = 0 \qquad (7.30)$$

Then;

$$\frac{d\chi(r,0)}{dz} = [A_1 JO(\lambda r)]\left[\lambda A_3 e^{\lambda 0} - \lambda A_4 e^{-\lambda 0}\right] \qquad (7.31)$$

$$\frac{d\chi(r,0)}{dz}\Big|_{z=0} = [A_1 JO(\lambda r)\lambda][A_3 - A_4] = 0 \qquad (7.32)$$

Since equation 7.32 is equal to zero;

$$A_3 = A_4 \qquad (7.33)$$

Since $A_3 = A_4$, Equation 7.29 becomes;

$$\chi(r,z) = [A_1 JO(\lambda r)A_3]\left[e^{\lambda z} - e^{-\lambda z}\right] \qquad (7.34)$$

If the hyperbolic functions is examined, it can be seen that;

$$\frac{e^{\lambda z} - e^{-\lambda z}}{2} = \cosh(\lambda z) \qquad (7.35)$$

If all constant defined as 'ϕ', general solution for Equation 7.35 can be written as;

$$\chi(r,z) = \phi J0(\lambda r)\cosh(\lambda z) \tag{7.36}$$

The above equation requires that the term $J0(\lambda R)$ should be zero since $\cosh(\lambda z)$ cannot be zero for all z values. Also ϕ cannot be zero since for ϕ=0, it becomes a trivial solution.

It also follows that the periodic $J0(\lambda R)$ term has n number of λR terms where it is equal to zero for n numbers of λR (zeros of $J0(\lambda R)$). If we call these values V_n;

$$J0(\lambda R) = J0(V_n) = 0 \tag{7.37}$$

$$\lambda R = V_n \rightarrow \lambda_n = \frac{V_n}{R} \tag{7.38}$$

then Equation 7.34 can be shown as;

$$\chi(r,z) = \sum_{n=1}^{\infty} \phi_n J0\left(\frac{V_n}{R}r\right)\cosh\left(\frac{V_n}{R}z\right) \tag{7.39}$$

Since, $C(r,z) = \chi(r,z) + C_s$,

$$C(r,z) = \sum_{n=1}^{\infty} \left(\phi_n J0\left(\frac{V_n}{R}r\right)\cosh\left(\frac{V_n}{R}z\right)\right) + C_s \tag{7.40}$$

Remember that C_{sol} is actually $C_{sol}(t)$. We are looking at the system at a given instant. Applying the boundry condition that;

$$C(r,L) = \sum_{n=1}^{\infty} \left(\phi_n J0\left(\frac{V_n}{R}r\right)\cosh\left(\frac{V_n}{R}L\right)\right) + C_s = C_{sol} \tag{7.41}$$

If Equation 7.41 is shown as;

$$\sum_{n=1}^{\infty} \left(\phi_n J0\left(\frac{V_n}{R}r\right)\right) = \frac{C_{sol} - C_s}{\cosh\left(\frac{V_n}{R}L\right)} = \varphi \tag{7.42}$$

It can be seen that the above equation is in the form of a Bessel Fourier series such that;

$$\varphi = \sum_{n=1}^{\infty} \left(\phi_n J0 \left(\frac{V_n}{R} r \right) \right) \tag{7.43}$$

ϕ_n can be found by applying Fourier Bessel transform;

$$\phi_n = \frac{\int_0^a \varphi r J0 \left(\frac{V_i}{R} r \right) dr}{\int_0^a r J0 \left(\frac{V_i}{R} r \right)^2 dr} \tag{7.44}$$

The solution of the integral is in the form;

$$\phi_n = \frac{2\varphi J1(V_i)}{V_i (J0 \, (V_i)^2 + J1 \, (V_i)^2)} \tag{7.45}$$

Since J0(V_i)=0 (roots of J0),

$$\phi_n = \frac{2\varphi}{V_i J1 \, (V_i)} = \frac{C_{sol} - C_s}{\cosh \left(\frac{V_n}{R} L \right)} \cdot \frac{2}{V_i J1 \, (V_i)} \tag{7.46}$$

Substituting for φ,

$$\phi_i = \frac{C_{sol} - C_s}{\cosh \left(\frac{V_n}{R} L \right)} \cdot \frac{2}{V_i J1 \, (V_i)} \tag{7.47}$$

Then C(r,z) gives;

$$C(r,z) = \sum_{i=1}^{n} \left(\phi_i J0 \left(\frac{V_i}{R} r \right) \cosh \left(\frac{V_i}{R} z \right) + C_s \right) \tag{7.48}$$

Then, Equation 7.48 gives the concentration equation as;

$$C(r,z) = 2(C_{sol} - C_s) \sum_{i=1}^{n} \frac{J0\left(\frac{V_i}{R}r\right)\cosh\left(\frac{V_i}{R}z\right)}{V_i J1(V_i)\cosh\left(\frac{V_i}{R}L\right)} + C_s \qquad (7.49)$$

In this model, a pore is situated in the z-axis between z=-L and z=+L and is symmetrical around z=0. In terms of the radial distances, the position of the pore is between r=-R and r=+R and there is also a complete symmetry around r=0. The concentration of drug in the pore changes with pore diameter (R) and pore length (L). Increasing r values indicate that the chitosan wall is approached while the chitosan solution concentration on the pore surface (r=R) is constant at a value C_s for all z. Hence, the highest drug concentration is present on the pore surface when r=R and z=0. At the point where the pore meets the chamber (z=L), drug concentration decreases while the concentration at the pore mouth (z=L) is constant at C_{sol}(t) for all r. Figure 7.5 shows how concentration changes with r and z, separately. If the concentration change with r is examined in three points (r=0.001 R, r=0.5 R and r=0.99 R) when R=1 μm and L=10 μm, it can be said that concentration shows a much sharper reduction for r=0.99R when moves away from z=0 as expected. Because, concentration difference is higher between pore surface and the chamber. The decrease is slower for the r=0.001 R since concentration is lower than surface concentration and difference is much lower between chamber and the point (r=0.001,z). Also, when the concentration change is studied for changing r values and for three z value (z=0.01 L, z=0.5 L, z=0.995 L), sharp increase is observed when getting closer to the pore surface (r=R) from r=0 for z=0.995 L as can be seen from the figure.
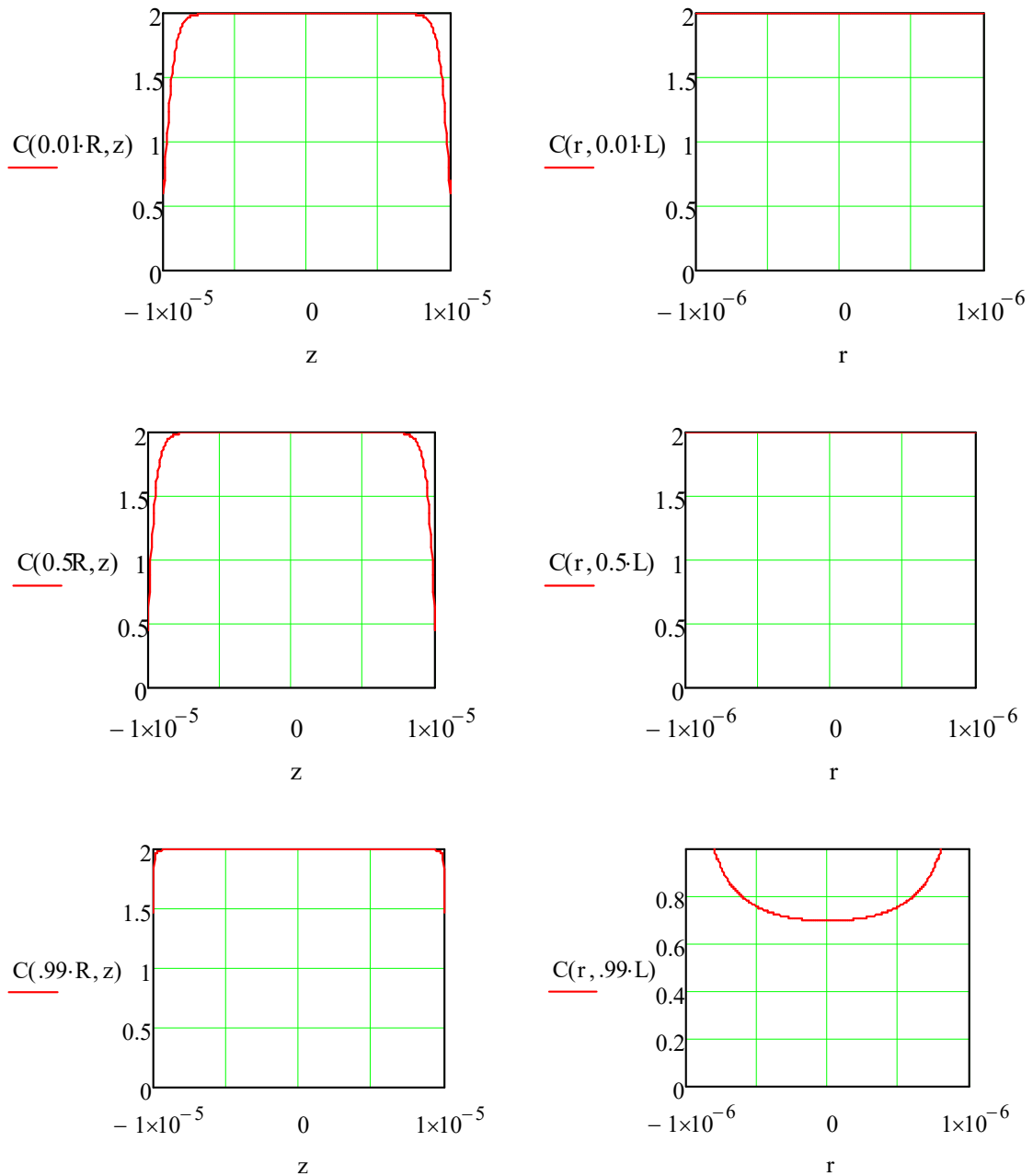
Figure 7. 5. Change of concentration with changing r and z values (R=1 µm and L=10 µm).

To observe the effect of the ratio of the pore diameter to pore length, the system was assumed to have pore diameter as 5 µm and length as 10 µm. Figure 7.6 shows the change of the concentration with r and z for the system. It can be cleary seen that concentration decreases slowly when compared the lower pore diameter through the z direction. In addition, the concentration inceases slowly through the r direction since the radius is higher. To sum up, it can be said that concentration inside the pore can be

thought to be equal to the surface concentration and same for all pore volume for the small pore diamaters. Otherwise, there is a concentration profile in the pores with higher diameters.
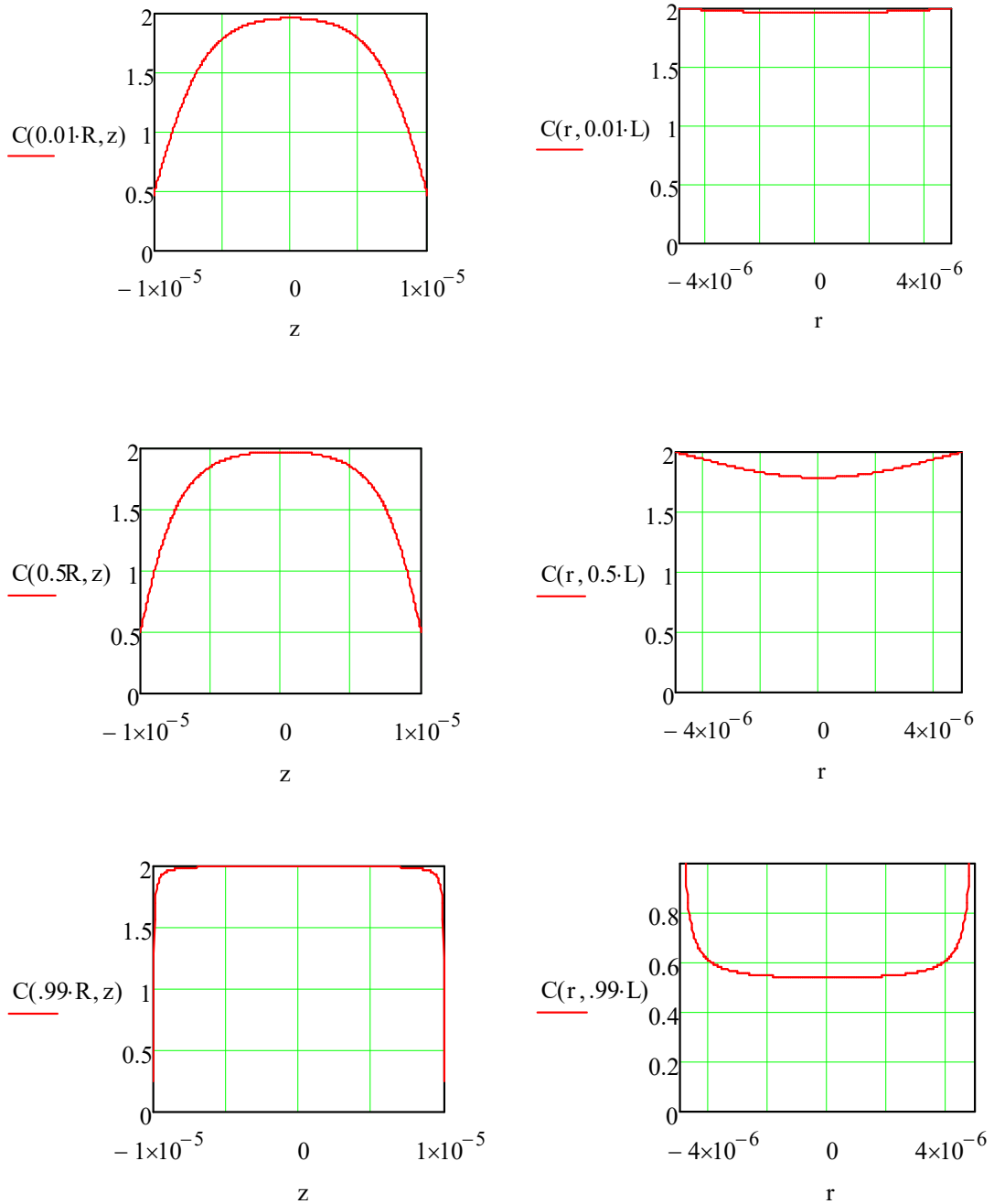
Figure 7. 6. Change of concentration with changing r and z values (R=5 μm and L=10 μm).

7.2.4. Development of the Flux Equations

The flux from the pore wall into the pores is equal to the amount of solute coming into the solution. It can be given by;

$$J_{in} = -2\pi RD \int_0^L \left(\frac{\partial}{\partial r} C(r,z)\right)_R dz \tag{7.50}$$

Since the change of concentration is obtained as;

$$\frac{dC(r,z)}{dr} = -2(C_{sol} - C_s) \sum_{i=1}^n \frac{\frac{V_i}{R} J_1\left(\frac{V_i}{R}r\right) \cosh\left(\frac{V_i}{R}z\right)}{V_i J_1(V_i) \cosh\left(\frac{V_i}{R}L\right)} \tag{7.51}$$

If Equation 7.51 is used in Equation 7.50;

$$J_{in} = 2\pi RD \int_0^L \left(\frac{\partial}{\partial r} C(r,z)\right)_R dz \tag{7.52}$$

$$= -2\pi RD \int_0^L 2(C_{sol} - C_s) \sum_{i=1}^n \frac{\frac{V_i}{R} J_1\left(\frac{V_i}{R}r\right) \cosh\left(\frac{V_i}{R}z\right)}{V_i J_1(V_i) \cosh\left(\frac{V_i}{R}L\right)}$$

When Equation 7.52 is simplified;

$$J_{in} = -4\pi D(C_{sol} - C_s) \int_0^L \sum_{i=1}^n \frac{\cosh\left(\frac{V_i}{R}z\right)}{\cosh\left(\frac{V_i}{R}L\right)} dz \tag{7.53}$$

Then, integration of Equation 7.53 gives;

$$J_{in} = -4\pi D(C_{sol} - C_s) \sum_{i=1}^n \frac{\sinh\left(\frac{V_i}{R}L\right)}{\frac{V_i}{R} \cosh\left(\frac{V_i}{R}L\right)} \tag{7.54}$$

The flux at the pore wall is obtained as;

$$J_{in} = 4\pi RD(C_s - C_{sol}) \sum_{i=1}^{n} \left(\frac{1}{V_i} \tanh\left(\frac{R}{L}V_i\right) \right) \tag{7.55}$$

This flux (J_{in}) should be equal to the flux from the pore into the solution at the pore mouth under steady state conditions (Figure 7.7).
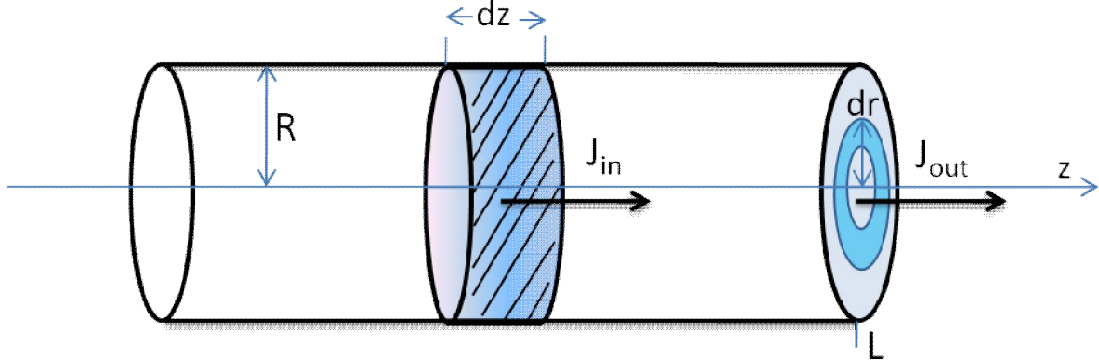
Figure 7. 7. Flux from the pore wall into the pores (J_{in}) and flux from the pore into the solution at the pore mouth (J_{out}).

The flux leaving the pore at the pore mouth can be given as;

$$J_{out} = -2\pi D \int_0^R \left(\frac{\partial}{\partial r} C(r,z) \right)_L r dr \tag{7.56}$$

Taking the derivative of the concentration equation with respect to L gives;

$$\left(\frac{dC(r,z)}{dz} \right)_L = -2 \left(\frac{C_{sol} - C_s}{R} \right) \sum_{i=1}^{n} \frac{J0\left(\frac{V_i}{R}r\right) \tanh\left(\frac{V_i}{R}L\right)}{J1(V_i)} \tag{7.57}$$

Evaluating this equation at the pore exit L and inserting it to the the J_{out} flux equation (7.56) gives;

$$J_{out} = -4\pi D \frac{C_{sol} - C_s}{R} \int_0^R \sum_{i=1}^{n} \frac{J0\left(\frac{V_i}{R}r\right) \tanh\left(\frac{V_i}{R}L\right)}{J1(V_i)} r dr \tag{7.58}$$

The flux leaving the pore at the pore mouth under steady state conditions is obtained as;

$$J_{out} = 4\pi R D (C_s - C_{sol}) \sum_{i=1}^{n} \left(\frac{1}{V_i} \tanh \left(\frac{R}{L} V_i \right) \right) \qquad (7.59)$$

7.2.5. Development of the Equation for Concentration Change in Solution

It can be seen that the steady-state conditions hold and the two fluxes are identical. Here, a is defined as R over L and the summation part is defined as f(a). It can be seen from Figure 7.8 that f(a) is equal to 1.25 a. As a result equation for concentration change in solution can be obtained as given here. The summation terms can be safely approximated by a simpler expression as follows:

$$\text{If; } a = \frac{R}{L}, \qquad f(a) = \sum_{i=1}^{n} \left(\frac{a}{V_i} \tanh \left(\frac{V_i}{a} \right) \right), \qquad f(a) = 1.25a = 1.25\frac{R}{L}$$
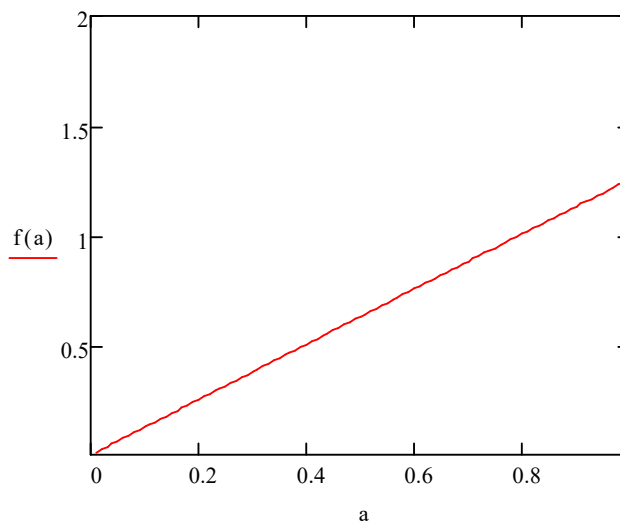
Figure 7. 8. Functions of f(a) and a.

If Equation 7.59 is divided by L and multiplied by R;

$$J_{out} = 4\pi LD(C_s - C_{sol}) \sum_{i=1}^{n} \left(\frac{R}{LV_i} \tanh \left(\frac{R}{L} V_i \right) \right) \qquad (7.60)$$

When a and f(a) terms used in Equation 7.60, it becomes;

$$J_{out} = 4\pi LD(C_s - C_{sol})f(a) \qquad (7.61)$$

As a result, Equation 7.59 can be obtained as;

$$J_{out} = \frac{dC(t)}{dt} = 5\pi DR(t)(C_s - C_{sol}) \qquad (7.62)$$

The equation given above is for a single pore and since η is the total number of pores and ϕ is the fraction of the drug in chitosan matrix, the total drug flux from the foam can be given as;

$$\frac{dC(t)}{dt} = a_1 R(t)(C_s - C_{sol}) \quad where \qquad a_1 = 5\eta\phi\pi D \qquad (7.63)$$

It can be seeen that the flux out of the pores follow a first-order expression for a constant pore radius (which would be equivalent to an instantaneous dissolution rate) is first-order. However, the dissolution of chitosan also leads a change of the pore radius which bring a higher-order dissolution rate (Figure 7.9).
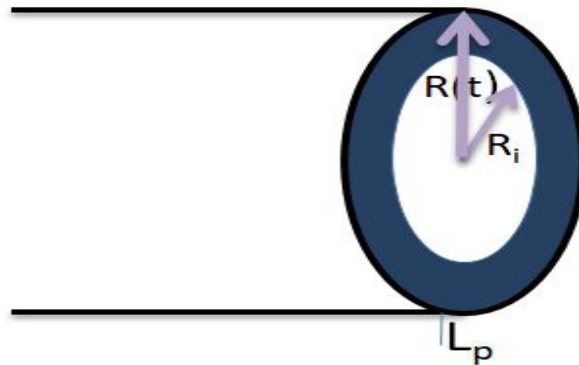
Figure 7. 9. Change of pore radius.

Differential amount of mass disssolving from the pore walls per unit solution volume can be given in terms of the change of the pore radius which is also changing concentration with time as chitosan dissolves;

$$dm(t) = dC(t) = 2\pi R(t)dR(t)\rho L_p \qquad (7.64)$$

Dividing both sides of Equation 7.64 with dt gives the differential amount of out flux from the single pore and change of concentration per unit solution volume;

$$J_{out} = \frac{dm(t)}{dt} = \frac{dC(t)}{dt} = 2\pi R(t)\frac{dR(t)}{dt}\rho L_p \qquad (7.65)$$

Since η is the total number of pores, ϕ is the fraction of the drug in chitosan matrix and b is defined as $b = 2\pi\rho L_p \phi\eta$, the total drug flux from the pore into solution can be given as;

$$J_{out} = \frac{dC(t)}{dt} = bR(t)\frac{dR(t)}{dt} \qquad (7.66)$$

Equating the two expressions for the rate of concentration change give (Equation7.63 and Equation 7.66);

$$a_1 R(t)(C_s - C_{sol})) = bR(t)\frac{dR(t)}{dt} \qquad (7.67)$$

$$\frac{dR(t)}{dt} = \frac{a_1}{b}(C_s - C_{sol}) \qquad (7.68)$$

If a_2 is defined as $a_2 = \frac{a_1}{b}$ and $a_2 = \frac{5D}{2\rho L_p}$,

$$\frac{dR(t)}{dt} = a_2(C_s - C_{sol})) \qquad (7.69)$$

Solution of the two equations (Equation 7.68 and 7.69) above gives;

151

$$R(t) = \sqrt{2\frac{a_2}{a_1}(C_s - C_1)\tanh\left[\frac{1}{2}\right]\left[\sqrt{2a_1 a_2(C_s - C_1)}(t + 2C_2)\right]} \tag{7.70}$$

where;

$$C_1 = -\frac{R_i^2 a_2}{2a_1} \tag{7.71}$$

$$C_2 = \frac{\operatorname{atanh}\left(\frac{R_i}{\sqrt{R_i^2 + \frac{2C_s a_2}{a_1}}}\right)}{\sqrt{R_i^2 a_1^2 + 2C_s a_2 a_1}} \tag{7.72}$$

for R(0)=Ri and for C(0)=0, Equation 7.70 is given as;

$$R(t) = \tanh\left(\operatorname{atanh}\left(\frac{R_i}{\sqrt{R_i^2 + \frac{2C_s a_2}{a_1}}}\right) + \frac{t\sqrt{R_i^2 a_1^2 + 2C_s a_2 a_1}}{2}\right)\sqrt{R_i^2 + \frac{2C_s a_2}{a_1}} \tag{7.73}$$

When the equation is simplified;

$$R(t) = \tanh\left(\operatorname{atanh}\left(\frac{R_i}{\sqrt{R_i^2 + \frac{2C_s a_2}{a_1}}}\right) + \frac{a_1 t}{2}\sqrt{R_i^2 + 2C_s\frac{a_2}{a_{1\,2}}}\right)\sqrt{R_i^2 + \frac{2C_s a_2}{a_1}} \tag{7.74}$$

Then, the expressions for a_1 and a_2 is put in Equation 7.74;

$$R(t) = \tanh\left(\operatorname{atanh}\left(\frac{R_i}{\sqrt{R_i^2 + \frac{C_s}{\pi\rho L_p \phi\eta}}}\right)\right. \tag{7.75}$$

$$\left. + \frac{5\eta\phi\pi Dt}{2}\sqrt{R_i^2 + \frac{C_s}{\pi\rho L_p \phi\eta}}\right)\sqrt{R_i^2 + \frac{C_s}{\pi\rho L_p \phi\eta}}$$

If α is defined as given in Equation 7.76;

$$\alpha = \sqrt{R_i^2 + \frac{C_s}{\pi \rho L_p \phi \eta}}$$ (7.76)

When α is used in Equation 7.75;

$$R(t) = \alpha \tanh\left[\operatorname{atanh}\left(\frac{R_i}{\alpha}\right) + \frac{5\eta\phi\pi D t}{2}\alpha\right]$$ (7.77)

After $R(t)$ is obtained, C(t) is found as;

$$C(t) = \frac{\tanh\left(\operatorname{atanh}\left(\frac{R_i}{\sqrt{R_i^2 + \frac{2C_s a_2}{a_1}}}\right) + \frac{t\sqrt{R_i^2 a_1^2 + 2C_s a_2 a_1}}{2}\right)^2 (a_1 R_i^2 + 2C_s a_2)}{2a_2} - \frac{a_1 R_i^2}{2a_2}$$ (7.78)

Simplified form of Equation 7.78 gives;

$$C(t) = \pi \rho L_p \phi \eta \left[\tanh\left(\operatorname{atanh}\left(\frac{R_i}{\sqrt{R_i^2 + 2C_s \frac{a_2}{a_1}}}\right)\right.\right.$$ (7.79)

$$\left.\left. + \frac{a_1 t}{2}\sqrt{R_i^2 + 2C_s \frac{a_2}{a_1}}\right)^2 \left(R_i^2 + 2C_s \frac{a_2}{a_1}\right) - R_i^2\right]$$

Then,

$$C(t) = \pi \rho L_p \phi \eta \left[\tanh\left(\operatorname{atanh}\left(\frac{R_i}{\sqrt{R_i^2 + \frac{2C_s a_2}{a_1}}}\right) + \frac{a_1 t}{2}\sqrt{R_i^2 + \frac{C_s}{\pi \rho L_p \phi \eta}}\right)^2 \left(R_i^2\right.\right.$$ (7.80)

$$\left.\left. + \frac{C_s}{\pi \rho L_p \phi \eta}\right) - R_i^2\right]$$

When the expressions for a_1 and a_2 is put in Equation 7.80;

$$C(t) = \pi \rho L_p \phi \eta \left[\tanh \left(\text{atanh} \left(\frac{R_i}{\alpha} \right) + \frac{5\eta\phi\pi Dt}{2} \alpha \right)^2 \alpha^2 - R_i^2 \right] \qquad (7.81)$$

Equation 7.81 can be simplified as;

$$C(t) = \pi \rho L_p \phi \eta \left[\left(\alpha \tanh \left(\text{atanh} \left(\frac{R_i}{\alpha} \right) + \frac{5\eta\phi\pi Dt}{2} \alpha \right) \right)^2 - R_i^2 \right] \qquad (7.82)$$

If total initial pore volume is given by V_i, mass ratio of dissolvable chitosan to solid chitosan is shown by α and κ which is the dissolution rate can be defined as;

$$V_i = \pi R_i^2 L \rho \eta \phi \qquad (7.83)$$

$$\alpha = \sqrt{1 + \frac{C_s}{V_i}} \qquad (7.84)$$

$$\kappa = \frac{5}{2} \pi D \eta \phi R_i \qquad (7.85)$$

When the definitions are used change of the radius and change of the concentration is found as;

$$R(t) = \alpha \tanh \left[\text{atanh} \left(\frac{R_i}{\alpha} \right) + \alpha \kappa t \right] \qquad (7.86)$$

$$R(t) = \alpha \tanh \left[\frac{1}{2} \ln \left(\frac{\alpha + R_i}{\alpha - R_i} \right) + \alpha \kappa t \right] \qquad (7.87)$$

$$C(t) = \pi L \rho \eta \phi [(R(t))^2 - R_i^2] \qquad (7.88)$$

To sum up, R(t) and C(t) can be given below;

$$R(t) = \alpha R_i \tanh\left[\text{atanh}\left(\frac{1}{\alpha}\right) + \alpha\kappa t\right] \tag{7.89}$$

$$R(t) = \alpha R_i \tanh\left[\ln\left(\sqrt{\frac{\alpha + 1}{\alpha - 1}}\right) + \alpha\kappa t\right] \tag{7.90}$$

$$C(t) = V_i\left[\left(\frac{R(t)}{R_i}\right)^2 - 1\right] \tag{7.91}$$

Figure 7.10 gives the change of drug concentration in the chamber and radius of the pore with time. It can be easily said that drug concentration in the chamber increases first. Then, increase rate decreases since the concentration difference is reduced by time between the chitosan wall and chamber. When the concentrations in the wall and chamber are equalized, concentration stays constant as can be seen from the figure. In addition, radius of the pore increases until chitosan wall reaches dissolution limit.
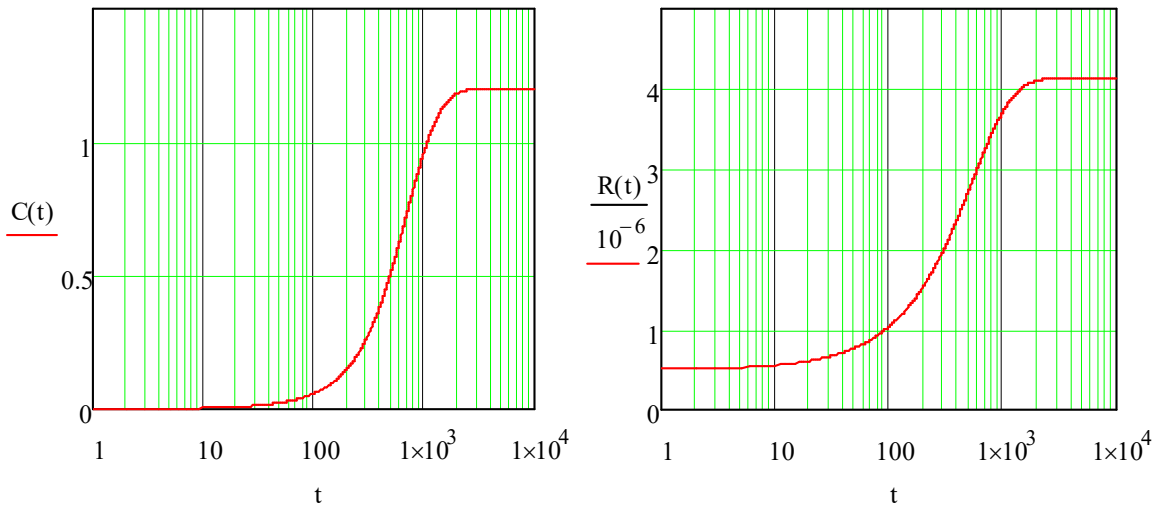
Figure 7. 10. Change of drug concentration in solution and pore diameter with time.

Then numerical solution was done to check the derived equations by using Mathematica. Equations used in the numerical solution are given below;

Given $\dfrac{dC(t)}{dt} = 5\eta\phi\pi DR(t)(C_s - C(t))$ $\qquad\qquad$ $\dfrac{dR(t)}{dt} = \dfrac{5D}{2L\rho}(C_s - C(t))$

C(0)=0 $\qquad$ R(0)=R$_i$ $\qquad$ $\begin{pmatrix} C_n \\ R_n \end{pmatrix} = Odesolve\left[\begin{pmatrix} C \\ R \end{pmatrix}, t, t_f, 100\right]$

7.2.6. Foam Calculation Sequence

It is important to determine the number of pores, volume of chamber, number of chamber, total surface area of chambers and total volume of chambers. In addition, pore properties such as volume of a single pore, unit number of per area, total number of pores and total pore volume are determined for the model. Then, total empty volume, total solid volume, total solid mass and foam volume are calculated. The foam model in calculating the number of pores in the foam structures is given in Figure 7.11.

d_w: 0.2 cm ; d_c: 0.8 cm; d_p: 0.05 cm

d_f =4 cm
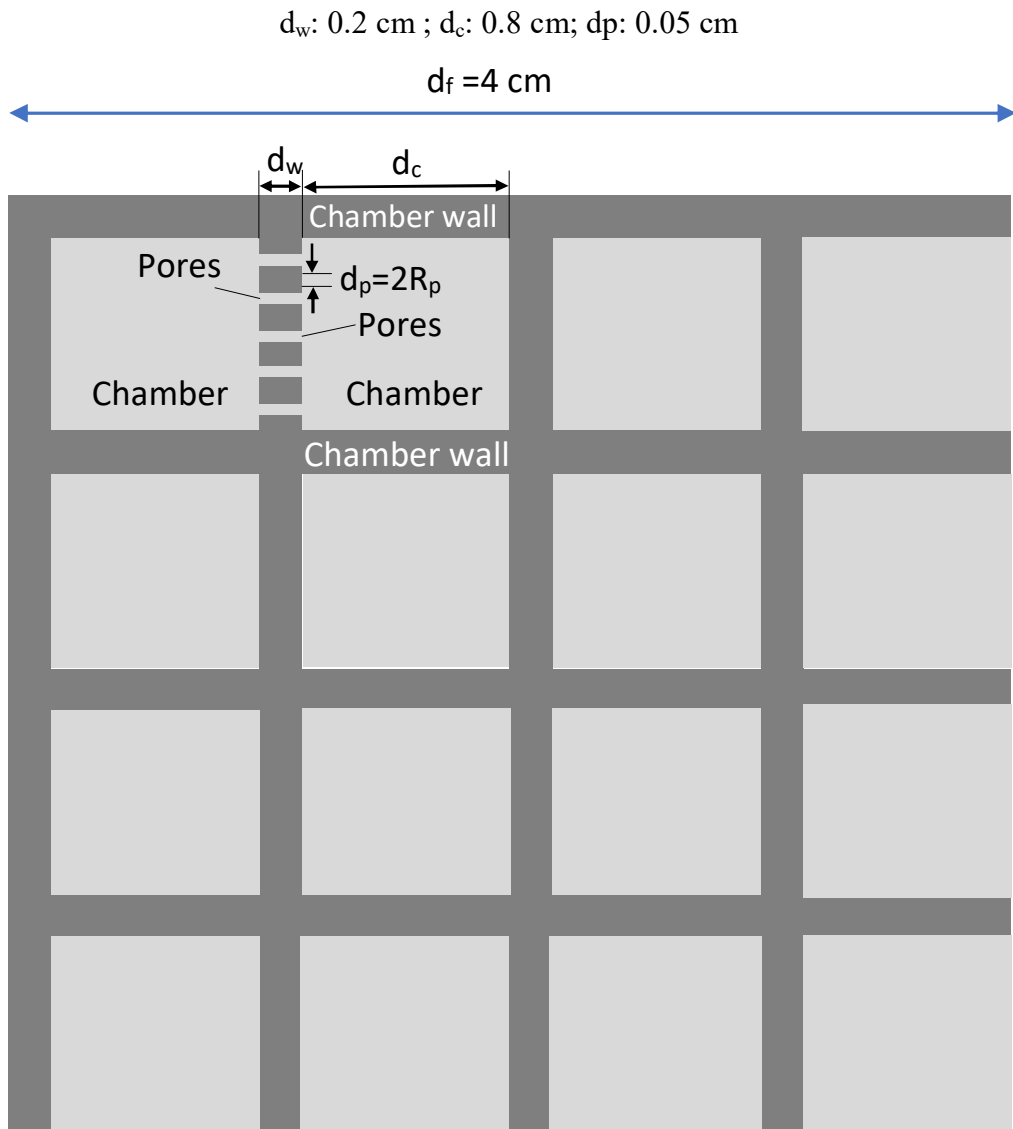
Figure 7. 11. The foam model in calculating the number of pores in the foam structures.

The sequence used in calculating the number of pores in a model foam structure in Figure 7.11 and the results are given in Figure 7.12. Pore properties such as volume of a single pore, unit number of per area, total number of pores and total pore volume are determined for the model. Then, total empty volume, total solid volume, total solid mass and foam volume are are calculated.

FOAM PROPERTIES

Volume of the whole foam: $V_f := 64 \cdot cm^3$

Size of one side of the whole foam: $d_f := \sqrt[3]{V_f}$ $d_f = 4 \cdot cm$

Solid density: $\rho := 1 \cdot \dfrac{gm}{cm^3}$

CHAMBER PROPERTIES

Chamber size: $d_c := 0.8 \cdot cm$

Volume of a single chamber $v_c := d_c^3$ $v_c = 0.512 \, cm^3$

Chamber wall thickness: $d_w := 0.2 \cdot cm$

Number of chambers: $N_c := \left(\dfrac{d_f}{d_c + d_w} \right)^3$ $N_c = 64$

Total surface area of chambers: $S_c := 6 \cdot d_c^2 \cdot N_c$ $S_c = 245.76 \, cm^2$

Total volume of chambers: $V_c := d_c^3 \cdot N_c$ $V_c = 32.768 \, cm^3$

PORE PROPERTIES

Radius of a pore: $R_p := 0.05 \, cm$

Volume of a single pore: $v_p := \pi \cdot R_p^2 \cdot d_w$ $v_p = 1.571 \times 10^{-3} \cdot cm^3$

Unit number of pores per area: $n_{pu} := 25 \cdot \dfrac{1}{d_c^2}$ $n_{pu} = 39.063 \dfrac{1}{cm^2}$

Total number of pores: $N_{pt} := n_{pu} \cdot \dfrac{S_c}{2}$ $N_{pt} = 4.8 \times 10^3$

Total Pore Volume: $V_p := N_{pt} \cdot v_p$ $V_p = 7.54 \, cm^3$

OVERALL FOAM PROPERTIES

Total empty volume: $V_e := V_c + V_p$ $V_e = 40.308 \, cm^3$

Total solid volume: $V_s := V_f - V_e$ $V_s = 23.692 \, cm^3$

Total solid mass: $m_s := V_s \cdot \rho$ $m_s = 23.692 \, gm$

Calculated Foam Volume: $Vf := V_e + V_s$ $V_f = 64 \cdot cm^3$

Figure 7. 12. The sequence used in calculating the number of pores in a model foam structure in Figure 7.10.

Then, the same the sequence used in calculating the number of pores in a real foam structure using the model in Figure 7.11. The volume of the foam is put into 100 mL release solution is 14 cm^3 and the mass of the same foam in 100 mL release solution

is 0.4 g. The number of pore was determined to the around 80 in 100 μm^2 by using SEM images. Figure 7.13 gives the results for the real foam property calculations.

REAL FOAM PROPERTY CALCULATIONS

> The volume of the foam that is put into 100 mL release solution is 14 cm3   (140 cm3 /L).
> The mass of the same foam in 100 mL release solution is 0.4 g (4.0 g/L).
> ALL CALCULATIONS BELOW ARE FOR 1 LITER SOLUTION.

Volume of foam in 1 L solution: $V_f := 140 \cdot cm^3$

Size of one side of the whole foam: $d_f := \sqrt[3]{V_f}$ $d_f = 5.192 \cdot cm$

Chitosan Solid density: $\rho := 1.1 \cdot \dfrac{g}{cm^3}$

CHAMBER PROPERTIES

Chamber size: $d_c := 150 \cdot \mu m$

Volume of a single chamber $v_c := d_c^3$ $v_c = 3.375 \times 10^{-6} \cdot cm^3$

Chamber wall thickness: $d_w := 10 \cdot \mu m$

Number of chambers: $N_c := \left(\dfrac{d_f}{d_c + d_w} \right)^3$ $N_c = 3.418 \times 10^7$

Total surface area of chambers: $S_c := 6 \cdot d_c^2 \cdot N_c$ $S_c = 4.614 \times 10^4 \, cm^2$

Total volume of chambers: $V_c := v_c \cdot N_c$ $V_c = 115.356 \cdot cm^3$

PORE PROPERTIES

Radius of a single pore: $R_p := 0.6 \cdot \mu m$

Volume of a single pore: $v_p := \pi \cdot R_p^2 \cdot d_w$ $v_p = 1.131 \times 10^{-11} \cdot cm^3$

Unit number of pores per area: $n_{pu} := 80 \cdot \dfrac{1}{100 \cdot \mu m^2}$ $n_{pu} = 8 \times 10^7 \cdot \dfrac{1}{cm^2}$

Total number of pores: $N_{pt} := n_{pu} \cdot \dfrac{S_c}{2}$ $N_{pt} = 1.846 \times 10^{12}$

Total Pore Volume: $V_p := N_{pt} \cdot v_p$ $V_p = 20.874 \cdot cm^3$

OVERALL FOAM PROPERTIES

Total empty volume: $V_e := V_c + V_p$ $V_e = 136.231 \cdot cm^3$

Total solid volume: $V_s := V_f - V_e$ $V_s = 3.769 \cdot cm^3$

Total solid mass: $m_s := V_s \cdot \rho$ $m_s = 4.066 \times 10^4 \, \dfrac{m}{kg \cdot s^2} \cdot gm$

Calculated Foam Volume: $V_f := V_e + V_s$ $V_f = 140 \cdot cm^3$

Figure 7. 13. The sequence used in calculating the number of pores in a real foam structure using the model in Figure 7.10.

7.3. Application of the Model to Real Data and Back Calculation of the System Parameters

The model developed was applied to the drug release data obtained. The resulting equations were obtained from the model development for the change of the pore radius due to chitosan dissolution and for the dissolution profile for chitosan;

$$R(t) = \frac{R_i(1 + \tanh(\alpha\kappa t))}{1 + \frac{1}{\alpha}\tanh(\alpha\kappa t)} \tag{7.86}$$

$$C_{ch}(t) = V_i\left[\left(\frac{R(t)}{R_i}\right)^2 - 1\right] \tag{7.91}$$

As given above;

$$V_i = \pi R_i^2 L \rho \eta \phi \tag{7.83}$$

$$\alpha = \sqrt{1 + \frac{C_s}{V_i}} \tag{7.84}$$

$$\kappa = \frac{5}{2}\pi D \eta R_i \phi \tag{7.85}$$

Defining a dimensionless pore diameter by dividing the time-dependent diameter with the initial pore diameter at t=0;

$$R_n(t) = \frac{R(t)}{R_i} \tag{7.94}$$

The known geometrical and physical system parameters in these equations are;

$R_i = 0.6 \ \mu m$ $\qquad\qquad \rho = 1100 \ kg/m^3$ $\qquad\qquad \eta=1.846 \times 10^{12} \ 1/L$

The other parameters D, L_p and κ in the equations are not known and must be determined.

Note that the $C_{ch}(t)$ is the concentration of chitosan in the release solution. Since a known amount of drug is present in the chitosan matrix at a ration φ, the drug dissolution profile can be obtained as a function of time by using chitosan dissolution profile.

Concentration of chitosan in solution: m_{ch}=40 g/L

Concentration of drug (Vancomycin) in solution: m_d=3 g/L

Concentration of drug (Curcumin) in solution: m_{d1}=0.2 g/L

Drug (Vancomycin) to chitosan ratio (φ): $\phi = \frac{m_d}{m_{ch}} = 0.075$

Drug (Curcumin) to chitosan ratio (φ₁): $\phi_1 = \frac{m_{d1}}{m_{ch}} = 0.005$

The drug dissolution results as a function of time from the release experiments are given below. Note here that $C_d(t)$ is the measured drug concentration in solution and $C_{ch}(t)$ is the corresponding chitosan concentration in solution such that $C_{ch}(t)=C_d(t)/\phi$ (assuming the drug is homogeneously dispersed in the chitosan matrix).

"Time, hr"	"Cd(t), g/L"	"Cch, (g/L)"
0.1600	0.0109	0.1453
1.0000	0.0199	0.2653
3.0000	0.0618	0.8240
6.0000	0.1069	1.4253
24.0000	0.2187	2.9160
48.0000	0.2671	3.5613
72.0000	0.2872	3.8293
96.0000	0.2961	3.9480
168.0000	0.3049	4.0653
192.0000	0.3016	4.0213
214.0000	0.3076	4.1013
238.0000	0.3000	4.0000

Equations 7.86 and 7.91 can be combined to a single equation for the change of chitosan concentration with time;

$$C_{ch}(t) = V_i \left[\left(\frac{1 + \alpha \tanh(\alpha \kappa t))}{1 + \frac{1}{\alpha} \tanh(\alpha \kappa t)} \right)^2 - 1 \right] \tag{7.95}$$

Equation 7.95 was fitted to the data from the table above using the Time (hr) and $C_{ch}(t)$ columns to give the following fit parameters;

$$\alpha = 1.0161$$

$$\kappa = 0.0302 \ 1/h$$

$$V_i = 122.01 \ g/L$$

Placing these model fit parameters and the known physical parameters for the system in Equation 7.83, Equation 7.84, Equation 7.85 yields the following unknown system parameter using;

$$L_p = \frac{V_i}{\pi R_i^2 \rho \eta}$$

$$C_s = (\alpha^2 - 1)V_i$$

$$D = \frac{2\kappa}{5\pi \eta R_i \phi}$$

which gives;

$$L_p = 53.1 \mu m \qquad C_s = 3.96 \frac{kg}{m^3} \qquad \frac{D}{10^{-15}} = 0.964 \ m^2/s$$

The corresponding chitosan and drug (vancomycin) dissolution profiles from Equation 7.86 and 7.91 is in the form given in Figure 7.14. As can be seen from the figure that the dissolution rates of chitosan and drug increase first and the increasing rate decreaces with time up to dissolution limits.

The chitosan dissolution profile
(Total chitosan concentration = 4 g/L)

The drug dissolution profile
(Total drug concentration = 0.3 g/L)
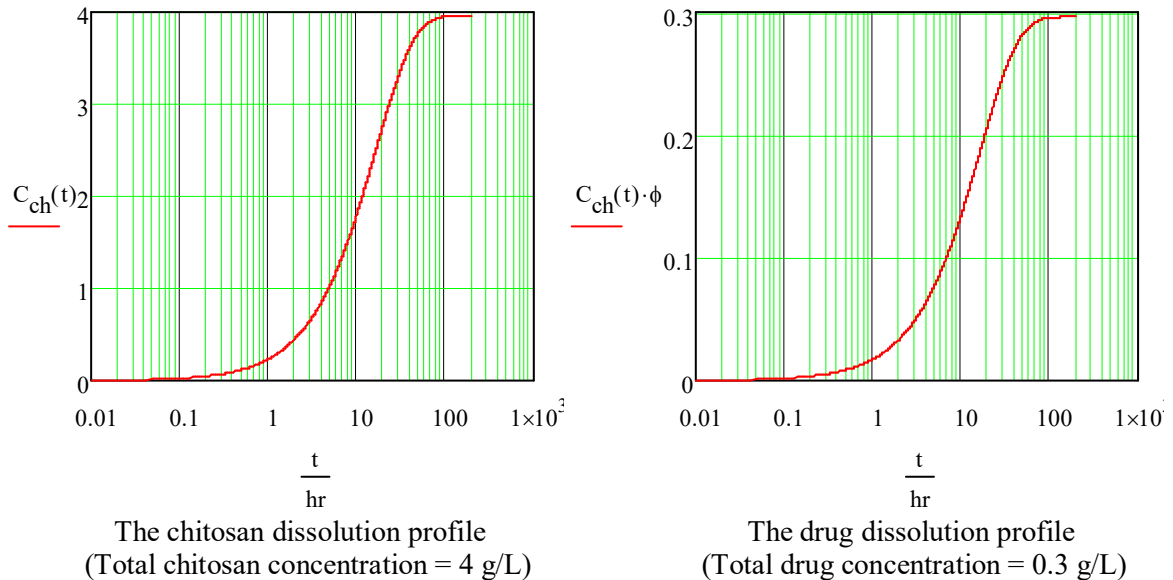
Figure 7. 14. The chitosan and drug dissolution profile.

Finally, the release data obtained were analyzed by the developed model. Figure 7.15 gives the dissolution of the chitosan and analysis of the data by model. The data can be said to fit perfectly. In addition, Figure 7.16 shows the graph of model fit analysis for hydrophilic (vancomycin) drug. It can be easily seen that the data fits the model very well. Hence, it can be said that the model is suitable for the vancomycin (hydrophilic) release mechanisms where drug is dispersed in the matrix. Also, assumptions made for the systems are found to be quite appropriate.

Morover, it can be seen that the model output parameter are reasonable physical entitites. The pore length comes out to be around 53.1 μm. Considering the wall thickness of around 10 μm, this higher number (53.1 μm) indicates a tortuosity of the pores within the walls.

Also, the very low diffusion coefficient of 0.964×10^{-15} m^2/s is in aggrement with the diffusion coefficients observed in the literature for large polymer molecules. Kwasniewska et al. showed that the diffusion coefficients of Heterogemini

163

Sulfobetaines molecules in water varied between 10^{-14} and 10^{-16} m^2/s and decreased with increasing polymer concentration (Kwaśniewska et al. 2015). Considering the high concentration profiles developed within the narrow pores of the chitosan matrix, the effective diffusion coefficient of 0.964×10^{-15} m^2/s is reasonable.

As for the solubility limit C_s, the predicted value of around 4.0 g/L at pH = 5.6 is reasonable considering (da Silva et al. 2018).
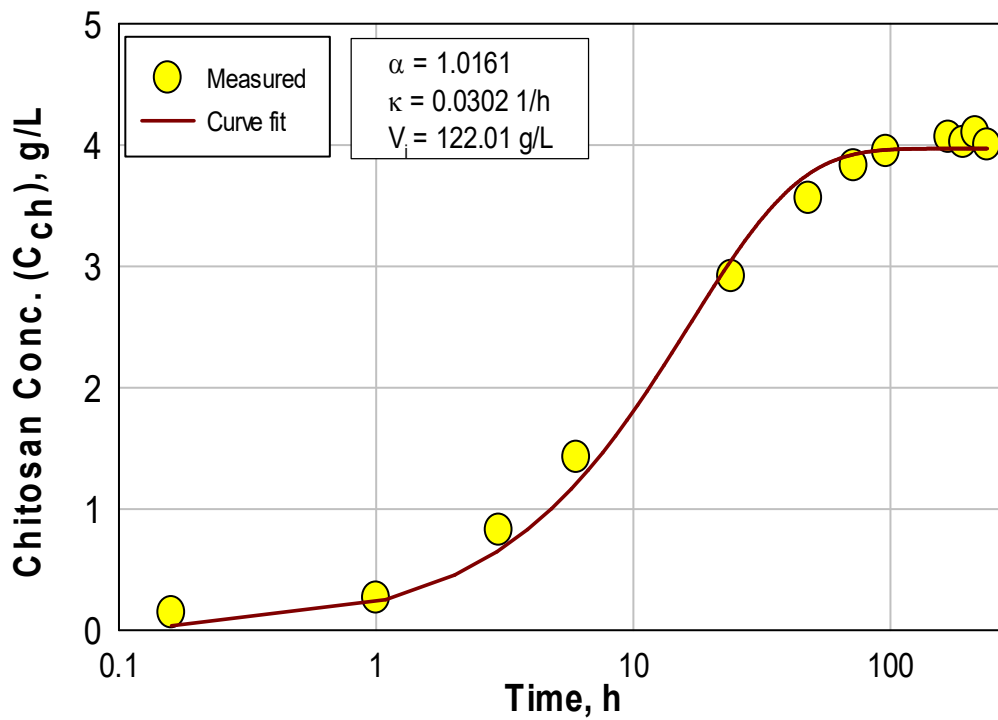
Figure 7. 15. Application of the model to the chitosan dissolution data.
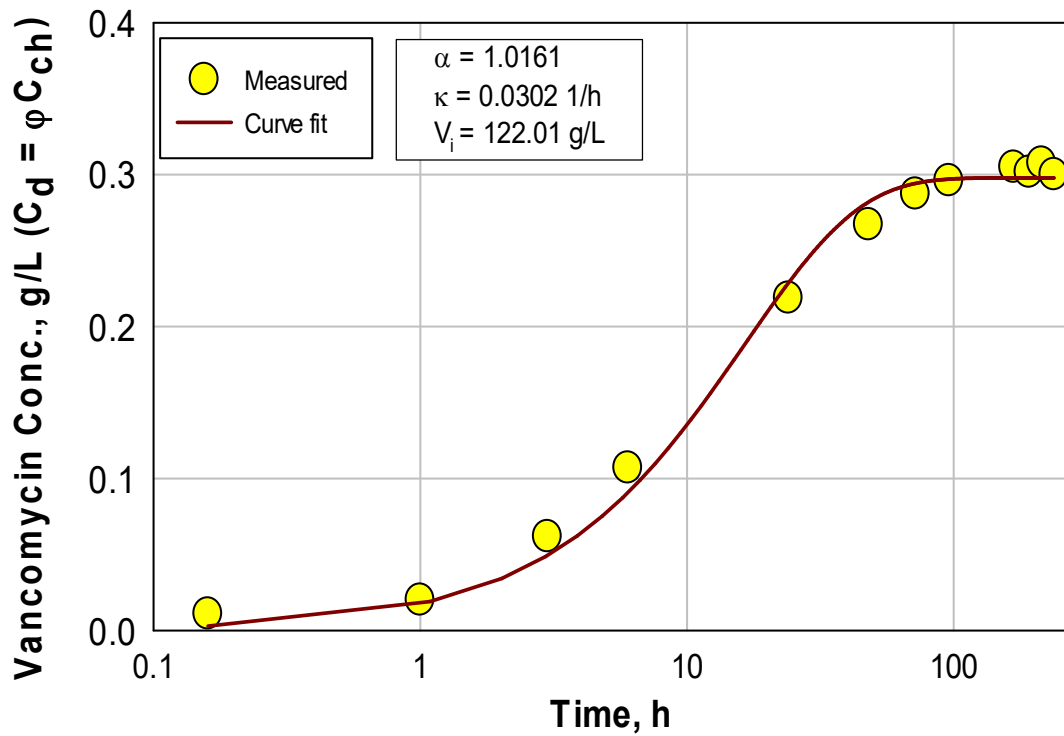
Figure 7. 16. Application of the model to the vancomycin release data.

Then, the model was applied to the curcumin (hydrophobic) release data. Although the model complies with the hydrophilic drug system, it can be seen from Figure 7.17 that the model does not fit well in systems in the presence of hydrophobic drug encapsulated micelles. Because, the system work for the systems where molecules dispersed in the chitosan matrix homogeneously. If the model is accepted for the system, κ value which is releated to the diffusion coefficient increases. This can be due to the presence of high amount of molecules in the micelles.
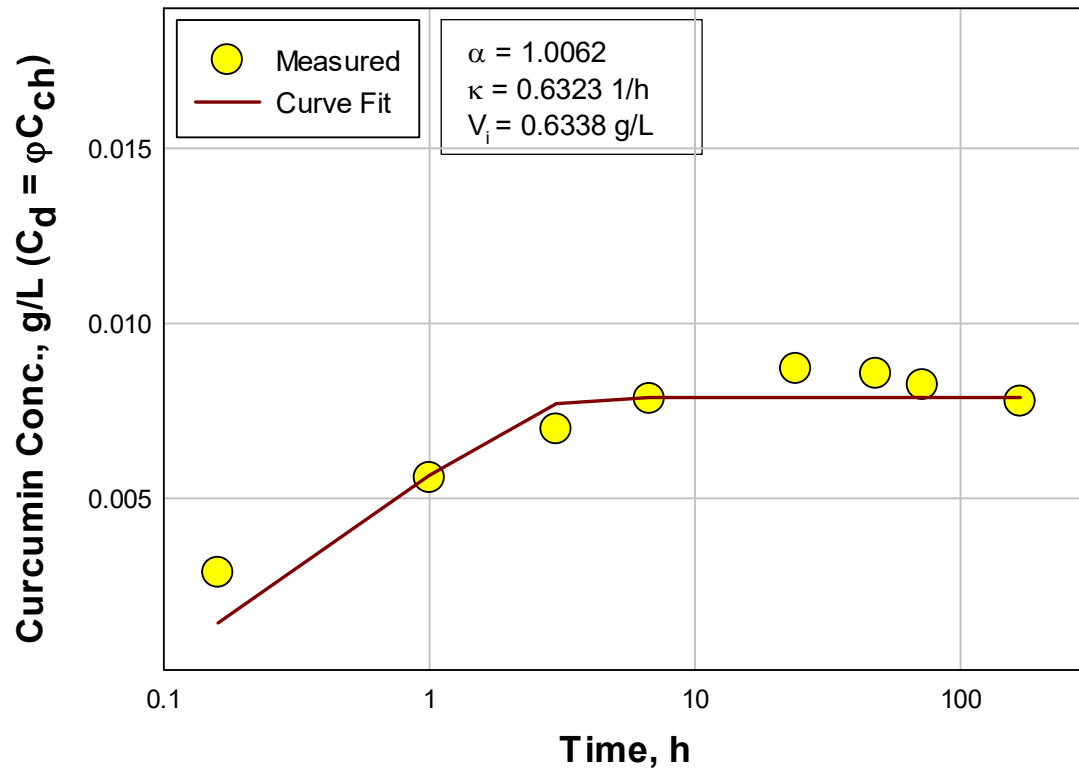
Figure 7. 17. Application of the model to the curcumin release data.

CHAPTER 8

SUMMARY AND CONCLUSIONS

In this thesis study, chitosan biofoams were produced by liquid (emulsion) templated method in the absence/presence of drug. The effect of experimental parameters on optimizing synthesis methods and optimizing foam-drug interactions has been studied in detail. The results of all these studies conducted and the conclusions made based on these studies were summarized in the following paragraphs.

In the first part of the study, O/W emulsions were produced using an ultrasonic probe in the absence of surfactants at four different chitosan concentrations. Chitosan was crosslinked by TPP. It was observed that chitosan amount has a large effect on the both the pore structure and the mechanical strength of foams. High chitosan concentrations resulted in more robust structures. Then, the oil droplets were obtained by ultrasonic probe in the presence of four types of surfactants (P-123, CTAB, SDS and TX-100) to increase both the stability and the number of oil droplets to form emulsions as templates. All structures were so brittle compare to the ones produced in the absence of surfactants. In the case of forming spontaneous emulsions, much smaller and ordered pores were produced but the foams were very brittle and distributed easily. High molecular weight chitosan was also tested to observe the effect of molecular weight on biofoam production. The pore structure was found to be more disordered and brittle compared to the low molecular weight chitosan.

In this study, SDS was used as an alternative cross linking agent in the absence of TPP. All SDS concentrations tested produced smaller sized porous structures compared to the ones crosslinked by TPP. Also, walls of the chitosan matrix showed porous structure. After freeze drying, no deformity in the structure was observed in the case of SDS crosslinking. The biofoams which were crosslinked by SDS have higher compressive strength values compared to the other foams produced with TPP (in this study and the literature). Different type of anionic surfactants were also tested as crosslinking agents to clarify the effect of surfactant structure on forming foams (Octadecyl sulfate sodium salt has straight chain similar to the SDS and mono-N-

dodecyl phosphate has helical chain) and both surfactants were also found to form porous structures. However, the walls of the foams did not have porous structure.

To clarify the role of oil phase in pore structure, chitosan foams were also produced in the absence of an oil phase. Even though these foams showed structural voids, there were no intrinsic micro pores in their framework. This observation suggested the presence of two types of pores in the structure. One is the structural voids (macropores) produced even in the absence of an oil phase (at least oil phase is not directly responsible) and the other one is the intrinsic micro pores (micropores) produced in the walls of the chitosan matrix. Besides the structural voids in foams, intrinsic micro pores with different size and shape were also observed in the presence of an oil phase. Then, effect of carbon chain length was examined by using three types of oil (pentane, hexane and heptane). For all the oil types, the structures had both structural voids and intrinsic micro pores. The foams had good mechanical strength compared with literature. They have better compressive strength than the foams produced in the absence of oil phase. It was observed that oil phase with smaller carbon chain produce higher micropore areas due to high volatility and low molecular weight. The foams produced in the absence of oil phase, on the other hand, has the smallest micropore area. This may be due to the absence of intrinsic micro pores.

To determine the porosity and water hold-up/release behavior of the chitosan foams, immerse tests were conducted. The results indicated that almost all foams can hold water nearly twenty times of their own weight. The water release tests showed that the release is slower for the higher chitosan concentrations. This can be due to high pore size and low porosity of the foams produced by high chitosan concentrations. The porosities of foams were calculated and concluded that the porosity of the foams depends on the amount of chitosan and oil phase. The porosity increases with decreasing chitosan concentration and decreasing oil concentration. Moreover, the porosity of all the foams are higher than the ideal value, 80 % mentioned in literature.

The second part of the study was an attempt to produce drug loaded chitosan biofoams using the same liquid (emulsion) templated method. The hydrophobic drugs used were curcumin and amphotericin-B (a model anti-inflammatory and antibiotic drugs) and the hydrophilic drug was a model antibiotic, vancomycin hydrochloride which is used to treat infections. Hydrophobic drug loaded biofoams were produced by thin film evaporation method coupled with the O/W emulsion template method.

Therefore this part of the study includes a detailed characterization of P-123 micelles with and without drug. However, a change in the size of micelles were not drastic.

In the third part of the study, the drug release behaviour of foams for both hydrophobic and hydrophilic drugs was examined. These studies were conducted in phosphate buffer at pH 5.6 for curcumin loaded biofoams at 37 ^{0}C. The release percentage of curcumin was found to increase with an increase in the amount of curcumin for the cases where chitosan was crosslinked by TPP. This percentage, on the other hand, was really low for the chitosan foams crosslinked by SDS most probably due to the possible interactions between drug, chitosan and SDS. In the case of vancomycin, the release was found to be higher at pH 5.6 than pH 8.2 due to the higher solubility of chitosan under acidic conditions. The release of vancomycin was also lower in the case of 4 % chitosan compared to the 2 % chitosan as expected due to its structure with lower porosity. The kinetics of drug releases were found to be presented better by second order kinetic model.

In the fourth part of the study, a mathematical model was developed to describe the kinetics of drug release from chitosan foams. According to this model, drug concentration in the chamber increases first. Then, increase rate decreases since the concentration difference is reduced by time between the chitosan wall and chamber. When the concentrations in the wall and chamber are equalized, concentration stays constant. In addition, radius of the pore increases until chitosan wall reaches dissolution limit. When the model is applied to the chitosan dissolution and vancomycin release data, it was demonstrated that model fits to the experimental data very well as expected. Since the model works with the molecules which are homogeneously dispersed in the chitosan matrix, the model does not fit the curcumin (in P-123 micelles) release data.

REFERENCES

Albaugh, Karen W, Scott A Biely, and Joseph P Cavorsi. 2013. "The effect of a cellulose dressing and topical vancomycin on methicillin-resistant Staphylococcus aureus (MRSA) and Gram-positive organisms in chronic wounds: a case series." *Ostomy Wound Manage* 59 (5):34-43.

Andrieux, Sébastien, Lilian Medina, Michael Herbst, Lars A Berglund, and Cosima Stubenrauch. 2019. "Monodisperse highly ordered chitosan/cellulose nanocomposite foams." *Composites Part A: Applied Science and Manufacturing* 125:105516.

Anitha, A, S Sowmya, PT Sudheesh Kumar, S Deepthi, KP Chennazhi, H Ehrlich, M Tsurkan, and R Jayakumar. 2014. "Chitin and chitosan in selected biomedical applications." *Progress in Polymer Science* 39 (9):1644-1667.

Arpornmaeklong, P, Pb Pripatnanont, and N Suwatwirote. 2008. "Properties of chitosan–collagen sponges and osteogenic differentiation of rat-bone-marrow stromal cells." *International journal of oral and maxillofacial surgery* 37 (4):357-366.

Budnyak, Tetyana M, Ievgen V Pylypchuk, Valentin A Tertykh, Elina S Yanovska, and Dorota Kolodynska. 2015. "Synthesis and adsorption properties of chitosan-silica nanocomposite prepared by sol-gel method." *Nanoscale research letters* 10 (1):87.

Chao, An-Chong, Shu-Huei Yu, and Guo-Syong Chuang. 2006. "Using NaCl particles as porogen to prepare a highly adsorbent chitosan membranes." *Journal of membrane science* 280 (1):163-174.

Chen, Xing, Li-Qiang Zou, Jing Niu, Wei Liu, Sheng-Feng Peng, and Cheng-Mei Liu. 2015. "The stability, sustained release and cellular antioxidant activity of curcumin nanoliposomes." *Molecules* 20 (8):14293-14311.

Cheng, Yan, Huijun He, Chunping Yang, Zhou Yan, Guangming Zeng, and Hui Qian. 2016. "Effects of anionic surfactant on n-hexane removal in biofilters." *Chemosphere* 150:248-253.

Croisier, Florence, and Christine Jérôme. 2013. "Chitosan-based biomaterials for tissue engineering." *European Polymer Journal* 49 (4):780-792.

Cruz-Tirado, JP, Ramon Sousa Barros Ferreira, Edward Lizárraga, Delia R Tapia-Blácido, NCC Silva, Luis Angelats-Silva, and Raúl Siche. 2020. "Bioactive Andean sweet potato starch-based foam incorporated with oregano or thyme essential oil." *Food Packaging and Shelf Life* 23:100457.

Cuomo, Francesca, Martina Cofelice, Francesco Venditti, Andrea Ceglie, Maria Miguel, Björn Lindman, and Francesco Lopez. 2018. "In-vitro digestion of curcumin

loaded chitosan-coated liposomes." *Colloids and Surfaces B: Biointerfaces* 168:29-34.

da Rosa Schio, Rejiane, Bruno C da Rosa, Janaína O Gonçalves, Luiz AA Pinto, Evandro S Mallmann, and Guilherme L Dotto. 2019. "Synthesis of a bio–based polyurethane/chitosan composite foam using ricinoleic acid for the adsorption of Food Red 17 dye." *International journal of biological macromolecules* 121:373-380.

da Silva, Suse Botelho, Malgorzata Krolicka, Lambertus AM van den Broek, August E Frissen, and Carmen Gabriela Boeriu. 2018. "Water-soluble chitosan derivatives and pH-responsive hydrogels by selective C-6 oxidation mediated by TEMPO-laccase redox system." *Carbohydrate polymers* 186:299-309.

Devi, M Pandima, M Sekar, M Chamundeswari, A Moorthy, G Krithiga, N Selva Murugan, and TP Sastry. 2012. "A novel wound dressing material—fibrin–chitosan–sodium alginate composite sheet." *Bulletin of Materials Science* 35 (7):1157-1163.

Dragostin, Oana Maria, Sangram Keshari Samal, Mamoni Dash, Florentina Lupascu, Andreea Pânzariu, Cristina Tuchilus, Nicolae Ghetu, Mihai Danciu, Peter Dubruel, and Dragos Pieptu. 2016. "New antimicrobial chitosan derivatives for wound dressing applications." *Carbohydrate polymers* 141:28-40.

Dutra, Lillian Maria Uchôa, Maria Elenir Nobre Pinho Ribeiro, Igor Marques Cavalcante, Débora Hellen Almeida de Brito, Luana de Moraes Semião, Raquel Freitas da Silva, Pierre Basílio Almeida Fechine, Stephen George Yeates, and Nágila Maria Pontes Silva Ricardo. 2015. "Binary mixture micellar systems of F127 and P123 for griseofulvin solubilisation." *Polímeros* 25 (5):433-439.

El-Hefian, Esam Abdulkader, Mohamed Mahmoud Nasef, and Abdul Hamid Yahaya. 2014. "Chitosan-based polymer blends: Current status and applications." *J. Chem. Soc. Pak* 36 (1):11.

Engel, Juliana B, Alan Ambrosi, and Isabel C Tessaro. 2019. "Development of biodegradable starch-based foams incorporated with grape stalks for food packaging." *Carbohydrate polymers* 225:115234.

Ferrer, Ana, Lokendra Pal, and Martin Hubbe. 2017. "Nanocellulose in packaging: Advances in barrier layer technologies." *Industrial Crops and Products* 95:574-582.

Franks, George V, Belinda Moss, and David Phelan. 2006. "Chitosan tissue scaffolds by emulsion templating." *Journal of Biomaterials Science, Polymer Edition* 17 (12):1439-1450.

Glenn, GM, and WJ Orts. 2001. "Properties of starch-based foam formed by compression/explosion processing." *Industrial Crops and Products* 13 (2):135-143.

Gunathilake, Thennakoon M Sampath Udeni, Yern Chee Ching, Cheng Hock Chuah, Hazlee Azil Illias, Kuan Yong Ching, Ramesh Singh, and Liou Nai-Shang.

2018. "Influence of a nonionic surfactant on curcumin delivery of nanocellulose reinforced chitosan hydrogel." *International journal of biological macromolecules* 118:1055-1064.

Hassan, MM, N Tucker, and MJ Le Guen. 2020. "Thermal, mechanical and viscoelastic properties of citric acid-crosslinked starch/cellulose composite foams." *Carbohydrate Polymers* 230:115675.

Hsieh, Chien-Yang, Sung-Pei Tsai, Ming-Hwa Ho, Da-Ming Wang, Chung-En Liu, Cheng-Hsuan Hsieh, Hsien-Chung Tseng, and Hsyue-Jen Hsieh. 2007. "Analysis of freeze-gelation and cross-linking processes for preparing porous chitosan scaffolds." *Carbohydrate Polymers* 67 (1):124-132.

Hu, Shihao, Shichao Bi, Dong Yan, Zhongzheng Zhou, Guohui Sun, Xiaojie Cheng, and Xiguang Chen. 2018. "Preparation of composite hydroxybutyl chitosan sponge and its role in promoting wound healing." *Carbohydrate Polymers* 184:154-163.

Huang, Xiaofei, Yongfu Sun, Jingyi Nie, Wentao Lu, Ling Yang, Zhiliang Zhang, Hongping Yin, Zhengke Wang, and Qiaoling Hu. 2015. "Using absorbable chitosan hemostatic sponges as a promising surgical dressing." *International journal of biological macromolecules* 75:322-329.

Ikeda, Takeshi, Kahori Ikeda, Kouhei Yamamoto, Hidetaka Ishizaki, Yuu Yoshizawa, Kajiro Yanagiguchi, Shizuka Yamada, and Yoshihiko Hayashi. 2014. "Fabrication and characteristics of chitosan sponge as a tissue engineering scaffold." *BioMed research international* 2014.

Indrani, Decky Joesiana, F Lukitowati, and Yoki Yulizar. 2017. "Preparation of Chitosan/Collagen Blend Membranes for Wound Dressing: A Study on FTIR Spectroscopy and Mechanical Properties." IOP Conference Series: Materials Science and Engineering.

Jayakumar, R, M Prabaharan, PT Sudheesh Kumar, SV Nair, and H Tamura. 2011. "Biomaterials based on chitin and chitosan in wound dressing applications." *Biotechnology advances* 29 (3):322-337.

Ji, Chengdong, Nasim Annabi, Ali Khademhosseini, and Fariba Dehghani. 2011. "Fabrication of porous chitosan scaffolds for soft tissue engineering using dense gas CO 2." *Acta Biomaterialia* 7 (4):1653-1664.

Kaisangsri, Nattapon, Ryan J Kowalski, Orapin Kerdchoechuen, Natta Laohakunjit, and Girish M Ganjyal. 2019. "Cellulose fiber enhances the physical characteristics of extruded biodegradable cassava starch foams." *Industrial Crops and Products* 142:111810.

Kanimozhi, K, S Khaleel Basha, and V Sugantha Kumari. 2016. "Processing and characterization of chitosan/PVA and methylcellulose porous scaffolds for tissue engineering." *Materials Science and Engineering: C* 61:484-491.

Karri, Veera Venkata Satyanarayana Reddy, Gowthamarajan Kuppusamy, Siddhartha Venkata Talluri, Sai Sandeep Mannemala, Radhakrishna Kollipara, Ashish

Devidas Wadhwani, Shashank Mulukutla, Kalidhindi Rama Satyanarayana Raju, and Rajkumar Malayandi. 2016. "Curcumin loaded chitosan nanoparticles impregnated into collagen-alginate scaffolds for diabetic wound healing." *International journal of biological macromolecules* 93:1519-1529.

Kedar, Uttam, Prasanna Phutane, Supriya Shidhaye, and Vilasrao Kadam. 2010. "Advances in polymeric micelles for drug delivery and tumor targeting." *Nanomedicine: Nanotechnology, Biology and Medicine* 6 (6):714-729.

Khan, Munezza A, and Mohammad Mujahid. 2019. "A review on recent advances in chitosan based composite for hemostatic dressings." *International journal of biological macromolecules* 124:138-147.

Kiran, Erdogan. 2016. "Supercritical fluids and polymers–The year in review–2014." *The Journal of Supercritical Fluids* 110:126-153.

Kumar, Majeti NV Ravi. 2000. "A review of chitin and chitosan applications." *Reactive and functional polymers* 46 (1):1-27.

Kwaśniewska, Dobrawa, Katarzyna Staszak, Daria Wieczorek, and Ryszard Zieliński. 2015. "Synthesis and interfacial activity of novel heterogemini sulfobetaines in aqueous solution." *Journal of surfactants and detergents* 18 (3):477-486.

Li, Chunyao, Tao Lou, Xu Yan, Yun-ze Long, Guangpeng Cui, and Xuejun Wang. 2018. "Fabrication of pure chitosan nanofibrous membranes as effective absorbent for dye removal." *International journal of biological macromolecules* 106:768-774.

Li, Zhensheng, Hassna R Ramay, Kip D Hauch, Demin Xiao, and Miqin Zhang. 2005. "Chitosan–alginate hybrid scaffolds for bone tissue engineering." *Biomaterials* 26 (18):3919-3928.

Lim, Jin Ik, Yong-Keun Lee, Jeon-Soo Shin, and Kook-Jin Lim. 2011. "Preparation of interconnected porous chitosan scaffolds by sodium acetate particulate leaching." *Journal of Biomaterials Science, Polymer Edition* 22 (10):1319-1329.

Lin, Wen-Ching, Da-Guang Yu, and Ming-Chien Yang. 2005. "pH-sensitive polyelectrolyte complex gel microspheres composed of chitosan/sodium tripolyphosphate/dextran sulfate: swelling kinetics and drug delivery properties." *Colloids and surfaces B: Biointerfaces* 44 (2-3):143-151.

Lin, Y, HE Huff, MH Parsons, E Iannotti, and F Hsieh. 1995. "Mechanical properties of extruded high amylose starch for loose-fill packaging material." *LWT-Food Science and Technology* 28 (2):163-168.

López-Montilla, Juan Carlos, Paulo Emilio Herrera-Morales, Samir Pandey, and Dinesh O Shah. 2002. "Spontaneous emulsification: mechanisms, physicochemical aspects, modeling, and applications." *Journal of dispersion science and technology* 23 (1-3):219-268.

Madeleine-Perdrillat, Claire, Thomas Karbowiak, Frédéric Debeaufort, Luc Delmotte, Cyril Vaulot, and Dominique Champion. 2016. "Effect of hydration on molecular dynamics and structure in chitosan films." *Food Hydrocolloids* 61:57-65.

Madeleine-Perdrillat, Claire, Thomas Karbowiak, Jesus Raya, Régis Gougeon, Philippe R Bodart, and Frédéric Debeaufort. 2015. "Water-induced local ordering of chitosan polymer chains in thin layer films." *Carbohydrate polymers* 118:107-114.

Madihally, Sundararajan V, and Howard WT Matthew. 1999. "Porous chitosan scaffolds for tissue engineering." *Biomaterials* 20 (12):1133-1142.

Mathias, Jean-Denis, Nicolas Tessier-Doyen, and Philippe Michaud. 2011. "Development of a chitosan-based biofoam: application to the processing of a porous ceramic material." *International journal of molecular sciences* 12 (2):1175-1186.

Michailidou, Georgia, Evi Christodoulou, Stavroula Nanaki, Panagiotis Barmpalexis, Evangelos Karavas, Susan Vergkizi-Nikolakaki, and Dimitrios N Bikiaris. 2019. "Super-hydrophilic and high strength polymeric foam dressings of modified chitosan blends for topical wound delivery of chloramphenicol." *Carbohydrate polymers* 208:1-13.

Miras, Jonathan, Susana Vílchez, Conxita Solans, and Jordi Esquena. 2013. "Chitosan macroporous foams obtained in highly concentrated emulsions as templates." *Journal of colloid and interface science* 410:33-42.

MITELUȚ, Amalia Carmen, Elisabeta Elena TĂNASE, POPA Vlad Ioan, and Mona Elena Popa. 2015. "Sustainable alternative for food packaging: Chitosan biopolymer-a review." *AgroLife Scientific Journal* 4 (2):52-61.

Moeini, Arash, Parisa Pedram, Pooyan Makvandi, Mario Malinconico, and Giovanna Gomez d'Ayala. 2020. "Wound healing and Antimicrobial effect of active Secondary Metabolites in Chitosan-based Wound dressings: A review." *Carbohydrate Polymers*:115839.

Mohanty, Soumyaranjan, Kuldeep Sanger, Arto Heiskanen, Jon Trifol, Peter Szabo, Marin Dufva, Jenny Emnéus, and Anders Wolff. 2016. "Fabrication of scalable tissue engineering scaffolds with dual-pore microarchitecture by combining 3D printing and particle leaching." *Materials Science and Engineering: C* 61:180-189.

Möbius, D., R. Miller, and V.B. Fainerman. 2001. *Surfactants: Chemistry, Interfacial Properties, Applications: Chemistry, Interfacial Properties, Applications*: Elsevier Science.

Netti, Paulo. 2014. *Biomedical foams for tissue engineering applications*: Elsevier.

Nguyen, Van Cuong, Van Boi Nguyen, and Ming-Fa Hsieh. 2013. "Curcumin-loaded chitosan/gelatin composite sponge for wound healing application." *International Journal of Polymer Science* 2013.

Noel, Scott P, Harry S Courtney, Joel D Bumgardner, and Warren O Haggard. 2010. "Chitosan sponges to locally deliver amikacin and vancomycin: a pilot in vitro evaluation." *Clinical Orthopaedics and Related Research®* 468 (8):2074-2080.

Nwe, Nitar, Tetsuya Furuike, and Hiroshi Tamura. 2009. "The mechanical and biological properties of chitosan scaffolds for tissue regeneration templates are significantly enhanced by chitosan from gongronella butleri." *Materials* 2 (2):374-398.

Ohtsuki, Chikara, Masanobu Kamitakahara, and Toshiki Miyazaki. 2009. "Bioactive ceramic-based materials with designed reactivity for bone tissue regeneration." *Journal of the Royal Society Interface* 6 (Suppl 3):S349-S360.

Ottenhall, Anna, Tiinamari Seppänen, and Monica Ek. 2018. "Water-stable cellulose fiber foam with antimicrobial properties for bio based low-density materials." *Cellulose* 25 (4):2599-2613.

Petrov, Petar, Jiayin Yuan, Krassimira Yoncheva, Axel HE Müller, and Christo B Tsvetanov. 2008. "Wormlike morphology formation and stabilization of "Pluronic P123" micelles by solubilization of pentaerythritol tetraacrylate." *The Journal of Physical Chemistry B* 112 (30):8879-8883.

Pires, Ana Luiza Resende, and Ângela Maria Moraes. 2015. "Improvement of the mechanical properties of chitosan-alginate wound dressings containing silver through the addition of a biocompatible silicone rubber." *Journal of Applied Polymer Science* 132 (12).

Sankar, PC Kavitha, G Rajmohan, and MJ Rosemary. 2017. "Physico-chemical characterisation and biological evaluation of freeze dried chitosan sponge for wound care." *Materials Letters* 208:130-132.

Shahidzadeh, Noushine, Daniel Bonn, Olivier Aguerre-Chariol, and Jacques Meunier. 1999. "Spontaneous emulsification: relation to microemulsion phase behaviour." *Colloids and Surfaces A: Physicochemical and Engineering Aspects* 147 (3):375-380.

Shaikh, Hina Kouser, RV Kshirsagar, and SG Patil. 2015. "Mathematical models for drug release characterization: a review." *World J. Pharm. Pharm. Sci* 4 (4):324-338.

Shao, Wei, Jimin Wu, Shuxia Wang, Min Huang, Xiufeng Liu, and Rui Zhang. 2017. "Construction of silver sulfadiazine loaded chitosan composite sponges as potential wound dressings." *Carbohydrate polymers* 157:1963-1970.

Shi, Chaoting, Caizhi Lv, Lan Wu, and Xiandeng Hou. 2017. "Porous chitosan/hydroxyapatite composite membrane for dyes static and dynamic removal from aqueous solution." *Journal of hazardous materials* 338:241-249.

Shirosaki, Yuki, Tomoyuki Okayama, Kanji Tsuru, Satoshi Hayakawa, and Akiyoshi Osaka. 2008. "Synthesis and cytocompatibility of porous chitosan–silicate hybrids for tissue engineering scaffold application." *Chemical Engineering Journal* 137 (1):122-128.

Siepmann, Juergen, and Nicholas A Peppas. 2011. "Higuchi equation: derivation, applications, use and misuse." *International journal of pharmaceutics* 418 (1):6-12.

Siepmann, Juergen, and F Siepmann. 2008. "Mathematical modeling of drug delivery." *International journal of pharmaceutics* 364 (2):328-343.

Silverstein, Michael S. 2014. "Emulsion-templated porous polymers: A retrospective perspective." *Polymer* 55 (1):304-320.

Singh, Lakhwant, Vipin Kumar, and Buddy D Ratner. 2004. "Generation of porous microcellular 85/15 poly (DL-lactide-co-glycolide) foams for biomedical applications." *Biomaterials* 25 (13):2611-2617.

Sionkowska, Alina, Beata Kaczmarek, and Katarzyna Lewandowska. 2014. "CHARACTERISATION OF CHITOSAN AFTER CROSS-LINKING BY TANNIC ACID." *Progress in the Chemistry and Application of Chitin and its Derivatives* (19):135-138.

Solans, Conxita, Daniel Morales, and Maria Homs. 2016. "Spontaneous emulsification." *Current Opinion in Colloid & Interface Science* 22:88-93.

Soykeabkaew, Nattakan, Pitt Supaphol, and Ratana Rujiravanit. 2004. "Preparation and characterization of jute-and flax-reinforced starch-based composite foams." *Carbohydrate Polymers* 58 (1):53-63.

Sreekumar, Sruthi, Francisco M Goycoolea, Bruno M Moerschbacher, and Gustavo R Rivera-Rodriguez. 2018. "Parameters influencing the size of chitosan-TPP nano- and microparticles." *Scientific reports* 8 (1):1-11.

Srinivasa, PC, and RN Tharanathan. 2007. "Chitin/chitosan—Safe, ecofriendly packaging materials with multiple potential uses." *Food Reviews International* 23 (1):53-72.

Su, K, Y Yang, Q Wu, Y Mao, and Y Hu. 2016. "Preparation of Polymeric Micelles of Curcumin with Pluronic P123 and Assessment of."

Talebian, Aazam, and Ardalan Mansourian. 2017. "Release of Vancomycin from electrospun gelatin/chitosan nanofibers." *Materials Today: Proceedings* 4 (7):7065-7069.

Testouri, A, C Honorez, A Barillec, D Langevin, and W Drenckhan. 2010. "Highly structured foams from chitosan gels." *Macromolecules* 43 (14):6166-6173.

van den Broek, Lambertus AM, Rutger JI Knoop, Frans HJ Kappen, and Carmen G Boeriu. 2015. "Chitosan films and blends for packaging material." *Carbohydrate polymers* 116:237-242.

Wan, Ying, Hua Wu, Xiaoying Cao, and Siqin Dalai. 2008. "Compressive mechanical properties and biodegradability of porous poly (caprolactone)/chitosan scaffolds." *Polymer Degradation and Stability* 93 (10):1736-1741.

Wójcik-Pastuszka, Dorota, Justyna Krzak, Bartosz Macikowski, Ryszard Berkowski, Bogdan Osiński, and Witold Musiał. 2019. "Evaluation of the Release Kinetics of a Pharmacologically Active Substance from Model Intra-Articular Implants Replacing the Cruciate Ligaments of the Knee." *Materials* 12 (8):1202.

Wu, Qiong, Vilhelm H Lindh, Eva Johansson, Richard T Olsson, and Mikael S Hedenqvist. 2017. "Freeze-dried wheat gluten biofoams; scaling up with water welding." *Industrial crops and products* 97:184-190.

Xianfang, Zeng, and Ruckenstein Eli. 1996. "Control of pore sizes in macroporous chitosan and chitin membranes [J]." *Ind Eng Chem Res* 35 (11):4169-4167.

Xie, Yu, Zeng-xing Yi, Jian-xun Wang, Tong-gang Hou, and Qiong Jiang. 2018. "Carboxymethyl konjac glucomannan-crosslinked chitosan sponges for wound dressing." *International journal of biological macromolecules* 112:1225-1233.

Xie, Yuling, Yanli Liu, Yan Wang, Siling Wang, and Tongying Jiang. 2012. "Chitosan matrix with three dimensionally ordered macroporous structure for nimodipine release." *Carbohydrate polymers* 90 (4):1648-1655.

Xu, Jiaojiao, Beihua Xu, Dan Shou, Xiaojing Xia, and Ying Hu. 2015. "Preparation and evaluation of vancomycin-loaded N-trimethyl chitosan nanoparticles." *Polymers* 7 (9):1850-1870.

Xu, Wei, Peixue Ling, and Tianmin Zhang. 2013. "Polymeric micelles, a promising drug delivery system to enhance bioavailability of poorly water-soluble drugs." *Journal of drug delivery* 2013.

Xu, Yongxiang, Dandan Xia, Jianmin Han, Shenpo Yuan, Hong Lin, and Chao Zhao. 2017. "Design and fabrication of porous chitosan scaffolds with tunable structures and mechanical properties." *Carbohydrate polymers* 177:210-216.

Zaric, Radica Zivkovic, Jasmina Milovanovic, Nikola Rosic, Dragan Milovanovic, Dejana Ruzic Zecevic, Marko Folic, and Slobodan Jankovic. 2018. "Pharmacokinetics of vancomycin in patients with different renal function levels." *Open Medicine* 13 (1):512-519.

Zhang, Fuqing, and Xiaogang Luo. 2015. "Systematic study on substituting petroleum-based polyols with soy-based polyol for developing renewable hybrid biofoam by self-catalyzing/rising process." *Industrial Crops and Products* 77:175-179.

Zhong, Xia, Chengdong Ji, Andrew KL Chan, Sergei G Kazarian, Andrew Ruys, and Fariba Dehghani. 2011. "Fabrication of chitosan/poly (ε-caprolactone) composite hydrogels for tissue engineering applications." *Journal of Materials Science: Materials in Medicine* 22 (2):279-288.

Zhou, Yiming, Shiyu Fu, Yunqiao Pu, Shaobo Pan, and Arthur J Ragauskas. 2014. "Preparation of aligned porous chitin nanowhisker foams by directional freeze–casting technique." *Carbohydrate polymers* 112:277-283.

Zhu, Guangshan, and Hao Ren. 2014. *Porous Organic Frameworks: Design, Synthesis and Their Advanced Applications*: Springer.

VITA

PERSONAL INFORMATION

Name: Aybike Nil OLCAY KURT   **E-mail:** aybikenil@gmail.com

EDUCATION

PhD   in Chemical Engineering 2014-2020, İzmir Institute of Technology, İzmir, Turkey
Thesis Tittle: Development of Chitosan Based Biofoams

MSc   in Environmental Engineering 2011-2014, İzmir Institute of Technology, İzmir, Turkey
Thesis Tittle: An Investigation of Dye-Surfactant Interactions in Aqueous Solutions
for Elucidating The Mechanisms of Ultrafiltration

BSc   in Business Administration 2007-2012, Anadolu University, Eskişehir, Turkey

BSc   in Chemical Engineering 2007-2011, İzmir Institute of Technology, İzmir, Turkey
Thesis Tittle: Enzymatic Degradation of Phthalate Esters

WORK EXPERIENCE

2013 - 2020	İzmir Institute of Technology , İzmir, Research Assistant
2012 - 2013	Atılım Metal Kauçuk Co, AOSB-İzmir, Production Engineer
2011 - 2012	Ege Suni Deri, Güzelcan Co., Torbalı-İzmir, Production Engineer

ACEDEMIC PROJECTS AND PUBLICATIONS

2019   **4th International Porous and Powder Materials Symposium**, Mugla/Turkey "Controling The Structural Voids And Intrinsic Micro Pores Of Chitosan Based Biofoams" **Oral Presentation and Publication.**

2017   **3th International Porous and Powder Materials Symposium**, Aydın/Turkey "Design of Chitosan Based Biofoams Using Micelles as Template" **Oral Presentation and Publication (**ISBN: 978-975-6590-09-6)**.**

2016   "Ancillary Effects of Surfactants on Filtration of Low Molecular Weight Contaminants Through Cellulose Nitrate Membrane Filters", **Published Article**, (Colloids and Surfaces A: Physicochem. Eng. Aspects 492 (2016) 199–206)

2016   **12. National Chemical Engineering Congress (UKMK12-2016),** İzmir/Turkey "Düşük Moleküler Ağirlikli Kirleticilerin Membran Filtre İle Etkileşiminin İncelenmesi" **Poster Presentation.**

2016   **5th World Congress on Materials Science & Engineering,** Alicante/Spain "Elucidating The Mechanism of Ultrafiltration for Wastewater Treatment in the Presence of Surface Active Molecules and Aggregates" **Oral Presentation.**

2015   **2nd International Porous and Powder Materials Symposium**, İzmir/Turkey "Ultrafiltration in the Presence of Surface Active Molecules and Aggregates" **Oral Presentation and Publication** (ISBN: 978-975-6590-07-2).

2015   **18th International Symposium on Environmental Pollution and its Impact on Life in the Mediterranean Region**, Crete/Greece "Elucidating the Mechanism of Ultrafiltration by Investigatıng of Dye-Surfactant Interactions in Aqueous Solutions" **Oral Presentation.**

2014   **11. National Chemical Engineering Congress (UKMK11-2014),** Eskişehir/Turkey "Yağ/Su Emülsiyon Sisteminin Bsa Proteini İle Stabilizasyonu" **Oral Presentation.**

2013   **1st International Porous and Powder Materials Symposium**, İzmir/Turkey "Capture of Low Molecular Weight Organic Contaminant within Micelle Structures in MEUF" **Oral Presentation and Publication** (ISBN: 978-975-6590-05-8).